Summer 8-31-2000

Turbulent mixing and chemical reaction in baffled stirred tank reactors : a comparison between experiments and a novel micromixing-based computational fluid dynamics model
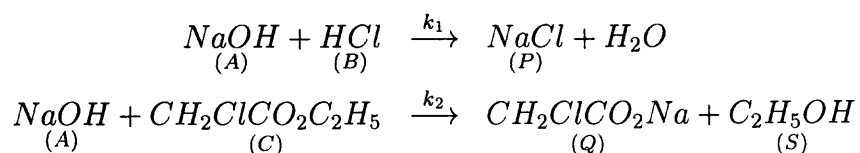
Otute Akiti
New Jersey Institute of Technology

ABSTRACT

TURBULENT MIXING AND CHEMICAL REACTION IN BAFFLED STIRRED TANK REACTORS: A COMPARISON BETWEEN EXPERIMENTS AND A NOVEL MICROMIXING-BASED COMPUTATIONAL FLUID DYNAMICS MODEL

by
Otute Akiti

The optimization of reaction processes to maximize the yield of a desired product while minimizing the formation of undesired by-products is one of the most important steps in process development for drug manufacturing or fine chemical production. In many situations the kinetics of product formation can be quite complex and involve a number of intermediate steps as well as parallel and serial reactions. This renders the systems sensitive to the operating conditions. Often, upon scale-up, a decrease in the yield of the desired product is experienced, while more undesired by-products are produced. A large number of interrelated variables influence the outcome of a process, and furthermore, most systems of process interest take place under turbulent conditions. Present methods for process design are inadequate because they involve the use of lumped parameters which fail to capture essential flow details and the rapid changes in the local concentration of reactants.

In recent years Computational Fluid Dynamics (CFD) has been successfully used to model the fluid dynamics of complex vessels (such as agitated reactors) and to predict the velocity distribution in turbulent systems such as mixers and reactors. In this work a novel approach based on the use of CFD coupled with micromixing models was used to predict the behavior of a multiple, competitive reaction system in cylindrical stirred tank reactors fitted with a variety of agitators. In particular, the following fast parallel competing reactions scheme (Bourne and Yu 1994) was modeled, and the results compared with original experimental data:

$$NaOH + HCl \xrightarrow{k_1} NaCl + H_2O$$
$$\underset{(A)}{} \quad \underset{(B)}{} \quad \quad \underset{(P)}{}$$

$$NaOH + CH_2ClCO_2C_2H_5 \xrightarrow{k_2} CH_2ClCO_2Na + C_2H_5OH$$
$$\underset{(A)}{} \quad \underset{(C)}{} \quad \quad \underset{(Q)}{} \quad \underset{(S)}{}$$

The reactor was operated in semi-batch mode, with the limiting reagent (A) being slowly added to the contents of the reactor in which the other reagents (B and C) were already dissolved. The final yield of the undesired product (S) was experimentally measured. The flow field in the reactor was simulated using the Reynolds Stress (RSM) turbulence model. The full impeller geometry was incorporated in the CFD simulation using the Multiple Reference Frames (MRF) model. The reaction zone was modeled in a Lagrangian way using a multi-phase *Volume of Fluid* (VOF) model (Hirt and Nichols 1981). The interaction of turbulence and reaction was accounted for by means of the engulfment-based models for micro-mixing (Baldyga and Bourne 1989a; Baldyga and Bourne 1989b; Baldyga et al. 1997).

The agreement between experimental velocity distribution data and the results of the simulations was generally good. The micro-mixing models, in conjunction with CFD, predicted a final yield in close agreement with the experimental data, demonstrating that the proposed approach can be successfully used to model turbulent reactive systems without the need for experimental input.

TURBULENT MIXING AND CHEMICAL REACTION IN BAFFLED STIRRED TANK REACTORS: A COMPARISON BETWEEN EXPERIMENTS AND A NOVEL MICROMIXING-BASED COMPUTATIONAL FLUID DYNAMICS MODEL

by
Otute Akiti

A Dissertation
Submitted to the Faculty of
New Jersey Institute of Technology
in Partial Fulfillment of the Requirements for the Degree of
Doctor of Philosophy in Chemical Engineering

Department of Chemical Engineering, Chemistry, and Environmental Science

August 2000

TURBULENT MIXING AND CHEMICAL REACTION IN BAFFLED STIRRED TANK REACTORS: A COMPARISON BETWEEN EXPERIMENTS AND A NOVEL MICROMIXING-BASED COMPUTATIONAL FLUID DYNAMICS MODEL

Otute Akiti

Dr. Piero M. Armenante, Dissertation Director   Date
Professor of Chemical Engineering, NJIT

Dr. Gordon Lewandowski, Committee Member   Date
Distinguished Professor of Chemical Engineering, NJIT

Dr. Robert Barat, Committee Member   Date
Associate Professor of Chemical Engineering, NJIT

Dr. Norman Loney, Committee Member   Date
Associate Professor of Chemical Engineering, NJIT

Dr. Pushpendra Singh, Committee Member   Date
Assistant Professor of Mechanical Engineering, NJIT

BIOGRAPHICAL SKETCH

Author: Otute Akiti

Degree: Doctor of Philosophy in Chemical Engineering

Date: August 2000

Undergraduate and Graduate Education:

- Doctor of Philosophy in Chemical Engineering,
  New Jersey Institute of Technology, Newark, New Jersey, 2000

- Master of Science in Chemical Engineering,
  Northeastern University, Boston, Massachusetts, 1995

- Bachelor of Science in Chemical Engineering,
  University of California at Berkeley, Berkeley, California, 1993

Major: Chemical Engineering

Presentations and Publications:

Otute Akiti and Piero M. Armenante, "A Computational and Experimental Study of Mixing
and Chemical Reaction in a Stirred Tank Reactor Equipped with a Down-pumping
Hydrofoil Impeller using a Micro-Mixing-Based CFD Model." Proceedings of the
10th European Conference on Mixing, Delft, The Netherlands, July 2–5, 2000.

Otute Akiti and Piero M. Armenante, "Mixing and Reaction in a Baffled Stirred Tank Re-
actor: A study of the Effects of Varying Viscosity on Mixing Sensitive Reactions
Using a Novel Micro-Mixing Based CFD Model." Annual Meeting of the American
Institute of Chemical Engineers, Dallas Texas, November 1999.

Otute Akiti and Piero M. Armenante, "A Computational and Experimental Study of Mixing
and Reaction in Stirred Tank Reactors using a Novel Micro-Mixing-Based Model"
Annual Meeting of the American Institute of Chemical Engineers, Dallas Texas,
November 1999.

Otute Akiti and Piero M. Armenante, "Mixing and Reaction in a Baffled Stirred Tank Re-
actor. Comparison Between Experiments and a Novel Micromixing Based CFD
Model" 17th Biennial North American Mixing Conference, Banff, Alberta, Canada,
August 15–20 1999.

Akiti et al, "Multiphasic or 'Pulsatile' Controlled Release System for the Delivery of Vaccines", in Human Biomaterials Applications, Humana Press Inc., 1996.

To my family

ACKNOWLEDGMENT

I would like to take this opportunity to say a few words of thanks to those who supported me and were instrumental in bringing this work to fruition.

I would firstly of like to thank my advisor, Professor Armenante, for his guidance and support during this project. He was not just a good advisor, but also a good teacher and I have benefitted tremendously from his excellent advice over the course of my studies here at NJIT.

I would also like express my sincere thanks to Dr. Gordon Lewandowski, Dr. Norman Loney, Dr. Robert Barat and Dr. Pushpendra Singh for serving as Committee Members.

A special thanks goes to Clint Brockway for his invaluable assistance with analytical laboratory equipment, and also to Larisa Krishtopa who filled in his big shoes after his departure. I would also like to thank Yogesh Gandhi in the chemical stockroom for his support. I would also like to thank Cindy Wos and Peggy Schel for their kind assistance with administrative work in the department.

I would like to thank Dr. Lanre Oshinowo, Dr. Liz Marshall and the rest of the Fluent support team for their technical assistance with using the Fluent CFD code.

This work was supported in part by a grant from the Emission Reduction Research Center at NJIT, and in particular the research institutes of the Schering Plough Corporation and the Bristol-Myers Squibb Corporation. Their support is gratefully acknowledged.

A special thanks to my friends here at NJIT, and the rest of the gang, who have contributed to making my experience as a student a most enjoyable one.

I would like to thank my parents, my brother and my sister for their patience and support.

To all the above, and anyone who I may have missed, thank you.

TABLE OF CONTENTS

TABLE OF CONTENTS
(Continued)

LIST OF TABLES

LIST OF FIGURES

Figure   **Page**

NOMENCLATURE

Symbol	Variable	Units
A	Impeller blade angle	radians
C	Impeller clearance off vessel bottom	m
C_i	Concentration of species i	$moles/m^3$
$\overline{C_i}$	Average concentration of species i	$moles/m^3$
C_i'	Fluctuating concentration of species i	$moles/m^3$
D	Impeller Diameter	m
D_k	Mass diffusivity of species k	m^2/s
E	Engulfment rate	$1/s$
F_i	External force	$N (Newtons)$
H	Liquid height	m
$J_{k,i}$	Mass flux of species k	kgm^2/s
N	Impeller speed	rev/s
N_{PO}	Impeller power number	—
P	Pressure	$Pa (Pascals)$
Po	Power dissipated by impeller	Watts
R	Vessel Radius	m
R_i	Reaction source term	—
Sc	Schmidt number	—
T	Tank diameter	m
U_{tip}	Impeller tip velocity	m/s
U	Degree of Mixing	—
V	Vessel Volume	m^3
V_{ei}	Engulfment volume	m^3
V_o	Initial dispersed phase volume	m^3
X_S	Yield of species S	—
c_P	Specific heat	$J/mol \cdot kg$
k_n	Kinetic rate constant for reaction n	$m^3/mol \cdot s$
n_b	Number of Impeller Blades	—
t	Time	s
u_i	Velocity vector	m/s
$\overline{u_i}$	Average velocity vector	m/s
u_i'	Fluctuating velocity vector	m/s
u_v	Axial velocity	m/s
v_v	Radial velocity	m/s
w_v	Tangential velocity	m/s
x_i	Cartesian coordinate components	m
Z	Vessel liquid height	m
z	Axial location in vessel	m

Greek Symbols	Variable	Units
δ_{ij}	Kronecker delta	—
ε	Turbulent energy dissipation rate	m^2/s^3
ϵ_{ijk}	Alternating unit tensor	—-
κ	Turbulent kinetic energy	m^2/s^2
μ	Molecular viscosity	$Pa \cdot s$
μ_t	Turbulent viscosity	$Pa \cdot s$
μ_{eff}	Effective viscosity ($\mu_t + \mu$)	$Pa \cdot s$
ν	Kinematic viscosity	M^2/s
ϕ	Mass fraction of species k	—
ρ_k	Mass density	kg/m^3
ρ_k	Mass density of phase k	kg/m^3
σ	Number of times feed is discretized	—
θ_{mix}	Mixing time	s
τ	Torque	$N(Newtons)$
Ω	Rotating speed of reference frame	rad/s
ω	Impeller speed	rad/s

CHAPTER 1

INTRODUCTION

1.1 Mixing in Industry and Research

Mixing processes are part of the infrastructure of the *Chemical Process Industries* (CPI). Mixing operations are encountered in industries such as: specialty chemicals, biotechnology, pharmaceutical, environmental (wastewater treatment), petroleum and polymer industries, to name a few, and serve to bring together the various process streams into contact to achieve desired objectives. These objectives include: the acceleration of heat transfer as a means of controlling temperature, the blending of liquids (homogenization), separation processes (e.g. solvent extraction), crystallization, and chemical reactions. Consequently, practically every plant contains a mixing process of some sort (Harnby et al. 1985).

As a result of their importance, mixing operations have been the subject of considerable study, and significant literature exists on the subject with the aim of furnishing design principles for many situations of industrial significance.

Economic losses that are incurred as a result of poor mixing are significant. In the United States alone, the output value from the chemical process industries is estimated at $750 billion (Tatterson et al. 1991). It is estimated that mixing related problems account for losses anywhere from 0.5 % to 3 % of that total. This translates into $1 billion–$20 billion in losses each year. In industries such as the pharmaceutical industry where the products require expensive reagents, are produced in relatively small quantities, and must meet exceptionally high purity standards, the losses are even more spectacular and may represent up 10 % of the turnover (Tatterson et al. 1991; Leng 1991; Smith 1990).

Despite their importance, mixing processes are still not well understood. This work focuses on addressing the problems that arise when mixing operations influence the outcome of chemical reactions.

1

1.2   Mixing and Chemical Reaction

1.2.1   The Mechanically Agitated Vessel

Because mixing operations cover a diverse spectrum of industries and applications, the equipment used for the purpose of mixing are equally diverse and include: mechanically agitated vessels, jet mixers, static mixers, extruders and mills.

This work focuses on the mechanically agitated tank, or stirred tank. The agitated vessel or stirred tank is widely used in the chemical process industries to effect mixing, especially where there is a need to maintain constant temperature and composition. The mechanical agitated vessel is typically a cylindrical vessel filled to some depth with the liquid of interest. The base of the tank may be flat, conical or spherical depending on the application. Baffles are included to prevent vortexing behavior when working with low viscosity liquids. The impeller is the device used to induce mixing. One more more impellers may be used. The impeller is generally mounted on a shaft which is driven by a motor. Heat transfer is effected by means of an external jacket or an internal cooling coil, or both. A schematic of a typical stirred tank is shown in Figure 1.1.

1.2.2   The Influence of Mixing on Chemical Reactions

This work focuses on mixing operations in *batch stirred tank reactors* (BSTR) with slow feed addition where reactions that are characterized as being "fast" and "complex", are taking place. In the BSTR one or several feed streams to the vessel are present while no exit streams are present. The BSTR is commonly encountered in industrial practice, and in particular the pharmaceutical industry. Such a reactor allows the control of temperature and helps prevent "runaway" reactions.

A "fast" reaction system, in the context of this work, refers to a system where the reaction time is on the order of magnitude, or shorter, than the time it would take to homogenize the contents of the mixing tank (blending time). This has important implications

motor/gearbox
drive unit

Feed

baffles

impeller

jacket for
heat transfer

vessel

(a) Side View

Baffles
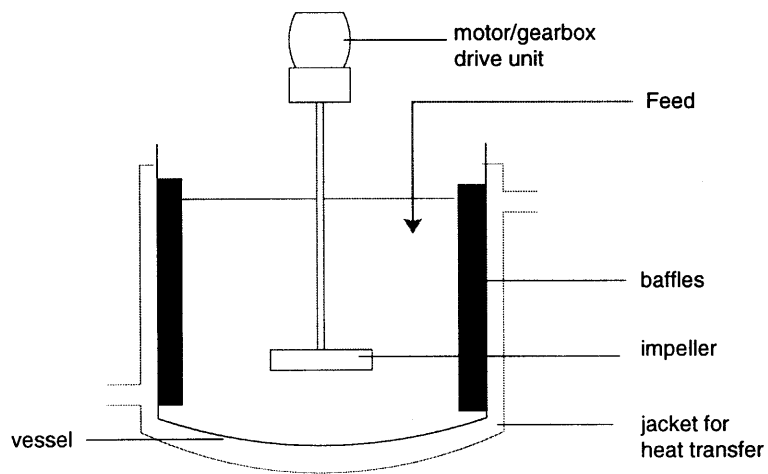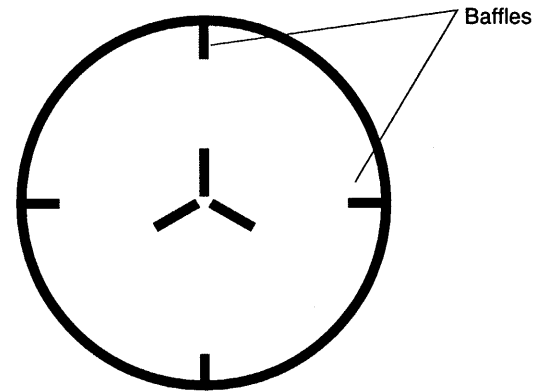
(b) Top View

Figure 1.1: Typical arrangement for a mechanically agitated vessel.

when "complex" reactions are involved.

A "complex" reaction system in this context is one where several interrelated reactions are taking place. An example of a complex reaction system would be a parallel competing reaction system of the following type:

$$A + B \xrightarrow{k_1} P \tag{1.1}$$

$$A + C \xrightarrow{k_2} S \tag{1.2}$$

where $k_1 \gg k_2$ and reactant A may react via two possible pathways.

Such a reaction scheme is commonly encountered in practice where a main reaction is taking place and unwanted side reactions are taking place alongside it. The unwanted side reactions may use up valuable reactants, produce species that reduce the purity of the desired product, or produce species that necessitate additional downstream processing steps in order to meet product specifications. This reduces the overall efficiency of the process.

When the reactions occurring are "fast", the reactants will be consumed before the contents of the mixing vessel are homogenized. In the example shown by Equations 1.1 and 1.2, this means that different amounts of Products P and S will be produced depending on the local environment Reactant A experiences. The manner in which this occurs is best illustrated by considering two extreme possibilities: the *the perfectly mixed system* and the *the completely segregated system.*

In a perfectly mixed system, with an initial equimolar mixture of reactants A, B and C, reactant A will "see" reactants B and C equally, and the final product distribution will depend solely on the kinetics. Because the first reaction is much faster than the second, $k_1 \gg k_2$, it will take place preferentially and little or no S product will form (Figure 1.2).

In a completely segregated system, where reactants B and C are segregated, and equal amounts of all the reactants are present initially, the reactions take place independently of each other such that reactant A sees both reactants B and C equally, and equal amounts of products P and S form (Figure 1.3).
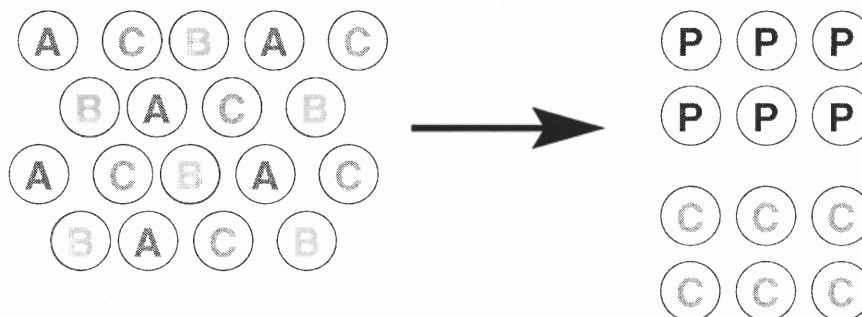
Figure 1.2: Reaction in a perfectly mixed environment
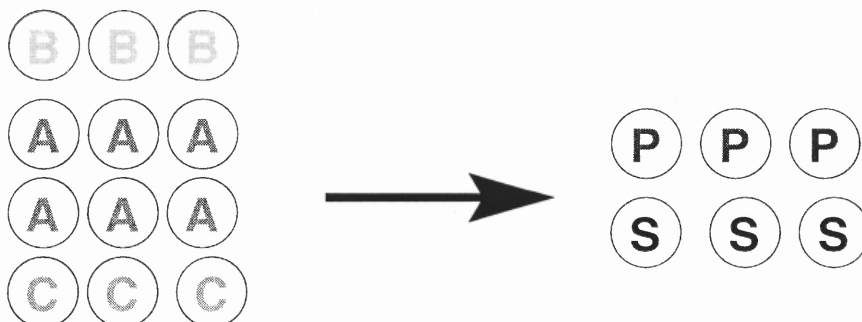
Figure 1.3: Reaction in a completely segregated environment

In a real system, where "fast" reactions are taking place, the system is neither in a state of complete mixedness nor is it in a state of complete segregation, and intermediate degrees of mixing are observed. This means that the kinetics as well as the hydrodynamics will dictate the final product distribution.

Most mixing problems occur in the scale-up stage because the prevailing hydrodynamics in large vessels is different from those in smaller ones where the processes are developed. Mixing times in small vessels are typically *small*, and often smaller than the characteristic reaction times; this means that reactions are more likely to take place in a homogeneous environment. Mixing times in large vessels (such as industrial reactors) are typically *large*. The mixing time in a 10,000 gallon reactor can easily exceed 10 minutes (Coy 1996). This means that reactions in an industrial reactor are likely to take place in an inhomogeneous environment when "fast" reactions are involved. Undesired by-products caused by mixing-sensitive reactions are more likely to be formed in large vessels than in small vessels even if the same reactions are considered. Over-designing rarely leads to a

better process. Successful prediction of the final product distribution upon scale-up will depend on a good understanding of the hydrodynamics and its influence on the kinetics.

For a long time, the approach used to analyze complex mixing systems was based on measurement and dimensional analysis. This involved the use of parameters such as: the *Power Number*, which is a measure of the power consumed by an impeller; the *Impeller Reynolds Number* which provides an indication of the level of turbulence in a reactor, and so on. While these parameters are useful, they describe an average, or overall reactor performance which, in many cases, masks inhomogeneities and gradients (concentrations, mixing intensity, temperature) that are important in determining the efficiency of a process. The lumping process wipes out the inhomogeneities and consequently leads to an erroneous estimation of the final product distribution. The inadequacy of using lumped parameters to designing systems when fast complex reactions were taking place was clearly demonstrated by Bourne and Yu (Bourne and Yu 1991).

In order to avoid the limitations of lumped parameter models, distributed parameter models based on actual system hydrodynamics must be used. This requires a more accurate knowledge of the local properties within the flow field of the reaction vessel. This involves gathering a huge amount of information that, in practice, cannot be obtained from experimentation. The only viable means of obtaining the necessary information is through numerical computation. In this work computational Fluid Dynamics (CFD) was employed for that purpose.

Computational Fluid Dynamics is an approach that involves the numerical solution of the the equations of motion (mass, momentum and energy) in a flow geometry of interest. These equations, together with subsidiary equations pertinent to the problem at hand, comprise a flexible and powerful tool. Examples of subsidiary equations that can be used in conjunction with CFD are:

- Equations for turbulence quantities

- Equations describing chemical species present in the flow

- Equations describing the dynamics of solid species, gas bubbles or other liquids dispersed in the flow domain

Computational Fluid Dynamics (CFD) has been successfully applied to model fluid flow in a variety of systems including stirred tanks (Ranade and Joshi 1990b; Ranade and Joshi 1989b; Brucato et al. 1998; Kresta and Wood 1991; Armenante and Chou 1994; Armenante et al. 1994).

The application of CFD to studying turbulent flow in batch stirred tank reactors where chemical reactions are taking place is not straightforward and the literature on the subject is sparse. In fact, CFD codes are unable to predict the product distribution in reactive flows exhibiting "fast" and "complex" chemistry. This is a result of the fact that CFD provides information about the local *bulk fluid flow* or *macromixing*, based on user defined boundary conditions. Chemical reaction is a molecular level process and takes place on the *microscale* which CFD does not resolve.

Micromixing models (Baldyga and Bourne 1989a; Baldyga and Bourne 1989b; Baldyga and Bourne 1984b; Baldyga and Bourne 1984a; Baldyga and Bourne 1984c; Bakker and van den Akker 1994; Bakker and van den Akker 1996) have been developed for purpose of modeling the effect of mixing on chemical reactions at the molecular level. Micromixing models do not contain any information about the bulk flow — the macromixing. A satisfactory means of linking information about the fluid dynamics to the kinetics to predict the outcome of complex reactive mixing systems is lacking in the literature.

Most work involving the computational modeling of mixing and chemical reaction, in stirred tanks, is based on a *network of zones* formulation (David et al. 1992; Bourne and Yu 1994; Wang and Mann 1992; Baldyga and Bourne 1988). Because this method requires experimentally derived correlations to describe the fluid flow, it is inadequate for investigating scale-up issues on novel systems. Work on modeling fast complex reaction systems using CFD was recently presented (Bakker and van den Akker 1994; Bakker and van den Akker 1996). The results reported were most encouraging. This method was,

however, unable to adequately predict the final product selectivities in all parts of the flow domain.

In this work, the final product yield of fast parallel competing reactions was studied for a variety of stirred tank configurations, all operated in semi-batch mode. A detailed description of the apparatus and method is presented in Chapter 4. An introductory overview is presented here.

A baffled stirred tank reactor was chosen for the study. The tank used was a flat bottomed cylindrical vessel having a diameter of 0.29 meters. The tank was filled with liquid up to a level equal to the vessel diameter. Four baffles of width one tenth of the tank diameter were equally spaced around the periphery of the tank. The impeller clearance, C, defined as the distance between the bottom of the tank and the center line of the impeller blades, was varied in some experiments. A variety of agitators were used. Different agitators produce different circulation patterns and different distributions of turbulent energy and dissipation for the same tank geometry. In this work the impellers used were:

- A radial flow impeller: Rushton Turbine

- An axial flow impeller: 6 Blade Pitched Blade Turbine (PBT) with the blades inclined at 45° to the horizontal

- A fluid foil impeller: The Chemineer High Efficiency Impeller (HE-3)
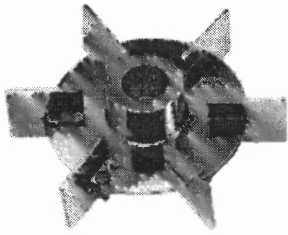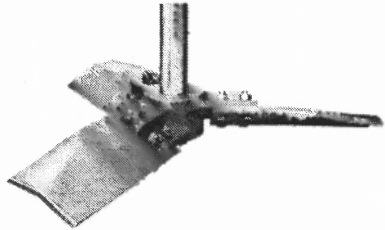
The three impellers used cover the majority of impeller types used in industrial practice for the agitation of low viscosity liquid systems. Schematic representations of the three impellers are presented in Table 1.1.

The mode of operation for the reactor system was semi-batch mode with the limiting reagent being slowly fed into the previously dissolved contents of the reaction vessel.

A summary of all the systems used for this work are presented in Table 1.2.

Studies were performed in both viscous and aqueous media in order to ascertain the effects of fluid viscosity of the complex chemistry. All simulation work was validated

Table 1.1: Overview of the impellers used

Figure of Impeller	Description
	The radial disk impeller is a high shear device that is commonly used in gas dispersion applications. This particular style is referred to as the Rushton impeller.
	The Chemineer HE-3 impeller is an example of a hydrofoil impeller. Hydrofoil impellers are the most efficient impellers for low viscosity blending applications (up to 2500 cps). They are also used in solid suspension applications where a relatively low percentage of solids are encountered.
	The pitched blade impeller finds its use in applications where a high flow velocity as well as moderate shear is required.

Table 1.2: Summary of systems under investigation

System	Impeller	Impeller Clearance	Process Fluid	Agitation Speed
A1	Rushton	T/3	Aqueous Water	100–300
A2	Rushton	T/3	Viscous Water	100–300
A3	Rushton	T/3	Aqueous Water	100–300
B1	Pitched Blade Turbine	T/3	Aqueous Water	100–400
B2	Pitched Blade Turbine	T/3	Viscous Water	100–400
C	Chemineer HE-3	T/3	Aqueous Water	100–400
D	Rushton	T/2	Aqueous Water	100–300

using original experimental data.

1.3 Objective

The overall objective of the present work was to develop a novel means of simulating mixing and chemical reaction in batch stirred tank reactors by using existing models for macromixing and micromixing as building blocks. A novel means of linking the various building blocks of the problem is introduced so as to provide a general purpose tool that can be used to predict the product distribution of fast complex reactions in BSTRs. All the numerical tools used in this work were validated using original experimental data.

The issues that need to be tackled when modeling mixing and chemical reaction in stirred tanks may be summarized as follows:

- An adequate description of the fluid flow in the geometry or interest

- An adequate description of the influence of turbulence on chemical reactions

- An adequate means of linking the description of the fluid flow with a mixing-sensitive reaction model that accounts for molecular level phenomena to ultimately yield a model that can be used to predict the course of fast complex reaction in stirred tanks.

The approach taken in this work to model the effects of mixing on complex reactions systems in this work may be be outlined as follows:

- CFD was used to obtain a quantitative description of the flow in stirred tanks.

- A micromixing model was selected to predict the influence of mixing on chemical reactions at the molecular level.

- A novel method to link macromixing and micromixing was used to successfully predict the product distribution of complex reaction systems.

- Original experimental work was conducted to collect data on the local fluid velocity distribution for all the systems studied. The collected data was used to validate the numerical predictions.

- Original experimental work was also conducted to determine the yield of complex parallel reactions under different operating conditions. These experimental results were used to validate the numerical predictions.

An outline of the work is summarized in Figure 1.4.

The critical step in the process is the coupling between information furnished by CFD and the information supplied by the micromixing models. The means for doing this is not generally agreed upon in the open literature and models that accomplish the task satisfactorily for stirred tank reactors are lacking. **Therefore specific the objective of this work is to develop a new model that successfully couples CFD with micromixing models to furnish a new tool that can be used for the design of BSTRs in which fast complex reactions are taking place.**

Fluid Mechanics   Kinetics

Experiment → Laser Doppler Velocimetry

Simulation → CFD + Turbulence Model

Competitive Fast Parallel Reactions

Micro-Mixing Model + Multiphase (VOF) Model

Novel Approach for Modeling Turbulent Reacting Flows
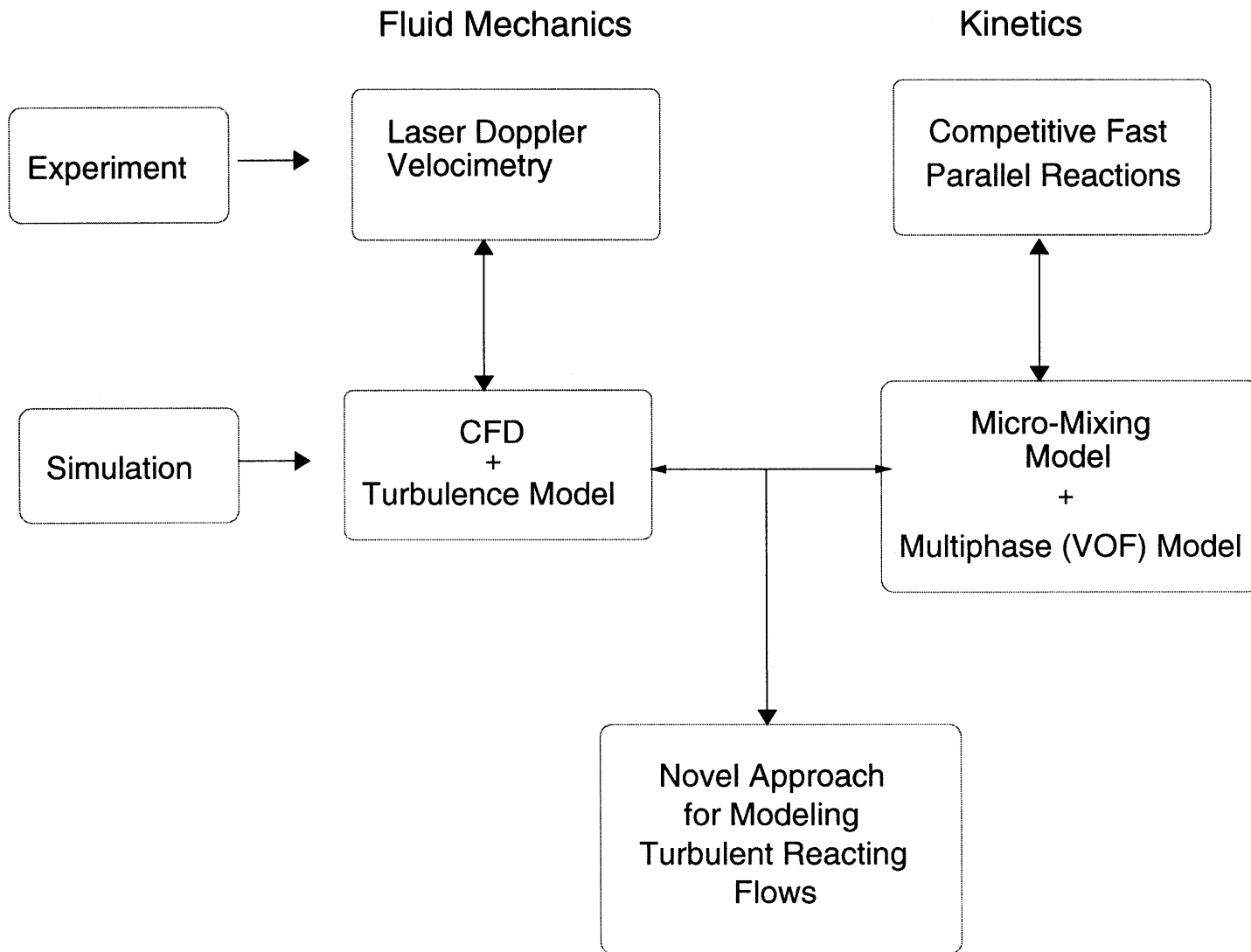
Figure 1.4: Outline of research work

CHAPTER 2

THEORETICAL BACKGROUND

2.1 Mixing Sensitive Reaction System

A parallel competitive reaction system that is sensitive to mixing effects (Baldyga and Bourne 1989b; Bourne and Yu 1991; Bourne and Yu 1994) was used to investigate the effect of mixing on chemical reactions. The reaction system is represented by Equation 2.1 and Equation 2.2. The first reaction (Equation 2.1) is an acid base neutralization reaction between *hydrochloric acid (HCl)* and *sodium hydroxide (NaOH)*. The second reaction (Equation 2.2), involves the hydrolysis of an ester, *ethyl-chloroacetate ($CH_2ClCO_2C_2H_5$)*.

$$\underset{(A)}{NaOH} + \underset{(B)}{HCl} \xrightarrow{k_1} \underset{(P)}{NaCl} + H_2O \qquad (2.1)$$

$$\underset{(A)}{NaOH} + \underset{(C)}{CH_2ClCO_2C_2H_5} \xrightarrow{k_2} \underset{(Q)}{CH_2ClCO_2Na} + \underset{(S)}{C_2H_5OH} \qquad (2.2)$$
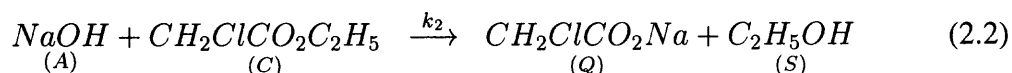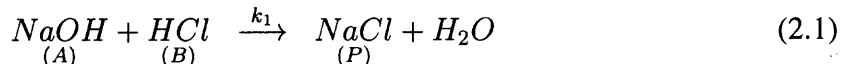
The rate constant k_1, for the first, faster, reaction is given by:

$$k_1 = 1.3 \times 10^8 m^3 mol^{-1} s^{-1} \text{ at } 25°C$$

while the rate constant k_2, for the second, slower (but still relatively fast) reaction, is given by the following Arrhenius rate expression (Bourne and Yu 1991):

$$k_2 = 2 \times 10^5 \exp(-3.887 \times 10^4 / RT)$$

This set of reactions is the well known Bourne reaction system # 4 (Baldyga and Bourne 1989b; Fox 1992; Bourne and Yu 1994). It is a well studied and characterized fast parallel competing reaction system. In this reaction scheme, component B, hydrochloric acid, and component C, ethyl-chloroacetate, compete for component A, sodium hydroxide. It is a well studied system because it is representative of reactions systems that are encountered in chemical reaction engineering practice where in addition to the primary reaction of interest, another competing reaction may also take place.

For this particular reaction set, the yield, X_S, of forming component S (undesired by-product) per mole of A (limiting reagent) fed to the system is of interest. The yield, X_S,

is defined as the moles of undesired by product S produced per mole of limiting reagent A fed to the system. It is expressed as follows in terms of the reaction products:

$$X_S = \frac{C_S}{C_P + C_S} \tag{2.3}$$

This yield varies depending on the system hydrodynamics as is explained below.

When the mixing is perfect (no segregation exists), the final yield X_S, is dictated solely by the kinetics and is given by:

$$X_S = \frac{C_S}{C_P + C_S} = \frac{k_2 C_C}{k_1 C_B + k_2 C_C} \tag{2.4}$$

For the above systems of equations, X_S is practically zero because $k_1 \gg k_2$.

When the segregation is intense (the reactions take place independently of each other), the yield becomes independent of the kinetics and is given by:

$$X_S = \frac{C_S}{C_P + C_S} \tag{2.5}$$

In the case where equal quantities of A, B and C are reacted, $X_S = 0.5$. *Intermediate degrees of mixing yields results between these two extremes and a means of evaluating the state of mixing on the reaction kinetics is necessary.*

2.2 Turbulent Reacting Flows

2.2.1 Overview

The process of turbulent mixing is extremely complex, largely because it involves a wide range of time and length scales. Mixing is initiated at the macroscale level and proceeds in a cascade like manner down to the microscale level. The macroscale level is important because it is the source of the mixing process. Chemical reactions, however, can only take place when the reacting species come into contact at the molecular level, the microscale level (Fox 1996; Baldyga and Pohorecki 1998; Bourne 1993; Villermaux and Falk 1996;

Bourne and Baldyga 1999). These scales and all those in between must be accounted for when modeling turbulent reacting flows.

For applications of chemical engineering interest, it is impossible to include a detailed description of all relevant turbulence scales into a CFD code, in particular those scales that take place at the sub-grid or molecular level, because the computational grid used for CFD calculations does not, and cannot extend down to such a fine scale. A computational grid used to describe a real physical system that contains a grid fine enough to resolve molecular scale phenomena would require computer resources that are well beyond the capacity of current computers. Furthermore, even with the present pace of computer development, this will not be possible in the foreseeable future.

Thus molecular level phenomena such as micromixing, molecular diffusion, and chemical reaction, must be modeled. The process of modeling can introduce significant simplifications into the physical description of the flow. In order to formulate acceptable algorithms for reacting flows, one must first understand and properly address the complex interactions between turbulence, molecular diffusion and chemical kinetics. At the very least, the following steps must be considered:

- Modeling the turbulence field in sufficient detail to resolve the rate controlling steps of turbulent mixing

- Modeling of the molecular diffusion and chemical reaction steps to predict the local reaction rate.

The specific importance of the modeling steps strongly depends on the type of flow under consideration. In this work, we are interested in single-phase, constant density flows with constant viscosity and equal mass diffusivities. Also, we are interested in mechanically agitated systems or stirred tanks.

2.2.2 Literature Review

A number of approaches have been developed to tackle the issue of turbulent reacting flows. The form taken by these models reflects the scientific field from which they were developed and the type of reacting flow system of interest. The problem has been studied actively for the last thirty years or so, unfortunately, in three major scientific areas that have largely ignored each other (Villermaux and Falk 1996). These are namely the areas of combustion, fluid mechanics and chemical reaction engineering. Fortunately, this trend is now changing. However, the established literature strongly reflects the previous state of affairs.

The most straightforward means of tackling the problem of turbulent reacting flows is to employ *direct numerical simulation* (DNS). This involves solving all pertinent equations directly without approximation or modeling. As mentioned earlier, this approach is not possible with complex real systems because of limitations of computer resources. Nonetheless for simple systems, DNS has proven to be a useful tool for gaining insights into the turbulent reacting process (Chakrabarti and Hill 1997).

Stemming from the discipline of fluid mechanics are models based on the Reynolds averaging approach. This approach is best illustrated by considering the following: For an irreversible second order reaction of the form:

$$A + B \longrightarrow R \tag{2.6}$$

The following transport equation for component j results:

$$\frac{\partial C_j}{\partial t} + U_i \frac{\partial C_j}{\partial x_i} = D \frac{\partial^2 C_j}{\partial x_i^2} - k_1 C_A C_B \tag{2.7}$$

Applying the Reynolds decomposition procedure (Denn 1980; Bird et al. 1960; Rodi 1984) for the concentration and the velocity yields:

$$C_j = \overline{C_j} + C_j' \quad U_i = \overline{U_i} + U_i' \tag{2.8}$$

The terms from Equation 2.8 are then inserted into Equation 2.7 to yield:

$$\frac{\partial \overline{C_j}}{\partial t} + \overline{U_i} \frac{\partial \overline{C_j}}{\partial x_i} = D \frac{\partial^2 \overline{C_j}}{\partial x_i^2} - \frac{\partial}{\partial x_i} \left(\overline{U_j' C_j'} \right) - k_1 \left(\overline{C_A C_A} + \overline{C_A' C_B'} \right) \tag{2.9}$$

In Equation 2.9 the turbulent transport term $\overline{U_i' C_j'}$ and the covariance $\overline{C_A' C_B'}$ are unclosed and must be modeled.

An infinite set of moments of the type

$$\overline{U_i' C_j'} \qquad \overline{U_j' C_j' C_k'}$$

can result from the Reynolds averaging procedure. The occurrence of these moments depends on the number of species involved in the reactions, the number of reactions and the phases within which these reactions are taking place. Also, except in the simplest of flows, these terms cannot be neglected, for they represent behavior of the reacting species at subgrid or molecular levels. Since chemical reactions can only occur when species come into contact at these levels, these terms are of prime importance when dealing with turbulent reacting flows involving complex chemistry.

First order closures were, historically, the first approach used to tackle the problem. This approach involves directly modeling the unclosed terms. The most common of these involves the use of Toor's hypothesis (Baldyga and Pohorecki 1998; Dutta and Tarbell 1989), which stipulates that the scalar covariance terms depend only on the hydrodynamics and not the kinetics. A number of models based on this approach are available in the literature. These have been shown to work well for simple reaction systems, while proving to be less adequate for systems involving complex chemistry (Dutta and Tarbell 1989; Wang and Tarbell 1993).

Second order closure models (Fox 1996) stem from fluid mechanics formulations and address some of the limitations of the first order closure models by developing transport equations for the nonlinear covariance terms. This in turn yields higher order unclosed terms which must be modeled. The *Turbulent Mixer Model* (Baldyga 1994; Baldyga 1989) and the *Spectral Relaxation Model* (Fox 1995) are notable examples of this method. This approach yields a relatively large number of equations that must solved and has limited their application to systems involving complex chemistry in tubular reactors that are conveniently modeled in two dimensions (2D) (Fox 1992; Pipino and Fox 1994; Kruis and

Falk 1996; Baldyga and Henczka 1997; Baldyga 1989; Baldyga 1994). Three dimensional (3D) problems, while theoretically feasible, are numerically intractable.

Micromixing models tackle the issue of turbulent reacting flows from a different angle. These models were developed primarily by chemical reaction engineers in recognition of the fact that the characteristic length and time scales present in the turbulent flow field are extremely important for predicting the yields in chemical reactors. The micromixing formulation has distinct advantages over the moment method approach:

1. Chemical reactions are treated exactly without modeling.

2. They require minimal computational resources.

3. Turbulent scale information is included in the model.

As a result of these advantages, micromixing models have elicited considerable interest in the chemical reaction literature. They are, however, not without their disadvantages:

1. The velocity and turbulence fields are not included in the model.

2. The coupling between the micromixing time scales and the turbulence time scales is not generally agreed upon, and is the subject of active research.

Several micromixing models have been presented in the literature and have been employed with limited success for the modeling of turbulent reacting flows in stirred tank reactors. These include the *Interaction by Exchange with the Mean* (IEM) model (Aubry and Villermaux 1975; David and Villermaux 1975; Villermaux and Falk 1996), the *Cylindrical Vortex Stretching Model* (Bakker and van den Akker 1994; Bakker and van den Akker 1996), the General Micromixing Models (GMM) (Villermaux and Falk 1994), and the *Engulfment Models* (Baldyga and Bourne 1984b; Baldyga and Bourne 1984a; Baldyga and Bourne 1984c; Baldyga and Bourne 1989a; Baldyga and Bourne 1989b; Baldyga et al. 1997). The Engulfment models are the most widely used because of their theoretical rigor

and ease of numerical implementation. The engulfment models form the foundation of this work and will be discussed in more detail in the following section.

The present research tackles the issue of modeling the influence of mixing on chemical reactions by developing a novel methodology based on CFD, and a new means of coupling the turbulent flow field with the micromixing process to yield a model that can be used to investigate turbulent reacting flows involving fast parallel competing reactions in stirred tank reactors.

2.3   Micromixing Models

The process of mixing is brought about by the onset of turbulence (Hinze 1975). The mixing process is initiated at the macroscale and proceeds down in a cascade-like manner to the microscale where chemical reactions can take place. In a mechanically agitated system for example, energy is imparted into the flow field by the impeller at the macroscale, and cascades down to the microscale. This is depicted schematically in Figure 2.1. In
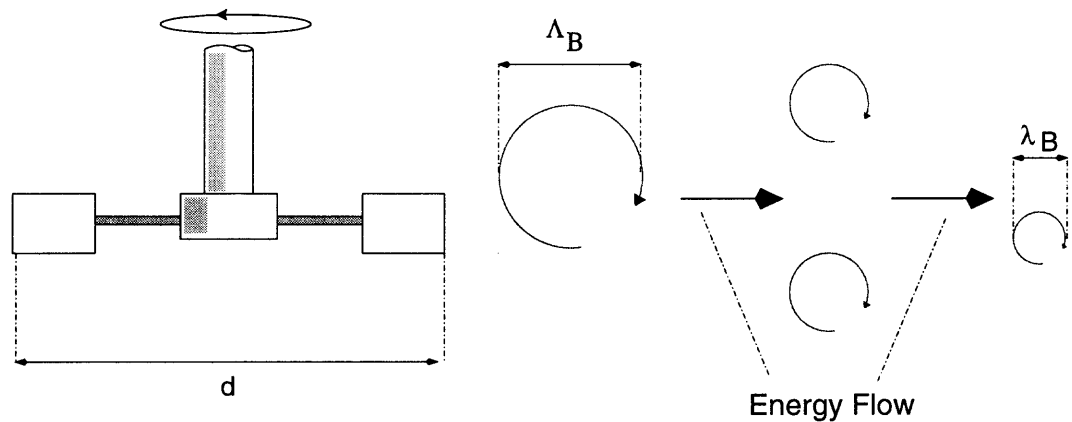
Figure 2.1: A simplified depiction of turbulence in a mechanically agitated system.

Figure 2.1, the turbulent cascade is shown to start on the scale of the agitator, d, proceed down to the Kolmogorov scale, Λ_B, and ultimately down to the Batchelor scale, λ_B.

The Kolmogorov scale is given by the following expression (Fox 1996; Hinze 1975):

$$\Lambda_B = \left(\frac{\nu^3}{\varepsilon}\right)^{1/4} \tag{2.10}$$

The Batchelor scale is given by the following expression (Fox 1996; Hinze 1975):

$$\lambda_B = \left(\frac{\nu D^2}{\varepsilon}\right)^{1/4} = Sc^{-1/2}\Lambda_B \tag{2.11}$$

In the process energy imparted by the agitator into the fluid, transfers with no loss until it reaches the Batchelor scale where it is ultimately dissipated by the action of viscous forces.

From turbulence theory (Hinze 1975; Rodi 1984), two important parameters are readily identified. These are namely: the *turbulent kinetic energy*, k_e, and *the rate of dissipation of turbulent kinetic energy*, ε. These two parameters serve to characterize the state of turbulence, and are important in the development of micromixing models. The turbulent kinetic energy, k_e, tells us how much energy is contained in the turbulent eddies initially. The rate of dissipation of k_e, ε, tells us how fast the energy contained in the eddies is dissipated at the microscopic level by viscous forces.

Though the process of turbulent mixing is extremely complex and a wide range of length and time scales exist between the macroscale and microscale, simpler stages in the mixing process can be identified (Bourne and Baldyga 1999):

- *The inertial convective stage:* Initially, different fluid elements are dispersed among each other. This takes place on a macroscopic scale.

- *The viscous convective stage:* Fluid elements stretch, deform and *engulf* each other. This takes place at a scale below the Batchelor scale.

- *The viscous diffusive stage:* The fluid elements become thin enough such that diffusion dominates and species are allowed to react, thereby eliminating concentration gradients.

These stages are represented schematically in Figure 2.2. Time constants can be identified

Inertial Convective   Viscous Convective   Viscous Diffusive
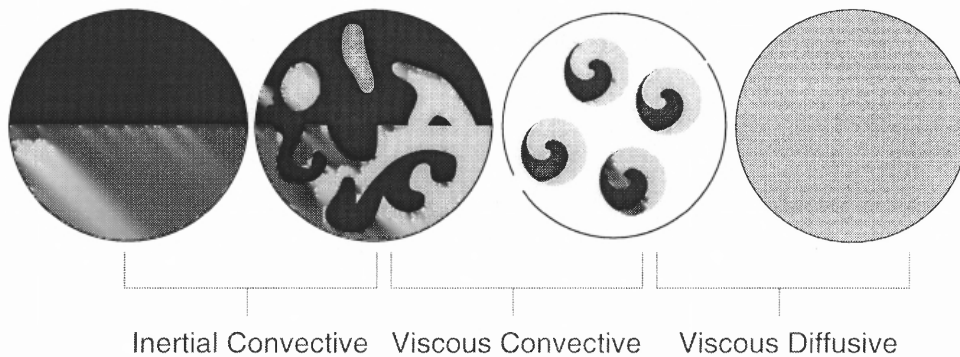
Figure 2.2: Principal stages of micromixing

for each stage in the cascade (Baldyga and Bourne 1984b; Baldyga and Bourne 1984a; Baldyga and Bourne 1984c; Villermaux and Falk 1996):

- Inertial convective range:

$$t_{ms} = \frac{k}{\varepsilon}$$

- The viscous convective range (engulfment):

$$t_E = \frac{1}{0.0578} \left(\frac{\nu}{\varepsilon}\right)^{1/2}$$

- The viscous–diffusive subrange:

$$t_D = \frac{Sc}{9.85 + 1.75 \times 10^{-2} Sc} \left(\frac{\nu}{\varepsilon}\right)^{1/2}$$

One or more of these mechanisms is usually found to be rate limiting, and hence controls the rate of mixing. Micromixing models and in particular, the engulfment family of micromixing models (Baldyga and Bourne 1984b; Baldyga and Bourne 1984a; Baldyga and Bourne 1984c; Baldyga and Bourne 1989a; Baldyga and Bourne 1989b; Baldyga et al. 1997) make use of this concept. They are discussed next.

2.3.1 The Standard Engulfment Model

The formulation of the engulfment models begins with an examination of the key physical processes that contribute to mixing on the molecular scale using information from fluid

mechanics. A mathematical model is then constructed from the information

From an analysis of the concentration spectrum, it was determined that (Baldyga and Bourne 1984b; Baldyga and Bourne 1984a; Baldyga and Bourne 1984c):

- Micromixing which proceeds by molecular diffusion, does not occur in the inertial-convective range.

- Mixing by molecular diffusion dominates in the viscous subrange.

- The viscous subrange is insensitive to diffusion when $k \approx k_K$ $(1/\Lambda_B)$, while when $k \approx k_B$ $(1/\lambda_B)$, diffusion is more important.

where k_K and k_B denote the Kolmogorov and Batchelor wave numbers respectively.

The key phenomena that govern the micromixing process are discussed next.

Deformation

Fluid deformation begins in the viscous convective subrange, where the fluid is deformed through the action of shear and elongation. The rate at which this process occurs is given by (Baldyga and Bourne 1984a; Baldyga and Bourne 1984d):

$$u = \frac{-\left(\epsilon/\nu\right)^{1/2} x}{\left(4 + \epsilon t^2/\nu\right)^{1/2}} \tag{2.12}$$

Vorticity (Engulfment)

Vorticity corresponds to the engulfment part of the model. This phenomenon refers to the curling and rotating of the velocity vector. Fluid deformation causes vortices to stretch and vorticity and kinetic energy to be transported from larger to smaller eddies. The nature of these energetically active, small scale motions in the fluid influence the regions where micromixing occurs.

Diffusion

Finally the fluid elements are small and thin enough such that molecular diffusion can take place. This occurs at scales below the Batchelor scale (viscous-diffusive subrange).

Implementation of the E Model

For aqueous systems where $Sc \ll 4000$, the *engulfment* step of the cascade is the rate limiting step (Baldyga and Bourne 1989a). This led to the development of the *Engulfment Model* (E-Model) (Baldyga and Bourne 1989a; Baldyga and Bourne 1989b).

The E-Model is based on the fact that mixing in the viscous convective subrange is rate limiting. Thus the E-Model visualizes a segregated reaction zone in a completely macromixed environment where the rate of transfer of bulk fluid into the reaction zone is characterized by the engulfment rate. Since chemical species react only when in contact at the molecular level, the engulfment rate controls the kinetics.

Segregrated reaction zone. Fluid is drawn in from the surroundings by the swirling fluid motion (engulfment).
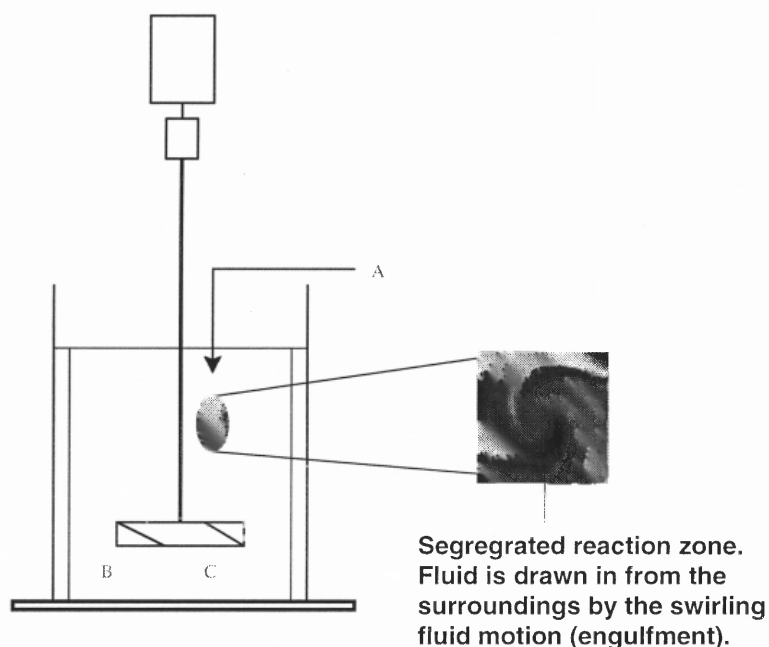
Figure 2.3: Schematic representation of the E-Model

The equations which comprise the E-Model, follow from a species mass balance between the segregated reacting zone and the macro-mixed bulk.

A mass balance on a substance i in the local environment of the growing eddy yields:

$$\frac{d\left(V_{ei}c_i\right)}{dt} = EV_{ei}\overline{c_i} + R_iV_{ei} \tag{2.13}$$

The volume of the reacting zone of fluid grows according to the following:

$$\frac{dV_{ei}}{dt} = EV_{ei} \tag{2.14}$$

Introducing Equation 2.14 into Equation 2.13 yields:

$$\frac{dc_i}{dt} = E\left(\overline{c_i} - c_i\right) + R_i \tag{2.15}$$

The parameter, E, is the rate of engulfment and is evaluated as follows (Baldyga and Bourne 1989a):

$$E = 0.05776(\varepsilon/\nu)^{1/2} \tag{2.16}$$

It depends on the state of turbulence through the parameter ε and the the fluid properties through the kinematic viscosity, ν.

2.3.2 The Modified Engulfment Model

A modification of the original E-Model was recently proposed where mixing in the inertial convective range of the turbulent spectrum was also accounted for (Baldyga et al. 1997). Mixing in this range is more commonly referred to as *mesomixing*, an intermediate stage of mixing between macromixing and micromixing by engulfment.

In this model, the rate of growth of micromixed volume is given by the following expression:

$$\frac{dV_B}{dt} = EV_B \left[1 - \frac{V_B \exp(-t/\tau_s)}{V_0}\right] \tag{2.17}$$

where V_B is the volume of fluid undergoing micromixing and $V_B = V_0$ when $t = 0$.

The parameter τ_s represents the time constant for mesomixing.

The substitution of Equation 2.17 into the E-Model formulation, yields the following expression for species C_i undergoing micromixing:

$$\frac{dC_i}{dt} = E \left(1 - \frac{V_B \exp(-t/\tau_s)}{V_0} \right) (\overline{C_i} - C_i) + R_i \qquad (2.18)$$

The primary difference between this model and the E-Model is the presence of two time scales. These are namely, the mesomixing time scale, τ_s and the engulfment time scale E. One of the objectives of this work is the assessment of whether or not the inclusion of the second time scale (τ_s) is important to modeling turbulent reactive systems in stirred tanks. The time constant for mesomixing is taken to be the scalar mixing rate k/ε.

2.4 Remarks

It possible to model the effect of mixing on chemical reactions without the need to approximate the reaction terms using micromixing models. This is the strength of using this approach. Unfortunately, micromixing models contain no information about the bulk flow of the system of interest which is necessary to fully describe and model the effects of mixing on chemical reactions in stirred tanks. In this work, the turbulent flow field will be obtained numerically using CFD.

CHAPTER 3

NUMERICAL SIMULATION

3.1 Modeling the Turbulent Flow Field

Numerical simulation of the flow field in stirred tanks was obtained using a general purpose, commercially available CFD package, FLUENT v4.5. The code numerically integrates the equations for transport over a user specified geometry and boundary conditions to provide a quantitative description of the flow field.

The flow phenomena encountered in the stirred tank are turbulent. Appropriate models to describe turbulent flow must be incorporated in the the simulation. The equations that will be solved are presented next.

3.1.1 Conservation Equations

The mass conservation equation, often termed the continuity equation, is represented as follows for incompressible flow (Bird et al. 1960; Denn 1980).

$$\frac{\partial u_i}{\partial x_i} = 0 \tag{3.1}$$

The conservation of momentum in a non-accelerating reference frame for flow is given by the following equation (Bird et al. 1960; Denn 1980):

$$\frac{\partial}{\partial t}\left(\rho u_i\right) + \frac{\partial}{\partial x_j}\left(\rho u_i u_j\right) = -\frac{\partial P}{\partial x_i} + \frac{\partial}{\partial x_j}\left(\tau_{ij}\right) + \rho g_i + F_i \tag{3.2}$$

The term F_i denotes external forces acting on the system and is zero if no such forces are present. The expression τ_{ij} is the stress tensor which represents the action of shear stresses on the fluid. It has the following expression:

$$\tau_{ij} = \left[\mu\left(\frac{\partial u_i}{\partial x_j} + \frac{\partial u_j}{\partial x_i}\right)\right] - \frac{2}{3}\mu\frac{\partial u_l}{\partial x_l}\delta_{ij} \tag{3.3}$$

For an incompressible fluid with constant viscosity, the stress tensor is simplified as

follows:

$$\tau_{ij} = \left[\mu \left(\frac{\partial u_i}{\partial x_j} + \frac{\partial u_j}{\partial x_i} \right) \right] \tag{3.4}$$

where μ is the molecular viscosity.

The conservation of species ϕ_k is described by the following equation:

$$\frac{\partial}{\partial t} \left(\rho \phi_k \right) + \frac{\partial}{\partial x_i} \left(\rho u_i \phi_k \right) = \frac{\partial J_{k,i}}{\partial x_i} + S_k \tag{3.5}$$

where ϕ_k denotes the mass fraction of species k and S_k is the source term. The mass diffusivity is expressed as follows for the isothermal case:

$$J_{k,i} = -\rho D_{k,\phi} \frac{\partial \phi_k}{\partial x_i} \tag{3.6}$$

3.1.2 Conservation Equations for Turbulent Flows

The equations of transport presented earlier are completely general. They form a closed set that describe the details of transport, including turbulent flow (Navier-Stokes Equations). The need for an alternative formulation for turbulent flows arises from the fact that turbulent flows contain apparently random and chaotic phenomena that are present at very small scales that need to be resolved. A computational grid sufficiently fine to resolve these scales for the system of interest demands far more resources than are possible with current computers. Should these phenomena not be resolved, the features and effects of the turbulent flow will not be captured (Hinze 1975; Fox 1996).

The Reynolds averaging technique is the most common approach employed for developing transport equations for turbulent flow. The technique consists of separating the instantaneous value of the velocity u_i, the pressure P, and the scalar quantity ϕ_i, into a mean and a fluctuating quantity as follows:

$$u_i = \overline{u_i} + u_i', \qquad P = \overline{P} + P', \qquad \phi_i = \overline{\phi} + \phi' \tag{3.7}$$

When these are substituted into the conservation equations and time averaging is applied, a new set of conservation equations results:

Continuity:

$$\frac{\partial \overline{u_i}}{\partial x_j} = 0 \tag{3.8}$$

Momentum:

$$\frac{\partial \overline{u_i}}{\partial t} + \overline{u_j}\frac{\partial}{\partial x_j}\overline{u_i} = -\frac{1}{\rho}\frac{\partial \overline{P}}{\partial x_j} + \frac{\partial}{\partial x_j}\left(\overline{\tau_{ij}} - \rho\overline{u_i'u_j'}\right) + \overline{F_i} + \overline{\rho g_i} \tag{3.9}$$

Species:

$$\frac{\partial \overline{\phi_k}}{\partial t} + \overline{u_i}\frac{\partial}{\partial x_j}\overline{\phi_k} = \frac{\partial}{\partial x_j}\left(D\frac{\partial}{\partial x_j}\overline{\phi_k} - \overline{u_i'\phi_k'}\right) + \overline{S_k} \tag{3.10}$$

The equations thus derived are exact since no assumptions have been made in deriving them. However, they no longer form a closed set since there is no information about the fluctuating terms, $\overline{\rho u_i'u_j'}$, also known as Reynolds stresses, and $\overline{u_i'\phi}$. These terms need to be modeled. The number of closure approximations to this set of equations is vast and serves as a testimony to the challenge that the problem presents (Rodi 1984). In this work, the *Reynolds' Stress Model* (RSM) will be used. The RSM while more computationally demanding than other available models, has been shown to consistently yield superior results (Brucato et al. 1998).

The Reynolds Stress (RSM) Model

In the RSM model, conservation equations for the individual stresses $\overline{u_i'u_j'}$ in Equation 3.9 are solved. This method yields unclosed terms of a higher order that need to be modeled. The implementation of the RSM model in FLUENT is as follows:

$$\frac{\partial \overline{u_i'u_j'}}{\partial t} + u_k\frac{\partial}{\partial x_k}\overline{u_i'u_j'} = \frac{\partial}{\partial x_k}\left(\frac{\mu_t}{\sigma_k}\frac{\partial}{\partial x_k}\overline{u_i'u_j'}\right) + P_{ij} + \Phi_{ij} - \varepsilon_{ij} + R_{ij} + S_{ij} + D_{ij} \tag{3.11}$$

where

P_{ij} is the stress production rate

Φ_{ij} a source/sink due to the pressure/strain correlation

ε_{ij} is the viscous dissipation

R_{ij} is the rotational term

S_{ij} and D_{ij} are curvature terms which arise when the equations are written in cylindrical coordinates.

The production term is computed without modeling assumptions as:

$$P_{ij} = -\left(\overline{u_i'u_j'}\frac{\partial}{\partial x_k}u_j + \frac{\partial}{\partial x_k}\overline{u_i'u_j'}\right) \tag{3.12}$$

The pressure/strain term is modeled as:

$$\Phi_{ij} = -C_3\frac{\varepsilon}{k}\left(\overline{u_i'u_j'} - \frac{2}{3}\delta_{ij}k\right) - C_4\left(P_{ij} - \frac{2}{3}\delta_{ij}P\right) \tag{3.13}$$

where $P = \frac{1}{2}P_{ii}$ and C_3 and C_4 are empirical constants with values of 1.8 and 0.6 respectively. The dissipation term is approximated by the isotropic dissipation rate ε:

$$\varepsilon_{ij} = \frac{2}{3}\delta_{ij}\varepsilon \tag{3.14}$$

The dissipation rate, ε, is determined by solving the following equations:

$$\frac{\partial}{\partial t}(\rho\varepsilon) + \frac{\partial}{\partial x_j}(\rho u_i\varepsilon) = \frac{\partial}{\partial x_j}\left(\frac{\mu_t}{\sigma_\varepsilon}\frac{\partial}{\partial x_j}\varepsilon\right) + C_{1\varepsilon}\frac{\varepsilon}{k}\left(G_k + (1 - C_{3\varepsilon})G_b\right) \\ -C_{2\varepsilon}\rho\frac{\varepsilon^2}{k} \tag{3.15}$$

G_k is the rate of production of turbulent kinetic energy:

$$G_k = \mu_t\left(\frac{\partial}{\partial x_i}u_j + \frac{\partial}{\partial x_j}u_i\right)\frac{\partial}{\partial x_i}u_i \tag{3.16}$$

and G_b is the generation of turbulence due to buoyancy:

$$G_b = -g_i\frac{\mu_t}{\rho\sigma_h}\frac{\partial}{\partial x_i}\rho \tag{3.17}$$

where

$$C_{1\varepsilon} = 1.44, \quad C_{2\varepsilon} = 1.92, \quad \sigma_\varepsilon = 1.3$$

The rotational terms are given by:

$$R_{ij} = -2\Omega_k \left[\overline{u'_j u'_m} \varepsilon_{ikm} + \overline{u'_j u'_m} \varepsilon_{jkm} \right] \qquad (3.18)$$

Further details of the RSM turbulence are presented in the literature (Rodi 1984).

3.2 Boundary Conditions

3.2.1 Boundary Conditions at Walls and Surfaces

Prior to solving the CFD model equations, appropriate boundary conditions must be imposed on the system.

The boundary conditions at the vessel walls, baffles, horizontal bottom, and shaft for all systems were those derived assuming no-slip. This implied that the shear stress near the solid surfaces is specified using wall functions, and that equilibrium between the generation and dissipation of turbulence energy is assumed (Rodi 1984; Fluent Inc. 1992). Wall functions are necessary because near the wall there is a transition from turbulent flow to laminar flow. The equations being solved are valid only in the turbulent regime. Thus in this transition zone and at the wall an alternate formulation is necessary.

The boundary conditions at the liquid surface was of the the zero-gradient, zero-flux type, which is equivalent to a frictionless impenetrable wall. The common symmetry boundary conditions are assumed at the symmetry axis for all systems (Ranade and Joshi 1990b).

3.2.2 Boundary Conditions for the Agitator

The most common method of applying boundary conditions for the agitator involves the use of time averaged, experimentally derived inputs as boundary conditions for the impeller region of the agitated vessel. This method has been employed extensively in the open literature for the simulation of fluid flow in stirred tanks (Ranade and Joshi 1990b; Kresta

and Wood 1991; Armenante et al. 1994; Armenante and Chou 1994; Armenante et al. 1997; Ranade and Joshi 1989b). While this method has been found to yield good overall results for the flow field, it fails to capture many features of the flow structure in the vicinity of the impeller. This has an adverse influence on the velocities predicted in the rest of the vessel.

Experimental observations have shown that there exists a strong inherent periodic unsteadiness due to the relative motion between the rotating impeller blades and the fixed baffles. These unsteady phenomena can be accommodated into the CFD model only if the model does not rely on the assumption of steady flow in the impeller region and the calculations are carried out in a time dependent manner.

The most accurate way of doing is this is to employ a fully time dependent CFD simulation. This is computationally extremely expensive in terms of memory use and computational time. In a time dependent simulation, small time steps are employed and convergence must be established at each time step before proceeding to the next one. The process is repeated until what is termed a time dependent steady state is achieved (Coy 1996; Harvey III and Rogers 1996).

A less expensive means of carrying out the calculations has been developed to overcome the limitations of using the steady state boundary conditions approach, while permitted the transient features of the agitator to be retained. This approach is termed the *Multiple Reference Frames* (MRF) approach (Luo et al. 1994). In the MRF formulation, the computational grid is divided into two or more sections, with some sections associated with a rotating reference frame and others associated with a stationary reference frame (Figure 3.1). Thus in simulating flow phenomena in a stirred tank, the part of the grid associated with the impeller is cast into a rotating frame of reference. The conservation equations are thus transformed into a rotating reference frame and the flow is computed in a steady state manner. The rest of the computational domain is stationary. At the interface between the two computational regions that are placed in two different frames of reference,
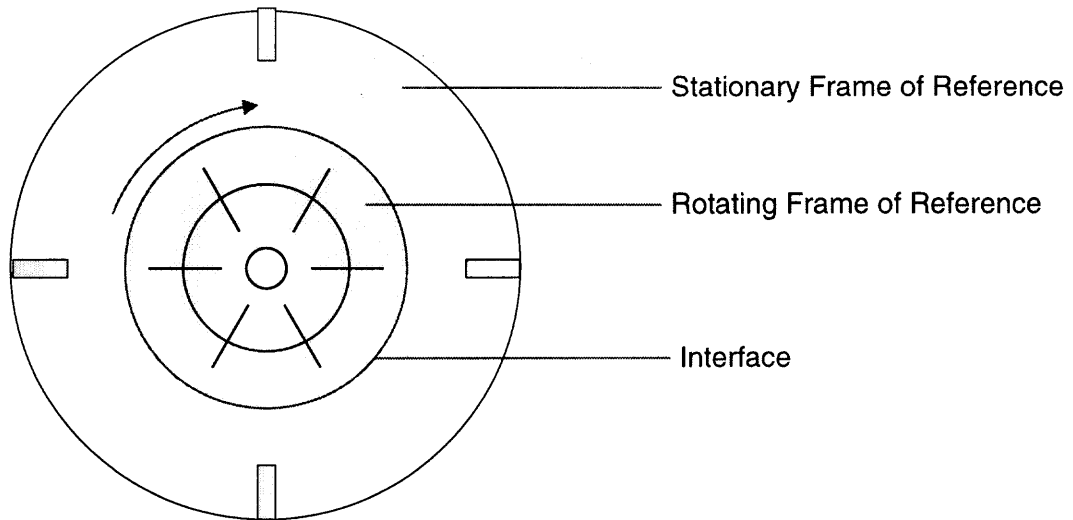
Figure 3.1: Illustration of the MRF model.

the two solutions are matched locally via appropriate transformations from one frame to another. This is tantamount to assuming steady flow conditions at the interface, a fact that has been verified using full unsteady state computations (Luo et al. 1994). For example, suppose computational cell P is placed on rotating frame 1, and its neighboring cell N in on rotating frame 2, then the velocities in cell N have to be converted to the same rotating frame as cell P in order to carry out the computations for cell P. This is necessary in order to facilitate the implicit coupling across the interface. The general velocity relationship for cells in two different frames of reference is given by:

$$u_{i,N}^{frame\ 1} = u_{i,N}^{frame\ 1} + \epsilon_{ijk} \left(\Omega_j^{frame\ 2} - \Omega_j^{frame\ 1} \right) x_k \qquad (3.19)$$

The motivation for carrying out a simulation in this manner is that an unsteady state simulation can be carried out in a steady state manner. This translates into considerable savings in computer resources. The MRF formulation also allows for the inclusion of the complete impeller geometry into the computation, thereby permitting a more realistic simulation. More importantly, transient features of the turbulent flow are preserved. This leads to a better prediction of turbulence.

3.2.3 Grid Generation

The conservation equations for mass, momentum, species, and turbulence quantities are solved using a control volume technique (Finlayson 1980; Griebel et al. 1998; Fluent Inc. 1992). The control volume technique involves the following:

- The computational domain is divided into discrete control volumes by means of a grid.

- The conservation equations are integrated on the individual control volumes to construct algebraic equations for the unknowns.

- The solution of the discretized conservation equations using algebraic techniques.

The numerical solution of differential equations can only be performed algebraically. The control volume technique is a means of converting differential equations to algebraic ones. The control volume technique employed in FLUENT consists of integrating the differential equations about each control volume to yield finite difference equations that consume each quantity on a control volume basis. The type of grid used in discretizing the equations is referred to a *non-staggered grid*. This means that the same grid and control volumes are used for integrating all the equations and variables of interest. The values of these variables are stored at the center of each control volume.

The computational grid necessary for the simulations was generated using MIXSIM v1.5, a grid generation package for stirred tanks that is part of the FLUENT software suite. The full 360° geometry of the stirred tank was used.

In order to obtain better predictions of turbulence, further modifications of the grid generated by MIXSIM was necessary. In particular, the impeller region was further refined in order to better capture the flow phenomena occurring there. It was also necessary to refine the parts of the grid where there was impinging flow. For the axial flow impellers, this was area close to the tank bottom, while for the radial flow impellers, this was the area close to the tank walls.

In the case of the Rushton impeller and the Pitched Blade Turbine, 20 grid lines were used to define the impeller region. For the Rushton impeller, the grid density in the vicinity of the tank wall was doubled by inserting five grid lines in that region. In the case of the Pitched Blade Turbine, the same procedure was applied to the base of the stirred tank. In the case of the Chemineer HE-3, the overall grid density was increased from the MIXSIM default of 40 cells per tank diameter to 60 cells per tank diameter. The impeller region was left unmodified because this particular impeller features complex geometric characteristics and was described using custom specifications furnished from the manufacturer (Chemineer Inc, Dayton, OH, USA). Modifications to the impeller region could alter the geometry of the impeller and lead to erroneous results.

For the axial flow impellers (PBT, HE-3), the MRF portion of the grid spanned the height of the computational grid, whereas for the radial flow impellers (Rushton turbine), the MRF zone did not span the entire height of the grid, rather it spanned a height of $0.25D$ to $0.5D$, where D is the impeller diameter. This was done in order to best capture the strong radial flow characteristics of the impeller.

The grid information employed for this work are summarized in Table 3.1.

3.3   Determining the Power Imparted to the System

The power delivered by each impeller to the system was computed by the CFD code by summing the cross product of the radius vector and the force vector at all nodes on the impeller surface. The radius vector originates on the shaft axis. The forces on the impeller include both shear forces and normal forces. Shear forces are computed from tangential velocity gradients at the surface, and the normal forces are computed from the surface pressure and cell area. The resulting torque is directed along the shaft axis.

The power imparted to the system by the impeller was then computed using the follow-

Table 3.1: Summary of Grids Used

System	Impeller	Impeller Clearance	Process Fluid	Grid Size (I,J,K)
A1	Rushton	T/3	Aqueous Water	145,40,89
A2	Rushton	T/3	Viscous Water	145,40,89
B1	Pitched Blade Turbine	T/3	Aqueous Water	146,34,85
B2	Pitched Blade Turbine	T/3	Viscous Water	146,34,85
C	Chemineer HE-3	T/3	Aqueous Water	145,32,82
D	Rushton	T/2	Aqueous Water	145,38,96

ing:

$$Po = \omega\tau \tag{3.20}$$

It has been shown through experimental data that the power consumption of an impeller, Po, is proportional to the cube of the rotational speed of the impeller, the fifth power of the impeller diameter, and the density of the fluid. The following relationship has been found to hold:

$$P = N_{Po}N^3 D^5 \rho \tag{3.21}$$

Solving for N_{Po} yields the following expression:

$$N_{Po} = \frac{P_o}{N^3 D^5 \rho} \tag{3.22}$$

This quantity is referred to as the power number. The power number for a wide range of system configurations is available in the open literature, mostly in the form of correlations. This allows the determination of the power imparted to the system by the impeller to be readily calculated.

The computed values for the power number and power draw were compared with the results from experiments conducted in the Mixing Laboratory in the department of Chemical Engineering, Chemistry and Environmental Science at the New Jersey Institute of Technology, and also with published correlations. The correlations used are summarized next:

3.3.1 Power Number Correlation for the Rushton Turbine

The correlation for N_{Po} is given by the following expression (Gray et al. 1982):

$$N_{Po} = 5.17 \left[\frac{C}{D}\right]^{0.29} \; for \; C/D < 1.1 \tag{3.23}$$

$$N_{Po} = 5.17 \; for \; C/D > 1.1 \tag{3.24}$$

3.3.2 Power Number Correlation for the Chemineer High Efficiency Impeller (HE-3)

No correlations are available in the literature for this impeller. However, studies have shown that in the turbulent regime, where N_{Po} is constant, and for the configuration used in this work, $N_{Po} = 0.282$ (Myers et al. 1994).

3.3.3 Power Number Correlation for the 6 Blade Pitched-Blade Turbine

The correlation for N_{Po} is given by the following expression (Rewaltker et al. 1990):

$$N_{Po} = 0.653T^{0.26} \left(\frac{T}{D}\right)^{0.11} \left(\frac{C}{T}\right)^{-0.23} n_b^{0.68} A^{1.82} \qquad (3.25)$$

3.3.4 Evaluation of the Impeller Reynolds Number

The impeller Reynolds number for stirred tanks is given as follows:

$$N_{Re} = \frac{\rho N D^2}{\mu} \qquad (3.26)$$

Equation 3.26 was used to compute the Reynolds number for all the systems under study.

3.4 Evaluation of Mixing Time

The mixing times for the systems studied were computed using published correlations. The mixing time for the purposes of this work is defined as the time taken to achieve 99 % uniformity as defined next.

3.4.1 Mixing Time for the Rushton Turbine

For the Rushton turbine, the mixing time correlation was taken from (Fasano and Penney 1991) and is given as follows:

$$t_{99} = \frac{-\log(1-U)}{aN\left[\frac{D}{T}\right]^b}\left[\frac{T}{Z}\right]^{0.5}$$

(3.27)

where:

U = Degree of Mixing (0.99) = 99% uniformity

For a 6 bladed radial disk, a = 1.06 and b = 2.17.

3.4.2   Mixing Time for the Chemineer High Efficiency Impeller

The mixing time correlation for the HE-3 was taken from from (Fasano et al. 1994) and is given by Equation 3.27.

For the HE-3 impeller, a = 0.272 and b = 1.67.

3.4.3   Mixing Time for the 6 Blade Pitched Blade Turbine

The mixing time correlation is taken from (Ranade et al. 1991).

$$\theta_{mix} = 72 \times R/U tip$$

(3.28)

3.5   A Novel Model Simulating Turbulent Reacting Flows

It has been shown in the literature that it is possible to describe the turbulent flow within an agitated vessel using CFD. It has also been shown in the literature that using micromixing models, it is possible to simulate without approximation, the influence of mixing on chemical reactions at the microscopic level. Missing from the picture is a means of linking the information furnished by CFD at the macroscopic level, with that furnished by the

micromixing models to result in a model that can be used to simulate and investigate the effects of mixing on chemical reactions in agitated tanks.

For such a model to be useful, it must be general enough such that no adjustable parameters are required and it must be numerically tractable, especially for turbulent flows in three dimensions. It must also require modest computational effort. There are presently no models in the open literature that satisfactorily meet these requirements. The present contribution addresses the issue.

3.5.1 Model Formulation

Visualization studies have shown that for semi-batch reactors with slow feed addition and fast complex chemistry, material fed into the reactor (the reaction zone) moves away from the feed point as the reactions takes place. This is a result of bulk motion or the macromixing aspect of the system. Also, it has been established that in the micromixing controlled regime, the reactions are practically complete before the reaction zone becomes fully dispersed throughout the tank volume (Bourne et al. 1995).

As the reaction zone moves through the tank volume, it experiences varying levels of turbulence intensity by virtue of the bulk motion. Since the reactions under consideration are sensitive to the turbulence intensity by virtue of the dissipation rate ε and the turbulent kinetic energy k, this bulk motion must be accounted for.

Therefore based on the known information about the ongoing phenomena in a BSTR, a novel model was developed for modeling the effect of turbulence on chemical reactions exhibiting complex chemistry in baffled stirred tanks with single slow feed addition.

In this work a novel approach is presented, whereby a multiphase model is used to represent the reacting fluid element as a separate and distinct phase. The model is outlined next and the details involved follow.

The slow feed addition to a batch reactor is a continuous process. For numerical purposes, this process must be expressed in discretized manner. This was accomplished as

follows:

- The total amount of feed material is divided (*discretized*) into several σ parts. Each part σ, is added to the reactor in sequence until the total feed has been fed into the system.

- Thus for a total feed volume Q, the part fed to the reactor at a time would be q, where $q = Q/\sigma$. The value of σ was chosen here to be sufficiently large so that the final results of the numerical simulation are independent of the value of σ.

- Each σ part is introduced into the reactor and allowed to react completely. During the computation process, the reaction zone was treated as a segregated environment surrounded by perfectly mixed bulk fluid. Thus, only the conditions within the reaction zone changed over time, while the bulk conditions remained static. Once the limiting reagent was consumed, the concentrations of all the species in the entire reactor, including the reaction zone, were updated via a mass balance. The next σ part of the feed was then added to the reactor.

- The procedure is repeated until all the feed is exhausted.

- For the purposes of this work a value of $\sigma = 50$ was used since higher values of *sigma* did not affect the final result.

A schematic representation of the approach is shown in Figure 3.2. The model is implemented as follows:

1. CFD is used to obtained a time averaged description of the turbulent flow field. It is assumed that the introduction of feed material does not influence the flow field. Since the feed volume introduced into the system is a small fraction of the tank volume, this is a reasonable assumption.

2. The feed material that is introduced into the tank is represented in a novel way by means of a multiphase model. Thus the reaction zone is represented as a separate and

H=T=0.29m
C = T/3
D = 0.1m

The influence
of micromixng
on the kinetics
is accounted
for with the
E-Model.

Flow field
is modeled
using CFD

Limiting reagent is
fed slowly into the vessel

The reaction zone is identified
by means of a multi-phase model
The location of the reaction zone
is tracked over time.

The impeller is modeled without
experimental input using the
MRF model.
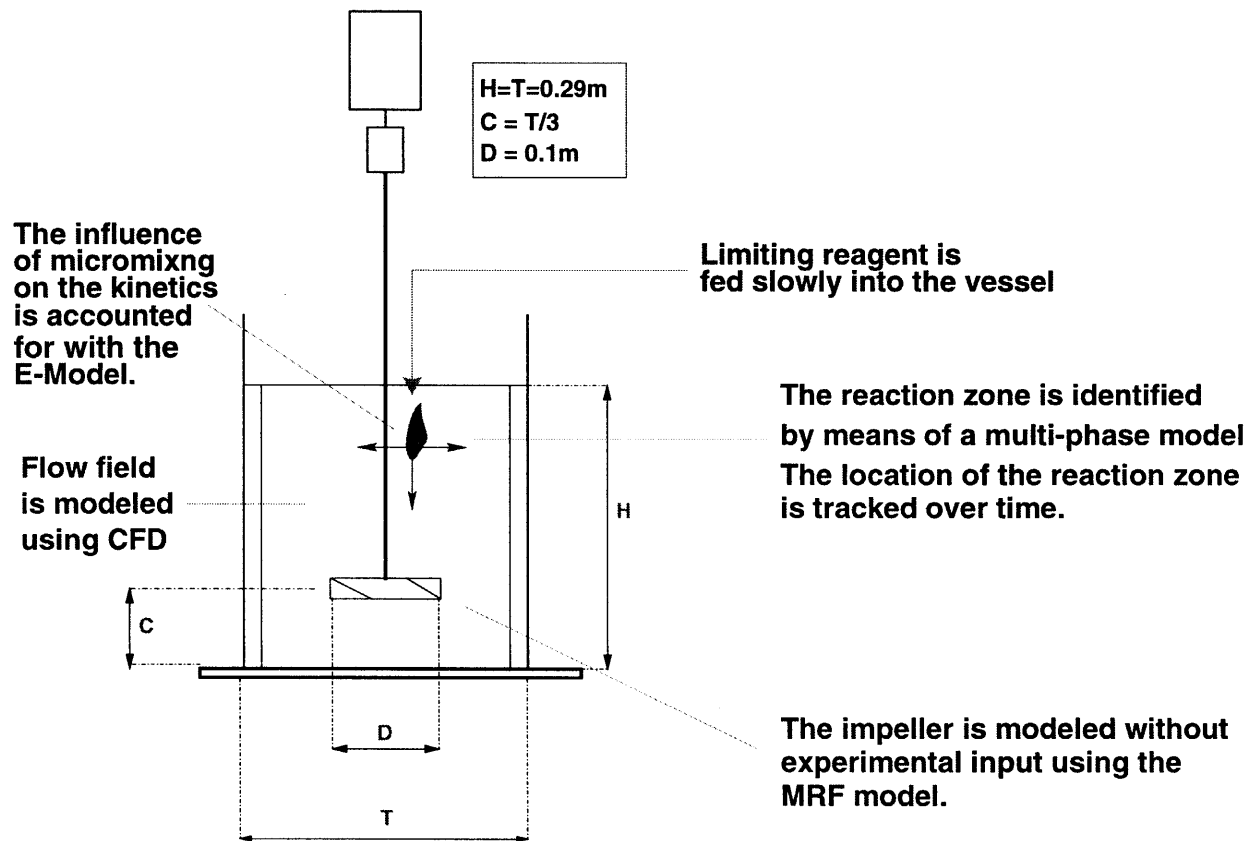
Figure 3.2: Outline of Proposed Model

distinct phase within the computational domain. Its properties can thus be specified independently of the bulk phase properties.

3. The feed material is then allowed to travel through the computational domain until dispersed. As it does so, it experiences varying levels of turbulence intensity by virtue of its position. The turbulence parameters k and ε are thus recorded as functions of time and position.

4. The time dependent history information is then used in conjunction with a micromixing model to evaluate the final product distribution of the reaction set.

The multiphase model which comprises an integral part of the novel approach is the VOF model. Its details are outlined next.

The VOF Free Surface Model

The *Volume of Fluid (VOF) model* (Hirt and Nichols 1981) is a multi-phase model designed for two or more fluids. It is optimized for the case where the interface between the fluids is of interest, but may be used for general multi-phase modeling. It is chosen for this work because of its simplicity and modest computational requirements.

The VOF model is implemented by solving a continuity equation for the volume fraction of the phases in the computational domain:

$$\frac{\partial \phi_k}{\partial t} + u_i \frac{\partial \phi_k}{\partial x_j} = S_{\phi_k} \tag{3.29}$$

Where the variable ϕ_k denotes the volume fraction of phase k. The source term, S_{ϕ_K} can be constructed to simulate mass transfer between the phases. In this work, it was set equal to zero.

The properties in the transport equations are determined by the presence of component phases at each point in the computational domain. For a two phase system, with the phases

represented by the subscripts 1 and 2, the following approximation is used:

$$\rho = \phi_1 \rho_2 + (1 - \phi_2) \rho_1 \tag{3.30}$$

In general, for an N-phase system, the volume fraction averaged mass density (ρ) is expressed as:

$$\rho = \Sigma \phi_k \rho_k \tag{3.31}$$

All other properties are computed in this manner, except for the specific heat, which is fraction averaged:

$$c_P = \frac{\Sigma \phi_k \rho_k c_{Pk}}{\Sigma \phi_k \rho_k} \tag{3.32}$$

A single momentum equation is solved throughout the computational domain, and the resulting velocity field is shared among the phases. The momentum equation is dependent on the volume fraction of each kth phase through the properties ρ and μ.

$$\frac{\partial}{\partial t}(\rho_j) + \frac{\partial}{\partial x_i}(\rho u_i u_j) = \frac{\partial P}{\partial x_j} + \frac{\partial}{\partial x_i}\mu\left(\frac{\partial u_i}{\partial x_j} + \frac{\partial u_j}{\partial x_i}\right) + \rho g_i + F_j \tag{3.33}$$

Equation 3.33 states that the dispersed phase moves *with* the bulk fluid with the fluid properties at each location being determined by the amount of each phase that is present.

Defining the reaction zone as a separate phase merely serves to distinguish it from the bulk phase and to keep track of its location as a function of time. Thus the shared fields approximation is suitable for our purposes.

The VOF model is used to track the path of the reaction zone as it moves within the vessel. At each position in time, the value of the rate of dissipation of turbulent kinetic energy, ε, which is needed to compute the engulfment parameter, E, is computed by taking the volume fraction average over all the cells occupied by the reacting fluid. Thus at any position in time, the value of ε is computed as follows:

$$\bar{\varepsilon} = \frac{\int \varepsilon \cdot dV_j}{\int dV_j} \rightarrow \frac{\Sigma \varepsilon \cdot \Delta V_j}{\Sigma \Delta V_j} \tag{3.34}$$

where V_j is the volume of a given cell occupied by the dispersed phase. It is computed according to: $V_j = V \times \phi_k$, where V is the volume of the cell in question, because the volume element may occupy one or several cells in the computational domain.

The time history of the turbulent kinetic energy is computed in a similar fashion.

A look-up table consisting of ε and k as a function of time is created. This look-up table was then be used in integrating the micromixing model equations.

3.6 Numerical Solution of the Micromixing Model Equations

3.6.1 Standard Engulfment Model

Using the formulation of the *E-Model* the reaction set can be expressed as follows for the three reacting species:

$$\frac{dC_A}{dt} = E\left(\overline{C_A} - C_A\right) - k_1 C_A C_B - k_2 C_A C_C \tag{3.35}$$

$$\frac{dC_B}{dt} = E\left(\overline{C_B} - C_B\right) - k_1 C_A C_B \tag{3.36}$$

$$\frac{dC_C}{dt} = E\left(\overline{C_C} - C_C\right) - k_2 C_A C_C \tag{3.37}$$

This apparently harmless looking set of differential equations is virtually impossible to solve with even the most rigorous collocation methods. This is because the k_1 term is so large that it introduces significant stiffness into the equation set. This problem is circumvented by applying a transformation to eliminate the k_1 term. This transformation is referred to as the W-Z transformation (Baldyga and Bourne 1984c).

Since the first reaction is extremely fast (nearly instantaneous), the species A and B cannot coexist. Use of this is made when applying the a transformation (Baldyga and Bourne 1984c) to eliminate the k_1 term. Using this formulation new variables are defined:

$$u = C_A - C_B \tag{3.38}$$

$$C_A = \frac{|u| + u}{2} \tag{3.39}$$

$$C_B = \frac{|u| - u}{2} \tag{3.40}$$

Where $|u|$ denotes the absolute value of u.

Equations 3.36 and 3.37 are then added to yield:

$$\frac{du}{dt} = E\left(\overline{u} - u\right) - k_2 C_C \left(\frac{|u| + u}{2}\right) \tag{3.41}$$

The equations that need to be solved are now Equations 3.41 and 3.37 in conjunction with Equation 3.39. These are readily solved using the method of Runge-Kutta (Finlayson 1980) and the time dependent, volume averaged values of ε obtained from the CFD simulation. The details of the specific Runge-Kutta code used for this work are presented in Appendix A.

The computational procedure involves integrating the E-Model equations until the limiting reagent is consumed. During this integration, the reaction zone was treated as a completely segregated zone. Thus the concentrations in the bulk of the tank, are treated as being constant. Only the concentrations within the reaction zone changes. Once the limiting reagent is completely consumed, the concentration of species in the entire tank (both the reaction zone and the bulk) are then updated by a mass balance, and the process repeated until all the feed had been added to the tank and reacted.

3.6.2 Modified Engulfment Model Equations

The procedure employed for solving the modified E-model equations are identical to those employed in solving the E-model equations. Applying the W-Z transformation results in the following set of equations:

$$\frac{du}{dt} = E\left(1 - \frac{V_B \exp(-t/\tau_s)}{V_0}\right)(\overline{u} - u) - k_2 C_C \left(\frac{|u| + u}{2}\right) \tag{3.42}$$

$$\frac{dC_C}{dt} = E\left(1 - \frac{V_B \exp(-t/\tau_s)}{V_0}\right)(\overline{C_C} - C_C) + k_2 C_A C_C \tag{3.43}$$

These equations are also readily solved using the method of Runge-Kutta.

CHAPTER 4

EXPERIMENTAL APPARATUS AND METHOD

4.1   Experimental Measurement of the Turbulent Flow Field

The computed velocity flow field and turbulence levels were experimentally verified using *Laser Doppler Velocimetry* (LDV). The laser Doppler Velocimeter is a widely accepted tool for fluid dynamic investigations in gases and liquids, as well as for moving surfaces. It has been used for more than three decades. Its non-intrusive principle, directional sensitivity, and high level of accuracy make it suitable for applications with reversing flow, chemical reactions, high temperature media, or rotating machinery, where physical sensors are difficult or impossible to use.

The principal advantage of using LDV to measure flow phenomena is that it is non intrusive so that the measurements are taken without disturbing the flow field in any way. Furthermore, the instrumentation has a very high spatial resolution, which enables the measurements to be made at very precise locations, due to the small measurement volume. The measurements are independent of temperature and the type of medium.

Measurements were taken for all the systems studied. The systems configuration is presented in Figure 4.6. The impeller details are presented in Figure 4.1.

4.1.1   Experimental LDV Setup

The LDV apparatus in the mixing laboratory of the department of Chemical Engineering, Chemistry and Environmental Science at NJIT (Figure 4.3), is a Dantec 55X series system (Dantec Measurement Technology USA, Mahwah, N.J. USA). It consists of a 750 mW Argon-Ion laser (Dantec Measurement Technology USA, Mahwah, N.J. USA) which produces a single multicolored laser beam. The laser beam is directed through an optical filter which filters out all the component colors except for green (wavelength 510 nm). The resulting laser beam is the passed through an optical train system where it is split into two.

47

Rushton Turbine
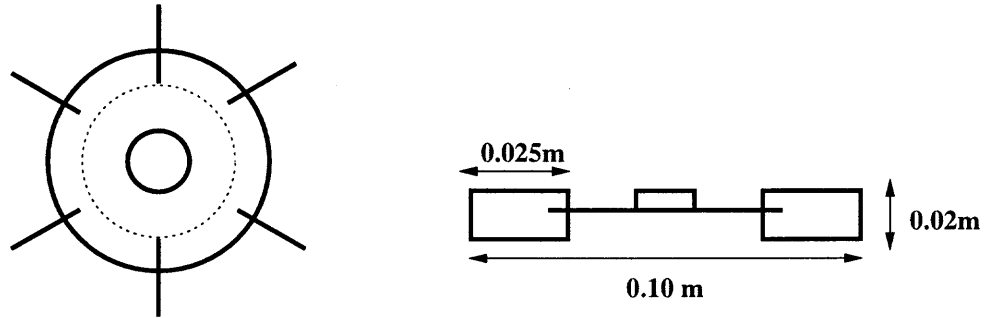
6 Blade Pitched Blade Turbine
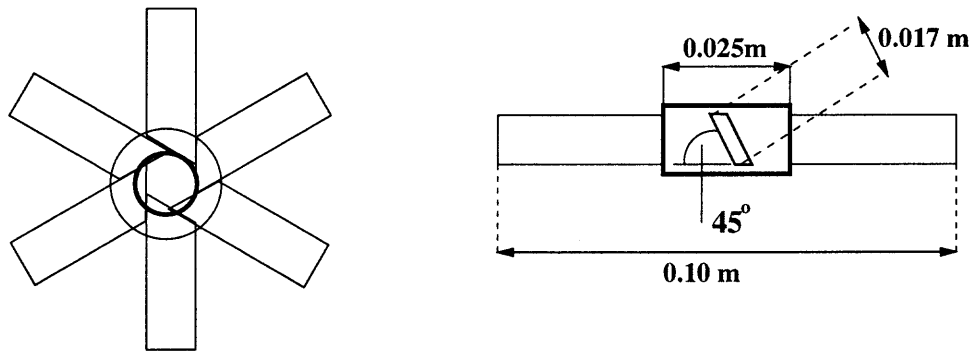
Chemineer HE-3
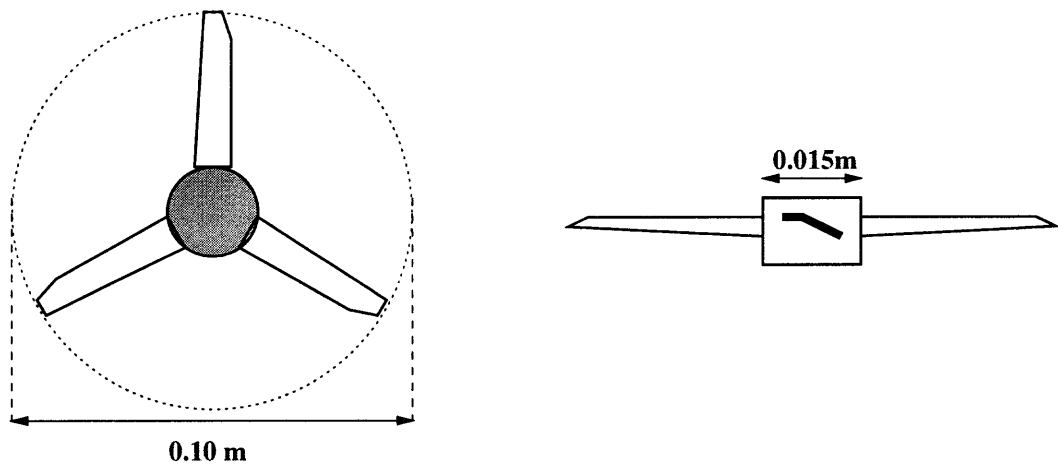
Figure 4.1: Details of impellers used

One of the split beams is passed through a Bragg cell. The Bragg cell is used to shift the frequency of the laser beam passing through it by 40 MHz. The use of the Bragg cell permits the distinction between positive and negative velocity measurements (TSI 1979).

The two beams are then passed through a beam expander system and then through a transmitting lens and focused at a single point 330 mm from the transmitting lens. This distance is equal to the focal length of the transmitting lens.
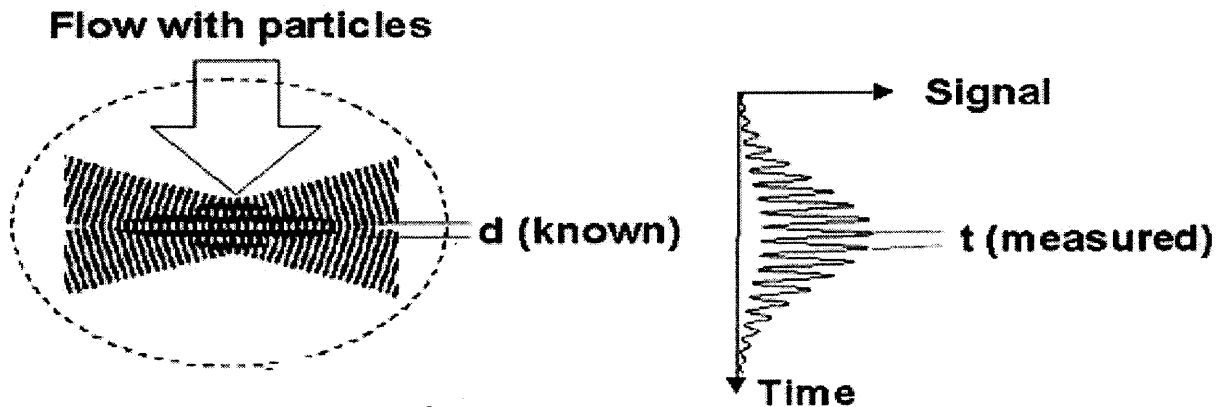
Figure 4.2: Laser Doppler Velocimetry fringe model

The beams form a fringe pattern at the point of intersection. The spacing of the fringes is a function of the frequency of the laser beam and the angle of the intersecting beams, which are known a priori. When a particle traverses the fringe pattern, it produces scattered light with a frequency that is equal to the velocity of the particle divided by the fringe spacing.

The scattered light from the tank, is captured by a photo-detector which reads the frequency of the incoming light. The frequency is converted to a voltage reading and ultimately to a velocity reading.

The receiver and data acquisition system are capable of taking hundreds of measurements in the same location, in a very short period of time. In this work, the system was configured such that 5000 measurements were sampled in period of 60 seconds or less. The precise time taken to sample the data is a variable quantity which depends on the data rate, the number of viable signals that reach the photo-detectors per second. It was thus possible
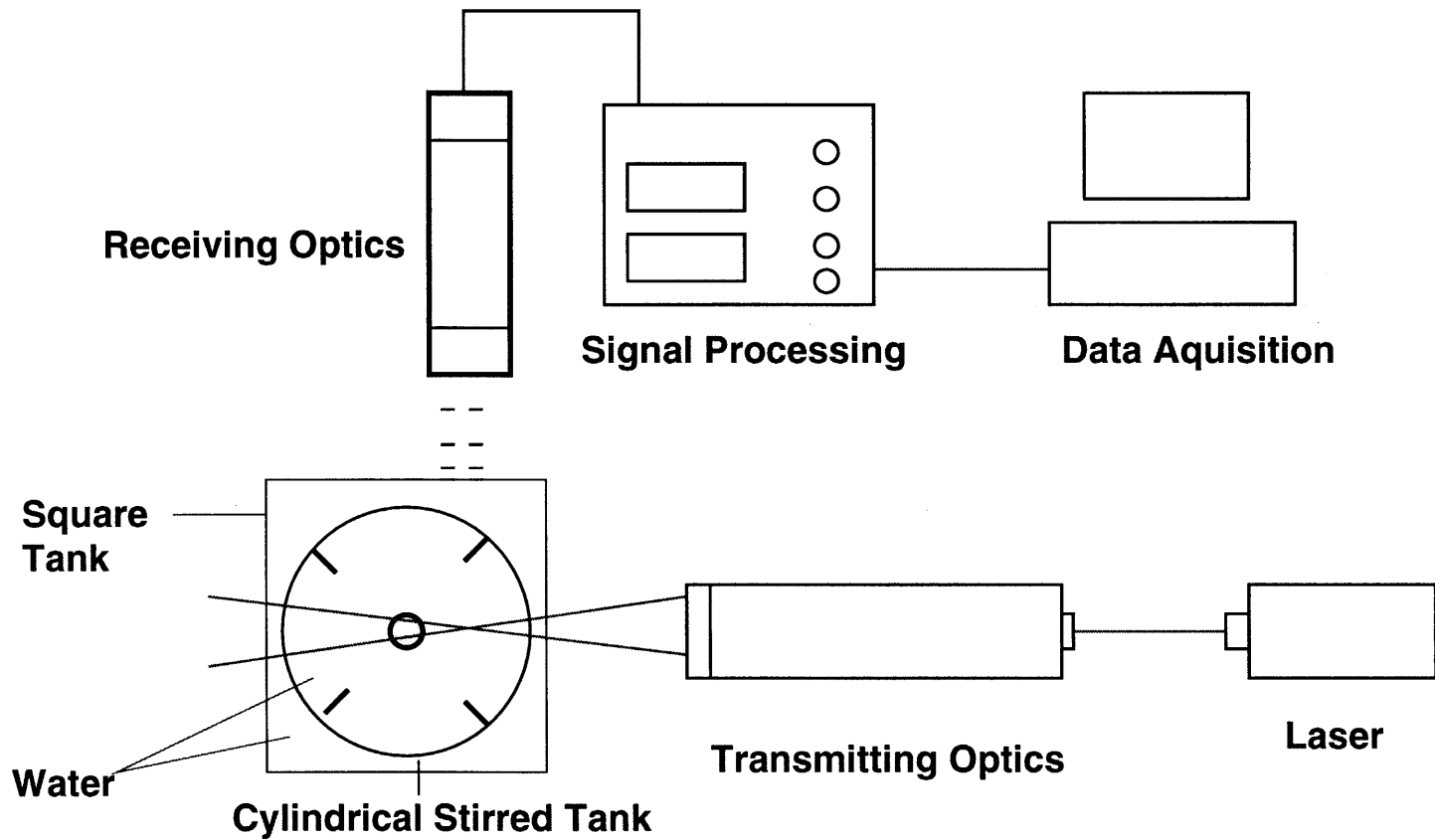
Figure 4.3: Laser Doppler Velocimetry apparatus

to measure not only the mean velocity component, but also the fluctuating component. The fluctuating components of the three dimensional velocity field were used to determine the turbulence intensity.

A clear Plexiglas cylindrical vessel was used for collecting the data. The diameter of the vessel was 0.29 meters and it was filled with water up to a height equal to its diameter. The use of clear Plexiglas enables the laser beams to enter the tank and the reflected light to reach the photo-detectors. Agitation was effected by a 1/8 HP motor (Model No. 455479, G. K. Heller Corp., Floral park, NY, USA) which was controlled by an external controller (Series H Motor Controller, G.K. Heller Corp, Floral park, NY, USA).

The cylindrical vessel was immersed in a clear Plexiglas square tank which was filled with water. The material used in making both tanks and the water have equal refraction indices. The use of the square tank eliminated optical distortion which would occur if the laser beams were to hit the curved surface of the cylindrical vessel directly.

The fluid within the tank was seeded with a small amount of neutrally buoyant 1.5 μm silver coated particles (T.S.I. Inc., Minneapolis, MN, USA). The particles were selected such that they follow the fluid flow patterns very closely.

Measurement in all regions of the tank was achieved by mounting the tank on a traverse system that could be moved in the x-y-z directions.

Because the LDV apparatus used was a 1D system, it was capable of measuring only one of the three velocity components at a time. The measurement of all three components was achieved by orienting the beam crossing in such a manner that the measurement in the desired direction could be made. This is summarized in Figure 4.4.

4.1.2 Measurements Provided by LDV

The LDV system provides the following measurements: u, v, w, u', v', w'. These parameters serve to characterize the mean flow in a flow domain as well as the level of turbulence in that flow domain.

(a) Tangential Measurement   (b) Axial Measurement   (c) Radial Measurement
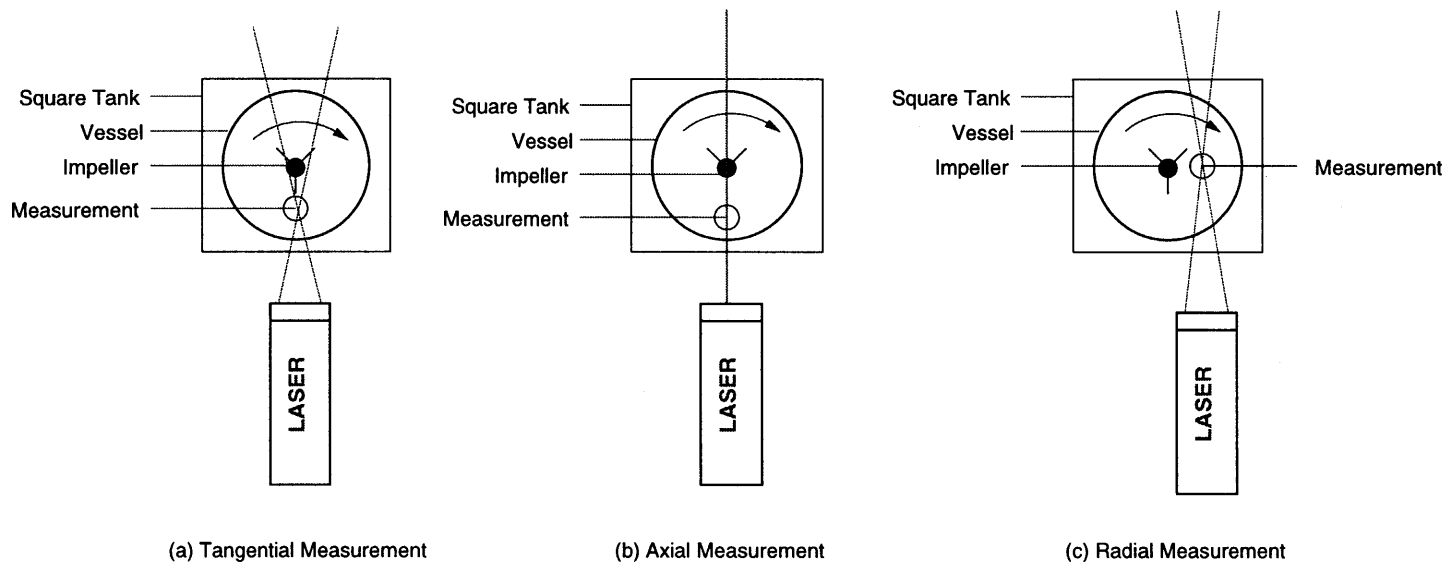
Figure 4.4: Position of the mixing vessel with respect to the laser assembly to measure all the velocity components.

The turbulent kinetic energy which arises in the turbulence model equations is evaluated in from the fluctuating velocity components as (Rodi 1984):

$$k_\varepsilon = \frac{1}{2}\left(u'^{\,2} + v'^{\,2} + w'^{\,2}\right) \tag{4.1}$$

4.2 Experimental Investigation of Power Draw

The power draw by the agitator was experimentally measured for each system investigated. A diagram of the apparatus is shown in Figure 4.5. The system was agitated by a 0.78 HP variable-speed motor (G. K. Heller Corp., Floral park, NY) with a maximum agitation speed of 1800 rpm. The rotational speed was measured with a digital tachometer connected to a photoelectric sensor (Cole-Parmer, Chicago, IL, USA), accurate to within ± 1 rpm. The tank consisted of an open flat-bottomed, cylindrical Plexiglas vessel, with four baffles evenly spaced around the periphery of the tank. The geometric characteristics of the tank are given in Figure 4.5. The impellers used and their geometric characteristics are given in Figure 4.1.

The shaft was a hollow aluminum tube fitted with strain gauges (Measurements Group Co. Raleigh, NC, USA, part No. CEA-06-187UV-350) mounted above the impeller. The gauges were electrically connected to a signal conditioner and an amplifier system (2120A system, (Measurements Group Co. Raleigh, NC) via a slip ring assembly (Airflyte Electronics Co., Bayonne, NJ, Part No. CAY1030-12-2) so that the torque and hence the power dissipated by the impeller could be experimentally determined. The data was collected and analyzed using a data acquisition system (Labtech Notebook) running on an Intel 486 personal computer. The value of each experimental variable was calculated by taking the average of 10 readings within a one second sampling time over a period of 60 seconds. The reproducibility of the experiments was within ± 5 % on average.

The power draw was calculated using Equation 3.20. The system configuration is depicted in Figure 4.5.
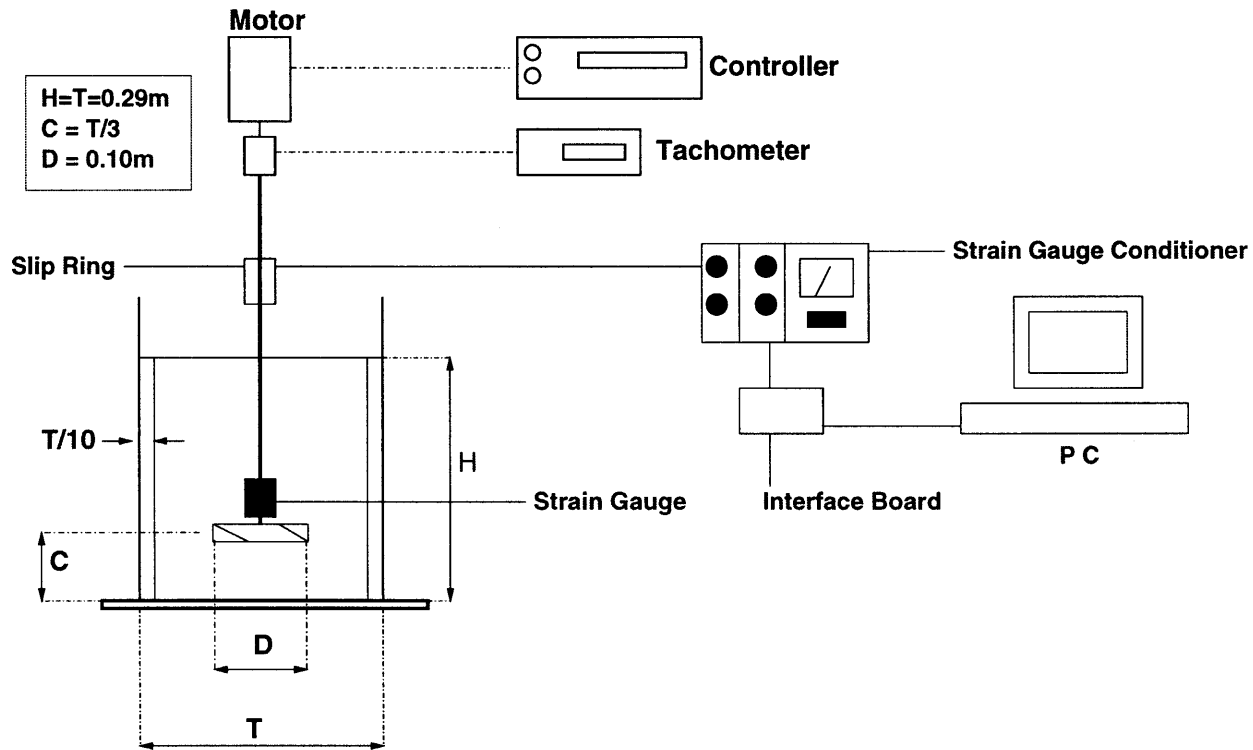
Figure 4.5: Experimental apparatus for the measurement of power draw.

Motor

Controller

H=T=0.29m
C = T/3
D = 0.10m

Tachometer

Slip Ring

Strain Gauge Conditioner

T/10

H

Strain Gauge

Interface Board

P C

C

D

T

4.3 Experimental Investigation of Micro-mixing

The apparatus used in studying the fast competitive parallel reactions is shown in Figure 4.6. Agitation was provided by 1/8 HP variable-speed motor (Model No. 455479, G. K. Heller Corp., Floral park, NY, USA) with a maximum agitation speed of 2000 rpm. The rotational speed was measured with a digital tachometer connected to a photoelectric pick-up sensor (Cole-Parmer, Chicago, IL, USA), accurate to within ± 1 rpm. The tank consisted of a 19 liter, flat bottomed, baffled cylindrical Plexiglas mixing vessel measuring $0.29m$ in diameter with four baffles equally spaced around the periphery of the vessel. The tank was filled with liquid to a height equal to the tank diameter. The tank was fitted with the impeller of choice depending on the system under investigation. The impellers used and their characteristics are presented in Table 1.1. The impeller details are presented in Figure 4.1.

The mixing tank was first charged with two reagents: hydrochloric acid and ethyl chloroacetate and, mixed until homogeneous. The limiting reagent, sodium hydroxide, was then fed to the tank in a controlled manner (slowly). A variable speed pump (Masterflex Model No. 7525-30, Cole Parmer, Chicago, IL, USA) was used to control the feed rate of the limiting reagent, sodium hydroxide. A flexible plastic tube (Tygon part No. 6408-64, Cole-Parmer, Chicago, IL, USA) connected to a glass tube of outer diameter 4.5 mm and inner diameter 3 mm, which was used to ultimately deliver the feed material to the tank.

The sodium hydroxide, was introduced at a much higher concentration than the other two reactants. The total number of moles of all three reactants was, however, equal.

A number of different feed points were investigated. These are shown in Figure 4.7. The impeller agitation speed was varied between 100 rpm and 400 rpm, depending on the system.

Details of the exact locations of these feed points are presented in Table 4.1.

The time taken to feed all the feed material (limiting reagent) into the reaction vessels was a variable quantity which depended on the system in question. The details are furnished

Motor

Controller

Tachometer

H=T=0.29m
C=T/3
D= 0.29m

Thermometer

A is feed slowly to system

B and C
are dissolved
and mixed in
system.

H

C

D

T

Feed

Pump

Magnetic Stirrer
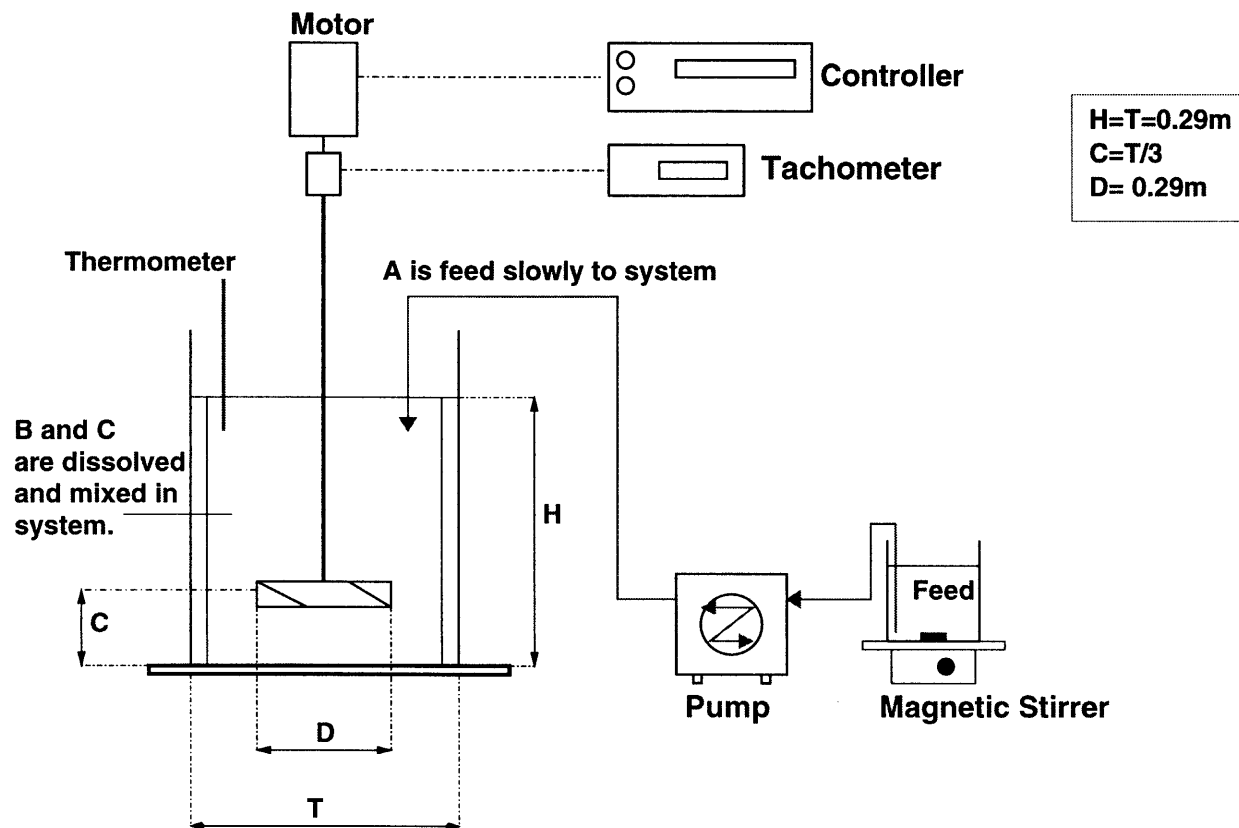
Figure 4.6: Experimental apparatus for the investigation of fast competitive parallel reactions.

in Chapter 5 where detailed results are presented. The actual locations used for each system studied are summarized in Table 4.2.

Published experimental data were used in evaluating Systems A1 and A2. For all the other systems, original experimental data were used.

In the present work, the initial concentrations of hydrochloric acid and ethyl chloroacetate in the tank was 18 moles/m^3. The initial concentration of sodium hydroxide was 900 moles/m^3 and was contained within a volume that was 1/50 the tank volume.

The yield is expressed in terms of component C, ethyl chloroacetate, consumed as follows:

$$X_S = \frac{V_o \cdot C_{Co} - (V_o + V_{Ao}) \cdot C_C}{V_{Ao} \cdot C_{Ao}} \tag{4.2}$$

or in terms of S, ethanol, formed:

$$X_S = \frac{(V_o + V_{Ao}) \cdot C_S}{V_{Ao} \cdot C_{Ao}} \tag{4.3}$$

where:

V_o the initial volume of material in the tank

V_{A_o} the volume of A (the limiting reagent) added to the tank

C_{Co} and C_{Ao} denote the initial concentrations of C and A respectively

C_C denotes the concentration of C, ethyl chloroacetate, at the end of the reaction

C_S denotes the concentration of S, ethanol, at the end of the reaction

In semi-batch mode where all conditions (e.g. temperature, stirrer speed, solution volumes and concentrations) are held constant, except for the feed time of the limiting reagent, X_S is found to vary with the feed time as shown in Figure 4.8 (Baldyga and Bourne 1992).

For sufficiently slow feed addition in excess of a critical feed time t_c, X_S is found to be independent of the feed rate, and is dependent upon micromixing. When the feed time
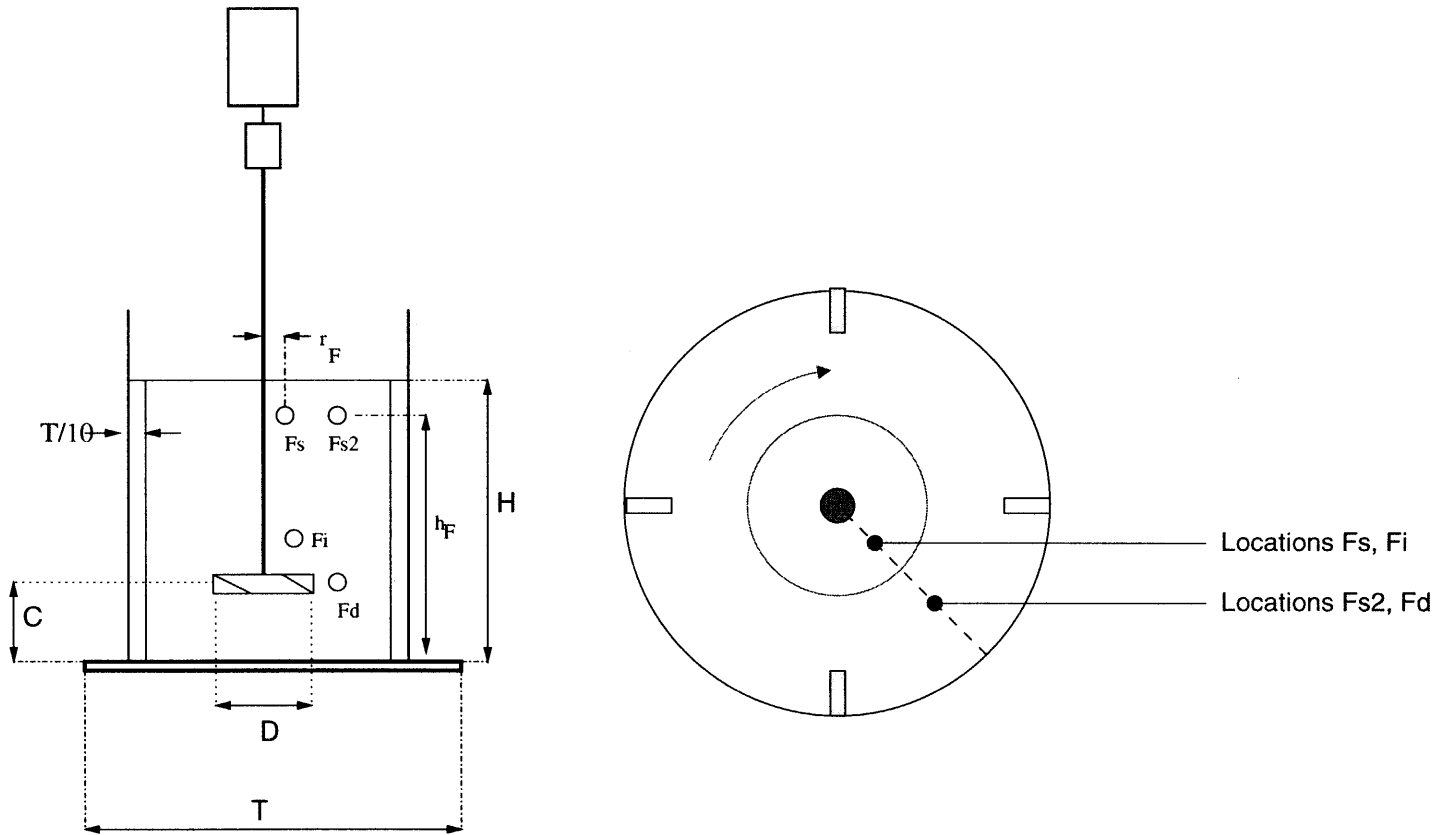
$$H = T = 0.29 \text{ m}$$
$$D = T/3$$

Figure 4.7: Feed point locations

Table 4.1: Summary of feed point locations

System	Fs	Fs2	Fi	Fd
A1,A2,B2,B2,C	$2r_F = 0.172D \quad h_F = 0.9H$	$2r_F = D \quad h_F = 0.9H$	$2r_F = 0.172D \quad h_F = 0.48H$	
D	$2r_F = 0.172D \quad h_F = 0.9H$		$2r_F = 0.172D \quad h_F = 0.48H$	$2r_F = D \quad h_F = 0.58H$

Table 4.2: Feed Point Locations used for Each System

System	Fs	Fs2	Fi	Fd
A1	X			
A2	X			
A3	X			
B1	X	X	X	
B2	X			
C	X		X	
D	X		X	X
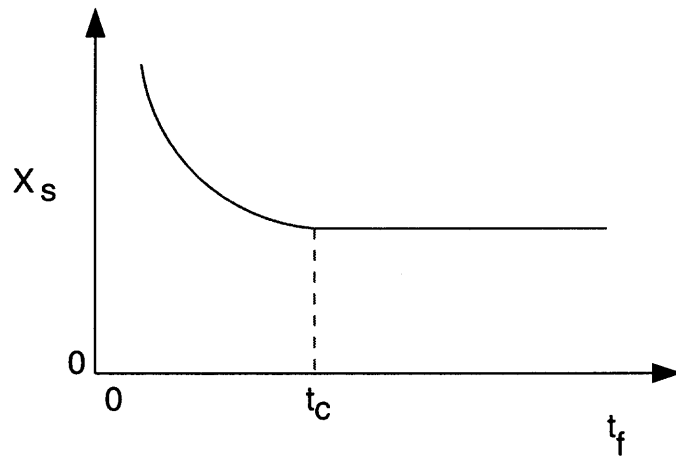
Figure 4.8: Schematic representation of how t_c varies with feed time

is shorter than the critical value t_c, it is observed that X_S increases with increasing feed rate and macroscale inhomogeneity plays a role in determining X_S. All experiments in this work were carried out in the micromixing controlled regime. The critical feed time t_c, is not a precise quantity (Baldyga and Bourne 1992; Bourne et al. 1995; Bourne and Yu 1994) and was determined experimentally for each system under investigation.

Ideally, t_c should be determined for each set of experimental conditions (feed position, agitation speed, fluid type etc.). This is not realistic. The method employed in this work was to determine the value for t_c under the "worst" set of experimental conditions for a particular system. This would be the longest value of t_c possible. This ensured that all subsequent reactions took place in the micromixing controlled regime. The "worst" set of experimental conditions corresponds to conditions where turbulence intensity is lowest — that is for feed at the lowest agitation speed with a feed position near the liquid surface.

A typical experimental run consisted of the following steps:

1. Measured volumes of concentrated hydrochloric acid and ethyl chloroacetate were added to the empty reaction vessel.

2. The vessel was then filled up to the desired volume with water to achieve the desired initial concentrations.

3. The sodium hydroxide feed vessel was charged with a highly concentrated solution of sodium hydroxide. Water was added to bring the volume and concentration to the desired initial volume and concentration.

4. The reaction vessel was thoroughly agitated in order to dissolve completely and homogenize the vessel contents. It took about 5 minutes to completely dissolve the ethyl chloroacetate at ambient conditions.

5. The feed tube was placed at the desired location.

6. A sample of the reaction vessel contents was taken and analyzed by gas chromatography in order to ascertain exactly the initial conditions of the reactor.

7. The agitation rate of the impeller was adjusted to the desired speed.

8. The pump was started and the sodium hydroxide solution fed at the desired feed rate to the reaction vessel contents until the reactions were complete (sodium hydroxide was consumed).

9. A sample of the reactor contents was taken and analyzed by gas chromatography for the final product distribution.

The product yield, X_S, can be simultaneously determined by measuring the concentration of ethyl chloroacetate, C_C, after the reaction is complete, or the concentration of ethanol, C_S, in the product mixture, or the concentration of hydrochloric acid, C_B, after the reactions are complete. In practice, C_B, cannot be determined by back titration because alkaline hydrolysis of ethyl chloroacetate also occurs during the titration. However, C_C and C_S can readily be determined by gas chromatography.

In this work an HP 5890 Series II gas chromatograph equipped with an FID detector was used (Hewlett Packard, Avondale, PA, USA). A packed column (Alltech 1 % AT-1000 on 60/80 graphpac packing in a C-5000 stainless steel casing, Alltech Associates, Deerfield, IL, USA) was used for the analysis of both C_C and C_S in final the product solution.

Calibration standards for the GC analysis of ethanol and the ethyl chloroacetate, were prepared and run prior to gathering each experimental set of data, or on a weekly basis — whichever was first.

The influence of fluid viscosity of the product yield of the reaction set was also investigated. Hydroxy-ethyl-cellulose (HEC) was used to alter the viscosity of water. Chemically, HEC contains ether linkages and hydroxyl groups in the side chains as well as in the cellulose backbone. It was chosen for use in the work for the following reasons (Bourne et al. 1995):

- Under the conditions used in this work, it does not react.

- Only small quantities are required in order to alter the viscosity of water ($< 1\%$ weight by volume).

- The viscosity of solutions containing HEC remains relatively constant over a wide range of pH values.

- Under the dilute conditions used in this work, HEC solutions remain Newtonian and exhibit no elasticity or pseudo-plasticity.

For the purposes of this work, a solutions containing 0.25% by weight of HEC in water were used. This had the effect of increasing the water viscosity eight fold to $8.3mPa \cdot s$ at ambient conditions. The viscosity of the solutions was measured using a Canon-Fenske viscometer.

CHAPTER 5

RESULTS AND DISCUSSION

For each system used in this work, CFD simulations were carried out in order to obtain the time averaged turbulent fluid velocity profile. The predicted velocity profile was verified experimentally using LDV. Once the velocity profile was computed, it was used for simulating the effect of turbulent mixing on chemical reactions. The details of the reactions used are presented in Section 4.3, and the manner whereby the simulations were used to simulate the effect of mixing on chemical reactions is detailed in Section 3.5.

In each of the following sections, the results for each system studied are presented. In each section, the details of the CFD setup are presented, followed by the results of simulating the flow field using CFD, as well as the comparison of CFD results with the experimentally obtained LDV data. All the LDV data presented are original experimental LDV data. These results are followed by the results obtained by using the novel model which combines CFD and micromixing models to predict the product yields of fast complex reactions. The predicted data are compared with the experimental data.

It is common practice to present standardized local values of mean and fluctuating velocities by relating their original values to the impeller tip speed, $\pi N D$. The velocities in all the figures used in this work are presented by dividing the actual velocity value by the impeller tip velocity. The turbulent kinetic energy is also presented in dimensionless form by dividing the actual value by the square of the impeller tip velocity. The sign conventions used are as follows:

- The positive axial flow is taken to be flow upwards from the base of the tank to the liquid surface

- The positive radial flow, is flow that moves away from the impeller shaft towards the tank wall

- The clockwise direction is taken to be the positive circumferential direction

5.1 Reproducibility of Experimental Data

In the flow measurements, the axial velocities were determined within an average standard deviation of ±11.7 %, the radial velocities within ±13.7 %, the tangential velocities within ±8.9 %, and the turbulent kinetic energy to within ±19.31 %. In all the ensuing plots presented, error bars indicating the standard deviation of repeated measurements are presented.

In the micromixing experiments, the final selectivities were determined to within an average of ±4.5 %. On all the graphs presented, error bars indicating the standard deviation of repeated experiments are shown.

In the power measurement experiments, the average error was ±3.5 %.

5.2 Effect of Feed Discretization of the Yield

It was explained earlier (Chapter 3), that in order to simulate the continuous process of slow feed addition numerically, a discretization procedure was necessary. In this work, the total feed material was discretized 50 times with each discretized aliquot fed to the tank in sequence until all the feed material was consumed. A value of 50 for the number of times the feed was discretized was sufficient. This will be shown on the following plots. Plots are shown for systems using the three types of impellers employed for this work. A plot is presented for data taken at the lowest agitation speed as well as the highest agitation speed for each system. On each plot data is presented for feed near the liquid surface as well as for feed closer to the impeller.

Figure 5.1 and Figure 5.2 show data for System D which is a Rushton based system. The system details are summarized in Table 1.2 and in Figure 4.6. The characteristics of the Rushton impeller are presented in Figure 4.1. In both plots its is seen that for the range of agitation speeds and feed locations under study in this work, the feed discretization value of 50 was adequate. Figure 5.3 and Figure 5.4 show data for System B1 which is a PBT
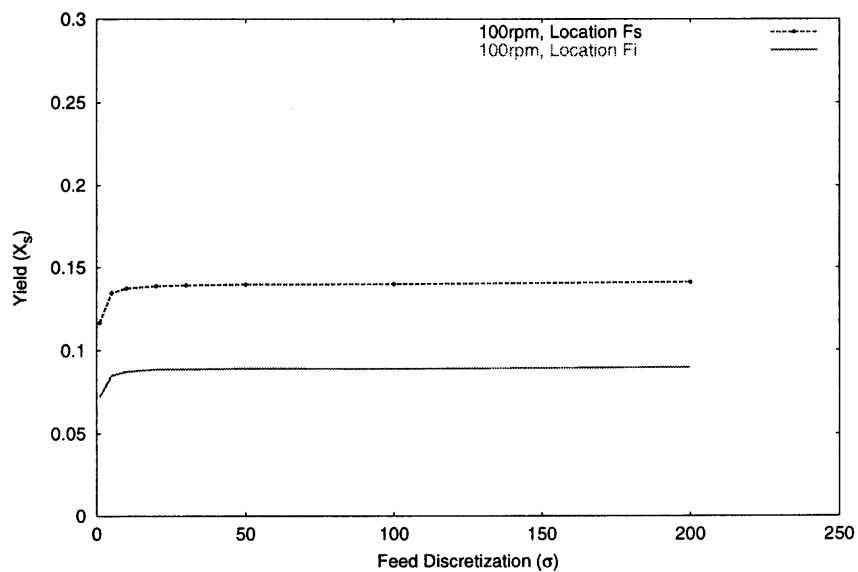
Figure 5.1: Effect of feed discretization on yield: System D, 100rpm
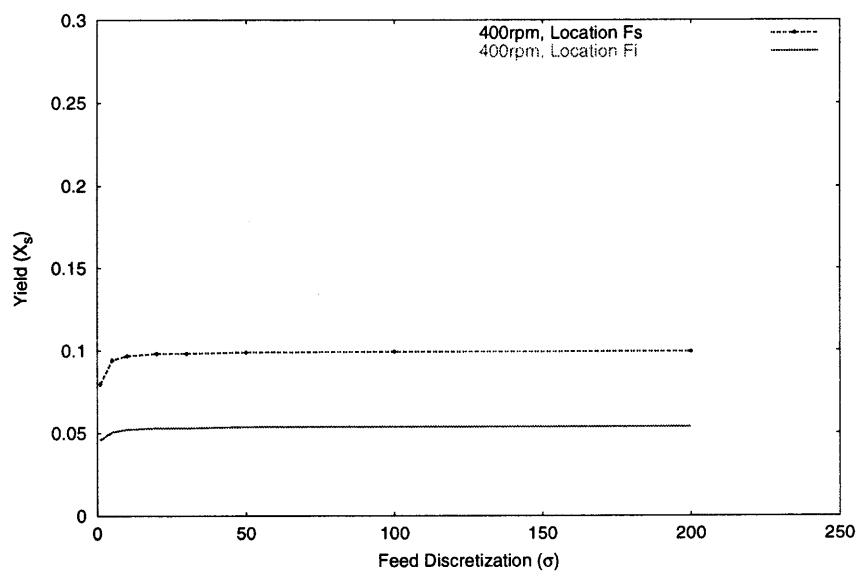
Figure 5.2: Effect of feed discretization on yield: System D, 300rpm

based system. The system details are summarized in Table 1.2 and in Figure 4.6. The characteristics of the PBT are presented in Figure 4.1. Once again its is seen that for the range of agitation speeds and feed locations under study in this work, the feed discretization value of 50 was adequate.
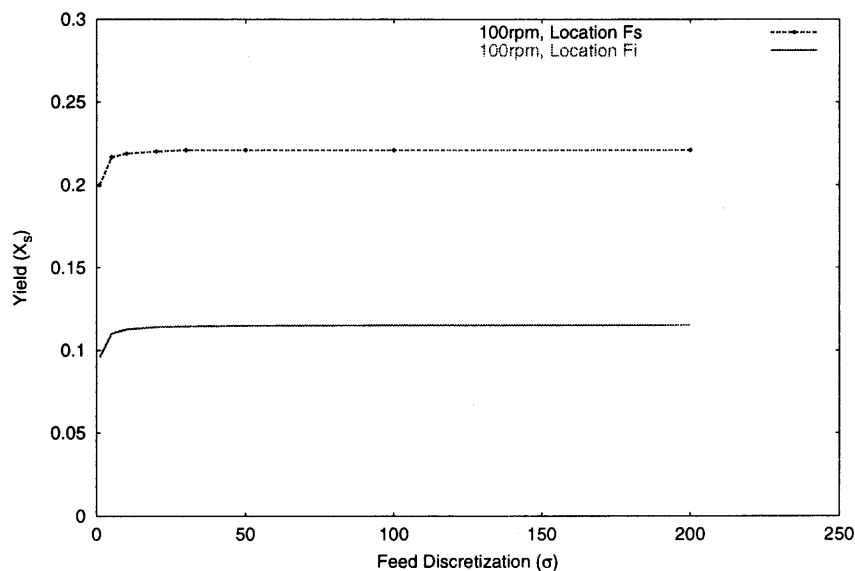
Figure 5.3: Effect of feed discretization on yield: System B1, 100 rpm
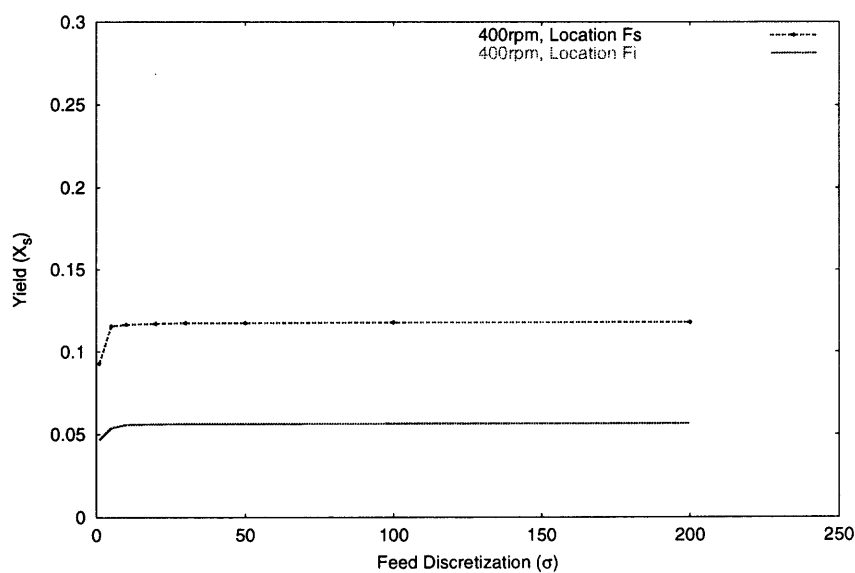
Figure 5.4: Effect of feed discretization on yield: System B1, 400 rpm

Figure 5.5 and Figure 5.6 show data for System C which is an HE-3 based system. The system details are summarized in Table 1.2 and in Figure 4.6. The characteristics of the HE-3 impeller are presented in Figure 4.1. Once again its is seen that for the range of agitation speeds and feed locations under study in this work, the feed discretization value of 50 was adequate.
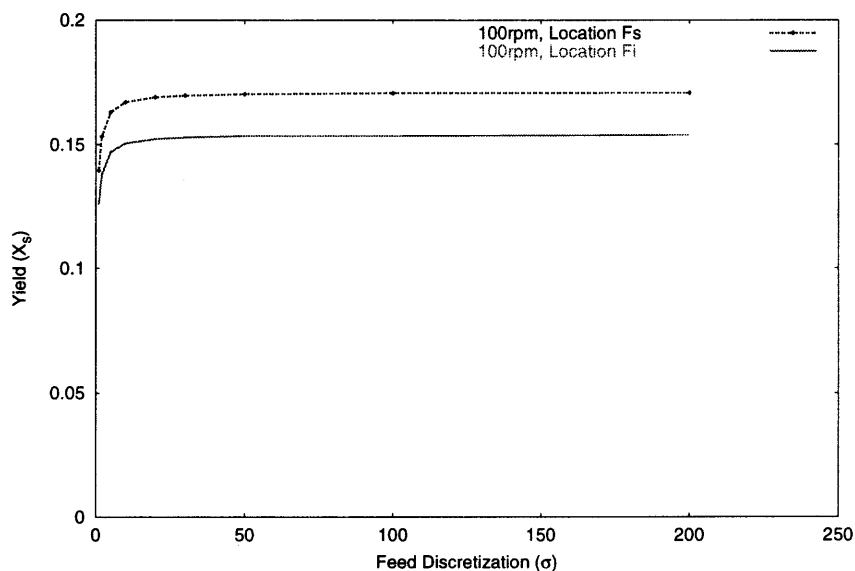
Figure 5.5: Effect of feed discretization on yield: System C, 400 rpm

5.2.1 Remarks

It is seen that for the wide range of configurations studied, the value of 50 for the the feed discretization σ, is more than adequate.
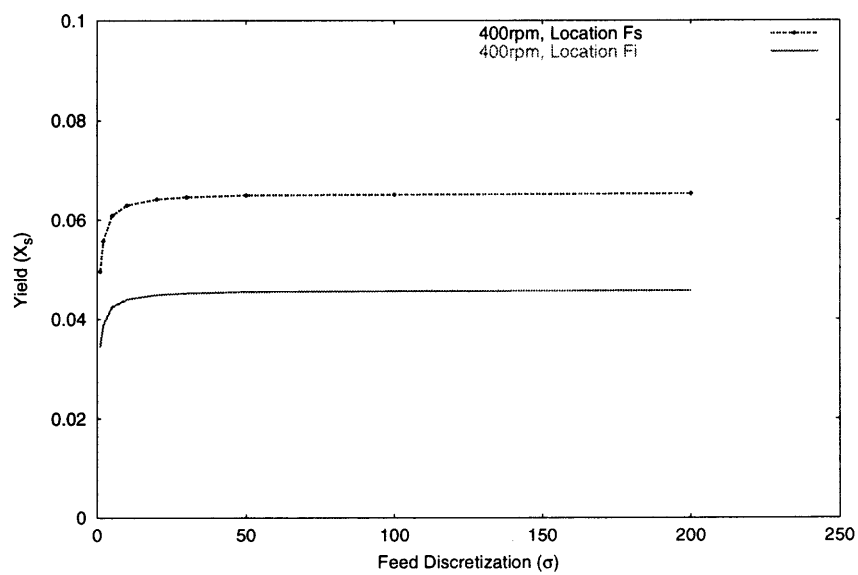
Figure 5.6: Effect of feed discretization on yield: System C, 400 rpm

5.3   Results for Systems A1, A2, A3
Rushton Turbine: Impeller off Bottom Clearance C = T/3

Systems A1, A2 and A3 consist of identical baffled cylindrical vessels fitted with a Rushton turbine. The difference between Systems A1 and A2 lies in the fact that in system A2, a viscous medium was used, while only water was used in system A1. System A3 is identical to System A1 in configuration. The difference between System A1 and System A3 lies in the fact that the reactant concentrations used for the kinetic studies are lower for System A3. The system details are summarized in Table 1.2 and in Figure 4.6.

5.3.1   System Configuration

Prior to carrying out simulations involving the influence of mixing and turbulence on fast parallel competitive reactions, the flow field was simulated using CFD and the simulation results verified using LDV. The system configuration and the axial locations in the vessel where the velocity profile was sampled using LDV are shown in Figure 5.7.

The tank geometries used for the CFD simulations are presented in Figures 5.8 – 5.9. In Figure 5.9, a cross-section of the tank showing the mesh details is shown. The mesh around the impeller is extremely fine as described in Chapter 3. This is necessary since strong gradients of velocity and turbulence exist. A fine grid is necessary to capture as much of the detail as possible, since the impeller generates the flow that prevails throughout the computational domain. It was also necessary to use a fine mesh at the tank wall because the fluid flow from the radial impeller impinges at the tank wall and creates a secondary source of turbulent flow there. The manner whereby this was done is also described in Chapter 3.

In Figure 5.8 and Figure 5.9 a region around the impeller is outlined. This is the MRF zone, the part of the computational domain which is solved in a rotating frame of reference.

Figure 5.10 shows a snapshot of the velocity profile for a simulation carried out at 300

z/T = 0.67

z/T = 0.50

z/T = 0.40

z/T = 0.26

z/T = 0.15

Data is sampled
in one of four
quadrants
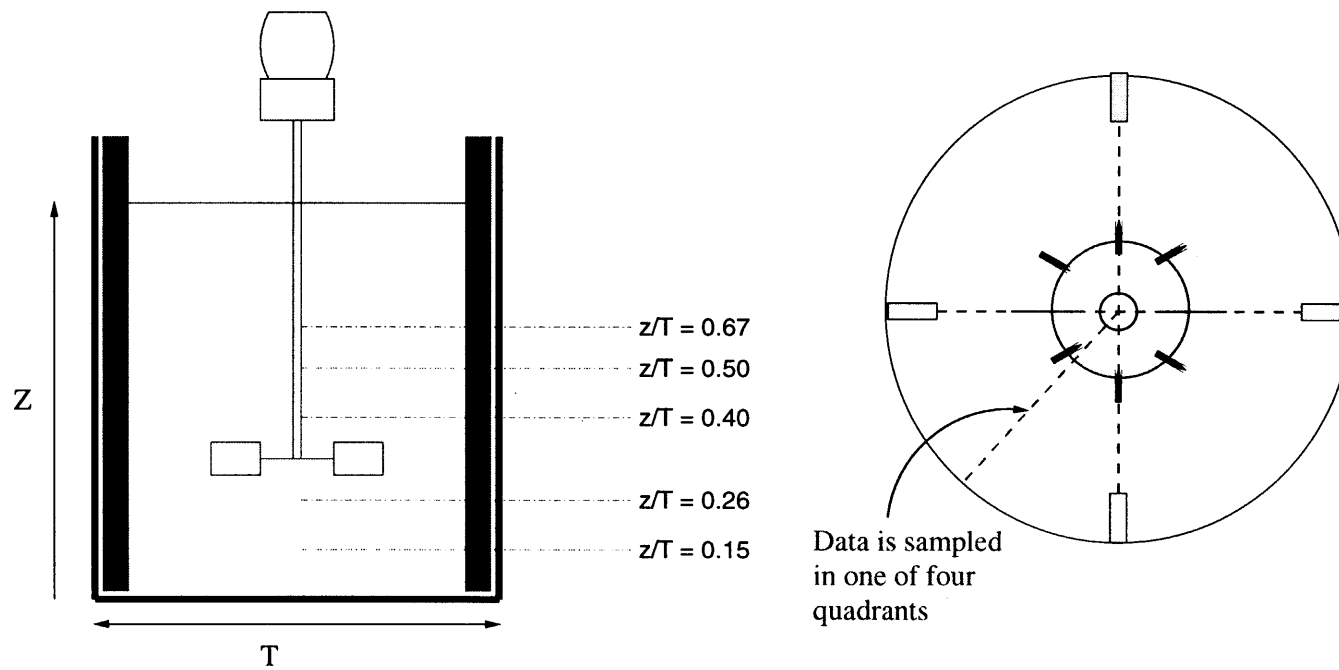
Figure 5.7: Stirred tank equipped with a Rushton turbine at an impeller clearance of T/3: Locations where LDV data was taken.

	Modified 3D Geometry Grid	Apr 08 2000
z	Outline	Fluent 4.52
x		Fluent Inc.
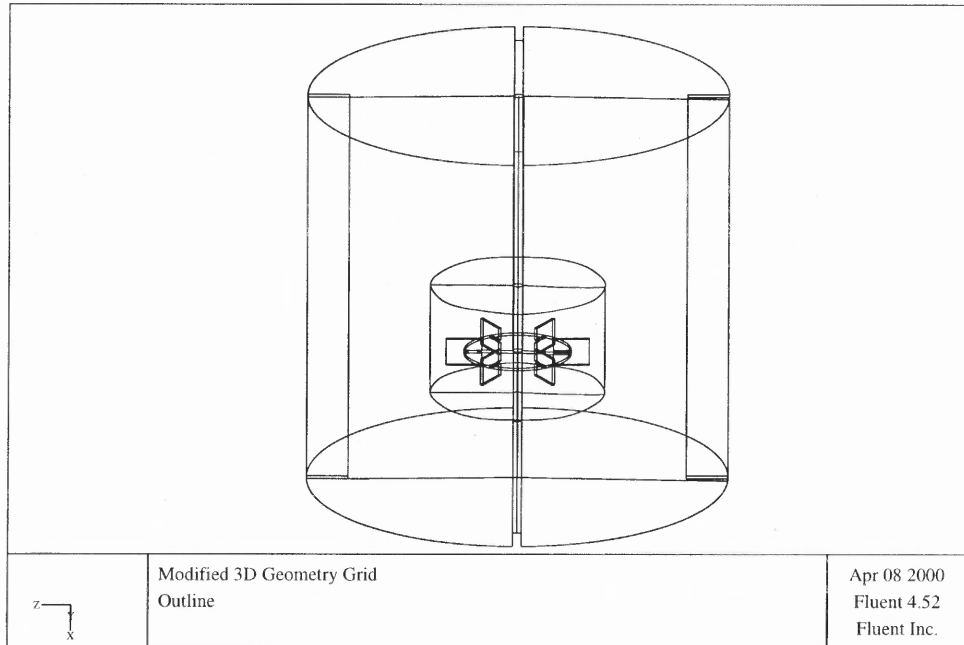
Figure 5.8: Stirred tank equipped with a Rushton turbine at an impeller clearance of T/3: Outline grid.

	Modified 3D Geometry Grid	Apr 08 2000
z	Grid (145 X 40 X 89)	Fluent 4.52
x	Slices: I=36, I=111	Fluent Inc.
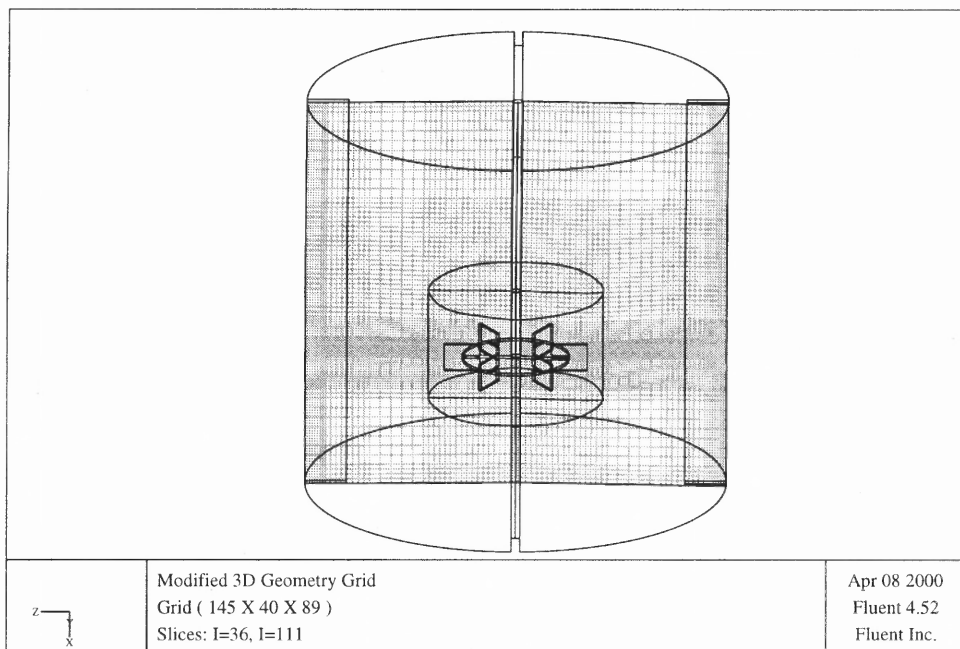
Figure 5.9: Stirred tank equipped with a Rushton turbine at an impeller clearance of T/3: Outline grid showing mesh details.

rpm. The velocity vectors shown are the resultant velocity vector for the axial, radial and tangential directions. The velocity profile shown is typical of what one would expect from a radial disk impeller. A turbulent jet is generated from the impeller and impinges on the tank wall. Four main circulation loops are evident. Two above the impeller mid-plane and two below it. Thus from a qualitative perspective, the simulation captures the main features of the turbulent flow generated by the Rushton turbine.

5.3.2   Comparison of LDV Data with FLUENT CFD Simulations for System A1

The LDV data was taken on a system with an impeller agitation speed of 200rpm. The CFD data presented here are for simulations carried out at 200rpm. The data are presented in dimensionless form as described earlier. The Rushton impeller produced four main circulation loops as shown in Figure 5.10. Near the tank wall and above the impeller the axial velocities are positive as the fluid is moving up. Near the shaft and above the impeller, the axial velocities are negative as the fluid returns to the impeller. These trends are reflected by the data, in particular in the region just above the impeller. Near the top of the tank, the flow is more horizontal and "quiet". This trend has been observed by other investigators of similar systems (Ranade and Joshi 1990a; Ranade and Joshi 1990b).

Below the impeller, the trend is reversed, but the main features of flow are the same. The simulation captures all these features adequately.

In the major part of the vessel, the radial velocities are very small as has been noted in the literature (Ranade and Joshi 1990a). Near the top of the tank and near the bottom, the radial velocities are negative indicating a recirculating flow to the the center of the tank. Near the impeller, the radial velocities are positive, indicating a discharge flow from the impeller region to the tank wall. Some negative radial velocities are also present in this region due to the presence of small recirculation loops.

The tangential velocities are high in the vicinity of the impeller stream due to the rotation of the impeller while in the general bulk, these velocities are small.
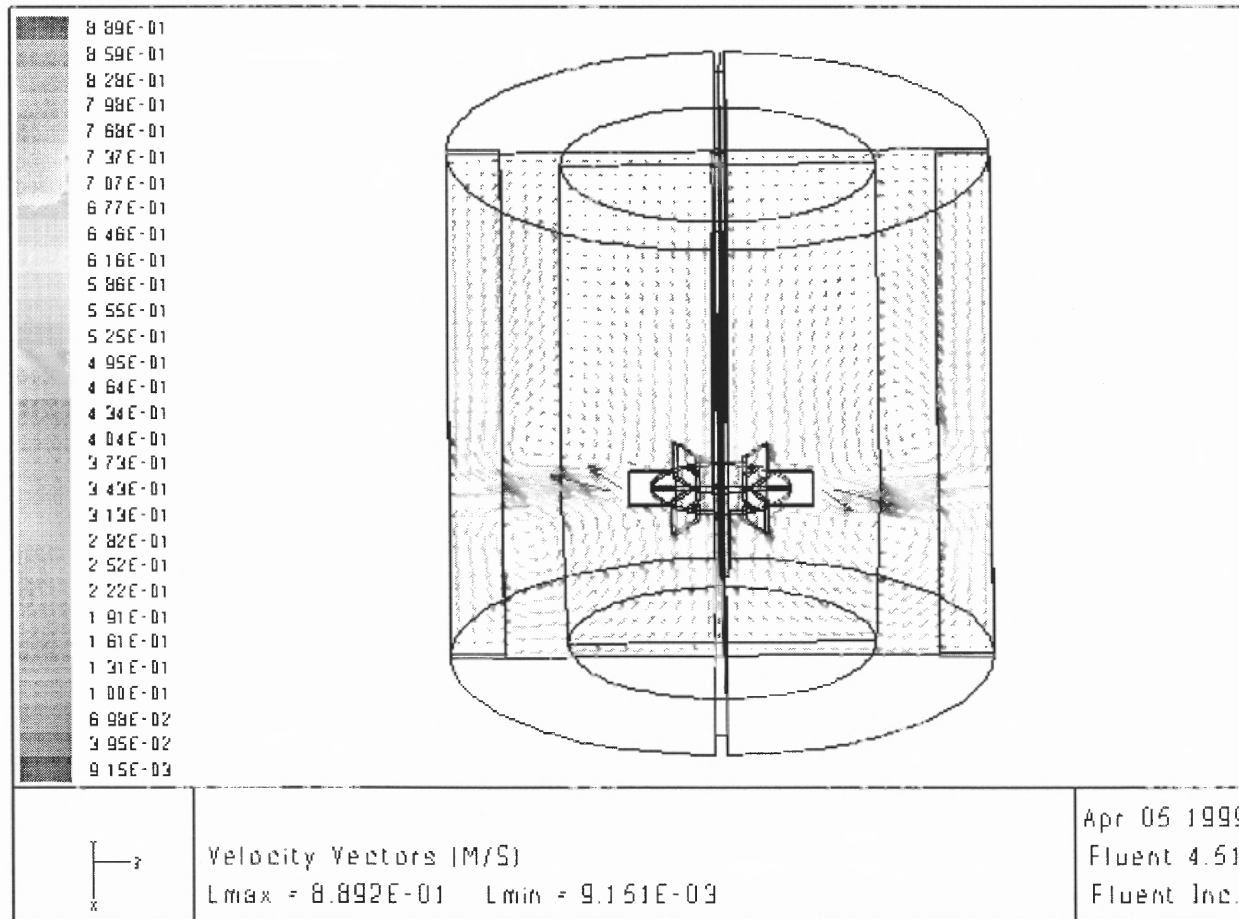
Figure 5.10: Stirred tank equipped with a Rushton turbine at an impeller clearance of T/3: Average velocity profile.
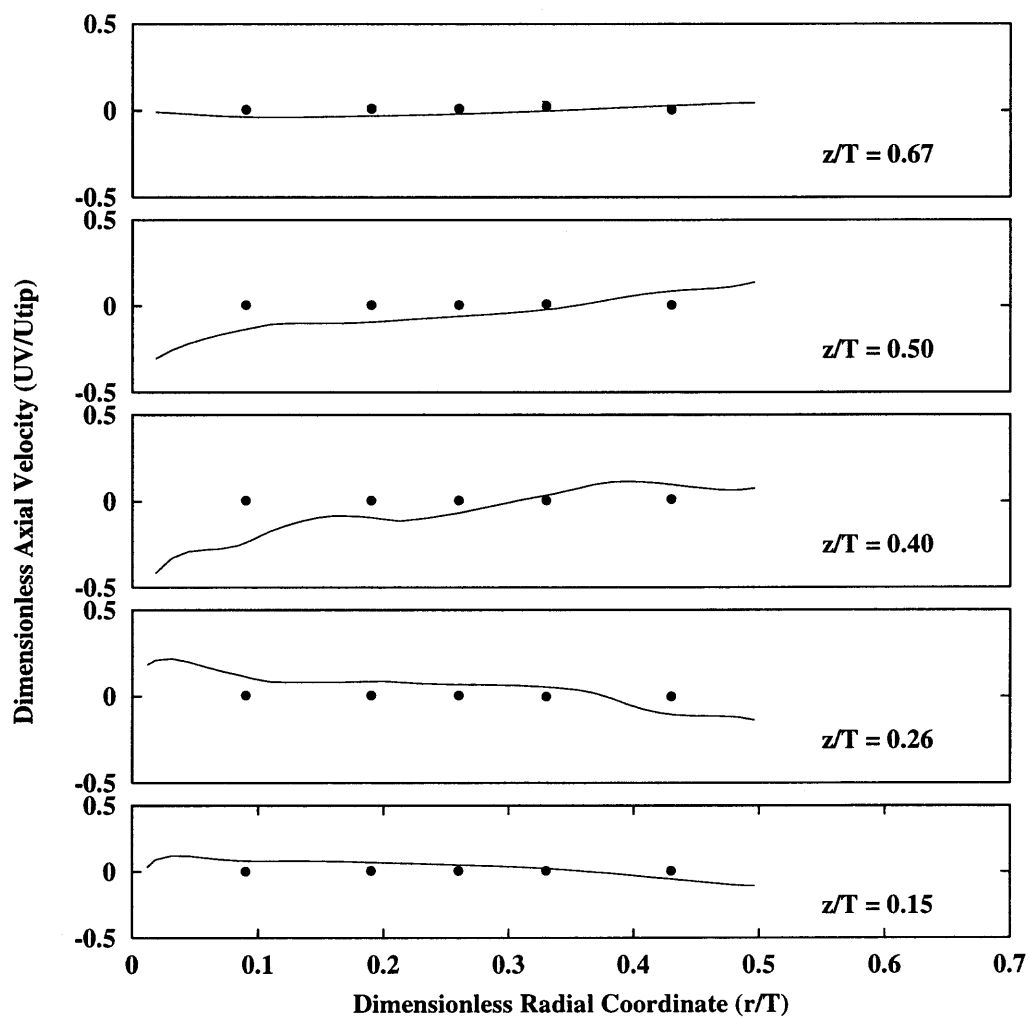
Figure 5.11: Stirred tank equipped with a Rushton turbine at an impeller clearance of T/3: Comparison of experimental axial velocity data with CFD simulation.
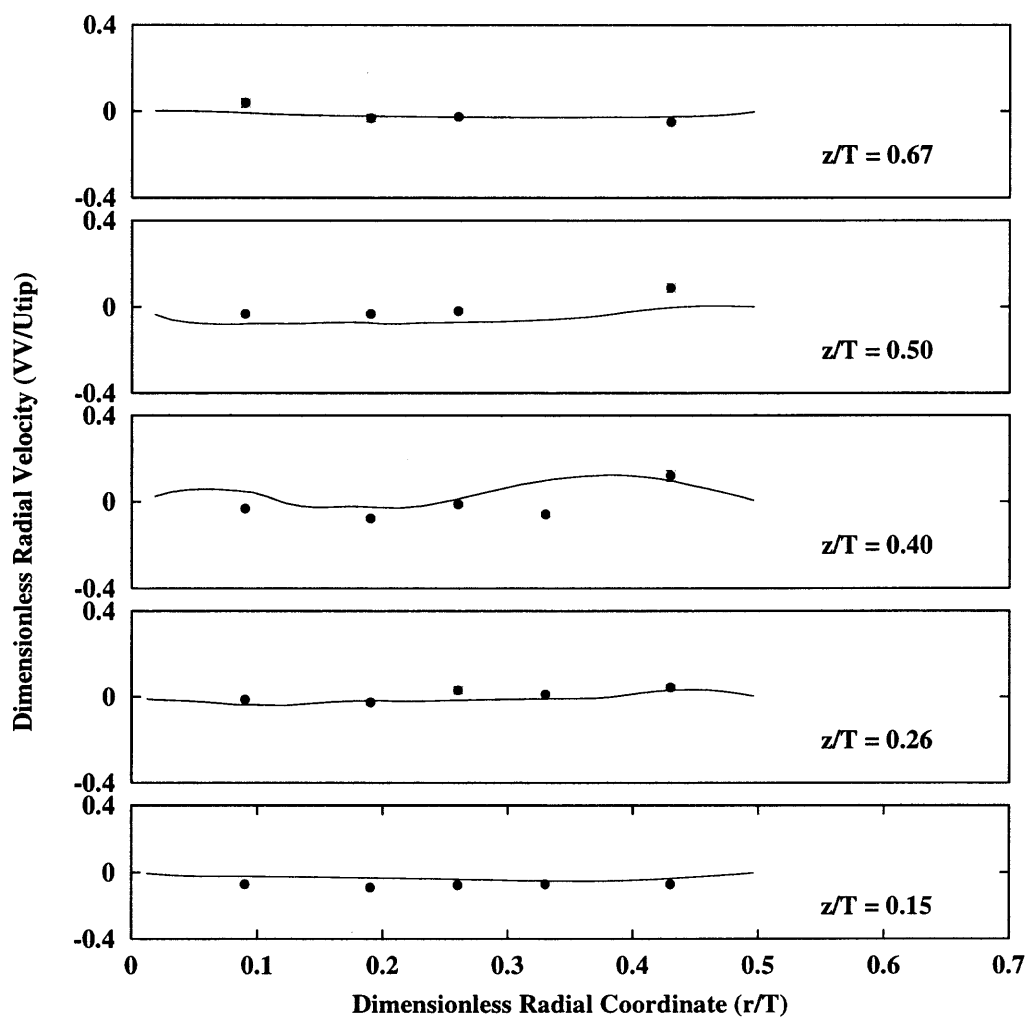
Figure 5.12: Stirred tank equipped with a Rushton turbine at an impeller clearance of T/3: Comparison of experimental radial velocity data with CFD simulation.
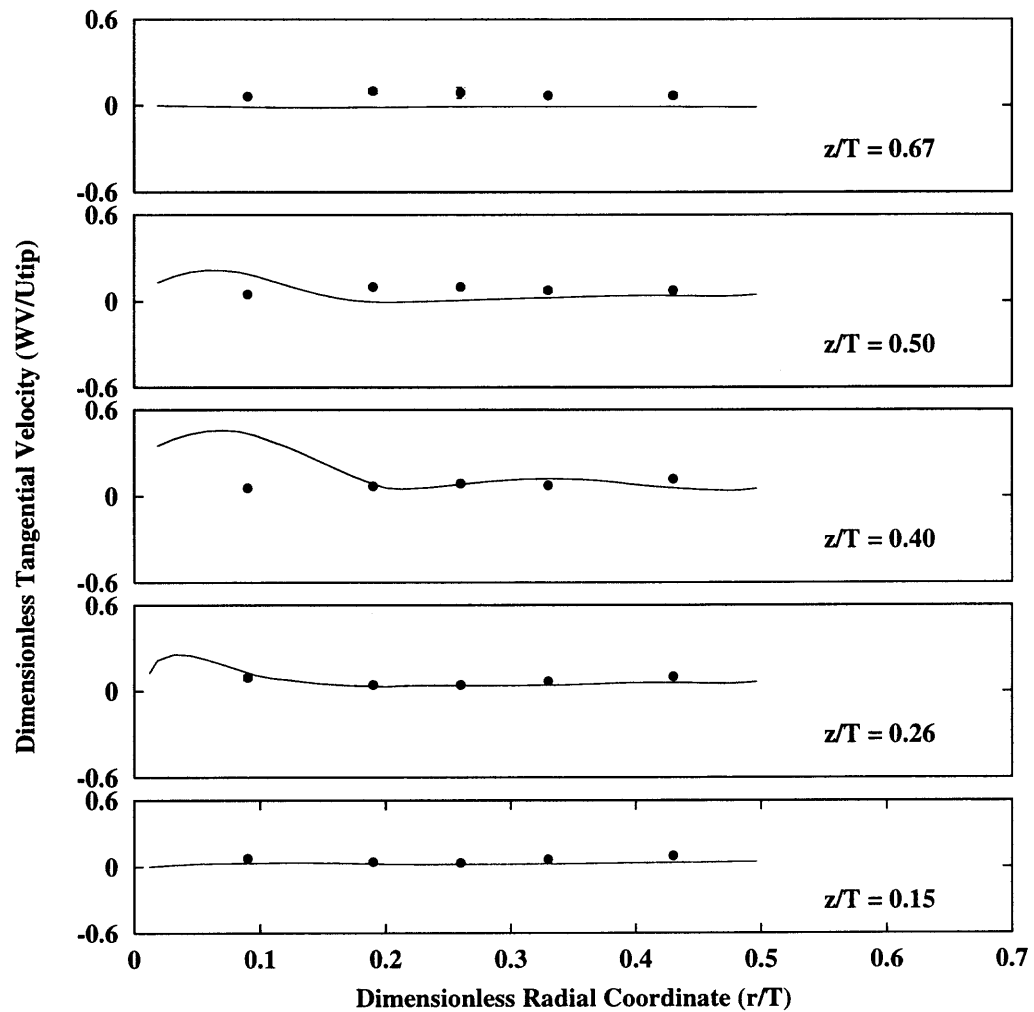
Figure 5.13: Stirred Tank equipped with a Rushton turbine at an impeller clearance of T/3: Comparison of experimental tangential velocity data with CFD simulation.

The profiles of turbulent kinetic energy is for the most part uniform. The CFD model has the tendency to under-predict the turbulence. The CFD model captures the main fea-
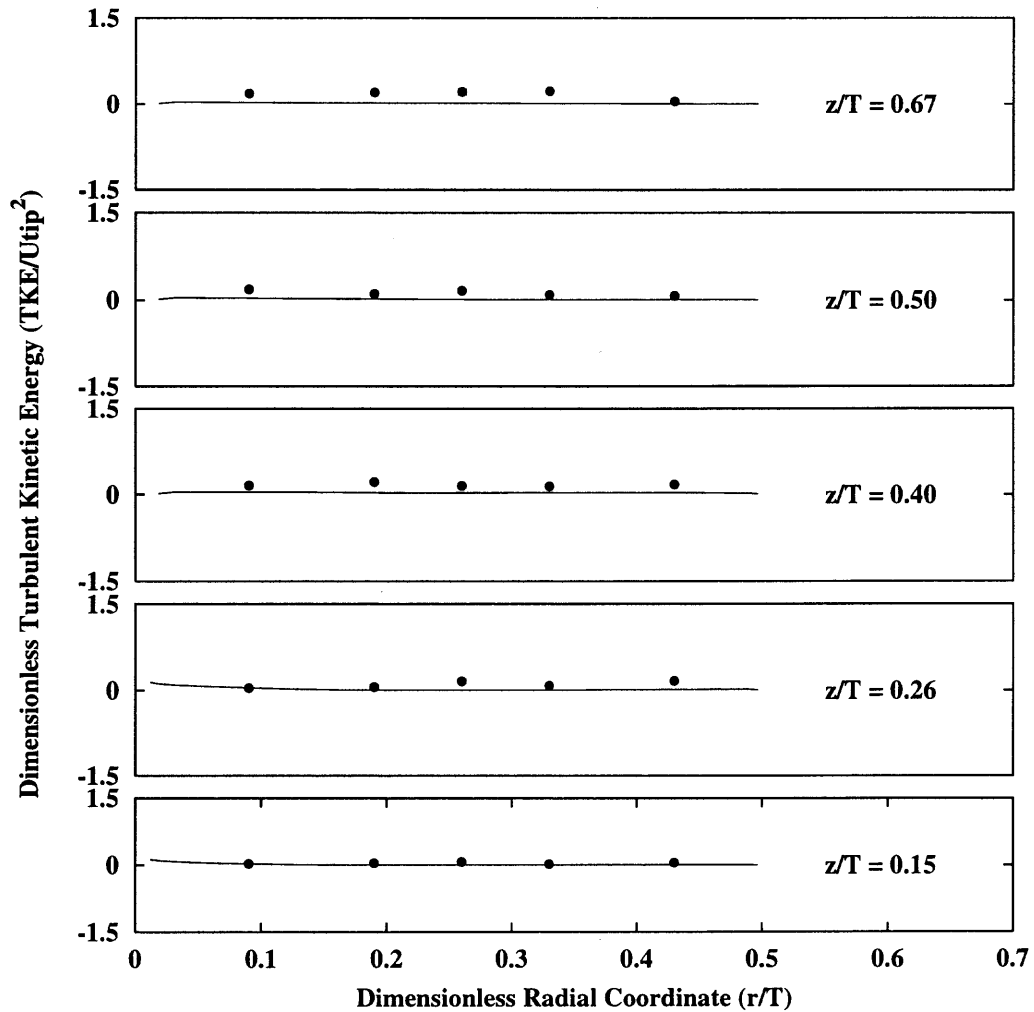
Figure 5.14: Stirred Tank Equipped with a Rushton Turbine at an Impeller Clearance of T/3: Comparison of Experimental Turbulent Kinetic Energy Data with CFD Simulation.

tures of the turbulent velocity field generated by the Rushton impeller well. Numerical discrepancies exist, but the results are nonetheless very encouraging.

5.3.3 Comparison of LDV Data with FLUENT CFD Simulations for System A2

In this section, the results of performing the simulation in a viscous medium which was prepared as described in Chapter 4 are presented.

The data presented here exhibit the same trends as for System A1. The data are presented next, followed by an overall discussion of the data.
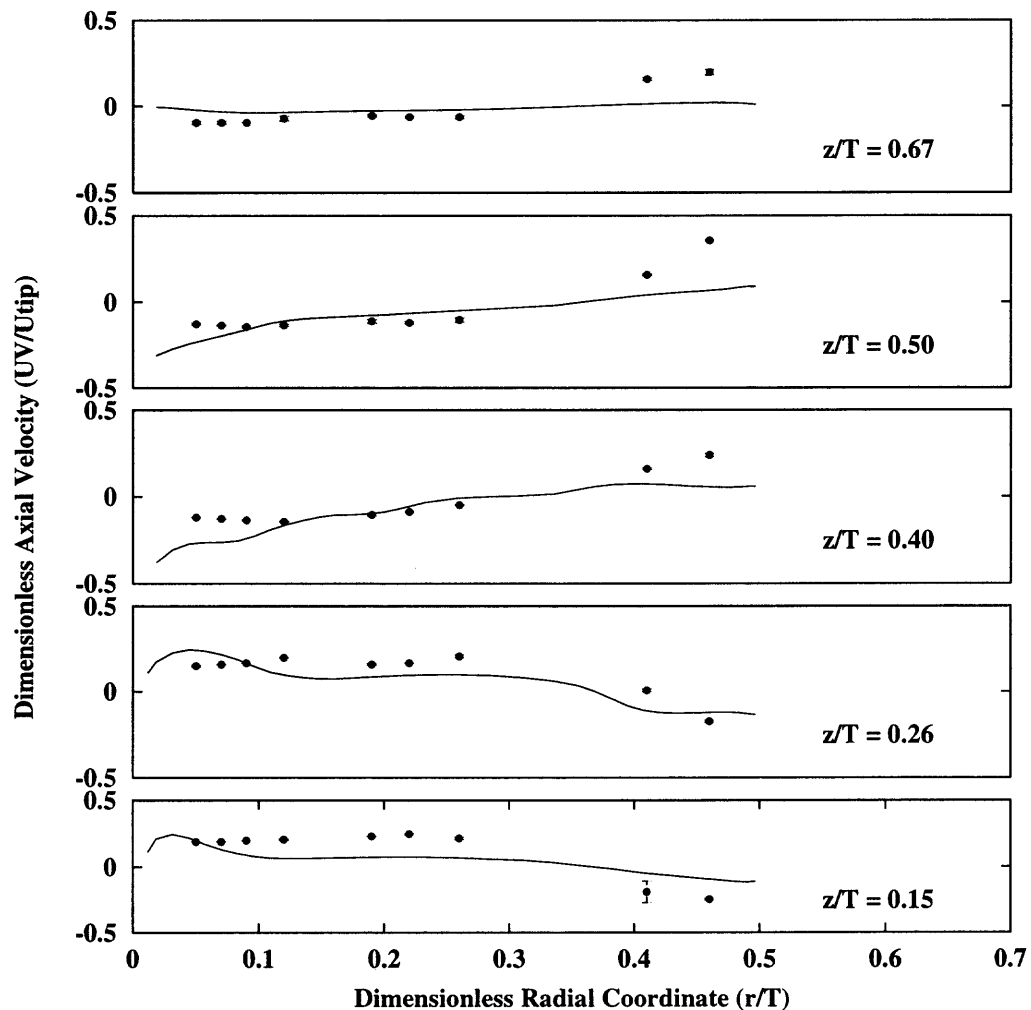
Figure 5.15: Stirred Tank Equipped with a Rushton turbine at an impeller clearance of T/3: Comparison of experimental axial velocity data with CFD simulation in viscous medium.

The same trends observed for the aqueous medium are observed for the viscous medium as well. The turbulence, though still under predicted, is better predicted for the viscous
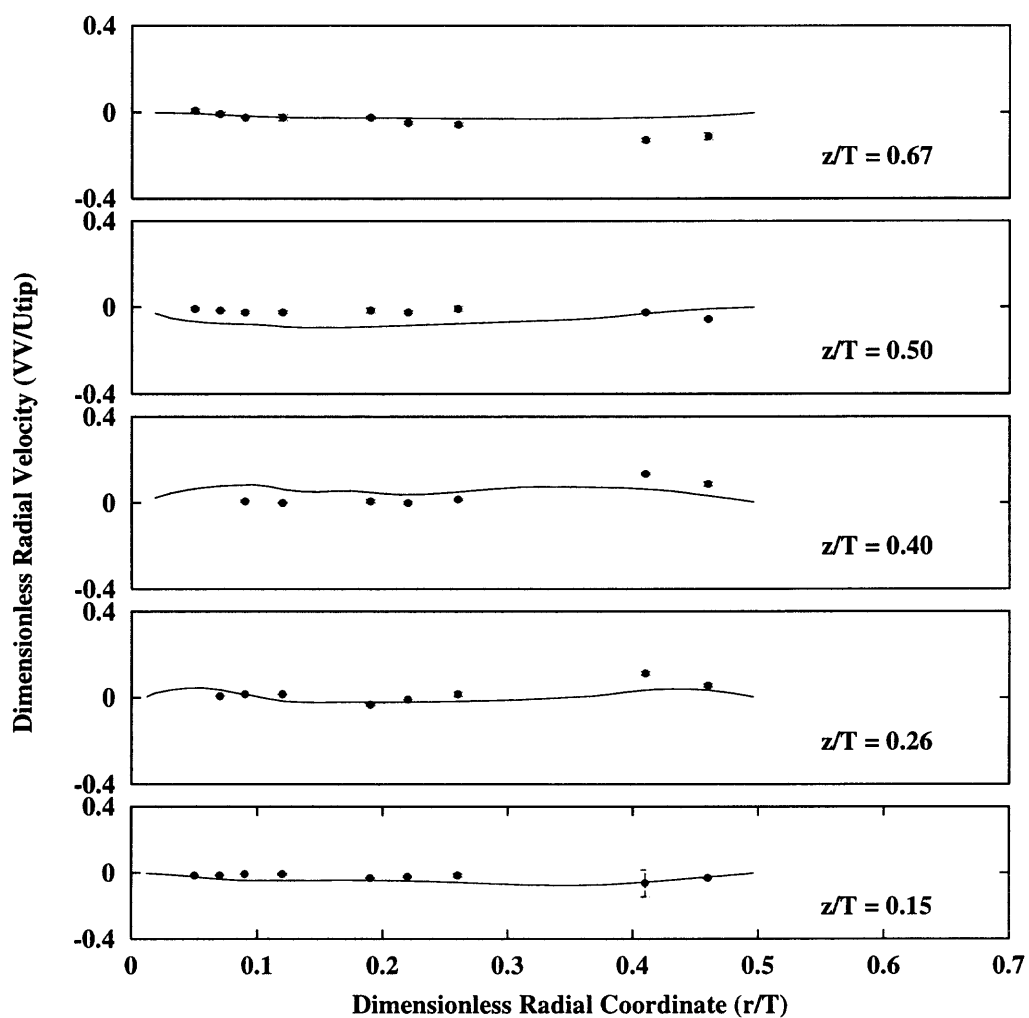
Figure 5.16: Stirred tank equipped with a Rushton turbine at an impeller clearance of T/3: Comparison of experimental radial velocity data with CFD simulation in viscous medium.
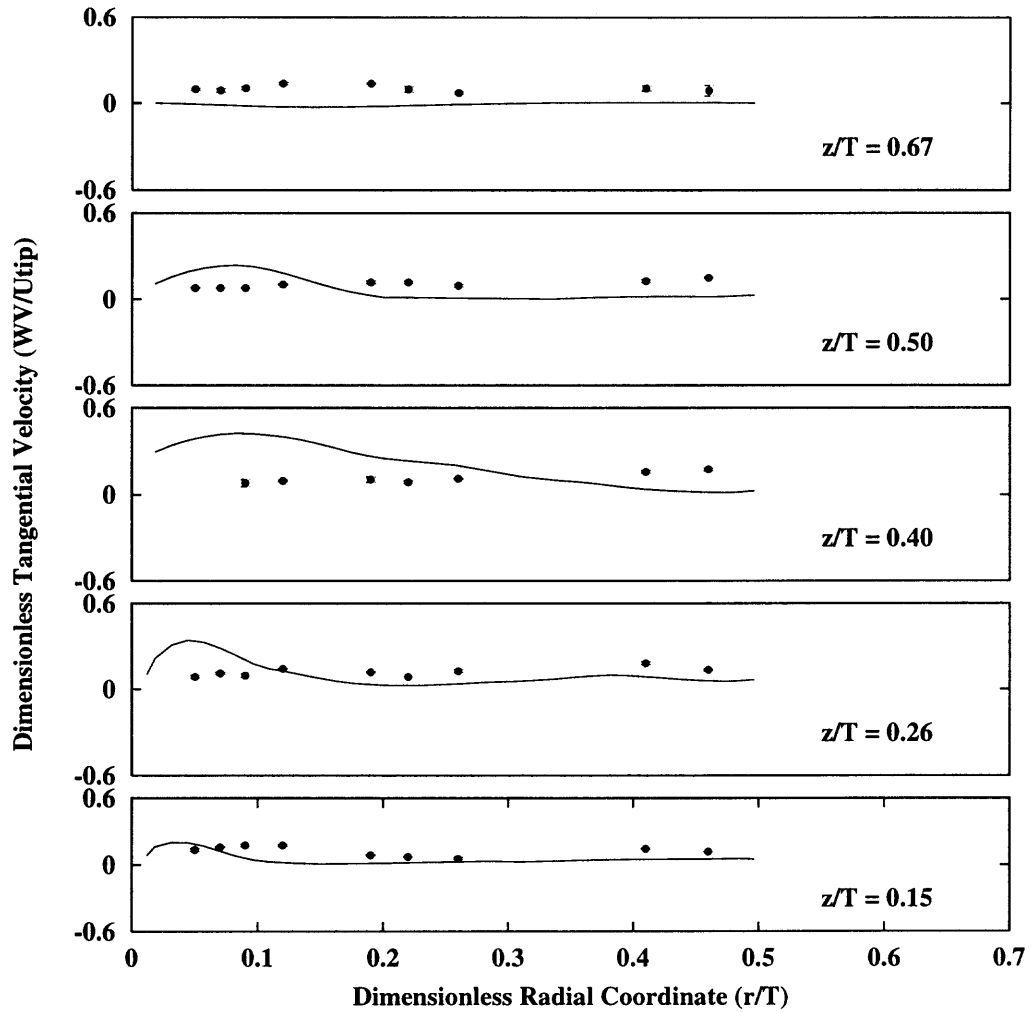
Figure 5.17: Stirred tank equipped with a Rushton turbine at an impeller clearance of T/3: Comparison of experimental tangential velocity data with CFD simulation in viscous medium.
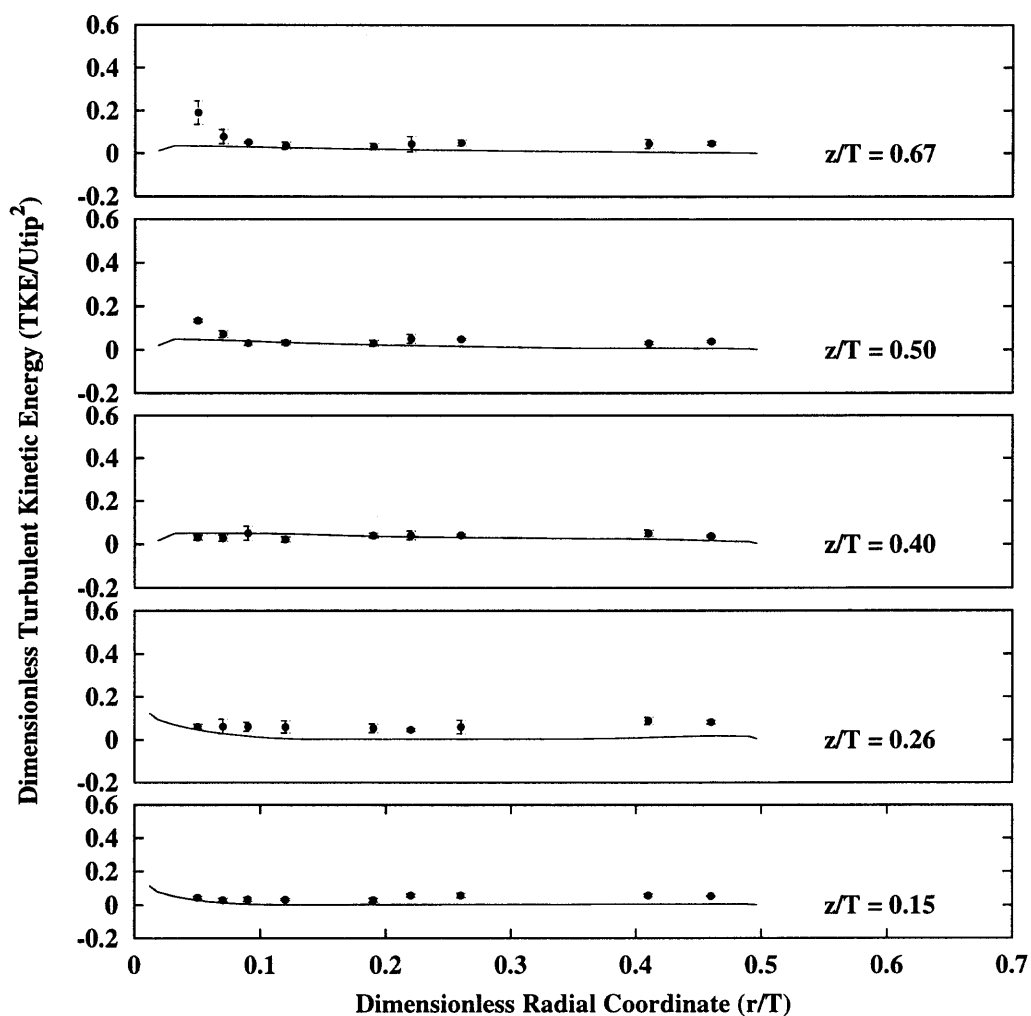
Figure 5.18: Stirred Tank equipped with a Rushton turbine at an impeller clearance of T/3: Comparison of experimental turbulent kinetic energy data with CFD simulation in viscous medium.

medium than for the aqueous medium, in particular in the bulk region of the tank above the impeller. The three velocity components yield similar velocity profiles as for the aqueous system.

5.3.4 Power Consumption

Table 5.1 shows how the computed power consumption of the system compares with experimentally measure power and published correlations. It is evident that the experimentally obtained values are in close agreement with those obtained from published correlations while, the computed power is under-predicted.

5.3.5 Comparison of Predicted Product Yields for System A1 with Experiment

In this section, the predicted yields for the parallel competing reaction set detailed in Section 4.3 are compared with the experimentally obtained results from the Literature (Bourne and Yu 1994; Bourne et al. 1995). The feed location simulated was location Fs (near the liquid surface) as outlined in Figure 4.7. Results obtained using both the standard E-Model as well as the modified E-Model are presented.

The first series of graphs (Figures 5.19– 5.20) show the concentration profile of the limiting reagent, sodium hydroxide, as a function of time. The final reaction time is the time taken for 99.99 % of the sodium hydroxide to be consumed. The graphs are presented for simulations at the lowest agitation speed (100 rpm), and at the highest agitation speed used for this system (300 rpm). The complete set of results are presented in Table 5.1.

It is clear that the two versions of the E-Model yield different reaction profiles for the limiting reagent. The two-parameter E-Model predicts initially, a longer time history profile the the standard E-Model. This can be explained from the fact that the two-parameter E-Model includes information about the initial break up of the reaction zone prior to engulfment. This initial break up of material is commonly referred to as mesomixing in the

Table 5.1: Power and mixing time results for systems A1 and A2

System	RPM	N_{Re}	Location	Reaction Time $t_{99.99}$(s)	Mixing Time t_{99}(s)	N_{Po} Simulation	Po(Sim) (W)	N_{Po} (correl)	Po (correl,W)	N_{Po} (exp)	Po (exp,W)
A1	100.00	18481	Fs	2.380	27.06	1.86	0.09	5.14	0.238	5.10	0.27
	200.00	36963		0.700	13.53	1.44	0.53	5.14	1.901	5.23	2.08
	300.00	55444		0.340	9.02	2.39	2.98	5.14	6.416	5.25	7.07
	100.00		Fi	1.420							
	200.00			0.440							
	300.00			0.180							
A2	100.00	2640	Fs	3.020		2.07	0.10			4.51	0.24
	200.00	5280		1.580		2.35	0.87			4.70	1.92
	300.00	7921		1.300		2.32	2.89			4.71	6.28
	100.00		Fi	2.320							
	200.00			0.960							
	300.00			0.520							

literature (Baldyga et al. 1997). The standard E-Model only considers the engulfment step. The initial longer time history means that the initial break up of the reaction zone influences the kinetics and it is important because the reactions under study are sensitive to the time history of their environment.

The computed reaction times are much smaller than the time taken to homogenize the tank contents. A comparison of the mixing times with the reaction times is presented in Table 5.1. This shows that the reactions are occurring under inhomogeneous conditions.

The reaction times are observed to be faster at high agitation speeds than at lower ones indicating that the role of micromixing diminishes with increasing agitation speed. This is consistent with the established theory. At the limit where the tank contents can be homogenized very quickly, a perfectly mixed reactor would result (CSTR) and micromixing will be unimportant. The first reaction, which is nearly instantaneous, will dominate, and the reaction time would be very small. This is but a hypothetical limit and is not realized in engineering practice for fast competitive reactions exhibiting complex chemistry.
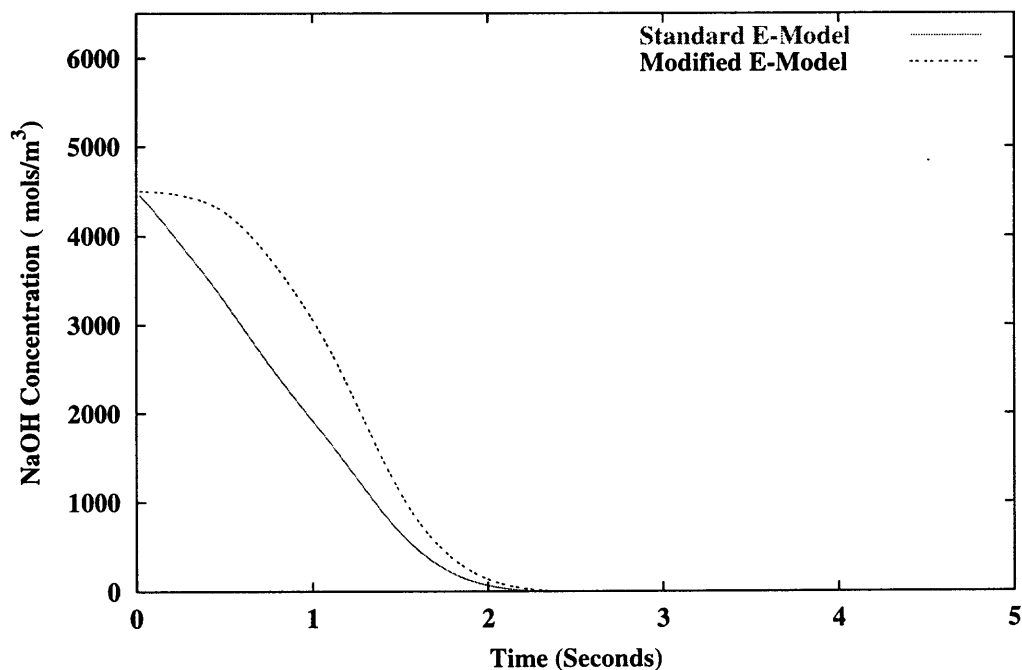
Figure 5.19: Reaction profile for system A1 at 100rpm. Feed location Fs.
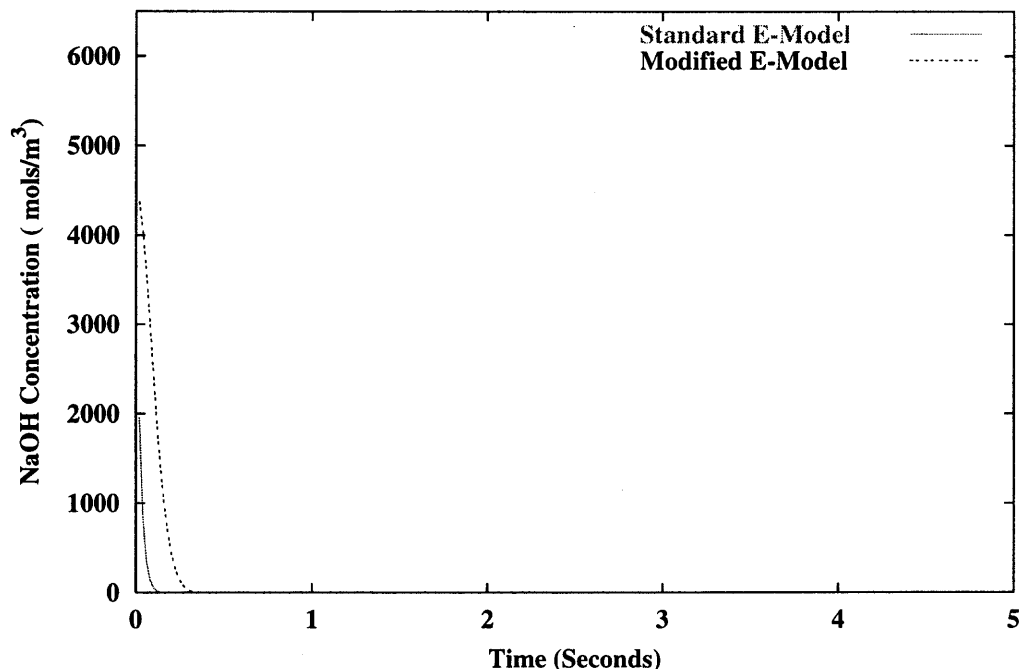
Figure 5.20: Reaction profile for System A1 at 300rpm. Feed location Fs.

Figure 5.21 shows the trajectory of the reaction zone within the stirred tank at 200rpm for feed near the surface. The reaction time for this configuration is given in Table 5.1. It is readily seen that for the reactions times under consideration, the reaction zone is hardly mixed, thereby affirming the assumptions on which the model is based, namely that the reactions are taking place in an segregated inhomogeneous environment. It is also seen that the model captures very well the ongoing phenomena within the stirred tank.

Figure 5.22 shows the variation of product yield with impeller agitation speed. Experimental results and predicted results for both micromixing models are presented on the same graph for ease of comparison.

From the data, two trends are readily apparent. Firstly the observed product yields are much higher than what would be observed in the absence of a micromixing model as explained in Section 1.2.2. Secondly, the product yields are observed to decrease as the agitation speed is increased.

The high product yields result because the product yield is sensitive to micromixing.
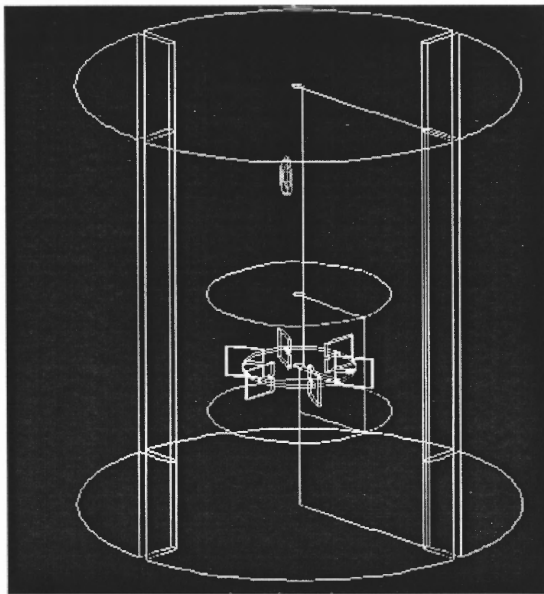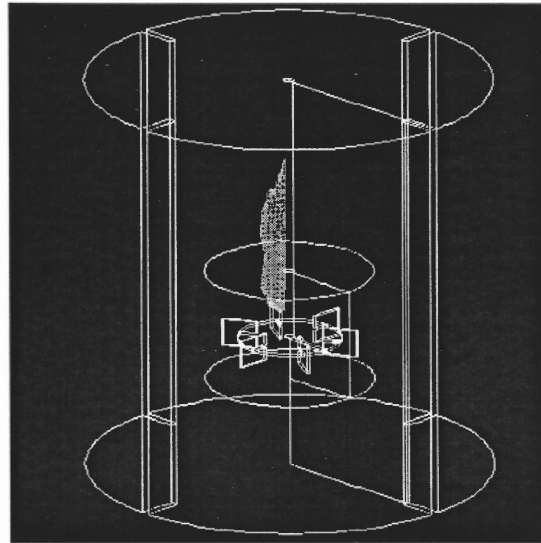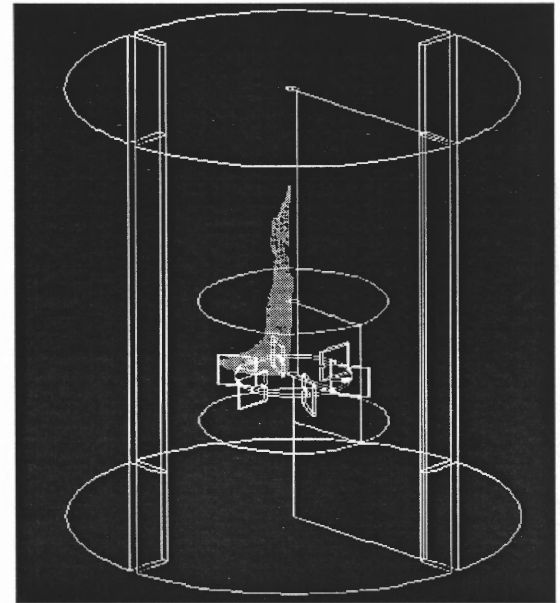
(a) t = 0.0 seconds   (b) t = 0.6 seconds   (c) t = 1.0 second

Figure 5.21: Reaction zone trajectory. System A1, feed near liquid surface at 200rpm.

Fine scale fluid deformation (mesomixing and engulfment) are rate limiting and hence the side reaction progresses to a greater extent than it would in a perfectly mixed system.

As the agitation speed is increased, the system approaches that of a perfectly mixed system, and the role of micromixing diminishes. The observed product yields are still relatively high in comparison to that of a perfectly mixed system.

The simulation predicts results in good agreement with the experimental data from the literature. The simulation results from both micromixing models over predicts the final selectivities somewhat, and this is a result of the fact that turbulence is over predicted for this particular system.
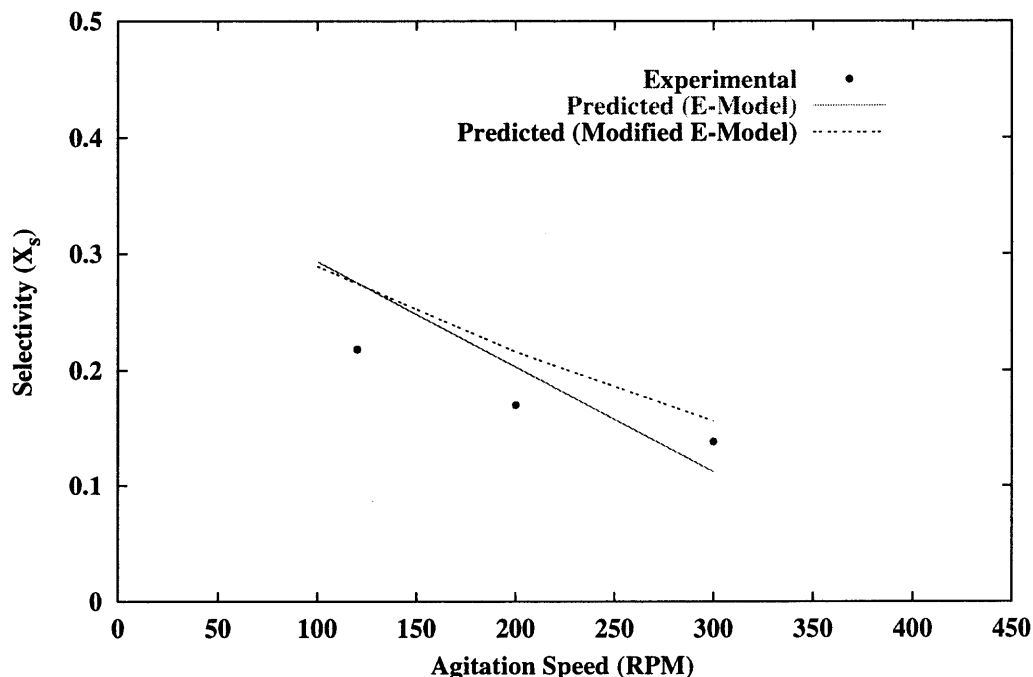
Figure 5.22: Variation of product yield with agitation speed for System A1. Feed location Fs.

5.3.6 Comparison of Predicted Product Yields for System A2 with Experiment

The results for System A2 are presented next. The trends observed for system A1 are observed for System A2 also. There are, however, differences that occur as a result of the

difference in viscosities.

In general, provided the flow remains turbulent, the change in viscosity has little influence on the bulk blending time (Bourne et al. 1995). Viscosity does, however, influence the fine scale structure of the fluid. Since the fine scale structure controls the rate of micromixing and hence controls the kinetics, it is expected that the viscosity will influence the yield of the fast competitive reaction system used in this work. The engulfment parameter which depends on the kinematic viscosity will be different for this system and hence different results are to be expected.

The flow regime in stirred tank tanks is considered turbulent when the Reynolds number exceeds a value of 1×10^4. For Reynolds numbers in the range of 2000 to 1×10^4, the flow is considered to be transitional. Also, in the turbulent regime, the power number is constant (Dickey and Fenic 1976) while lower in the transitional regime. The results presented in Table 5.1 reflect this. The power number obtained for the viscous system are slightly lower than those obtained for the aqueous system. However, it has been shown that even at the lowest Reynolds numbers employed in this work, for this particular system, excellent fluid turn over is obtained in the entire vessel (Bourne et al. 1995). Thus it seems certain that fully developed turbulence is present for this system.

The reaction time history plots for this system exhibit the same trends as for System A1 (Figure 5.23 and Figure 5.24). The reaction times are, however, longer than for System A2 than for System A1 under the same conditions. This is a result of the increase in viscosity. An increase in viscosity slows the engulfment process i.e. the engulfment parameter is decreased, as viscous forces are more prominent. Since engulfment strongly influences the kinetics, the overall reaction time is longer. This is further evidence that micromixing controls the kinetics.

Although the modified E-Model produces a different reaction profile than the standard E-Model, the overall reaction times predicted by the two models do not differ significantly. This indicates that, as the fluid viscosity is increased, the engulfment stage of micromixing,

the stage which results from the action of viscous forces, is more dominant.

Shown next is a plot showing the variation of product yield with impeller agitation speed (Figure 5.25) The trends observed for System A1 are observed here too. By-product formation decreases with increasing agitation speed.
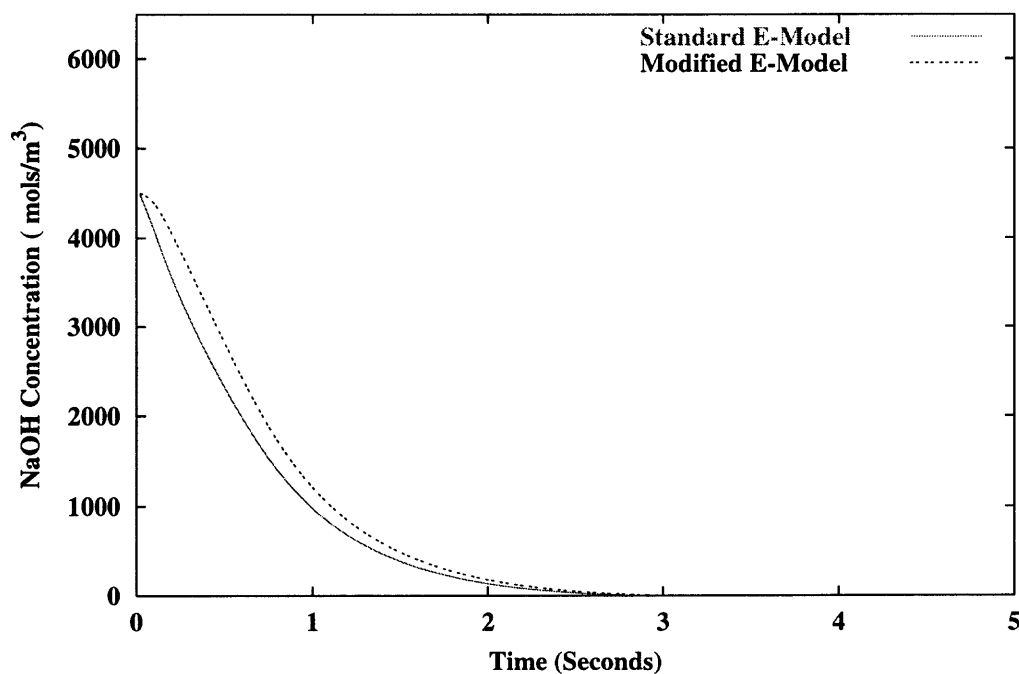
Figure 5.23: Reaction time for System A2 at 100rpm. Feed location Fs.

5.3.7 Comparison of Predicted Product Yields for System A3 with Experiment

In this section results for System A3 are presented. System A3 is identical to system A1 in its configuration except that lower initial concentrations of reactants were used. This was done in order to remain consistent with the results presented in later sections.

For the experimental phase of the work, the minimum feed time necessary for micromixing to be rate controlling was determined experimentally. The manner in which this is done and the reasons why it was necessary are detailed in Section 4.3.

For this system, it was determined that a feed time of $\approx$ 35 minutes (Figure 5.26) was
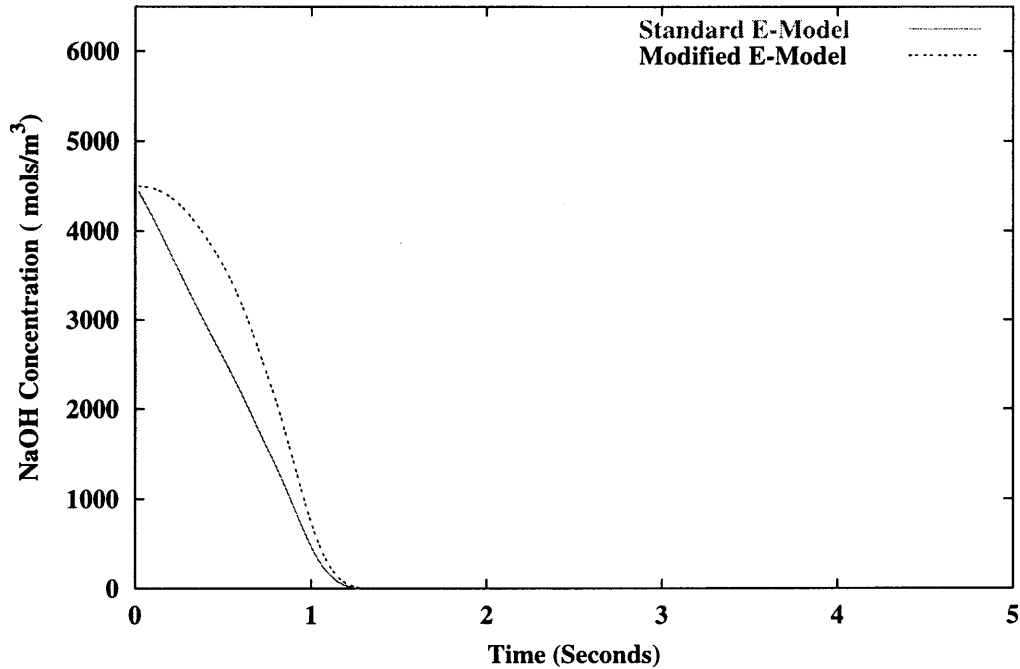
Figure 5.24: Reaction time for System A2 at 300rpm. Feed location Fs.

sufficient to ensure that micromixing was dominant. This was the feed time used for all the experimental runs.

As is evidenced here, except for the fact the the use of lower feed concentrations results in faster reaction times and lower yields, all the trends observed in Section 5.3.2 are observed here also. The reaction is faster at higher agitations speeds than at lower ones and the inclusion of mesomixing parameter into the model results in the prediction of a slower rate of reaction than when only the standard E-Model is considered.

The yield is observed to decrease with increasing agitation speed as expected and observed earlier. The modified E-Model is observed to provide a better prediction of the product yield than the standard E-Model. Both results are, however, most encouraging.
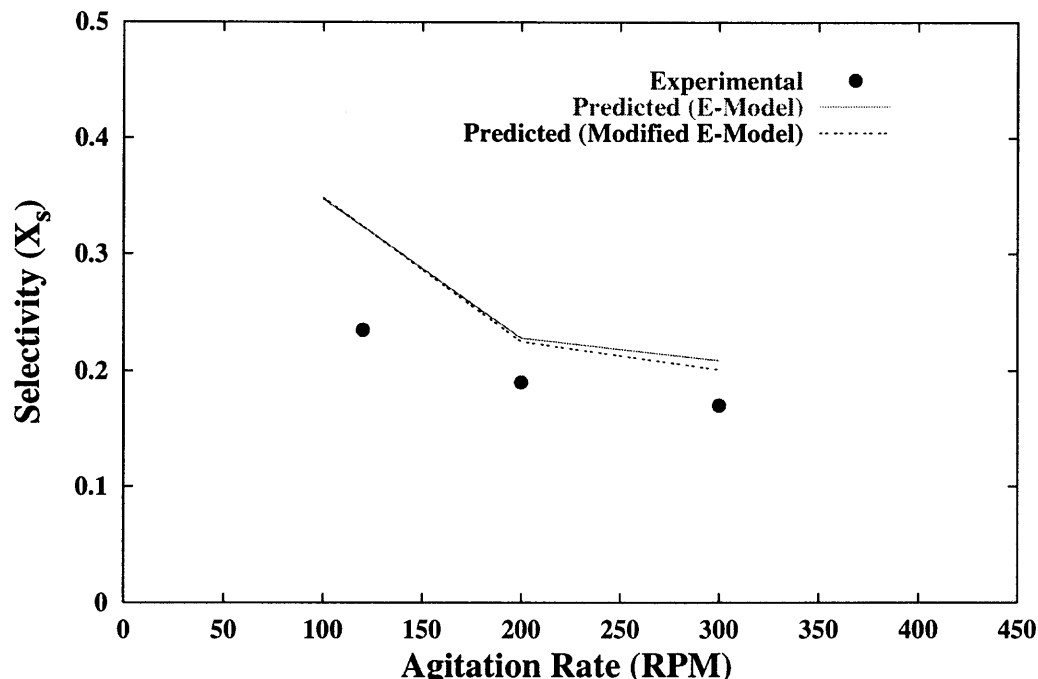
Figure 5.25: Variation of product yield with agitation speed for System A2. Feed location Fs.

5.3.8 Remarks

Mixing and chemical reaction were successfully simulated for the systems which consist of a baffled cylindrical stirred tank fitted with a Rushton turbine at an impeller off bottom clearance of one third the liquid height. System A2 differs from system A1 in that a high viscosity medium was used. System A3 differs from system A1 in that lower initial reactant concentrations were used.

The turbulence generated by this impeller was in general under-predicted. This led an over-prediction of the reaction product yields. The prediction of turbulence was slightly better for the viscous medium than for the aqueous medium. Nonetheless, the model serves to provide insights into the micromixing process and the main trends of the process are also captured. Reaction is slower at lower agitations speeds and the by-product yields higher, indicating that the role of micromixing is more important when macromixing is slower.

The increase in fluid viscosity was observed to slow down the rate of micromixing and
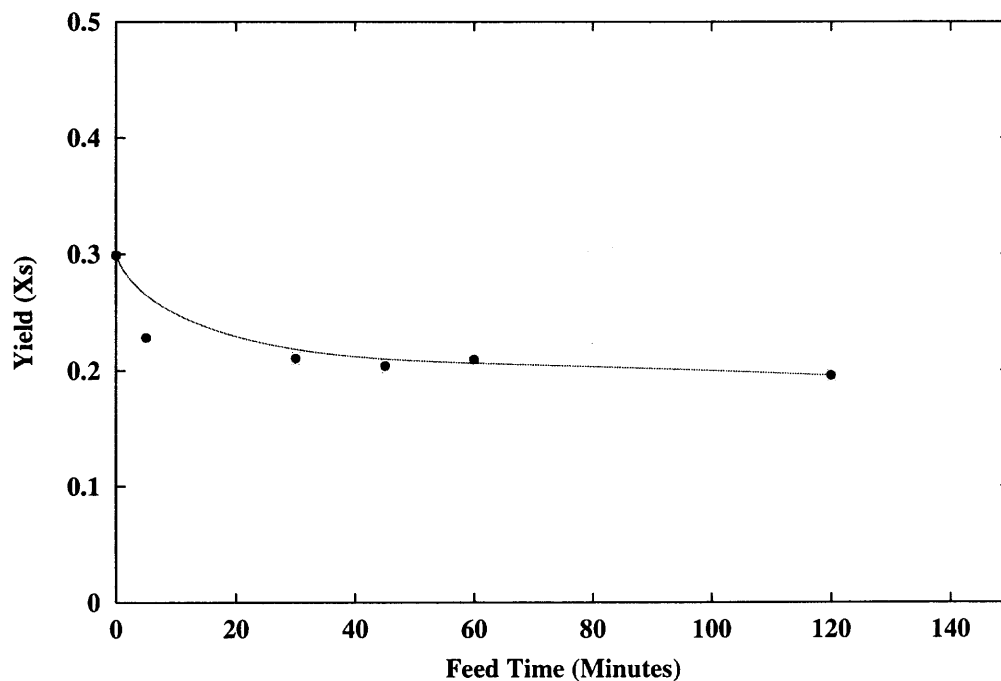
Figure 5.26: Variation of product yield with feed time for System A3
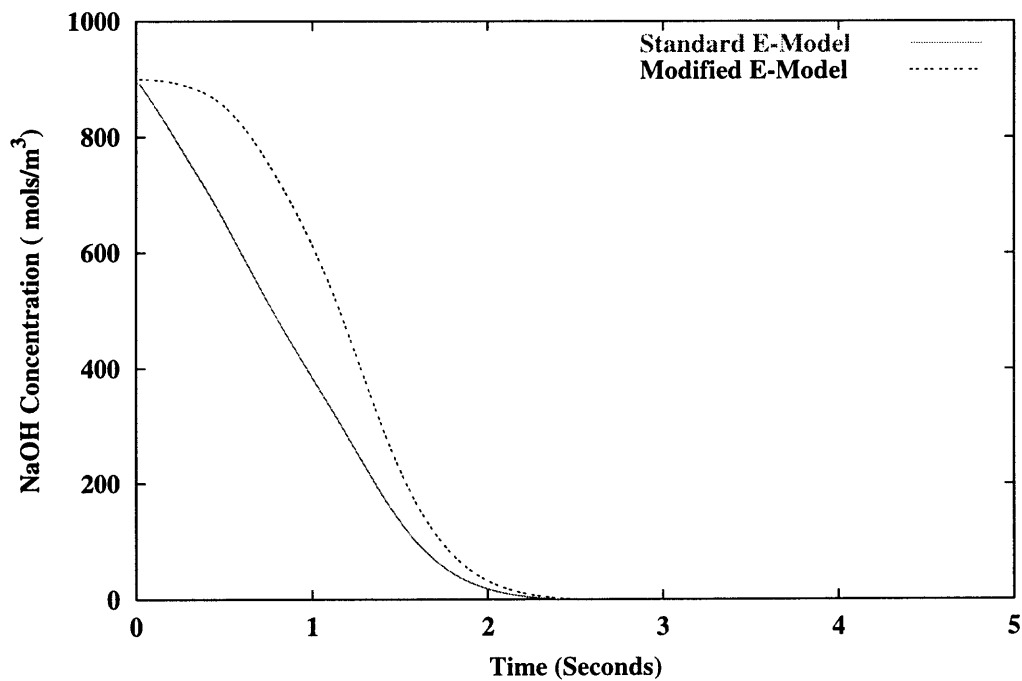
Figure 5.27: Reaction profile for System A2 at 100rpm. Feed location Fs.
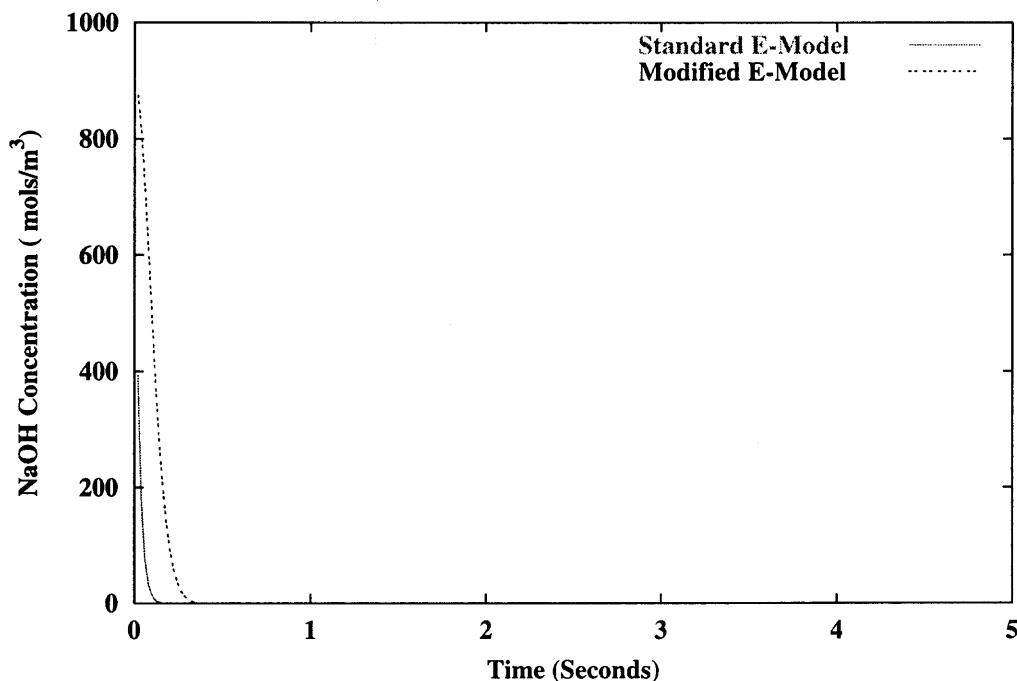
Figure 5.28: Reaction profile for System A3 at 300rpm. Feed location Fs.

hence increase the by-product yields. Thus in more viscous media, micromixing effects are more important than in aqueous media.

The under-prediction of turbulence for the Rushton impeller could be attributed to micro instabilities (trailing vortices) present in the impeller region. These micro-instabilities are an important source for the turbulence generated by this impeller. Because these instabilities are transient in nature and occur at very small scales, it is very difficult to capture them in a computational grid. This consequently leads to an under prediction of the turbulence generated by the impeller. The Rushton turbine has been observed to generate two such instabilities per blade (Zhou and Kresta 1996). The use of the MRF model which is an steady state approximation of a transient process may fail to capture these phenomena in sufficient detail. It is possible that only a fully time dependent computation in conjunction with a turbulence model that can capture these phenomena will improve the prediction of turbulence. A grid sufficiently small to capture their presence would not be feasible.

Despite its limitation, the CFD model has served to provide insights into the turbulent
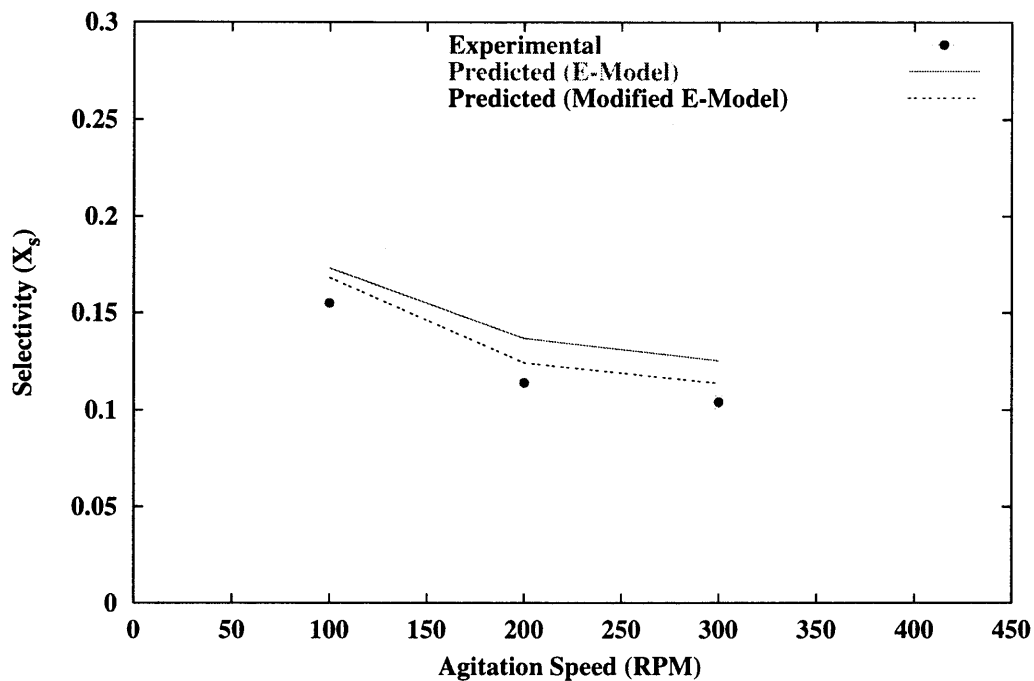
Figure 5.29: Variation of Product Yield with Agitation Speed for System A3. Feed Location Fs.

mixing process.

5.4 Results for Systems B1 and B2

Pitched Blade Turbine: Impeller off Bottom Clearance C = T/3

The pitched blade turbine is commonly used in industrial practice because it requires less power than a Rushton impeller while providing a high fluid turn over rate. In this section, results for Systems B1 and B2 are presented. The difference between the two lies in the fact that in System B2, a viscous medium was used, while only water was used in System B1. The system details are summarized in Table 1.2 and in Figure 4.6.

5.4.1 System Configuration

Prior to carrying out simulations involving the influence of mixing and turbulence on fast parallel competitive reactions, the flow field was simulated using CFD and the simulation results verified using LDV. The system configuration and the axial locations in the vessel where the velocity profile was sampled using LDV are shown in Figure 5.30. The data was sampled in one of four quadrants midway between the baffles due to system symmetry.

The tank geometries used for the CFD simulations are presented in Figures 5.31 – 5.32. In Figure 5.32 a cross-section of the tank showing the mesh details is shown. The mesh around the impeller is extremely fine as detailed in Chapter 3. This is necessary since strong gradients of velocity and turbulence exist there. A fine grid is necessary to capture as much of the detail as possible, since the impeller generates the flow that prevails throughout the computational domain. It was also necessary to use a fine mesh at the tank bottom because the fluid flow from the axial impeller impinges there and creates a secondary source of turbulent flow. The details of how this was done are also outlined in Chapter 3.

In Figure 5.31 and Figure 5.32 a region around the impeller is outlined. This is the MRF zone, the region in the computational domain that is solved in a moving reference frame. For an axial impeller such as the pitched-blade turbine, this region spans most of the height of the tank because the flow generated by the impeller is primarily axial.
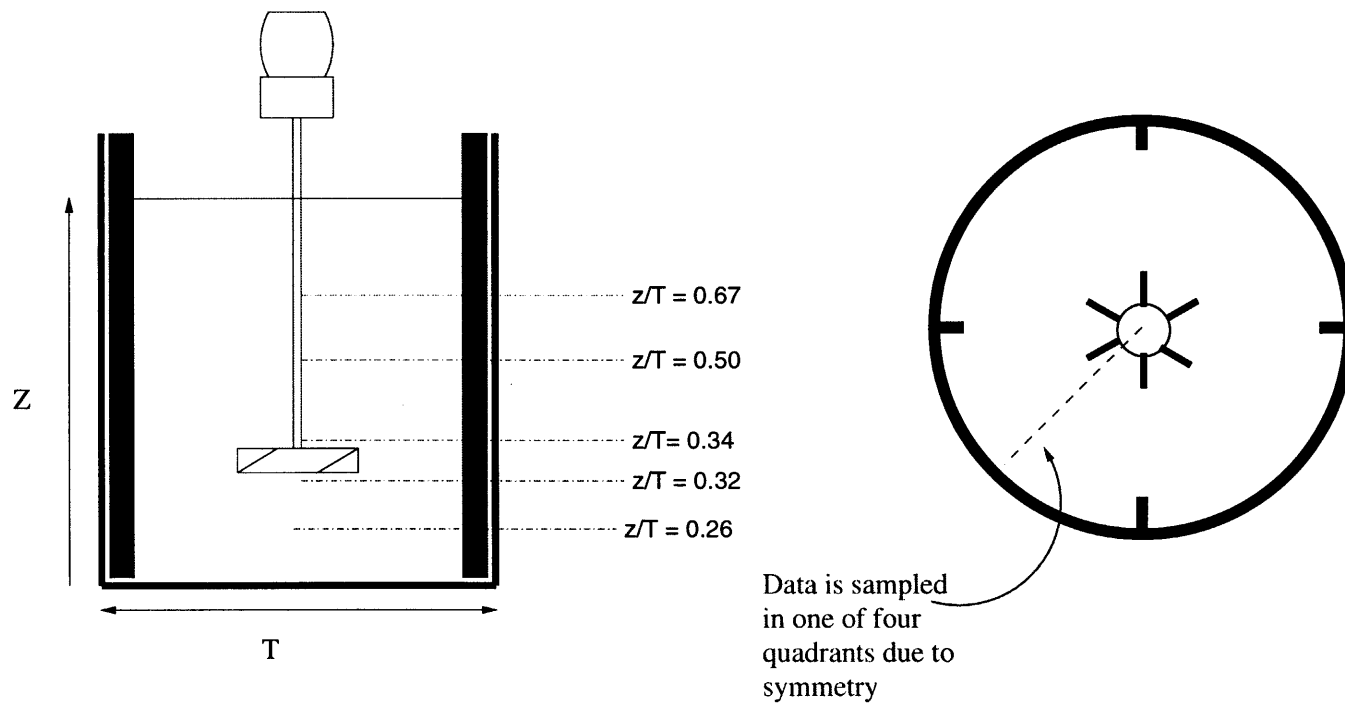
Figure 5.30: Stirred tank equipped with a pitched blade turbine at an impeller clearance of T/3: Locations where LDV data was taken.

z/T = 0.67

z/T = 0.50

z/T = 0.34

z/T = 0.32

z/T = 0.26

Z

T

Data is sampled
in one of four
quadrants due to
symmetry

Modified 3D Geometry Grid	Apr 08 2000
Outline	Fluent 4.52
	Fluent Inc.
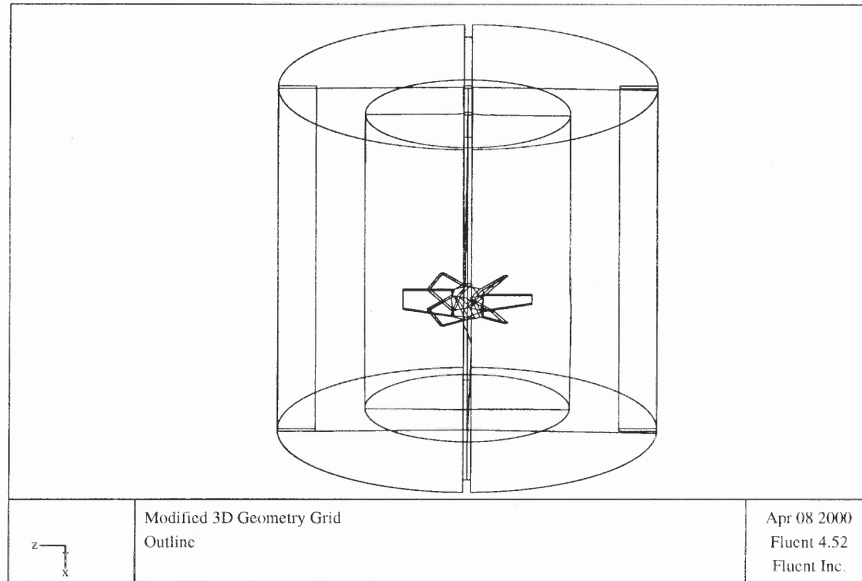
Figure 5.31: Stirred tank equipped with a pitched blade turbine at an impeller clearance of T/3: Outline grid.

Modified 3D Geometry Grid	Apr 08 2000
Grid (145 X 34 X 85)	Fluent 4.52
Slices: I=36, I=111	Fluent Inc.
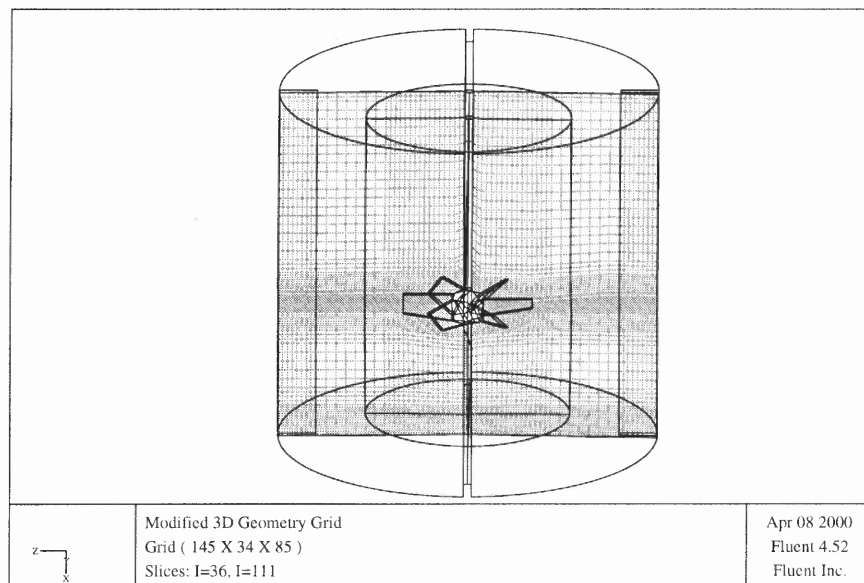
Figure 5.32: Stirred tank equipped with a pitched blade turbine at an impeller clearance of T/3: Outline grid showing mesh details.

Figure 5.33 shows a snapshot of the velocity profile for a simulation carried out at 300 rpm. The velocity vectors shown are the resultant velocity vectors for the axial, radial and tangential directions. The velocity profile shown is typical of what one would expect from an axial flow impeller. A turbulent jet is generated from the impeller and impinges on the tank base. Two main circulation loops are evident. One on each side of the impeller. Thus from a qualitative perspective, the simulation captures the main features of the turbulent flow generated by the pitched-blade impeller.

5.4.2   Comparison of LDV Data with CFD Simulations for System B1

LDV data was taken on a system with an impeller agitation speed of 300rpm. The CFD data presented here is for simulations carried out at 300rpm.

The pitched blade impeller produces two main circulation loops as shown in Figure 5.33. Near the tank wall along the entire length of the vessel axial velocities are positive as the fluid is moving up. Near the shaft and above and below the impeller, the axial velocities are negative as the fluid returns to the impeller and is pumped away towards the tank base. These trends are reflected by the data, in particular in the region just above the impeller. Near the top of the tank, the flow is more horizontal and "quiet". This trend has been observed by other investigators of similar systems (Ranade and Joshi 1989b; Ranade and Joshi 1989a).

Below the impeller, near the middle of the tank, positive velocities are observed indicating the presence of a small recirculation loop there. This feature has also been reported in the literature (Ranade and Joshi 1989b; Ranade and Joshi 1989a) and is characteristic of similarly configured agitation systems.

Because the flow produced by the pitched-blade turbine is primarily axial in nature, the radial components of the velocity are expected to be low. This is evidenced by the simulation and verified by experiment as Figure 5.35 shows.

In the vicinity of the impeller region, the radial velocities are higher indicating that
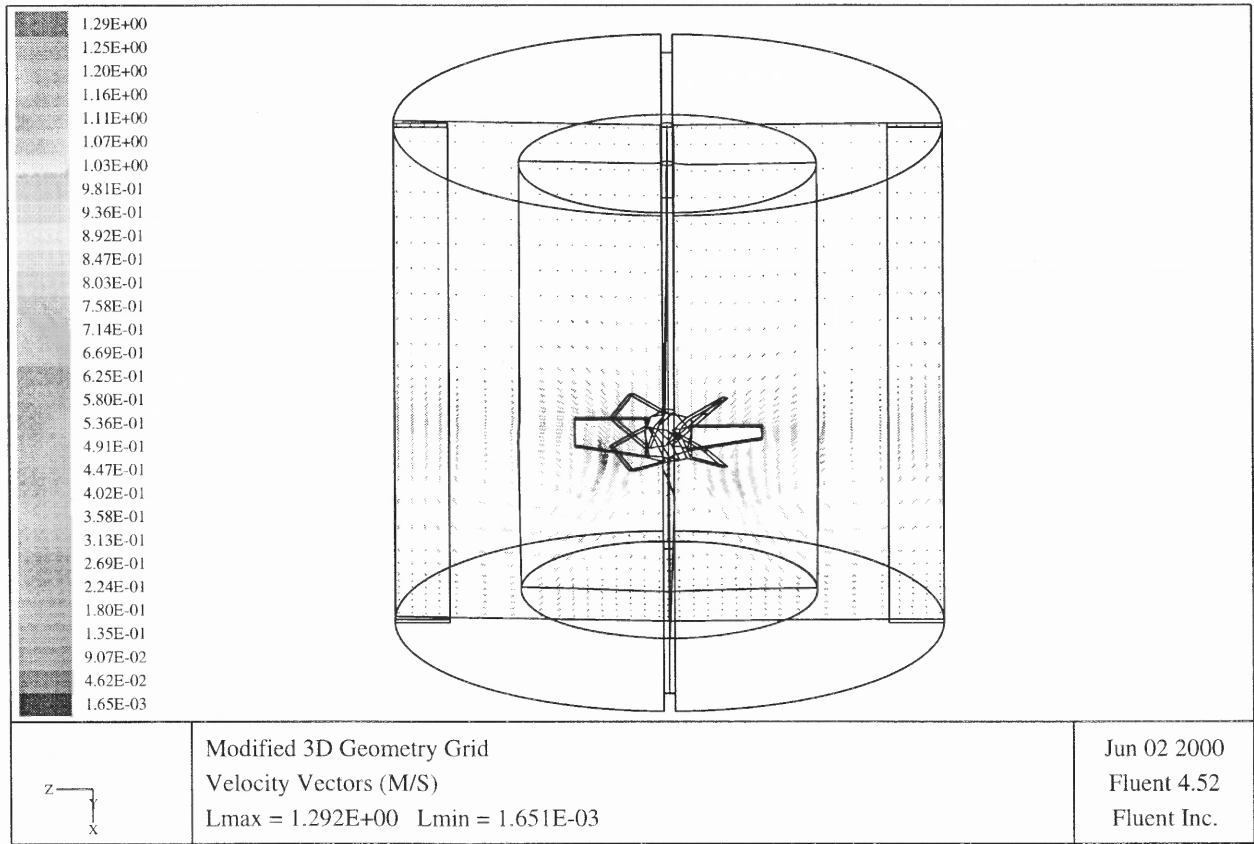
Figure 5.33: Stirred tank equipped with a pitched blade turbine at an impeller clearance of T/3: Velocity profile.
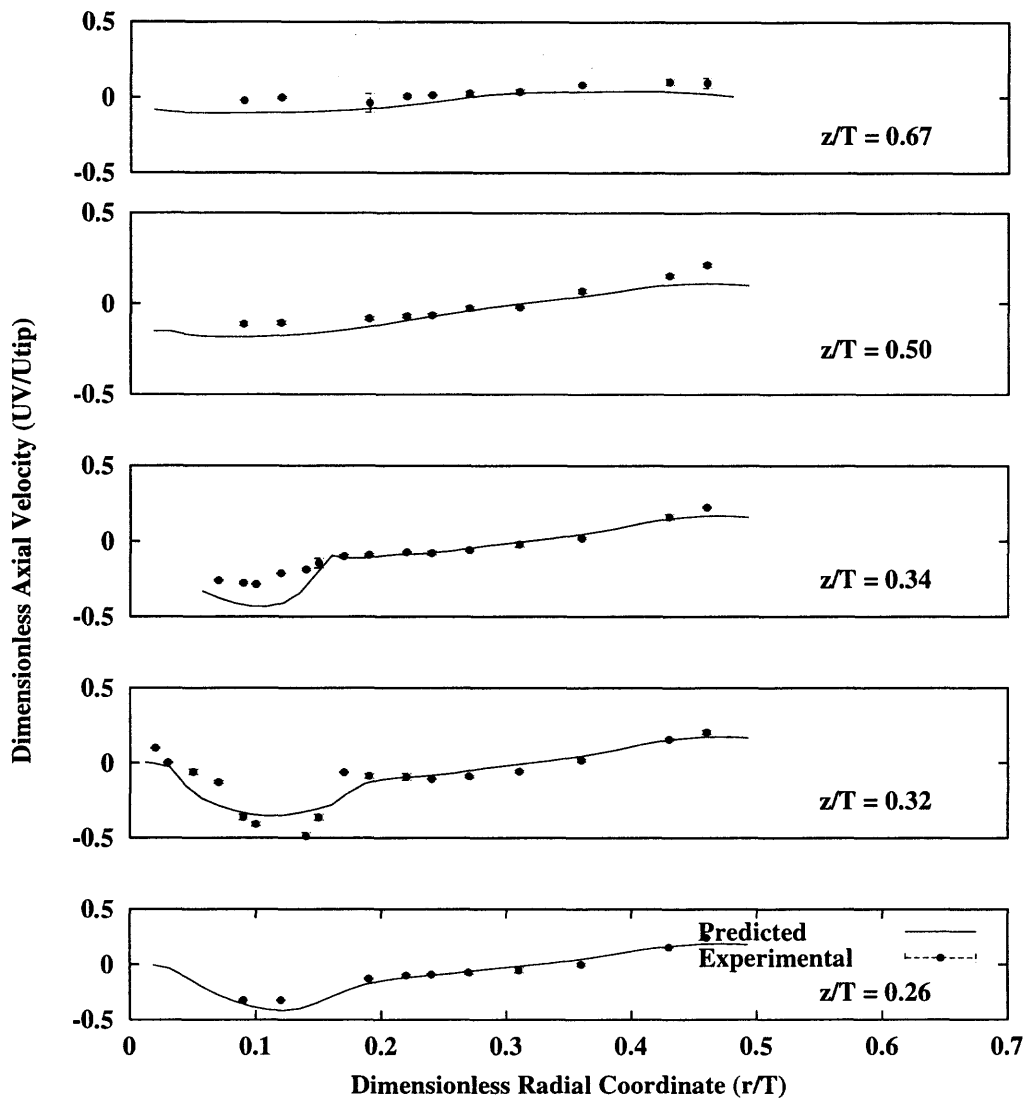
Figure 5.34: Stirred tank equipped with a pitched blade turbine at an impeller clearance of T/3: Comparison of experimental axial velocity data with CFD simulation.

the impeller imparts a some radial motion to the flow. In the rest of the vessel, the radial velocity profiles are flat.
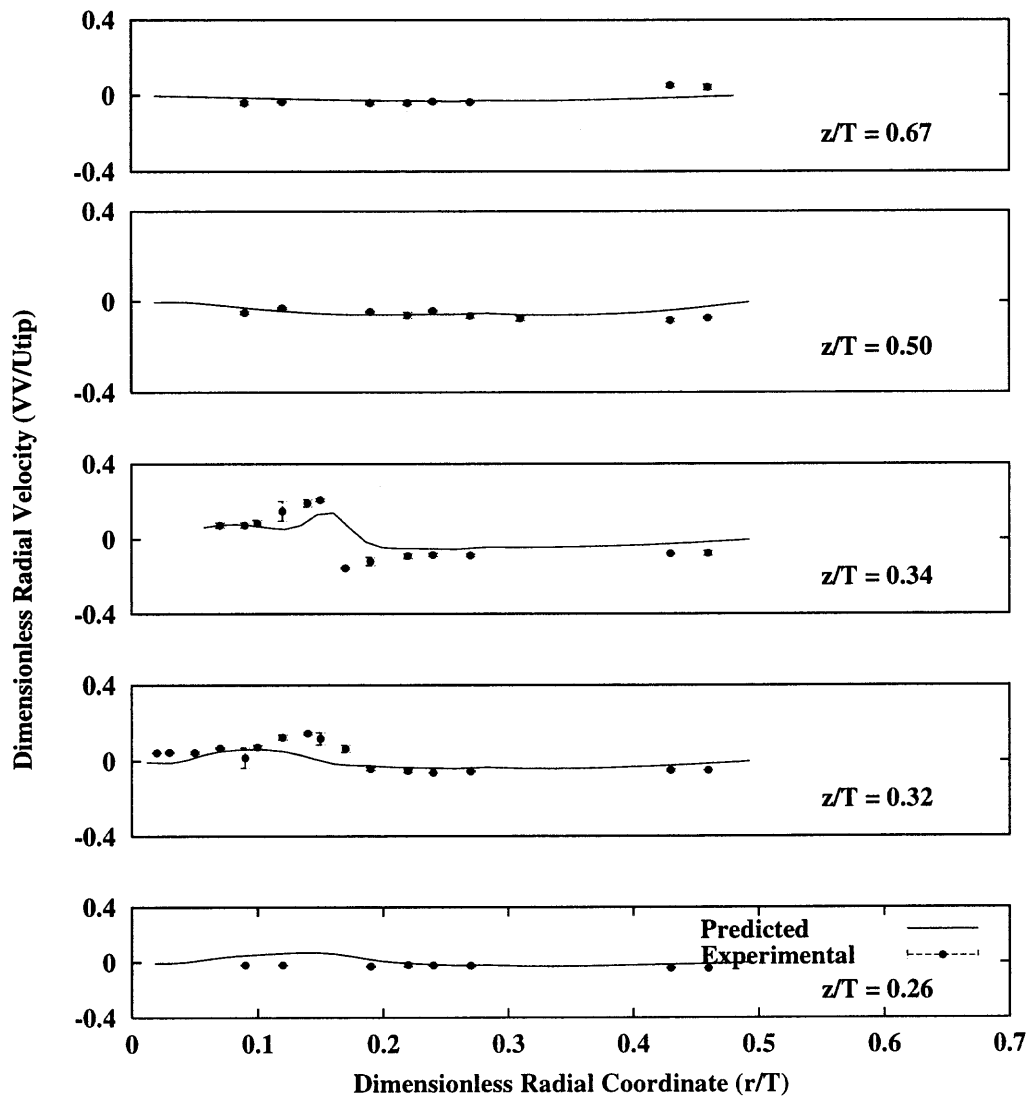
Figure 5.35: Stirred tank equipped with a pitched blade turbine at an impeller clearance of T/3: Comparison of experimental radial velocity data with CFD simulation.

In the case of the tangential velocity (Figure 5.36), the results show that near the impeller shaft and along the height of the tank, swirling motion is evident. This swirling motion dies out near the tank walls. The agreement between the predicted values and the experimentally obtained ones is satisfactory.

Near the top of the vessel the profiles of turbulent kinetic energy are flat. Closer to the
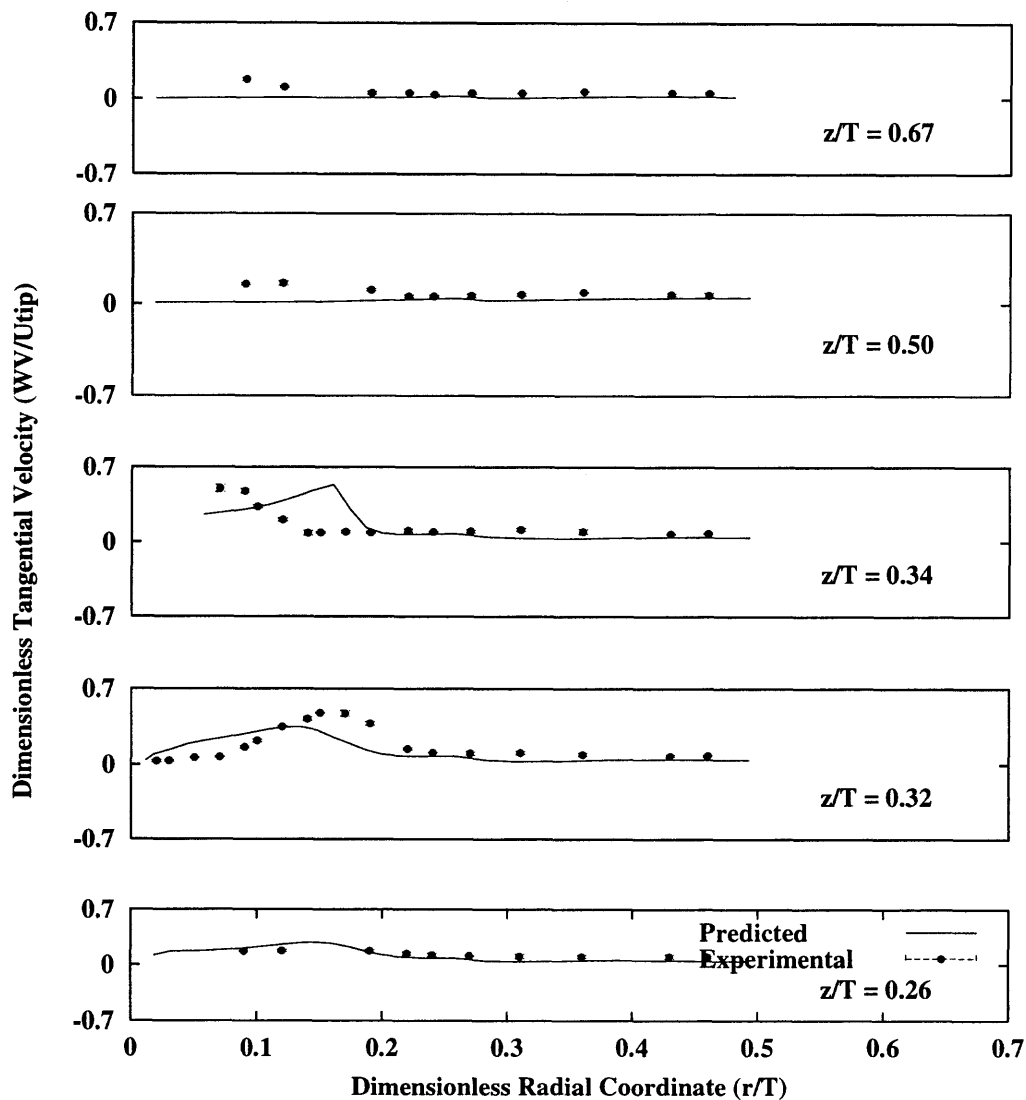
Figure 5.36: Stirred tank equipped with a pitched blade turbine at an impeller clearance of T/3: Comparison of experimental tangential velocity data with CFD simulation.

impeller, higher values are observed. The agreement between the experimental values and the predicted values is satisfactory.
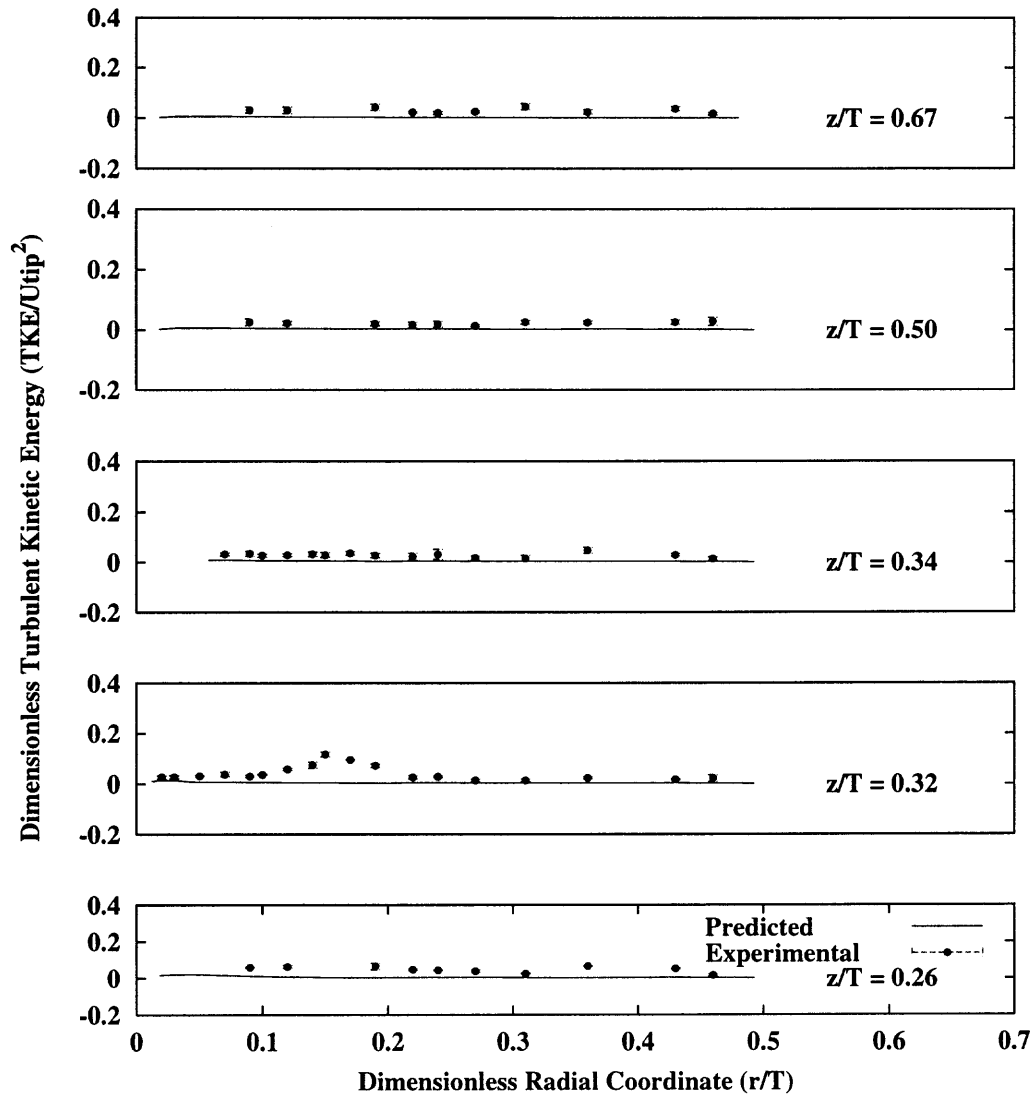
Figure 5.37: Stirred Tank Equipped with a Pitched Blade Turbine at an Impeller Clearance of T/3: Comparison of Experimental Turbulent Kinetic Energy Data with CFD Simulation.

The CFD model captures the main features of the turbulent velocity field generated by the pitched-blade impeller. Numerical discrepancies exist, but the results are satisfactory overall.

5.4.3   Comparison of LDV Data with CFD Simulations for System B2

In this section, the results of performing the simulation in a viscous medium are presented. The viscosity of the medium was $8.3 \times 10^{-3} Pa \cdot s$ and the manner whereby this was done is presented in Chapter 4.
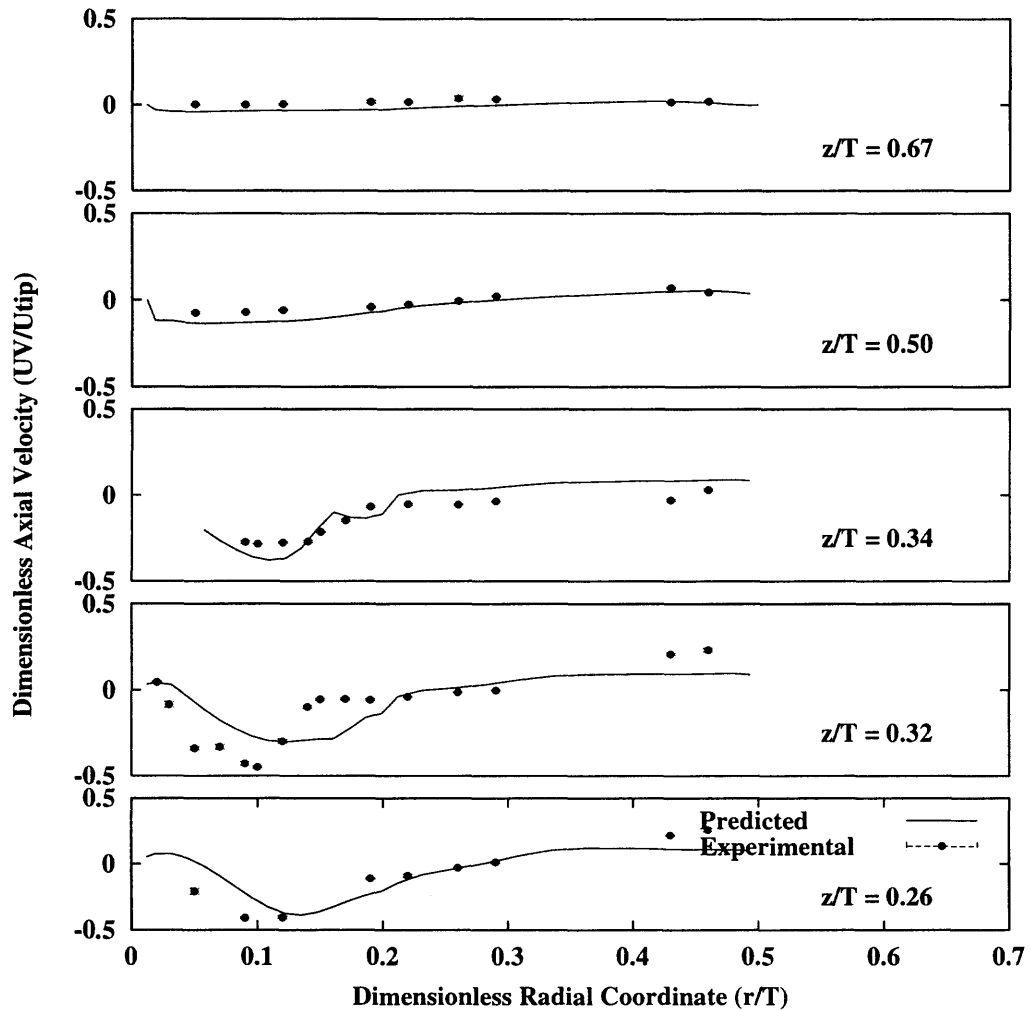
Figure 5.38: Stirred tank equipped with a pitched blade turbine at an impeller clearance of T/3: Comparison of experimental axial velocity data with CFD simulation in viscous medium.
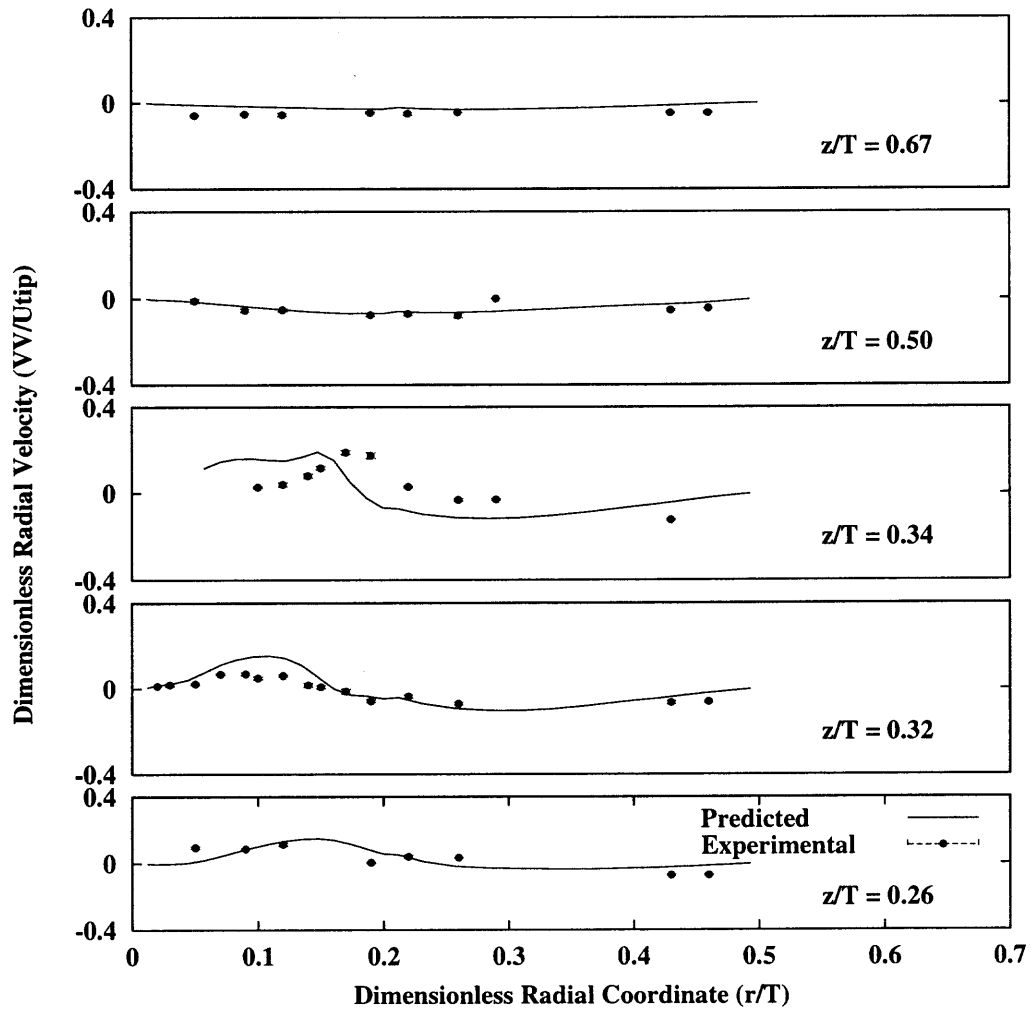
Figure 5.39: Stirred tank equipped with a pitched blade turbine at an impeller clearance of T/3: Comparison of experimental radial velocity data with CFD simulation in viscous medium.
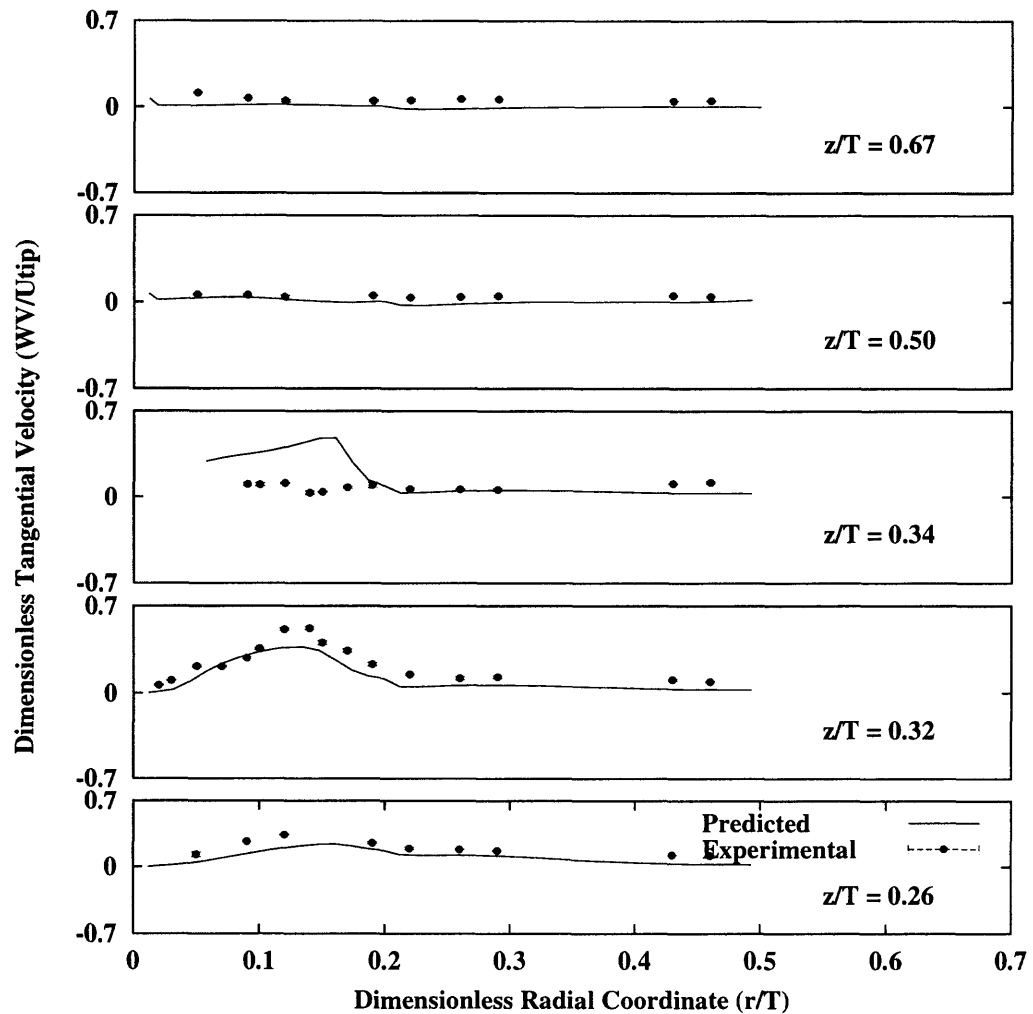
Figure 5.40: Stirred tank equipped with a pitched blade turbine at an impeller clearance of T/3: Comparison of experimental tangential velocity data with CFD simulation in viscous medium.
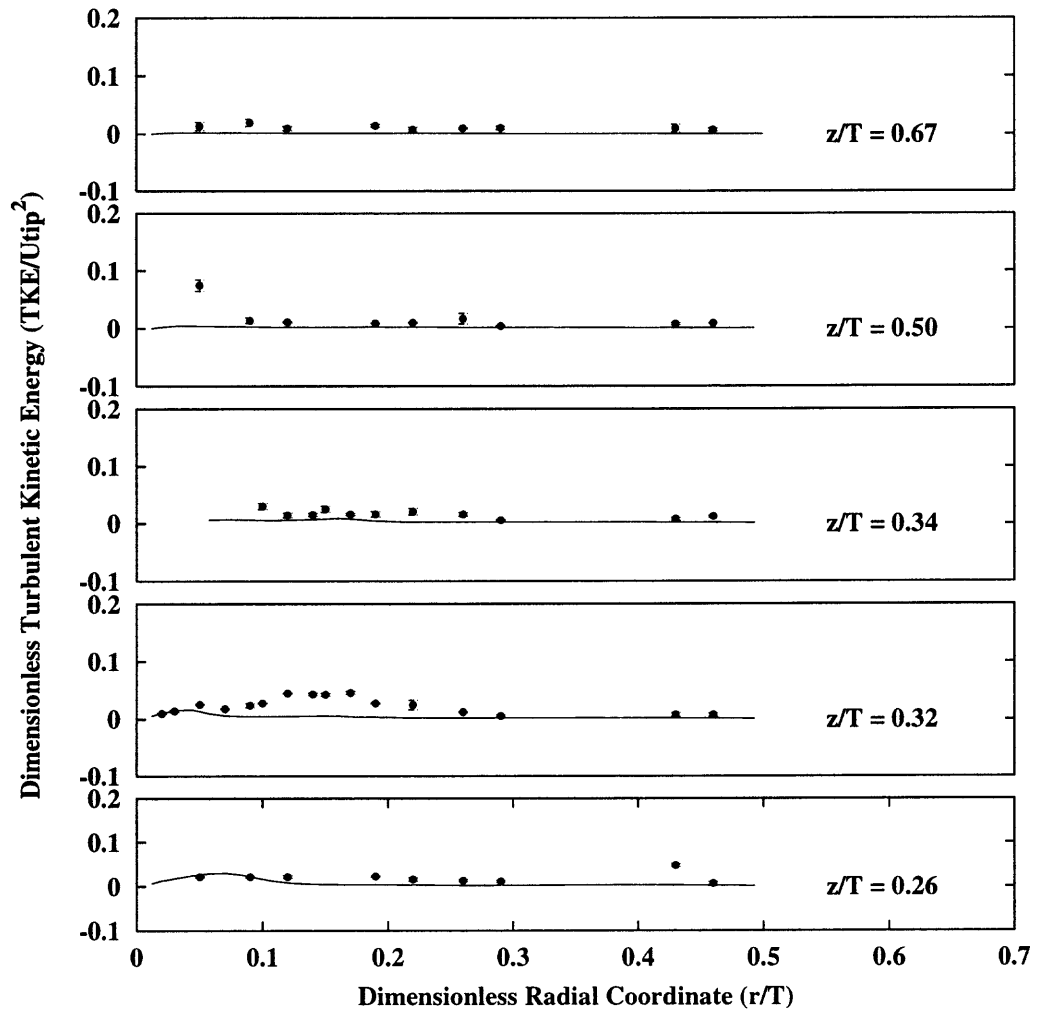
Figure 5.41: Stirred tank equipped with a pitched blade turbine at an impeller clearance of T/3: Comparison of experimental turbulent kinetic energy data with CFD simulation in viscous medium.

5.4.4 Remarks

The same trends observed for the aqueous medium are observed for the viscous medium as well. The CFD model is able to furnish without experimental input, a quantitative description of the turbulent flow field.

5.4.5 Power Consumption

Table 5.2 shows how the computed power consumption of the system compares with experimentally measured power, as well as that computed using published correlations. It is evident that the experimentally obtained values are in good agreement with those obtained from published correlations. The computed power using CFD is also close to the experimentally observed values, as well as the published correlations.

5.4.6 Comparison of Predicted Product Yields in Aqueous Medium with the Model

In this section, the predicted yields for the parallel competing reaction set detailed in Section 4.3 are compared with the experimentally obtained results. The feed locations simulated are locations Fs and Fs2 (near the liquid surface) and Fi (in the impeller suction stream) as outlined in Figure 4.7. Results obtained using both the standard E-Model as well as the modified E-Model are presented on each plot.

Before proceeding with the experimental phase of the study, it was necessary to experimentally determine the minimum feed time necessary for micromixing to be rate controlling as explained in Section 4.3. The results of this study are presented in Figure 5.42. After $\approx$ 50–60 minutes, the product yield was observed to be independent of the feed rate, thus the feed time employed for all subsequent simulations was taken to be 60 minutes.

In the following series of graphs (Figures 5.43 – 5.46) the concentration profile of the limiting reagent, sodium hydroxide, is shown as a function of time. The graphs are presented for a feed location near the liquid surface (Fs) and for one in the vicinity of the

Table 5.2: Power and mixing time characteristics for Systems B1 and B2

System	RPM	N_{Re}	Location	Reaction Time (s)	Mixing Time (s)	N_{Po}(Sim)	Po(Sim) (W)	N_{Po} (correl)	Po (correl,W)	N_{Po} (exp)	Po (exp,W)
B1	100	18481	Fs	2.90	20.21	0.75	0.04	1.50	0.069	0.67	0.04
	200	36963		2.55	10.11	0.81	0.32	1.50	0.554	1.29	0.50
	300	55444		1.60	6.74	0.78	1.03	1.50	1.870	1.24	1.62
	400	73926		1.05	5.05	0.76	2.37	1.50	4.432	1.30	4.16
	100		Fs2								
	200										
	300										
	400										
	100		Fi	1.45							
	200			0.54							
	300			0.39							
	400			0.36							
B2	100	2004	Fs	4.02		0.75	0.04			1.40	0.07
	200	4008		2.03		0.78	0.30			1.39	0.55
	400	8016		1.86		0.85	2.65			1.27	3.96
	100		Fi	3.84							
	200			1.26							
	400			1.05							
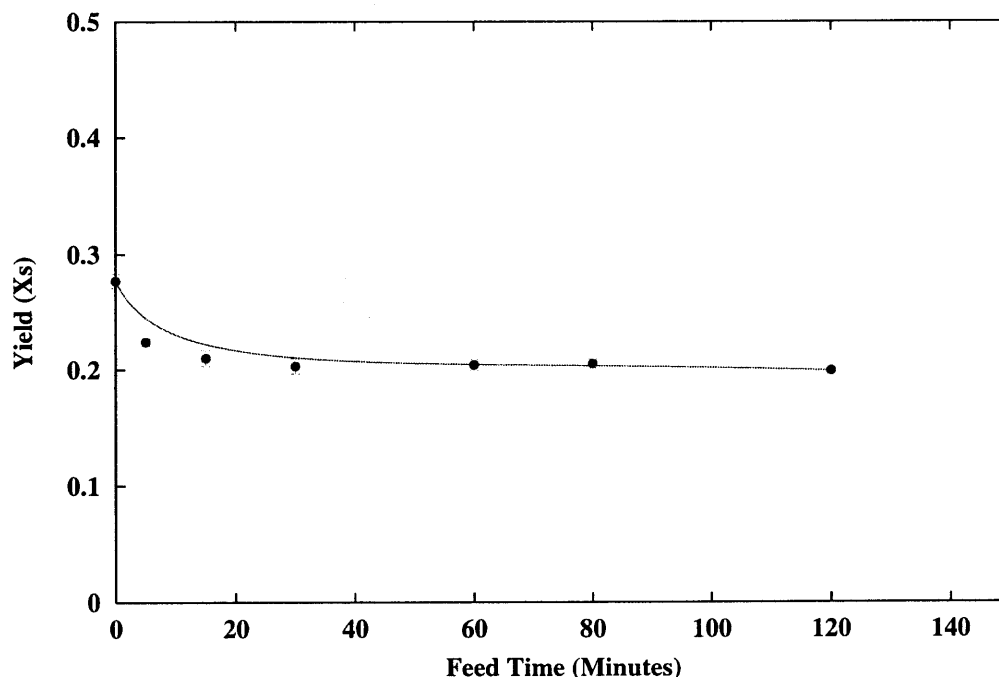
Figure 5.42: Variation of Product Yield with Feed Time for System B1. Feed Location Fs.

impeller (Fi), and for both micromixing models at the lowest agitation speed (100 rpm), and at the highest agitation speed used for this system (400 rpm).

Once again, it is evident that the two versions of the E-Model yield different time histories for the limiting reagent. The two-parameter E-Model consistently predicts a slower initial time history profile the the standard E-Model. As discussed earlier, this can be explained from the fact that the two-parameter E-Model includes information about the initial breakup of the reaction zone prior to engulfment (mesomixing).

These reaction times are much smaller than the time taken to homogenize the tank contents. A comparison of the mixing times with the reaction times is presented in Table 5.2.

The reaction times are observed to be faster at high agitation speeds than at lower ones as expected.
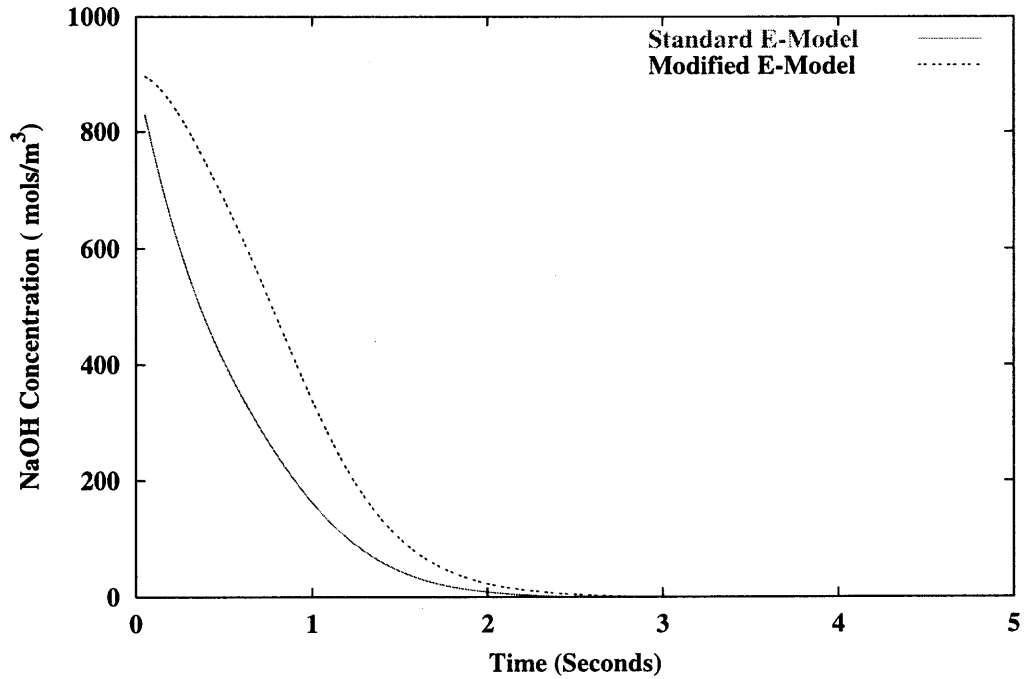
Figure 5.43: Reaction time for system B1 at 100rpm. Feed location Fs.
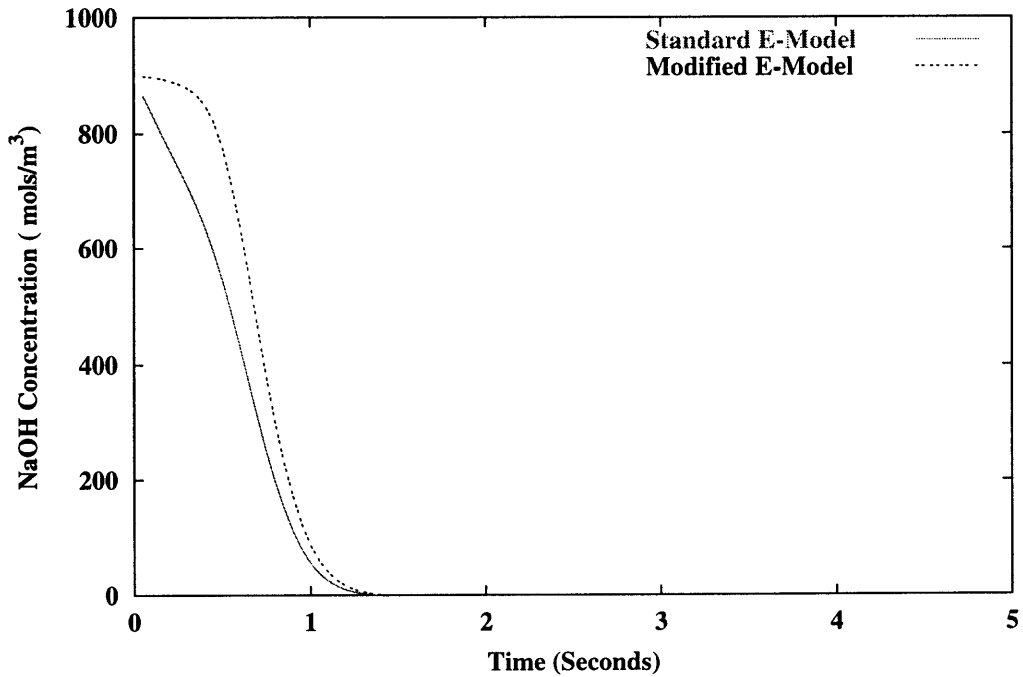
Figure 5.44: Reaction time for system B1 at 100rpm. Feed location Fi.
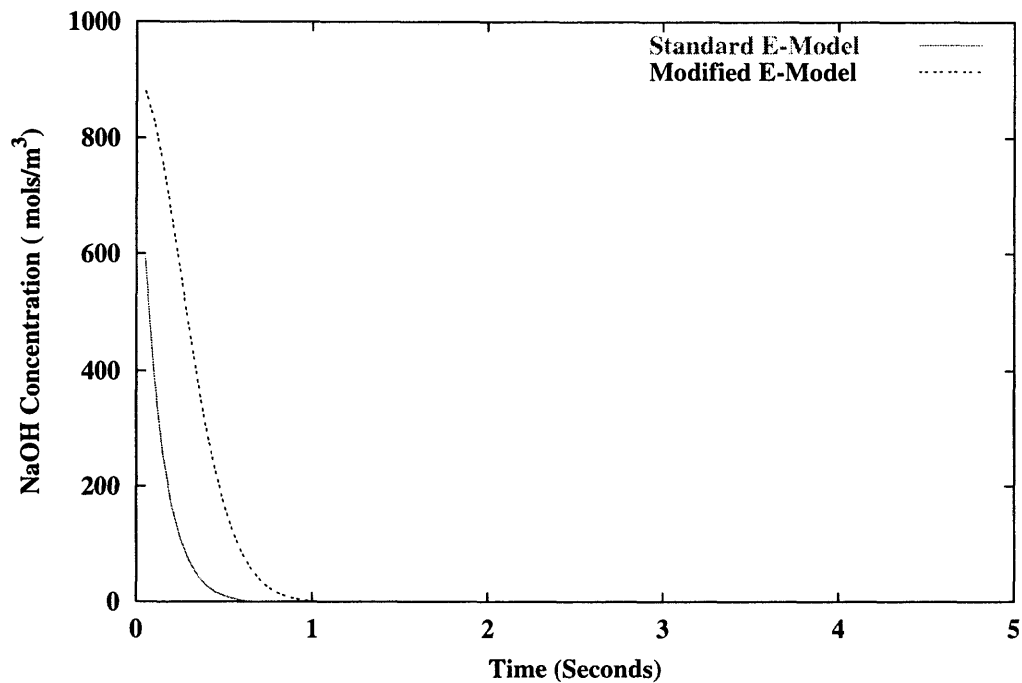
Figure 5.45: Reaction time for system B1 at 400rpm. Feed location Fs.
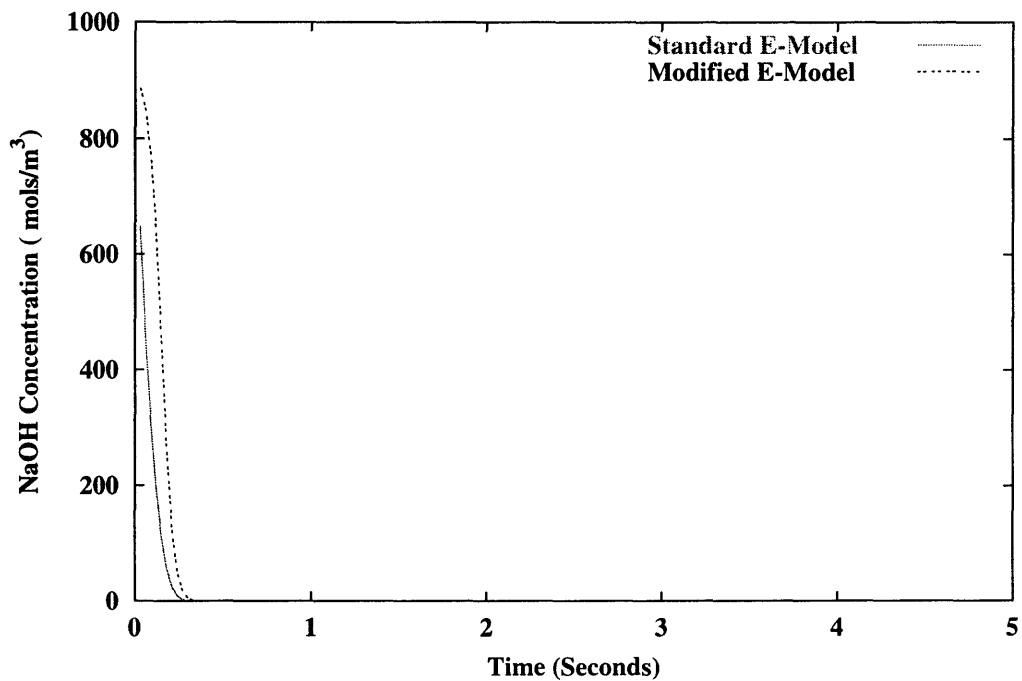
Figure 5.46: Reaction time for system B1 at 400rpm. Feed location Fi.

A comparison of the reaction zone trajectories shown in Figures 5.47 and 5.48, show that for the short reaction times under consideration, the reaction zone mostly retains its integrity. This means that the manner in which the model is used to account for the effects of mixing on the kinetics is adequate — the reactions are taking place in a segregated zone that is only a small part of the entire reactor volume.

The next series of plots (Figure 5.49 – Figure 5.51) show how the model performs at predicting the final product yields for the reaction system.

In all cases, the trends observed for System A1 and System A2, are observed here. The by-product yield decreases with increasing agitation rate. When the feed is introduced in the vicinity of the impeller, less by-product is formed than when the feed is introduced near the liquid surface. The role of turbulence is thus important in determining the outcome of the reactions.

Feed locations Fs (Figure 5.49) and Fs2 (Figure 5.50) yield similar results indicating that near the liquid surface, the level of turbulence is similar irrespective of the radial position. In both cases, the by-product yields are over predicted. A reflection of the fact that the turbulence was under predicted in the CFD simulation. The results are however most encouraging. In particular, it is evident that the modified E-Model does a better job of predicting the final product yield that the standard E-Model.

For feed location Fi (Figure 5.51, the model largely under predicts the final product yields, and the two micromixing models yield similar results. The results are nonetheless very encouraging.

5.4.7 Comparison of Predicted Product Yields in Viscous Medium with the Model

The results for System B2 are presented next. Experiments and simulations were carried out for feed location Fs. The trends observed for System B1 are observed for System B2 also. There are, however, differences that occur as a result of the difference in viscosities.

It was first necessary to determine the minimum feed time necessary to ensure that
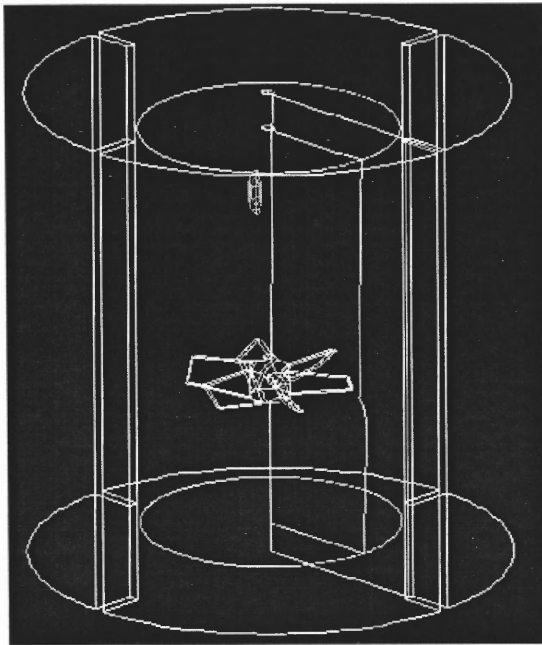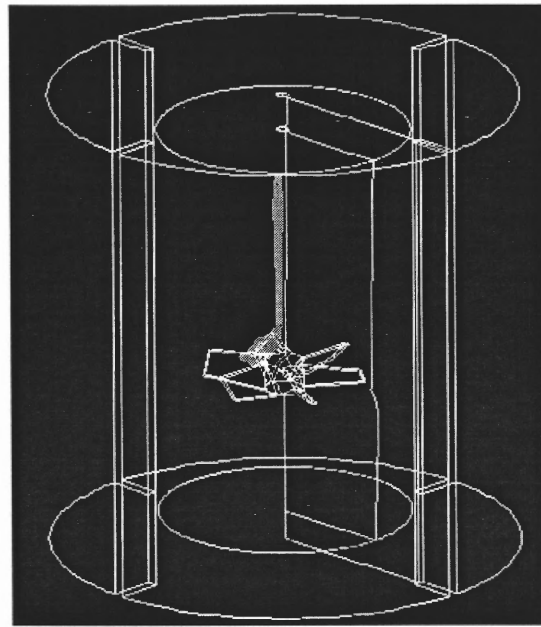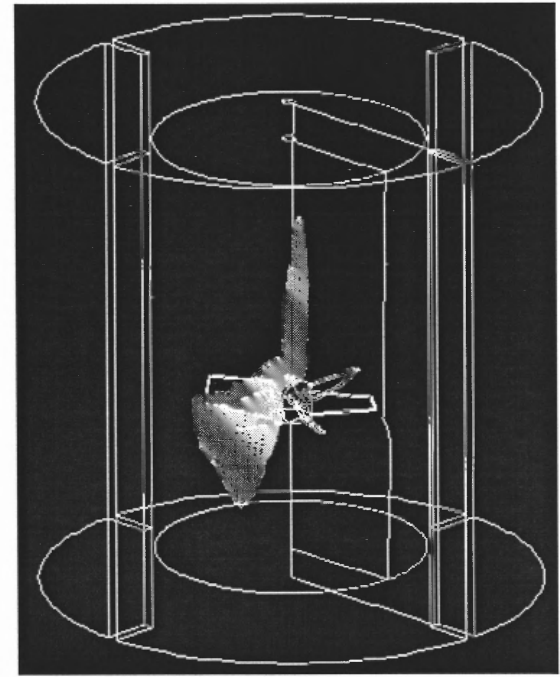
(a) t = 0.0 seconds   (b) t = 0.6 seconds   (c) t = 1.2 seconds

Figure 5.47: Reaction zone trajectory. System B1, feed near surface, 400rpm.
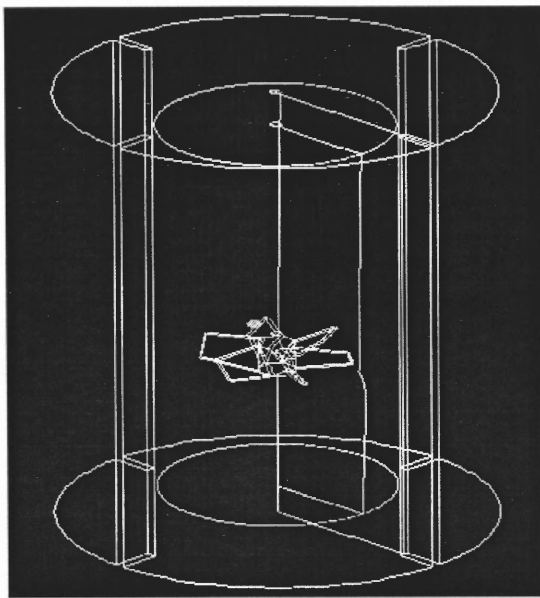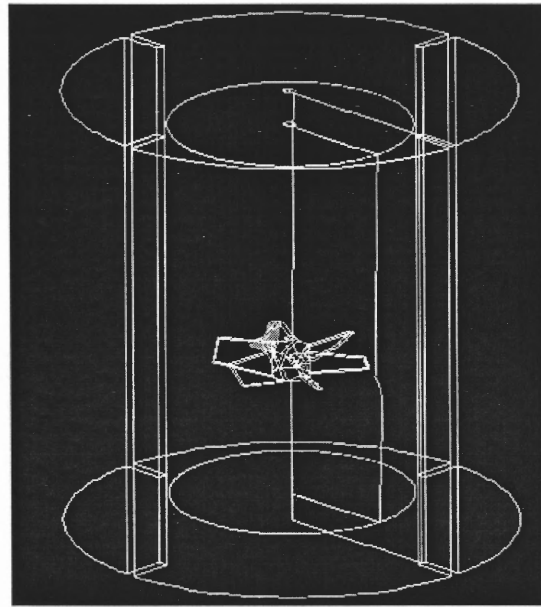
(a) t = 0.0 seconds   (b) t = 0.2 seconds   (c) t = 0.6 seconds
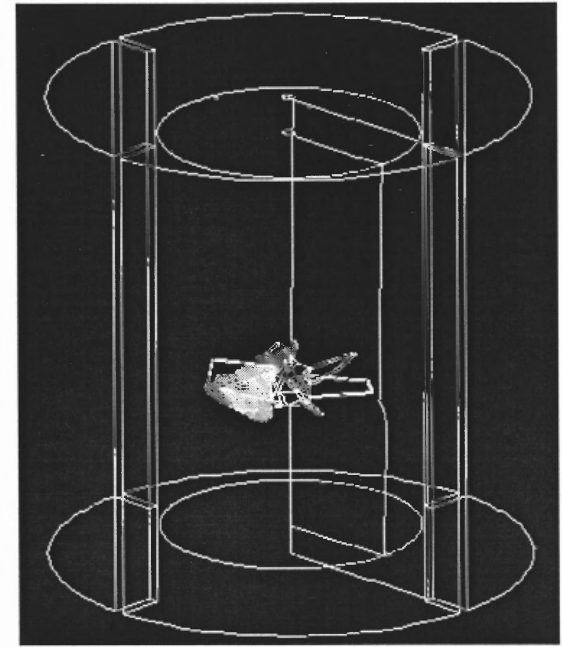
Figure 5.48: Reaction zone trajectory. System B1, feed above impeller, 400rpm.
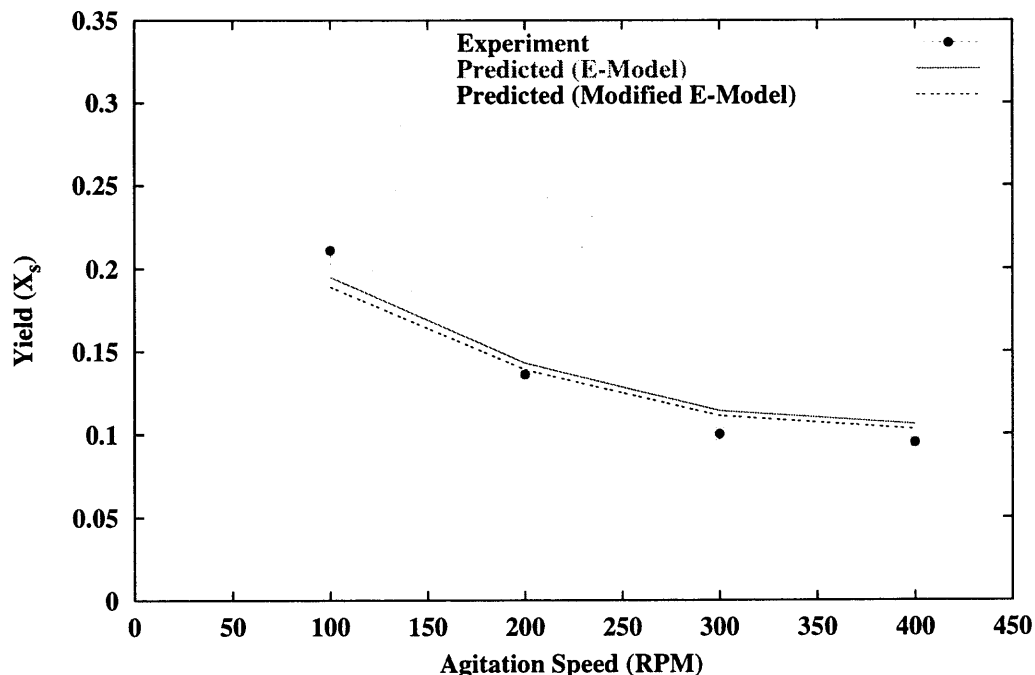
Figure 5.49: Variation of Product Yield with Agitation Speed for System B1. Feed Location Fs.

micromixing was the dominant mode of mixing. The results are presented in Figure 5.52. From these result a feed time of 60 minutes was used in all the experimental runs.

The data presented in Table 5.2 show that the power number for this system is largely constant and similar to that obtained for System B1. Using this fact and the arguments made earlier for System A2, we can assume that the flow for this system is turbulent.

The reaction time history plots (Figures 5.53 – 5.56) for this system exhibit the same trends as for System A1, A2 and B1. The complete set of results are presented in Table 5.2. The reaction times are longer for system B2 than for System B1. This results from the increase in viscosity which slows down the engulfment process, i.e. the engulfment parameter is decreased. Since engulfment strongly influences the kinetics, the overall reaction time is longer.
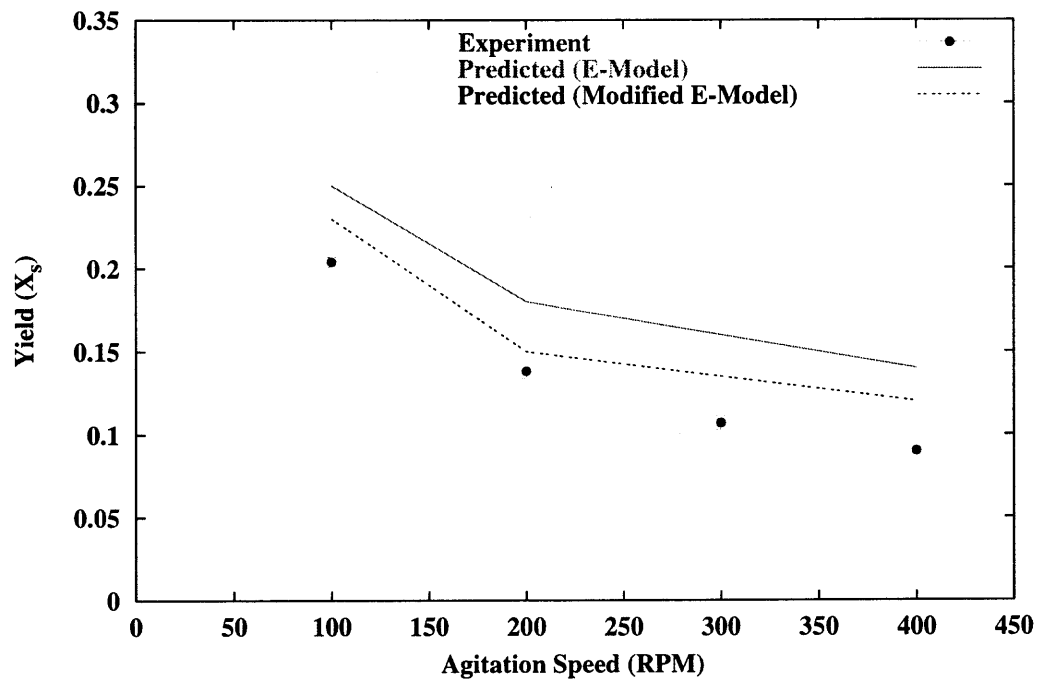
Figure 5.50: Variation of Product Yield with Agitation Speed for System B1. Feed Location Fs2.
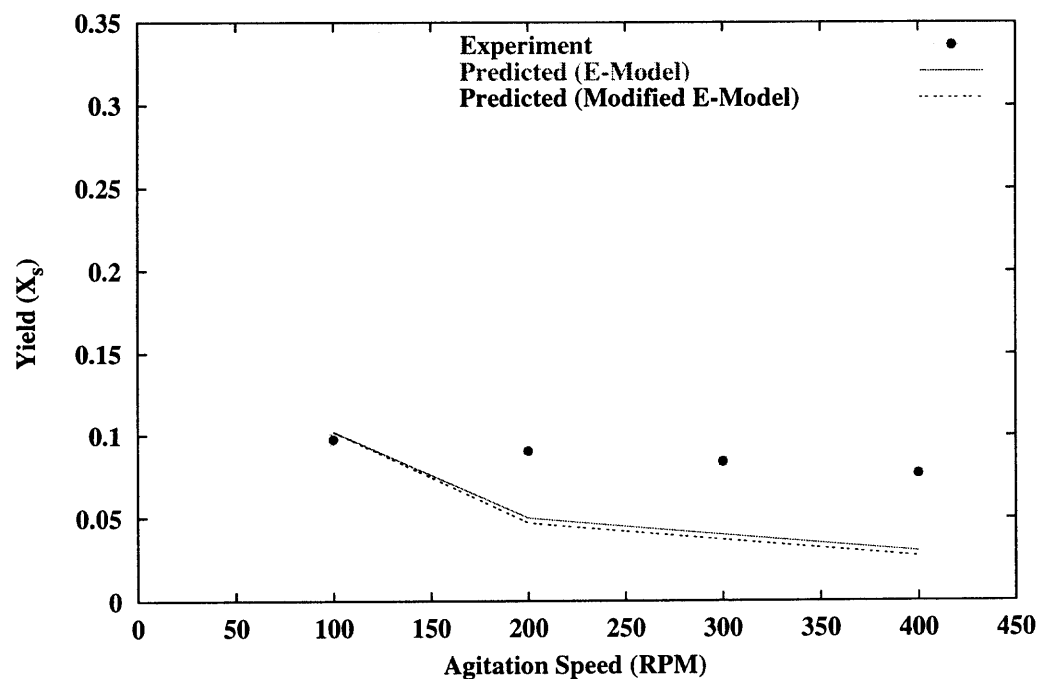
Figure 5.51: Variation of Product Yield with Agitation Speed for System B1. Feed Location Fi.
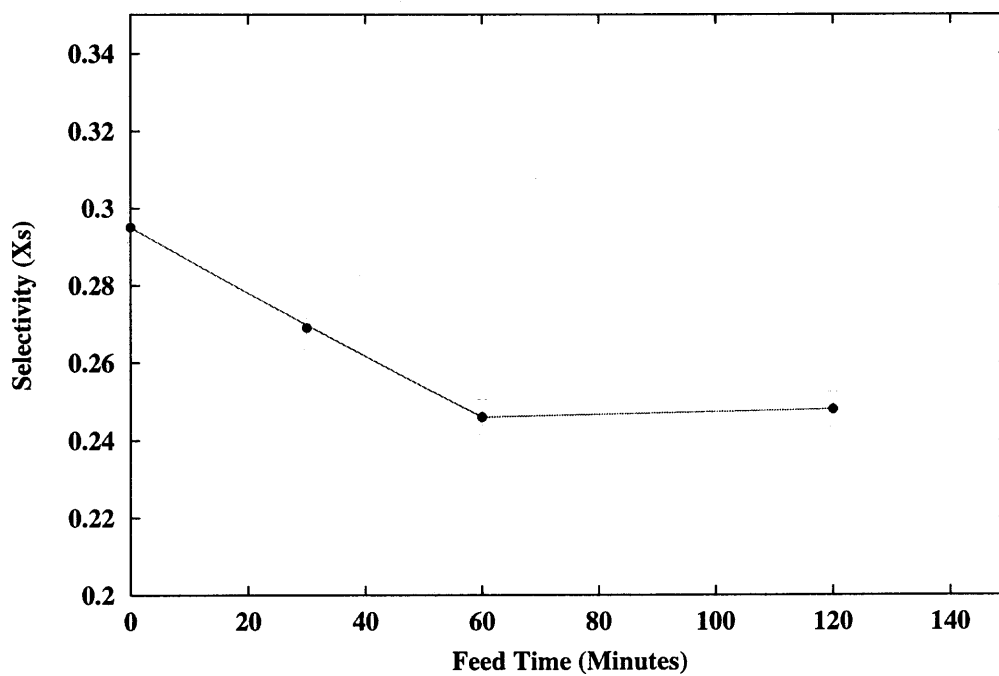
Figure 5.52: Variation of Product Yield with Feed Time for System B2
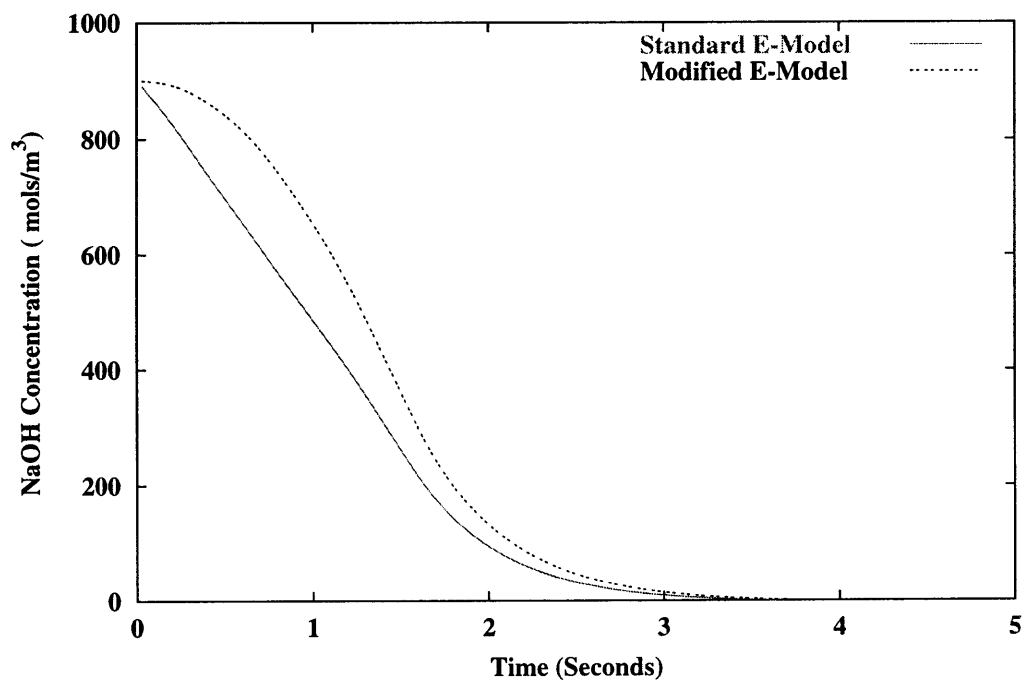
Figure 5.53: Reaction time for system B2 at 100rpm. Feed location Fs.
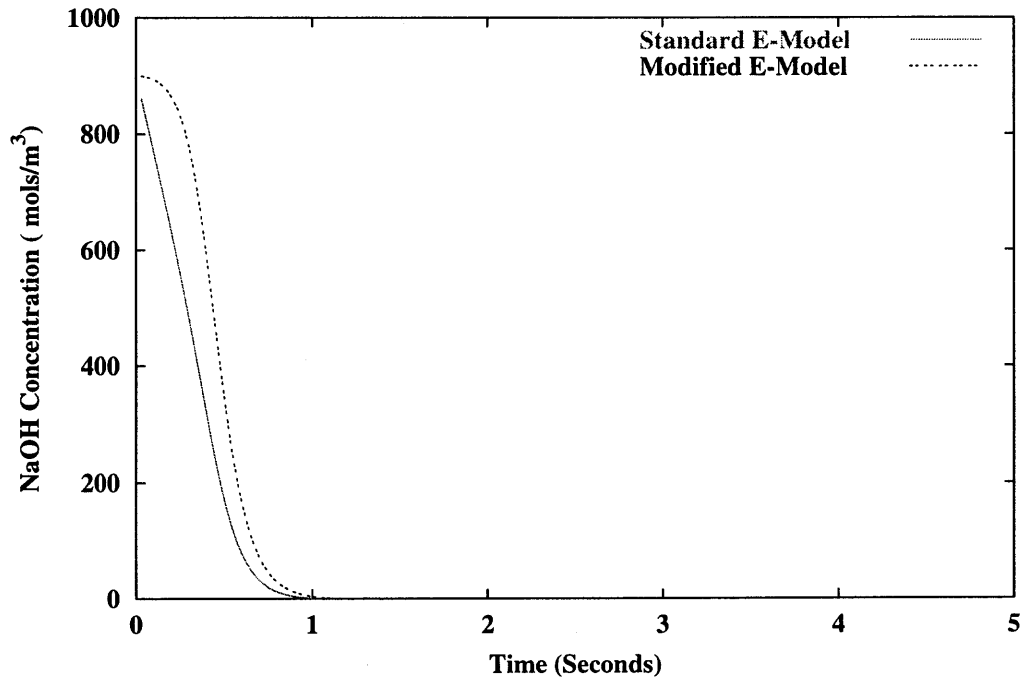
Figure 5.54: Reaction time for system B2 at 100rpm. Feed location Fi.
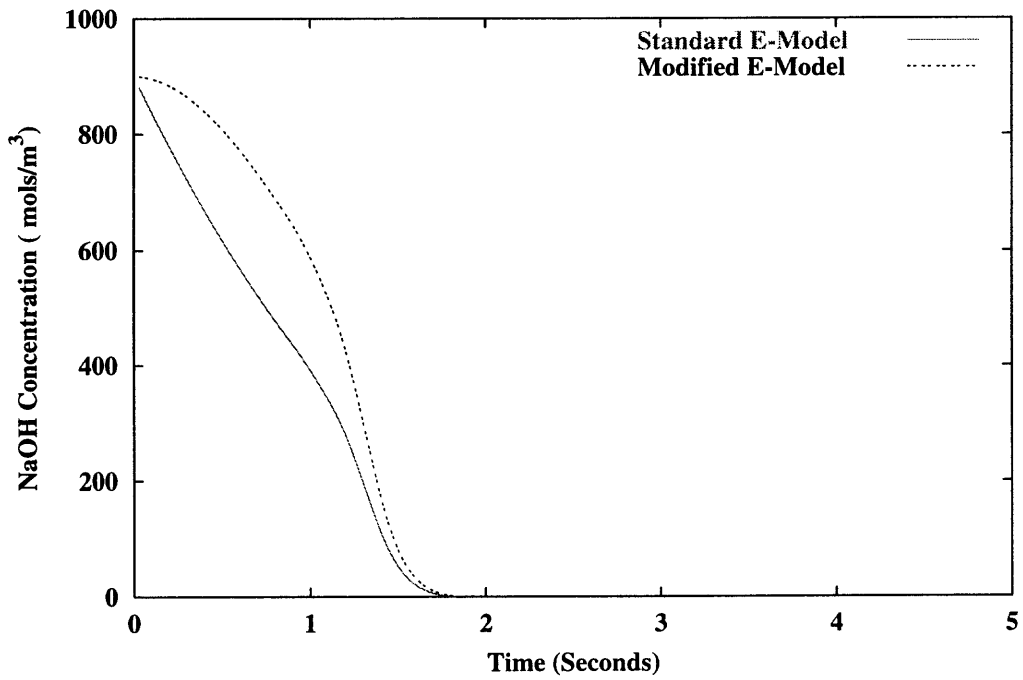
Figure 5.55: Reaction time for system B2 at 400rpm. Feed location Fs.
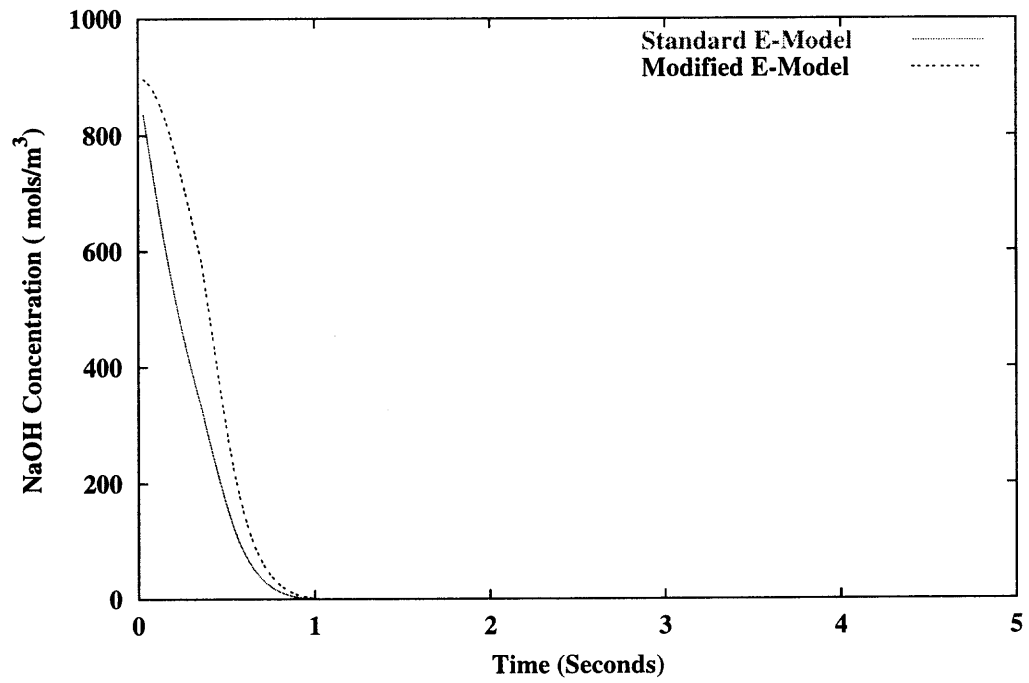
Figure 5.56: Reaction time for system B2 at 400rpm. Feed location Fi.

Shown next are plots showing the variation of the by-product yield with impeller agitation speed (Figures 5.57 – 5.58). The by-product yield was observed to decrease with increasing agitation speed. The model reasonably predicts the final product distributions. Both version of the E-Model yield very similar results. This could be explained by the fact that in the more viscous medium, the engulfment process is slower, and hence rate determining for the micromixing process. Thus mesomixing, even if it were present, would occur on a time scale much faster than mixing by engulfment and consequently would not influence the final product distribution significantly.
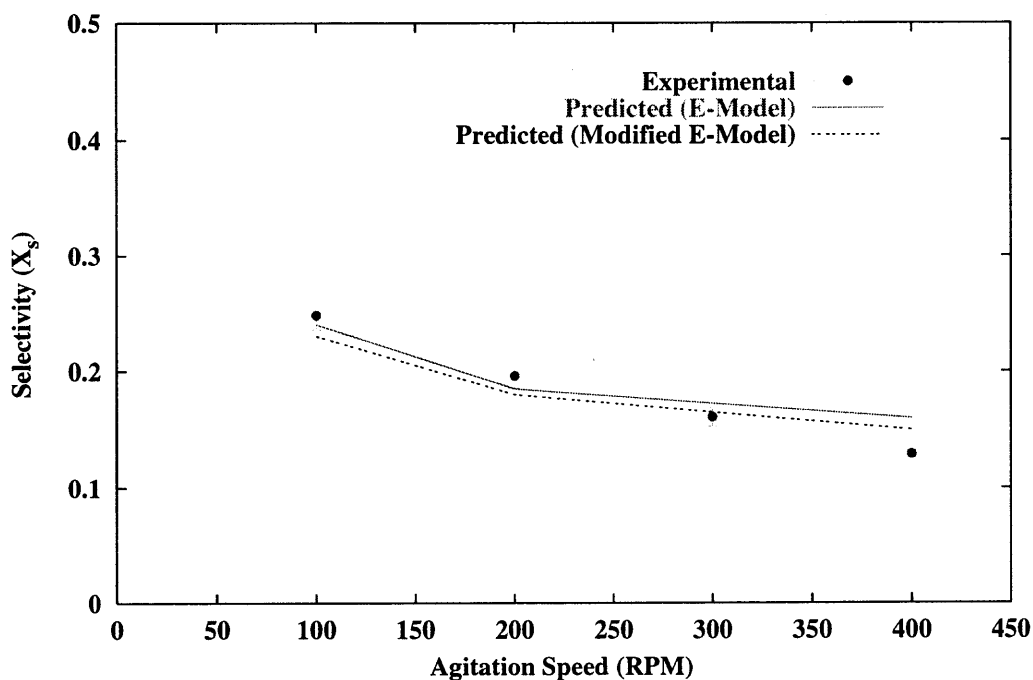
Figure 5.57: Variation of Product Yield with Agitation Speed for System B2. Feed Location Fs.

Increasing the fluid viscosity has the effect of increasing the yield of by-product. This result is consistent with established theory. Increasing the fluid viscosity results in a decrease in the rate of engulfment at the molecular level. This means that at microscopic scale local inhomogeneities persist for a longer time thereby permitting the slower side reaction to take place for a longer time before new material from the surrounding bulk is introduced.
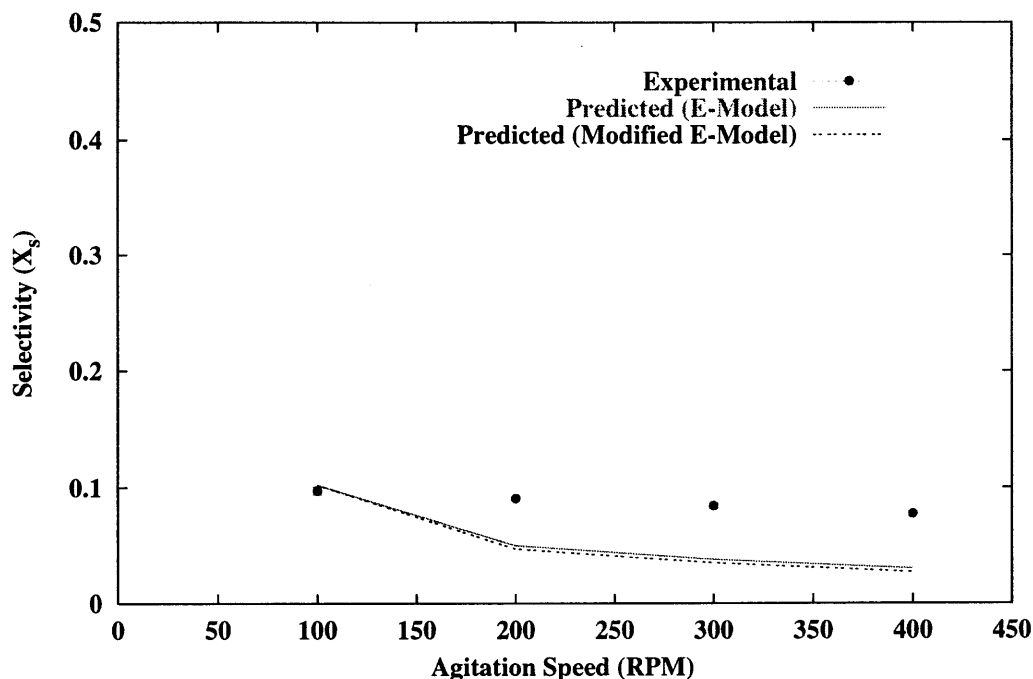
Figure 5.58: Variation of Product Yield with Agitation Speed for System B2. Feed Location Fs.

The result is a higher rate of by-product formation.

5.4.8 Comparison of System B1 and System B2

The product yields observed for System B2 (viscous medium) were observed to be higher that for System B1 (aqueous medium) when the same conditions and feed point were considered. In Figure 5.59, the results for feed location Fs (near the liquid surface) are superimposed for ease of comparison.

5.4.9 Remarks

The model was successfully used to predict the effect of mixing on the by-product yield for the reaction system under study. It is evident that increasing the fluid viscosity significantly impacts the kinetics and hence the formation of by-products.
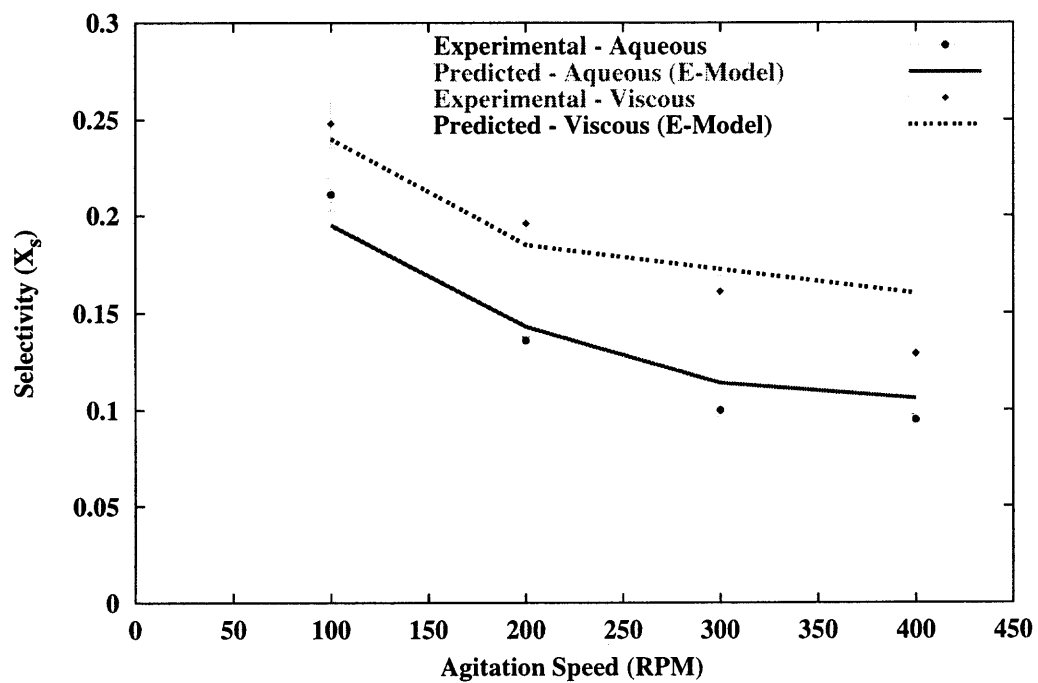
Figure 5.59: Comparison of System B1 and System B2: Feed location Fs.

5.5   Results for System C

Chemineer High Efficiency Impeller (HE-3): Impeller off Bottom Clearance C = T/3

The Chemineer High Efficiency impeller (HE-3) is a hydrofoil impeller. Hydrofoil impellers are popular for low viscosity applications because of their low power requirements and high pumping capacities. In this section, results are presented for a system fitted with a Chemineer HE-3 impeller. The system is configured as described in Table 1.2 and in Figure 4.6.

5.5.1   System Configuration

Prior to carrying out simulations involving the influence of mixing and turbulence on fast parallel competitive reactions, the flow field was simulated using CFD, and the simulation results verified using LDV. The system configuration and the axial locations in the vessel where the velocity profile was sampled using LDV are shown in Figure 5.60. Data was sampled in each of four quadrants and averaged. This was done because the combination of the three impeller blades and the four baffles on the tank results in a system that is non symmetrical, thus there was no repeating cyclic geometry to exploit.

The tank geometry used for the CFD simulations are presented in Figures 5.61 – 5.62. In Figure 5.62 a cross-section of the tank showing the mesh details is shown. A fine grid as described in Chapter 3 was used as this was necessary to capture as much of the flow detail as possible.

In Figure 5.61 and Figure 5.62 a region around the impeller is outlined. This is the MRF zone. The region in the computational domain that is solved in a moving reference frame. For a axial impeller such as the HE-3, this region does spans most of the height of the tank because the flow generated by the impeller is primarily axial.

Figure 5.63 shows a snapshot of the velocity profile for a simulation carried out at 300 rpm. The velocity vectors shown are the resultant velocity vectors for the axial, radial

z/T = 0.67

z/T = 0.52

z/T= 0.34

z/T = 0.32

z/T = 0.26

Data from each of four planes
midway between the baffles was
sampled and averaged
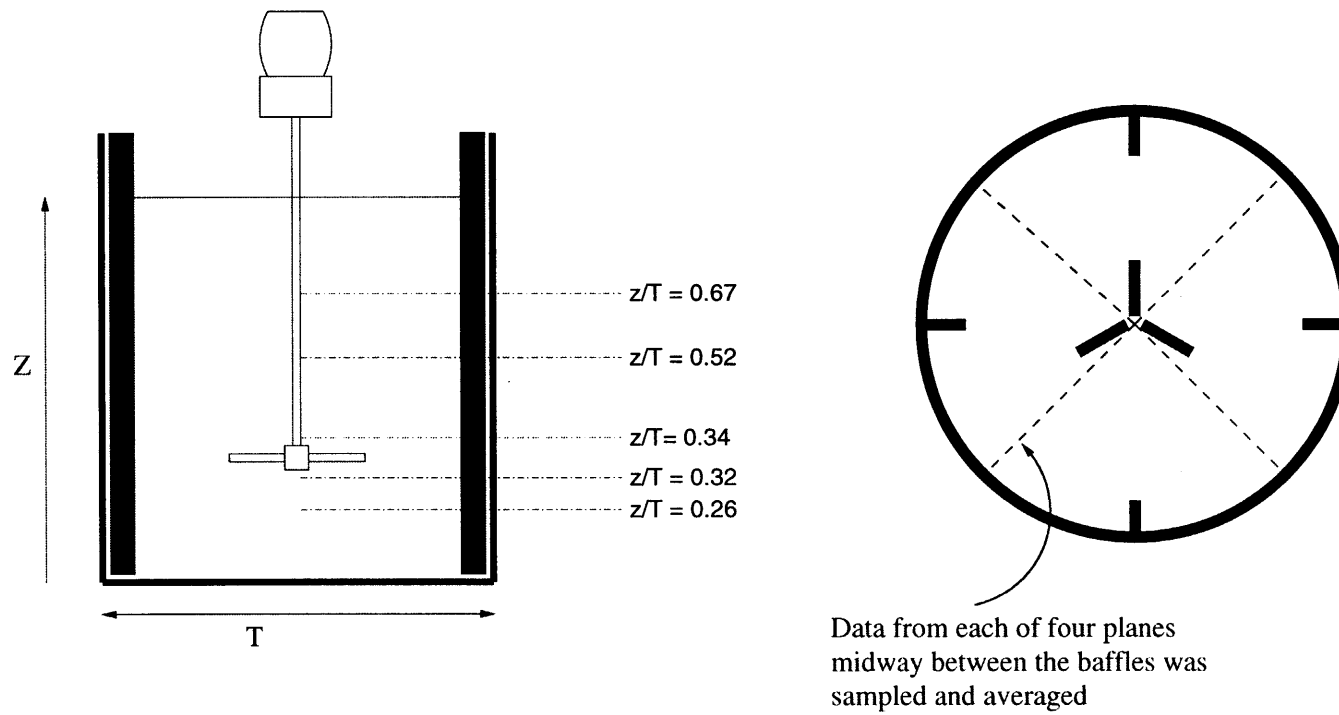
Figure 5.60: Stirred tank equipped with a Chemineer High Efficiency impeller at a clearance of T/3: Locations where LDV data was taken.

Modified 3D Geometry Grid	Apr 08 2000
Outline	Fluent 4.52
	Fluent Inc.
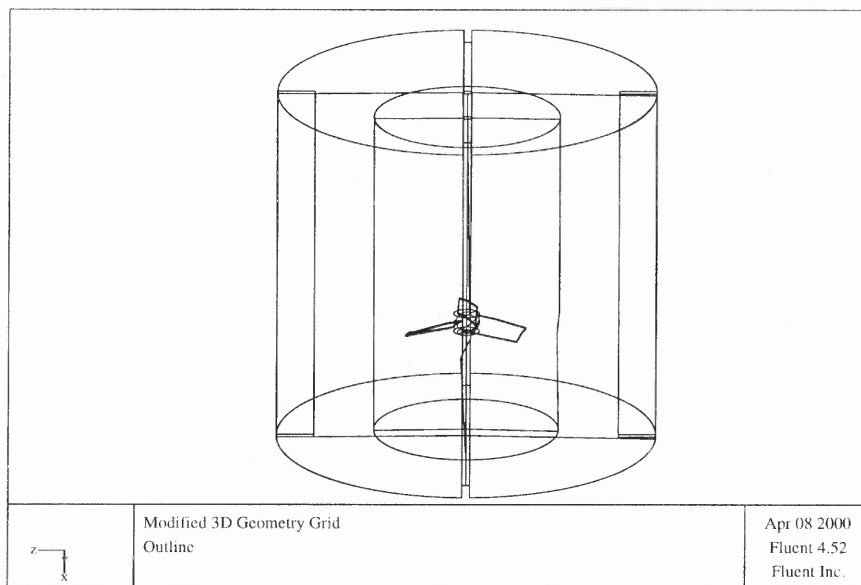
Figure 5.61: Stirred Tank Equipped with a Chemineer High Efficiency Impeller at an impeller clearance of T/3: Outline grid.

Modified 3D Geometry Grid	Apr 08 2000
Grid (145 X 32 X 82)	Fluent 4.52
Slices: I=36, I=111	Fluent Inc.
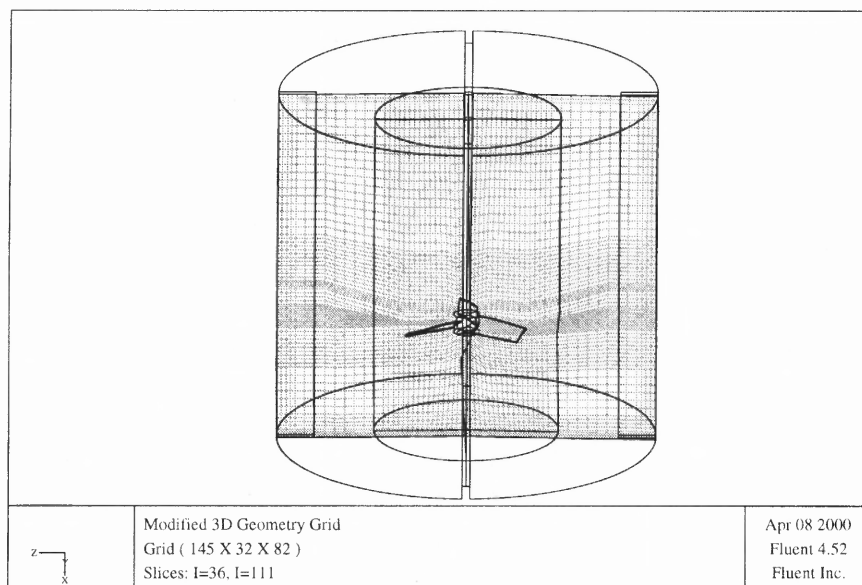
Figure 5.62: Stirred tank equipped with a Chemineer High Efficiency impeller at an impeller clearance of T/3: Outline grid showing mesh details.

and tangential directions. The velocity profile shown is typical of what one would expect from an axial flow impeller. A turbulent jet is generated from the impeller and impinges on the tank base. Two main circulation loops are evident. One on each side of the impeller. Thus from a qualitative perspective, the simulation captures the main features of the turbulent flow generated by the HE-3.

5.5.2   Comparison of LDV Data with FLUENT CFD Simulations

The LDV data was taken on a system with an impeller agitation speed of 330rpm and compared with data from the numerical simulation.

The HE-3, like the PBT, produces two main circulation loops as shown in Figure 5.63. Near the tank wall along the entire length of the vessel axial velocities are positive as the fluid is moving up. Near the shaft and above and below the impeller, the axial velocities are negative as the fluid returns to the impeller and is pumped away towards the tank base. These trends are reflected by the data. Near the top of the tank, the flow is more horizontal and "quiet". This trend has been observed by other investigators of similar systems (Jaworski et al. 1996).

Because the flow produced by the HE-3 is primarily axial in nature, the radial components of the velocity are expected to be low. This is evidenced by the simulation and verified by experiment as Figure 5.65 shows.

The results show that near the impeller shaft and along the height of the tank, swirling motion is evident. This swirling motion dies out near the tank walls. The tangential component is still small in magnitude in comparison to the axial component of the velocity. The agreement between the predicted values and the experimentally derived ones is good.

Near the top of the vessel the profiles of turbulent kinetic energy are flat. Closer to the impeller, higher values are observed. The agreement between the experimental values and the predicted values is satisfactory.

	8.10E-01
	7.82E-01
	7.54E-01
	7.27E-01
	6.99E-01
	6.71E-01
	6.44E-01
	6.16E-01
	5.88E-01
	5.61E-01
	5.33E-01
	5.05E-01
	4.78E-01
	4.50E-01
	4.22E-01
	3.94E-01
	3.67E-01
	3.39E-01
	3.11E-01
	2.84E-01
	2.56E-01
	2.28E-01
	2.01E-01
	1.73E-01
	1.45E-01
	1.18E-01
	8.99E-02
	6.22E-02
	3.45E-02
	6.80E-03

	Modified 3D Geometry Grid	Jun 09 2000
z—y, x	Velocity Vectors (M/S)	Fluent 4.52
	Lmax = 8.098E-01 Lmin = 6.804E-03	Fluent Inc.
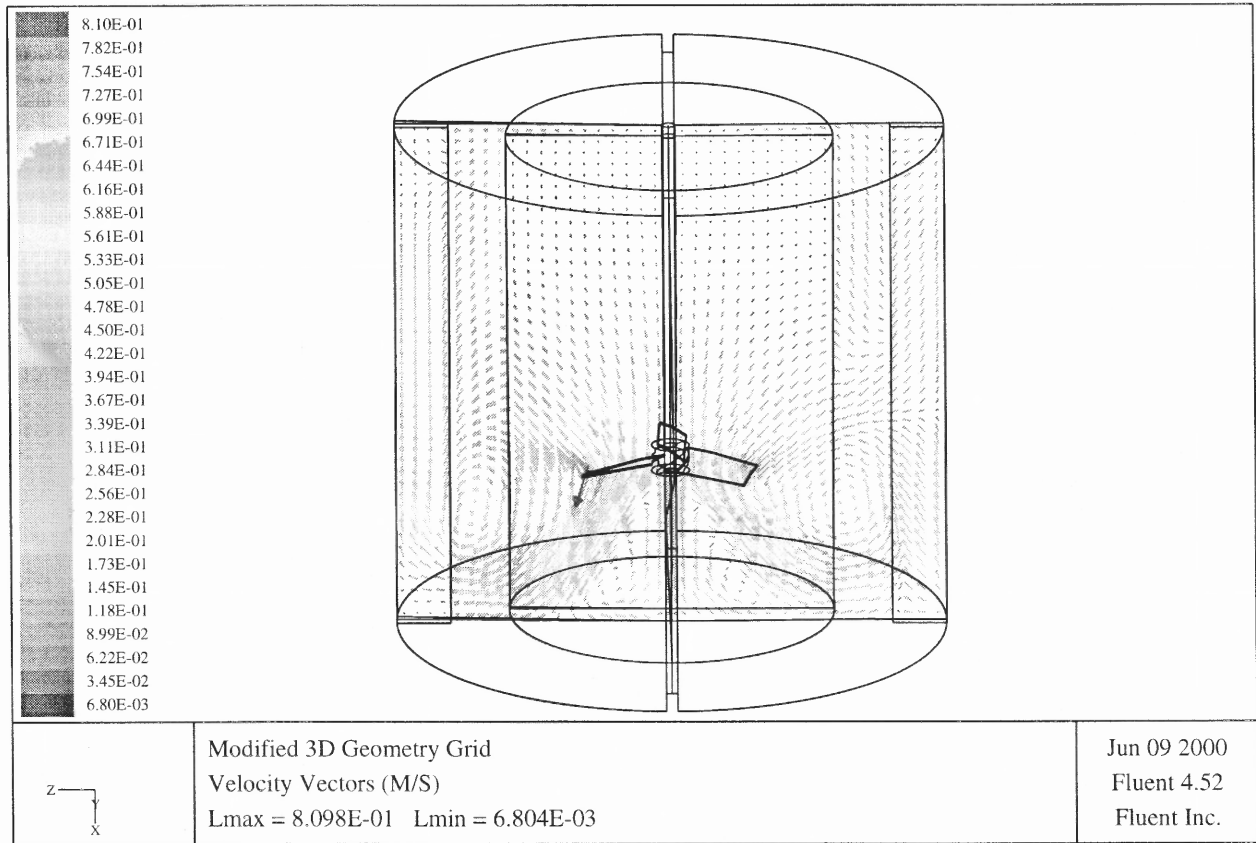
Figure 5.63: Stirred Tank Equipped with a Chemineer High Efficiency Impeller at an impeller clearance of T/3: Velocity profile.
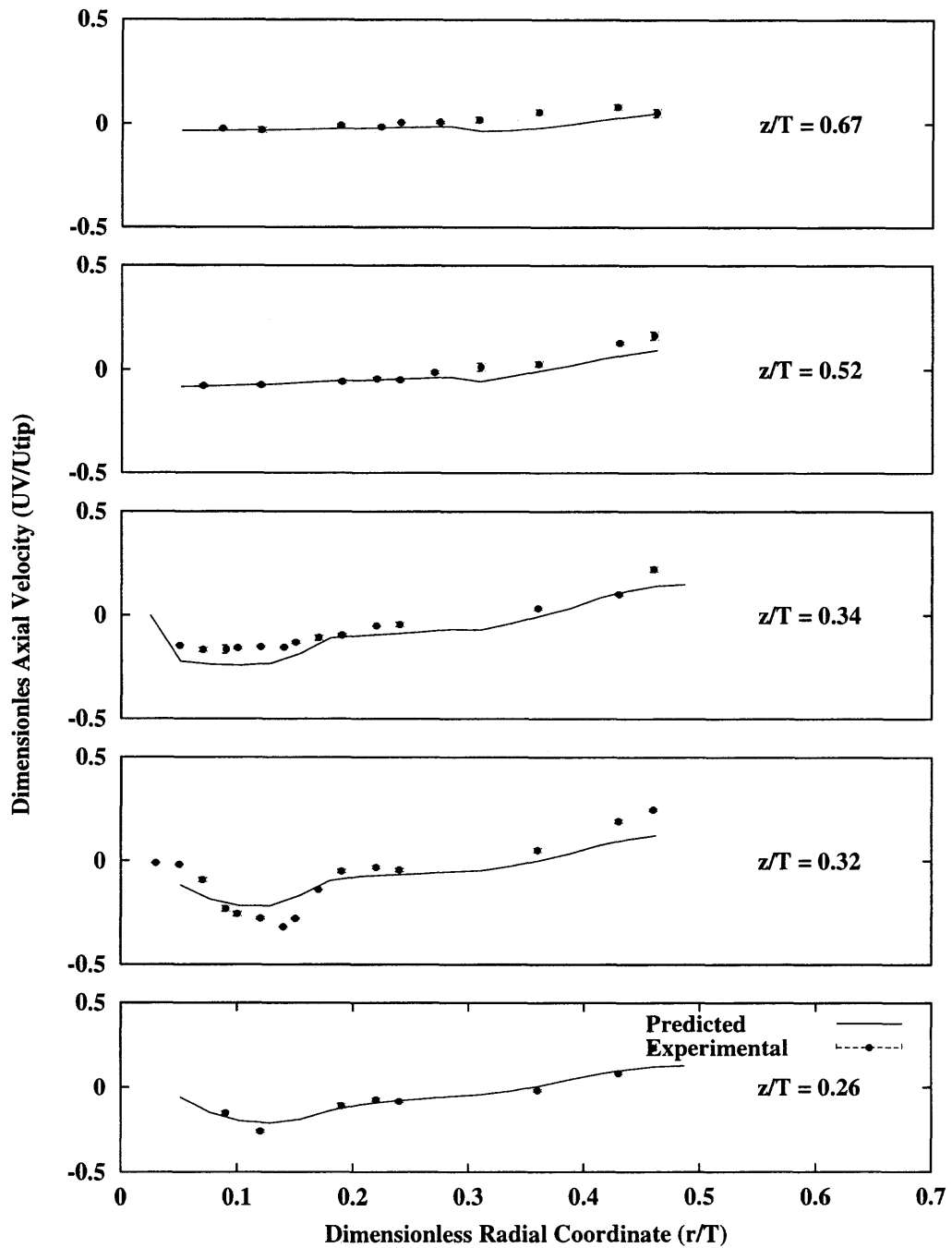
Figure 5.64: Stirred Tank equipped with a Chemineer High Efficiency impeller at an impeller clearance of T/3: Comparison of experimental axial velocity data with CFD simulation.
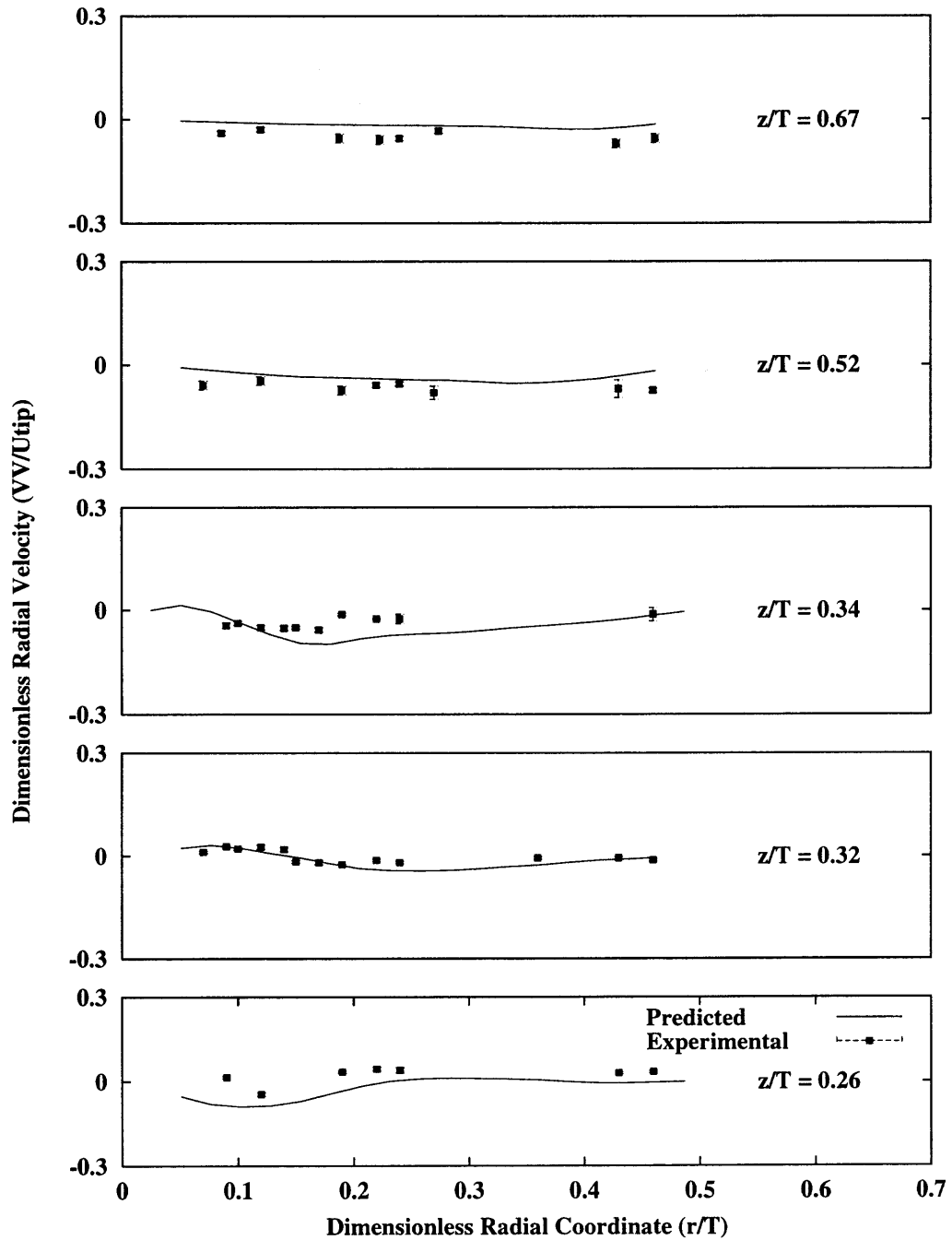
Figure 5.65: Stirred tank equipped with a Chemineer High Efficiency impeller at an impeller clearance of T/3: Comparison of experimental radial velocity data with CFD simulation.
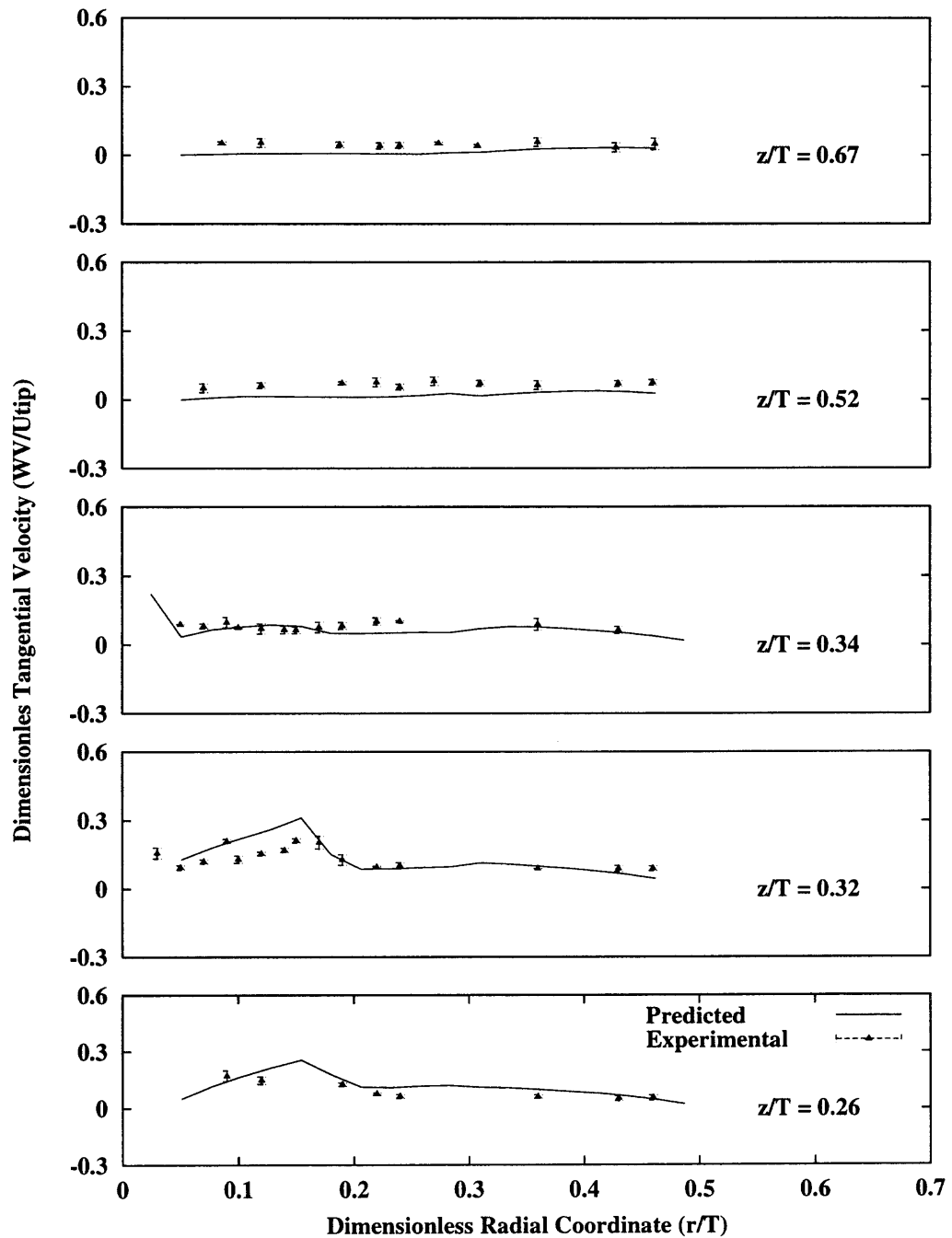
Figure 5.66: Stirred tank equipped with a Chemineer High Efficiency impeller at an impeller clearance of T/3: Comparison of experimental tangential velocity data with CFD simulation.
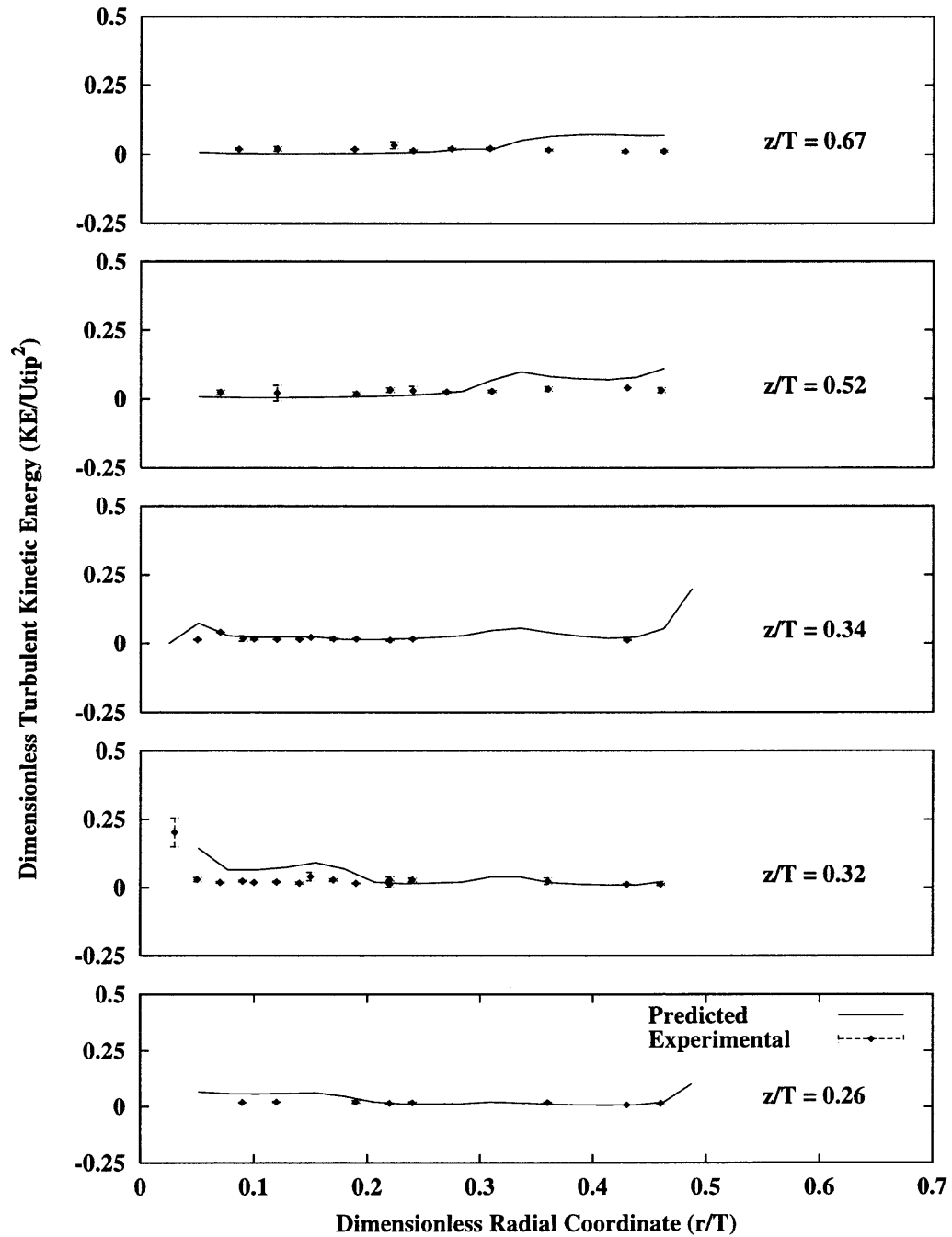
Figure 5.67: Stirred Tank Equipped with a Chemineer High Efficiency Impeller at an Impeller Clearance of T/3: Comparison of Experimental Turbulent Kinetic Energy Data with CFD Simulation.

5.5.3 Power Consumption

Table 5.5.3 shows how the computed power consumption of the system compares with experimentally measured power values presented in the literature. It is evident that the experimentally obtained values are in close agreement with those obtained from published correlations. The computed power using CFD is also close to the experimentally observed values, as well as the published correlations. In Table 5.5.3, some of the experimental data are annotated with an asterisk. These are data points that could not be accurately sampled because the signal produced by the strain gauges was extremely low for the system used. These data points should thus be regarded with the understanding that they may not be altogether accurate.

5.5.4 Remarks

The CFD model captures the main features of the turbulent velocity field generated by the HE-3. Numerical discrepancies exist, but the results are overall satisfactory.

5.5.5 Comparison of Predicted Product Yields with the Model

In this section results are presented to show how well the model is able to predict the final by-product distribution for System C.

The first step in the experimental investigation of the influence of mixing on the reaction kinetics, was the determination of the minimum feed time to ensure that micromixing was rate controlling. The results of this study are presented in Figure 5.68. From the results, it was determined that a feed time of at least 90 minutes was necessary to ensure that the reactions were conducted in a micromixing controlled regime. Thus a feed time of 90 minutes was used for all the experimental runs.

In the following series of graphs (Figures 5.69 – 5.72) the concentration profile of the limiting reagent, sodium hydroxide, is shown as a function of time. The graphs are

Table 5.3: Power and mixing time results for System C

System	RPM	N_{Re}	Location	Reaction Time $t_{99.99}$(s)	Mixing Time t_{99} (s)	N_{Po}(Sim)	Po(Sim) (W)	N_{Po} (correl)	Po (correl,W)	N_{Po} (exp)	Po (exp,W)
C	100	18481	Fs	2.710	61.51	0.19	0.01	0.28	0.013	0.93*	0.05*
	200	36963		1.240	30.76	0.27	0.11	0.28	0.104	0.48*	0.19*
	300	55444		1.000	20.5	0.32	0.51	0.28	0.352	0.34	0.44
	400	73926		0.675	15.38	0.39	1.22	0.28	0.834	0.35	0.108
	100		Fi	1.940							
	200			0.615							
	300			0.425							
	400			0.395							
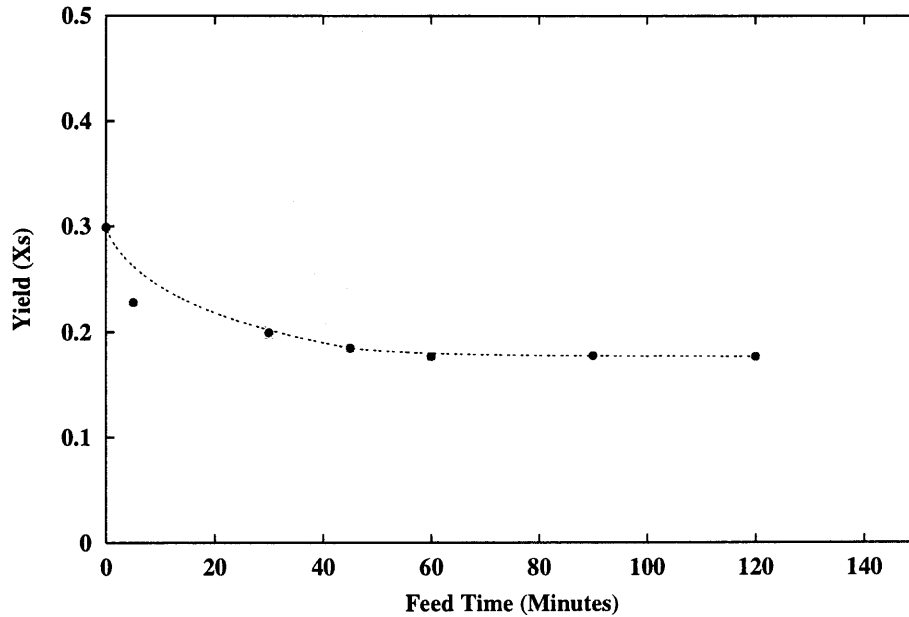
Figure 5.68: Variation of Product Yield with Feed Time for the HE-3

presented for a feed location near the liquid surface (Fs) and for one in the vicinity of the impeller (Fi), and for both micromixing models at the lowest agitation speed (100 rpm), and at the highest agitation speed used for this system (400 rpm). The complete set of results are presented in Table 5.5.3.

It is evident that the two versions of the E-Model yield different time histories for the limiting reagent. The two-parameter E-Model consistently predicts a longer time history profile the the standard E-Model. As discussed earlier, this can be explained from the fact that the two-parameter E-Model includes information about the initial breakup of the reaction zone prior to engulfment (mesomixing).

The incorporation of mesomixing into the model results in a longer overall reaction time. These reaction times are however much smaller than the time taken to homogenize the tank contents. A comparison of the mixing times with the reaction times is presented in Table 5.5.3.

The reaction times are observed to be faster at higher agitation speeds than at lower ones as expected. In comparison to System B1, the time taken to deplete the limiting reagent is

similar.
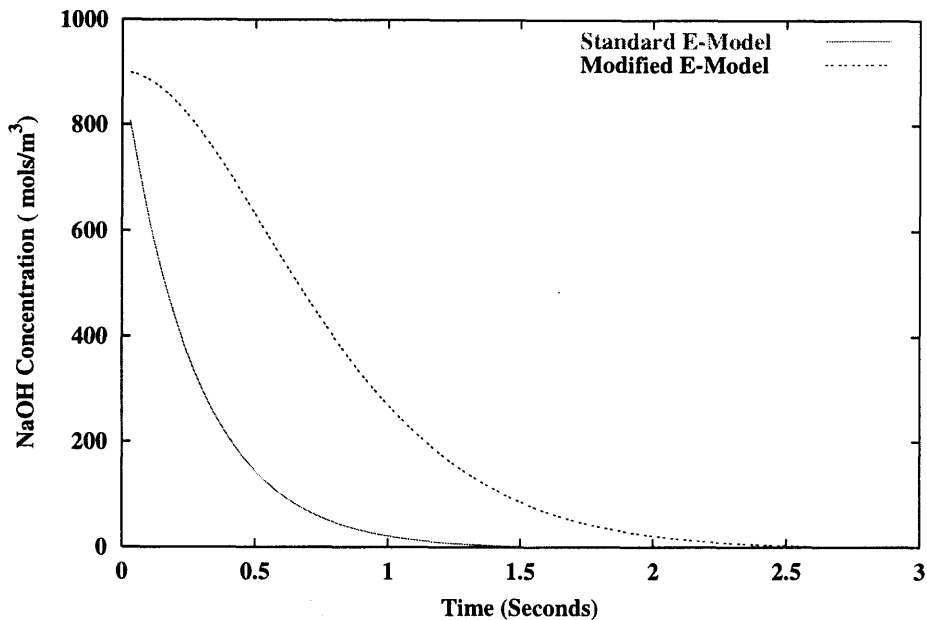
Figure 5.69: Reaction profile for system C at 100rpm. Feed location Fs.
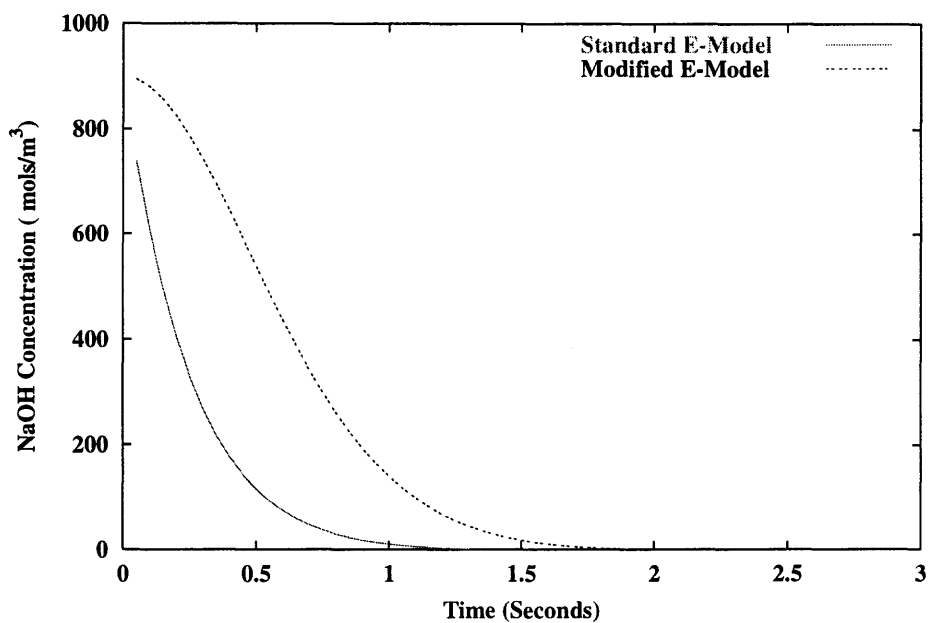
Figure 5.70: Reaction profile for system C at 100rpm. Feed location Fi.
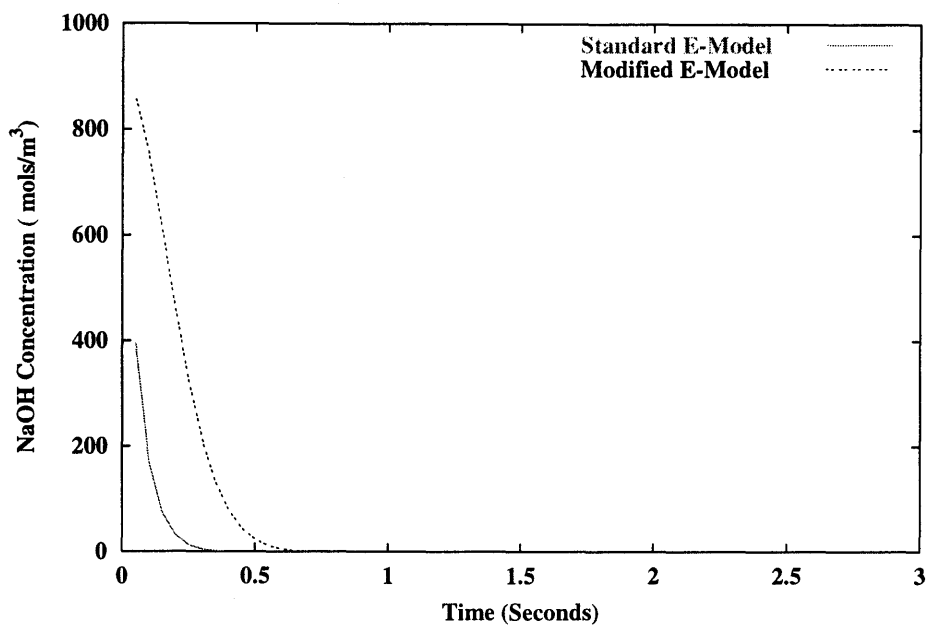
Figure 5.71: Reaction time for system C at 400rpm. Feed location Fs.
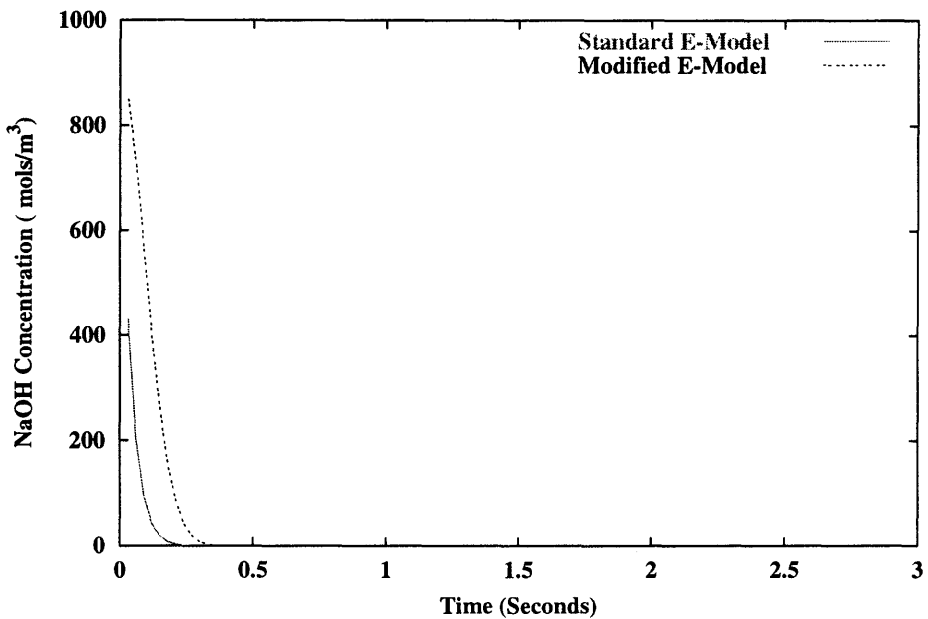
Figure 5.72: Reaction time for system C at 400rpm. Feed location Fi.

The next series of plots (Figure 5.73 and Figure 5.74) show how well the model performs at predicting the final product yields for the reaction system.

In both cases, the trends observed earlier, are observed here. The by-product yield decreases with increasing agitation rate. When the feed is introduced in the vicinity of the impeller less by-product is formed than when the feed is introduced near the liquid surface.

It is evident here that the modified E-Model does a better job of predicting the final product yield that the standard E-Model, in particular for the feed point Fs.
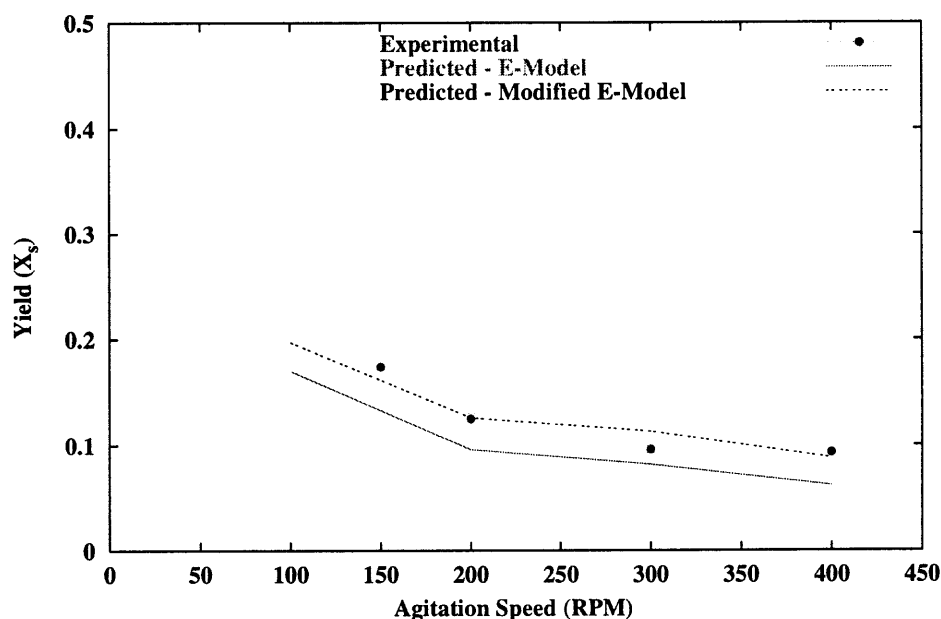
Figure 5.73: Variation of by-product yield with agitation speed for the HE-3. Feed location Fs.

5.5.6 Remarks

The model was successfully used to predict the effect of mixing on the by-product yield for the reaction system under study.
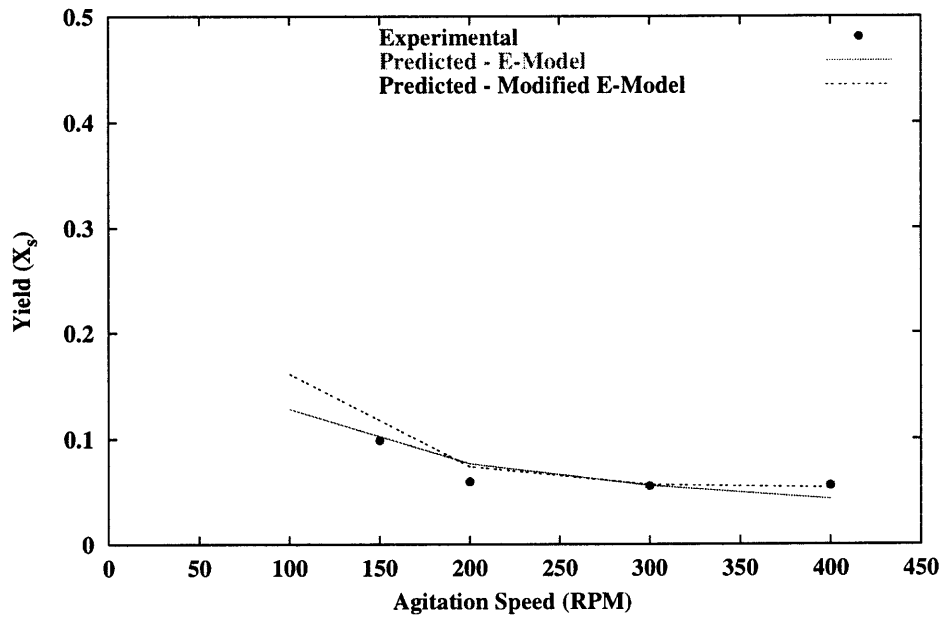
Figure 5.74: Variation of by-product yield with agitation speed for the HE-3. Feed location Fi.

5.6   Results for System D

Rushton Turbine: Impeller off Bottom Clearance C = T/2

Systems D consists of a baffled cylindrical vessel fitted with a Rushton turbine, such as Systems A1, A2. The difference between System D and the others lies in the fact that in system D, the impeller was placed at an impeller off bottom clearance of T/2 rather than T/3. The system details are summarized in Table 1.2 and in Figure 4.6.

5.6.1   System Configuration

Prior to carrying out simulations involving the influence of mixing and turbulence on fast parallel competitive reactions, the flow field was simulated using CFD and the simulation results verified using LDV. The system configuration and the axial locations in the vessel where the velocity profile was sampled using LDV are shown in Figure 5.75.

The tank geometry used for the CFD simulations are presented in Figures 5.76 – 5.77. In Figure 5.77 a cross-section of the tank showing the mesh details is shown. The mesh around the impeller is extremely fine so as to capture as much of the flow detail as possible. It was also necessary to use a fine mesh at the tank wall because the fluid flow from the radial impeller impinges at the tank wall and creates a secondary source of turbulent flow there. The manner whereby this was done is outlined in Chapter 3.

5.6.2   Comparison of LDV Data with FLUENT CFD Simulations

LDV data was taken on a system with an impeller agitation speed of 300rpm. The CFD data presented here is for simulations carried out at 300rpm. As shown earlier, the Rushton impeller produces four main circulation loops as shown in Figure 5.78. The axial velocity results are presented in Figure 5.79. For this particular configuration, the loops are equal due to the system symmetry. Near the tank wall and above the impeller the axial velocities are positive as the fluid is moving up. Near the shaft and above the impeller, the axial
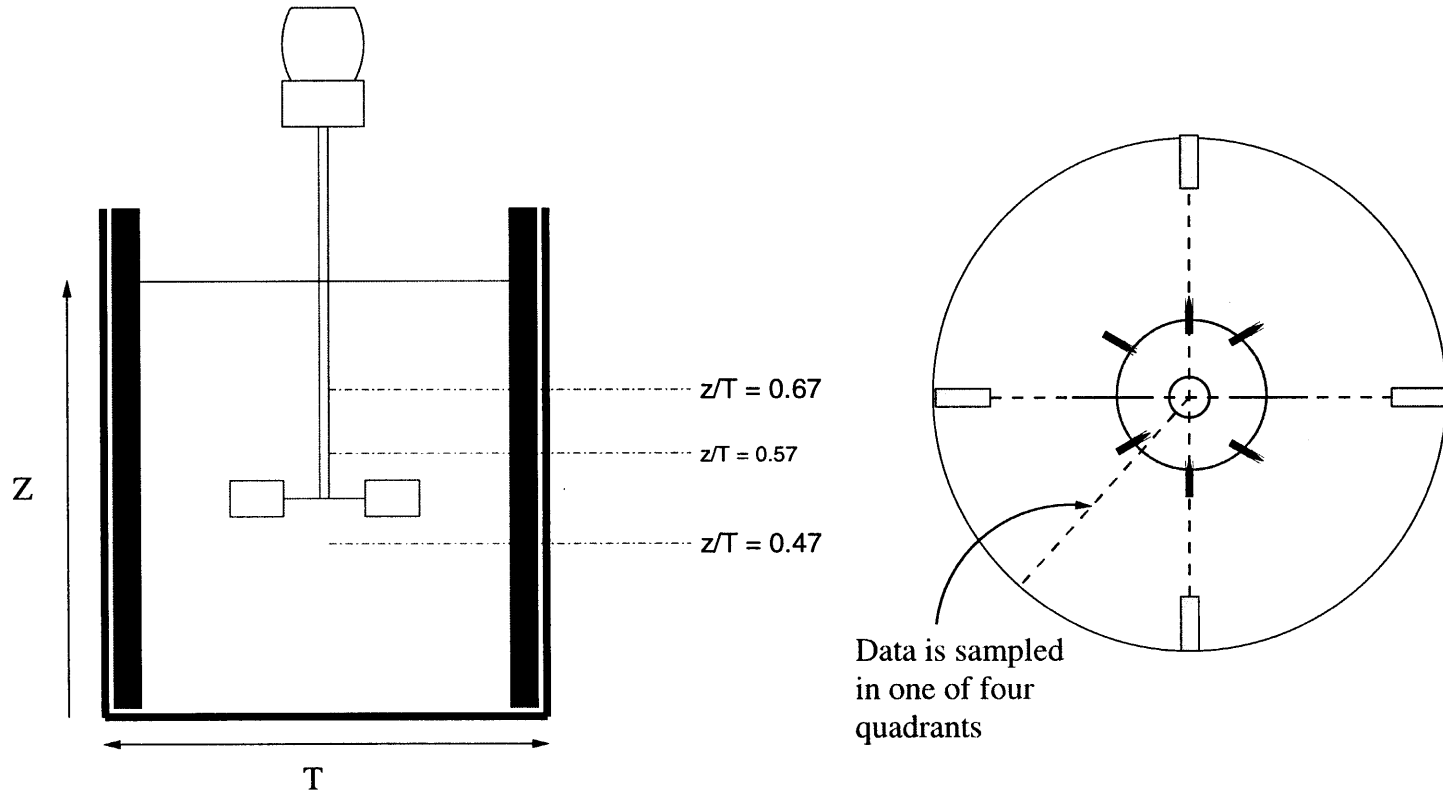
Figure 5.75: Stirred tank equipped with a Rushton turbine at an impeller clearance of T/2: Locations where LDV data was taken.

x	Modified 3D Geometry Grid	Apr 08 2000
z	Outline	Fluent 4.52
		Fluent Inc.
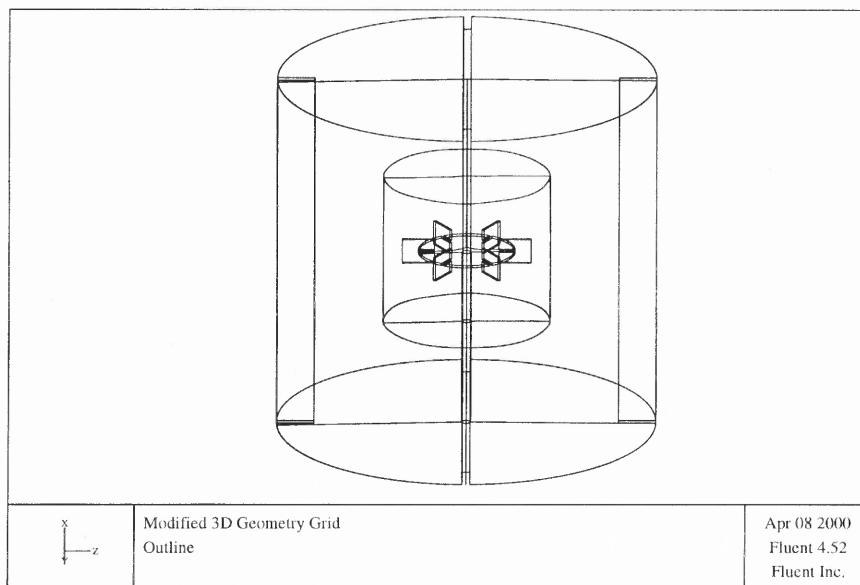
Figure 5.76: Stirred tank equipped with a Rushton turbine at an impeller clearance of T/2: Outline grid.

x	Modified 3D Geometry Grid	Apr 08 2000
z	Grid (145 X 38 X 96)	Fluent 4.52
	Slices: I=36, I=111	Fluent Inc.
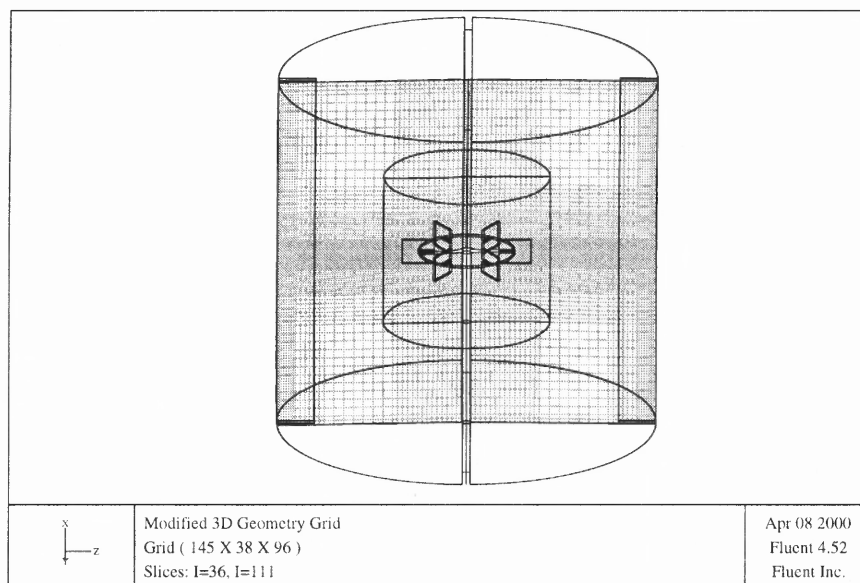
Figure 5.77: Stirred Tank equipped with a Rushton turbine at an impeller clearance of T/2: Outline grid showing mesh details.
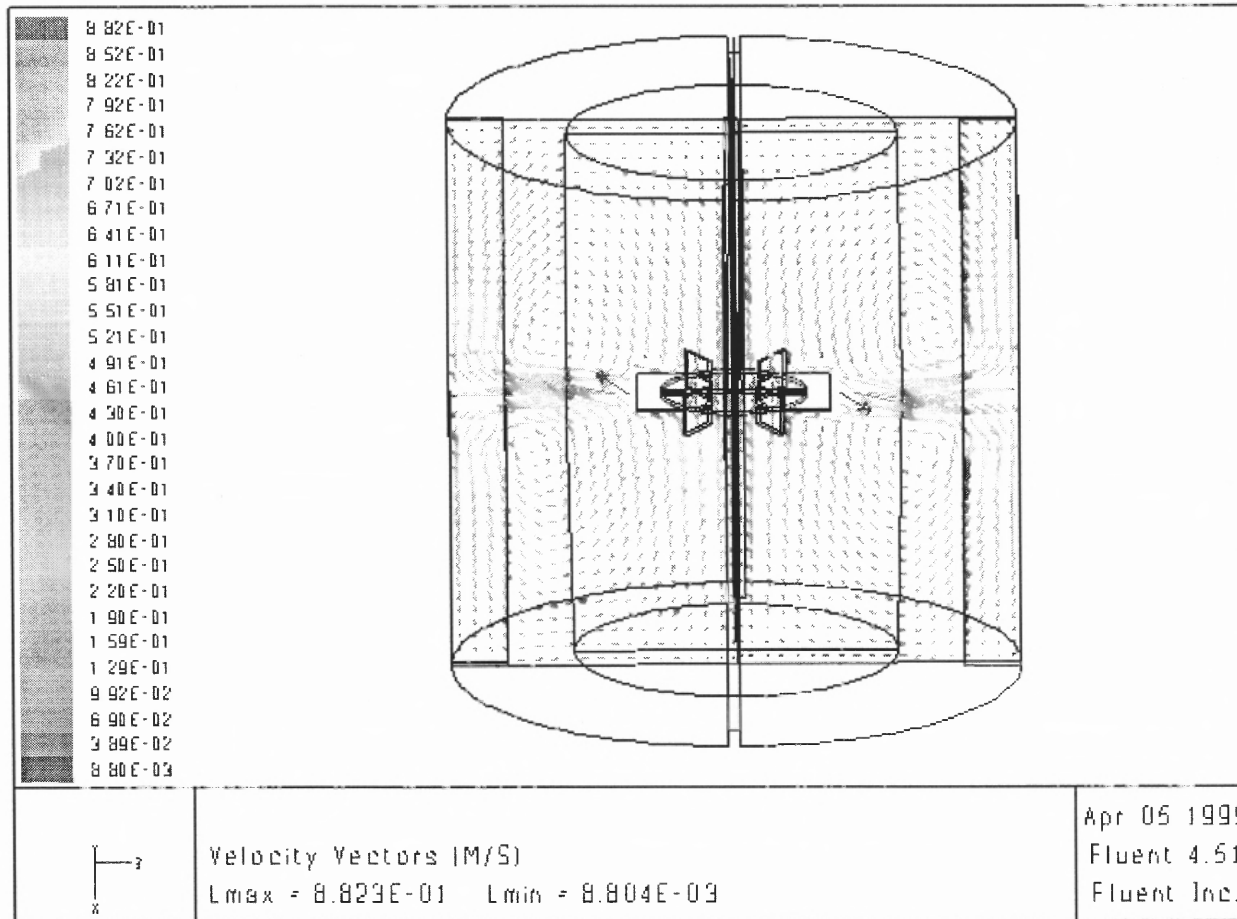
Figure 5.78: Stirred tank equipped with a Rushton turbine at an impeller clearance of T/2: Velocity profile.

velocities are negative as the fluid returns to the impeller. These trends are reflected by the data, in particular in the region just above the impeller. Below the impeller, the trend is reversed, but the main features of flow are the same.
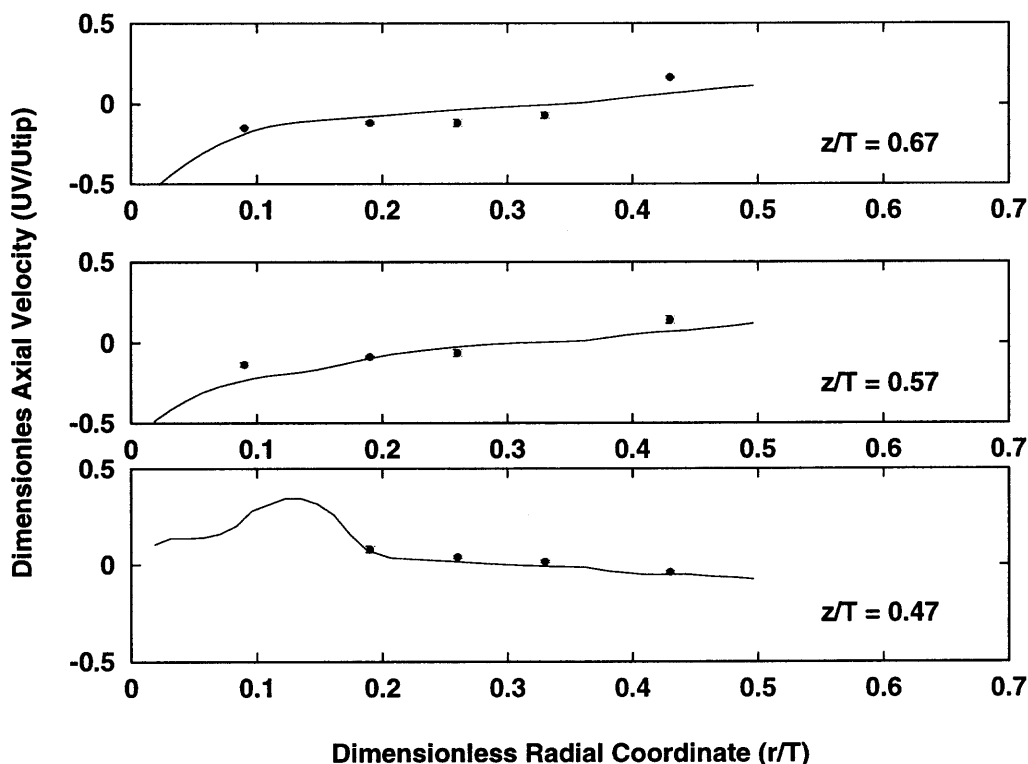
Figure 5.79: Stirred tank equipped with a Rushton turbine at an impeller clearance of T/2: Comparison of experimental axial velocity data with CFD simulation.

The radial velocity results are presented in Figure 5.80. In the upper portion of the vessel, the radial velocities are negative, indicating a return of fluid from the tank walls to the center of the tank as is shown in Figure 5.78.

The tangential velocity results are presented in Figure 5.81. The tangential velocities are high in the vicinity of the impeller stream due to the rotation of the impeller while in the general bulk, these velocities are small.

In regions far from the impeller, the predicted profiles of the turbulent kinetic energy are generally good. The overall results are quite good.
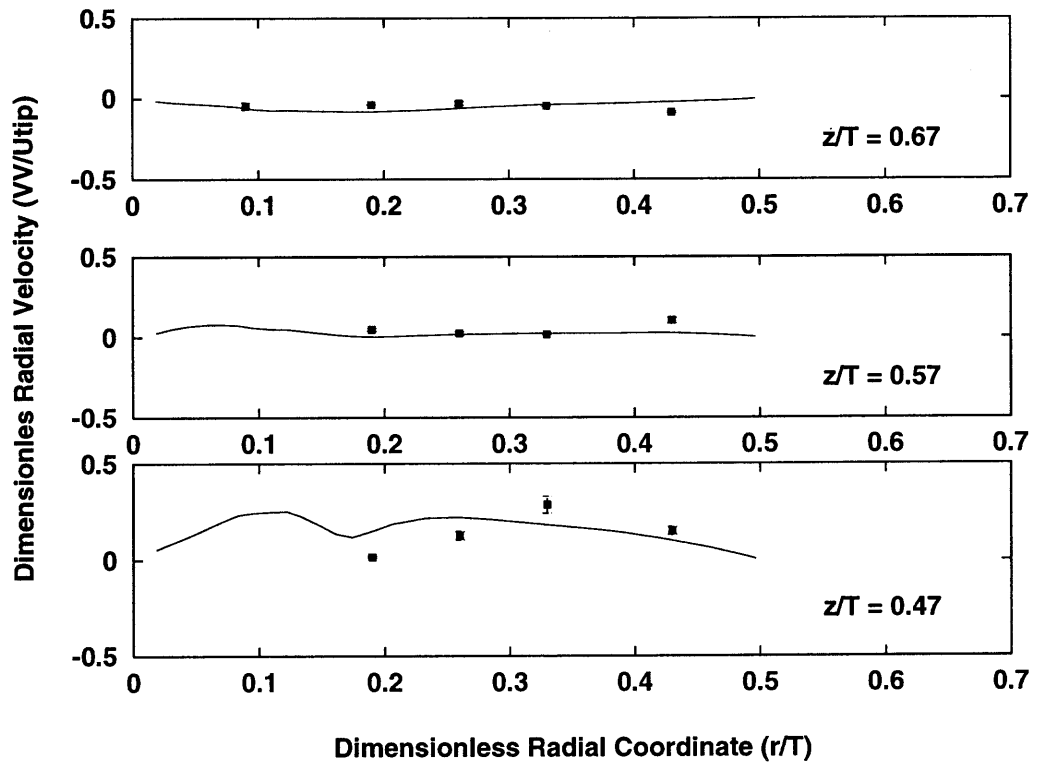
Figure 5.80: Stirred tank equipped with a Rushton turbine at an impeller Clearance of T/2: Comparison of experimental radial velocity data with CFD simulation.
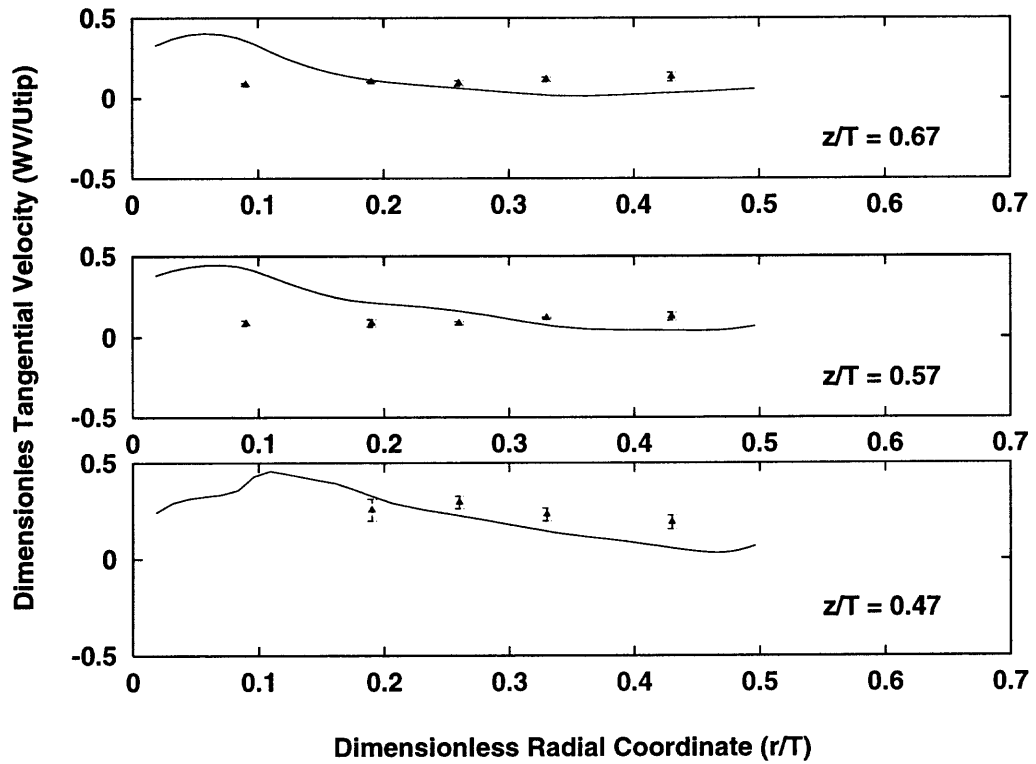
Figure 5.81: Stirred tank equipped with a Rushton turbine at an impeller clearance of T/2: Comparison of experimental tangential velocity data with CFD simulation.
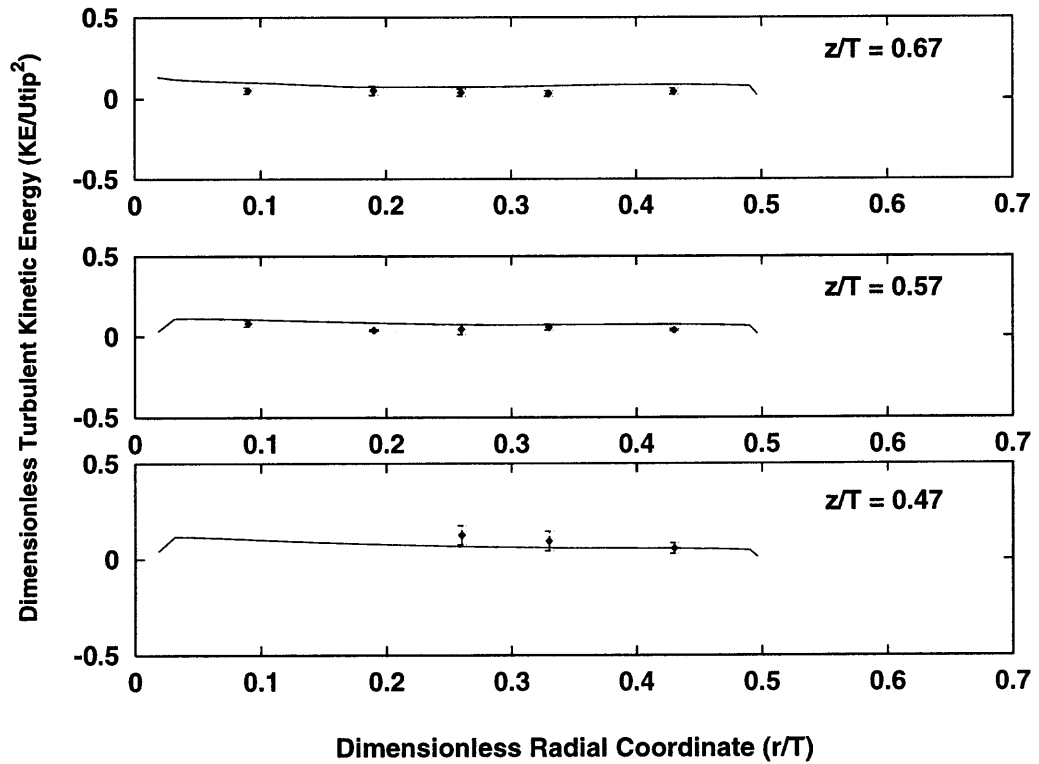
Figure 5.82: Stirred tank equipped with a Rushton turbine at an impeller clearance of T/2: Comparison of experimental turbulent kinetic energy data with CFD simulation.

5.6.3   Remarks

The CFD model captures the main features of the turbulent velocity field generated by the Rushton impeller. While numerical discrepancies exist, the overall agreement between the LDV data and the CFD model is good.

5.6.4   Power Consumption

Table 5.4 shows how the computed power consumption of the system compares with experimentally measure power and published correlations. It is evident that the experimentally obtained values are in close agreement with those obtained from published correlations while the computed power is under-predicted.

5.6.5   Comparison of Predicted Product Yields with the Model

In this section, the predicted yields for the parallel competing reaction set detailed in Section 4.3 are compared with the experimentally obtained results from our laboratory. The feed locations simulated are locations Fs (near the liquid surface), location Fi (in the impeller suction stream), and location Fd (the impeller discharge stream) as outlined in Figure 4.7. Results obtained using both the standard E-Model as well as the modified E-Model are presented on each graph.

As with all systems investigated, it was necessary to determine the minimum feed time required to establish a system where micromixing was rate controlling. The results of the study are presented in Figure 5.83. It is seen that a feed time of 20 minutes is sufficient to ensure that micromixing is rate controlling.

The following series of plots (Figures 5.84– 5.87) show the concentration profile of the limiting reagent, sodium hydroxide, as a function of time. The graphs are presented for feed locations Fs and Fi, and for both micromixing models at the lowest agitation speed (100 rpm), and at the highest agitation speed used for this system (300 rpm). The complete

Table 5.4: Power and mixing time characteristics for System D

System	RPM	N_{Re}	Location	Reaction Time $t_{99.99}$(s)t_{99}	Mixing Time (s)	N_{Po}(Sim)	Po(Sim) (W)	N_{Po} (correl)	Po (correl,W)	N_{Po} (exp)	Po (exp,W)
D	100	18481	Fs	0.920	27.06	1.86	0.09	5.17	0.239	4.84	0.24
	200	36963		0.630	13.53	2.33	0.53	5.17	1.911	5.25	2.00
	300	55444		0.380	9.02	2.39	2.98	5.17	6.450	5.03	6.76
	100		Fi	0.720							
	200			0.900							
	300			0.270							
	100		Fd	0.880							
	200			0.270							
	300			0.190							
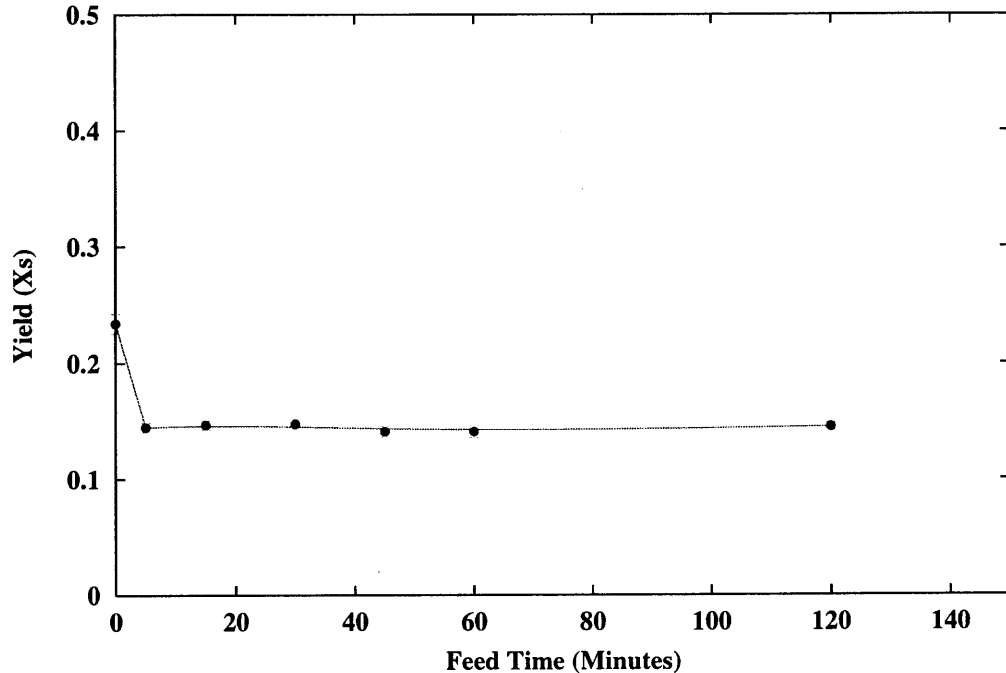
Figure 5.83: Variation of product yield with feed time for System D

set of data is presented in Table 5.4.

Again, it is evident that the two versions of the E-Model yield different time histories for the limiting reagent. The overall reaction time predicted by both models are similar and much smaller than the mixing time for this vessel.

The reaction times are observed to be faster at high agitation speeds than at lower ones indicating that the role of micromixing diminishes with increasing agitation speed. This is consistent with the trends observed for the other systems studied.

The predicted selectivities follow the previously observed trends: by-product formation decreases with increasing agitation rate and feeding material in the vicinity of the impeller results in lower by-product yields also.

The amount of by-product formation for all three locations are similar. With less by-product being formed in the impeller discharge stream than at the other two points in the system, indicating the higher level of turbulence that prevails there.
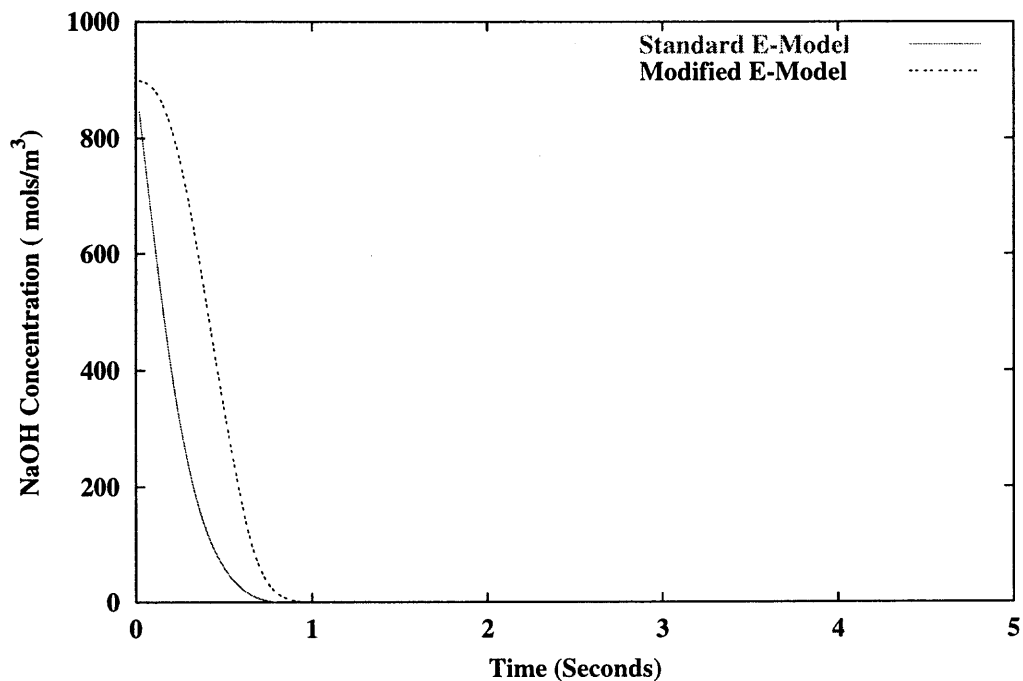
Figure 5.84: Reaction profile for System D at 100rpm. Feed location Fs.
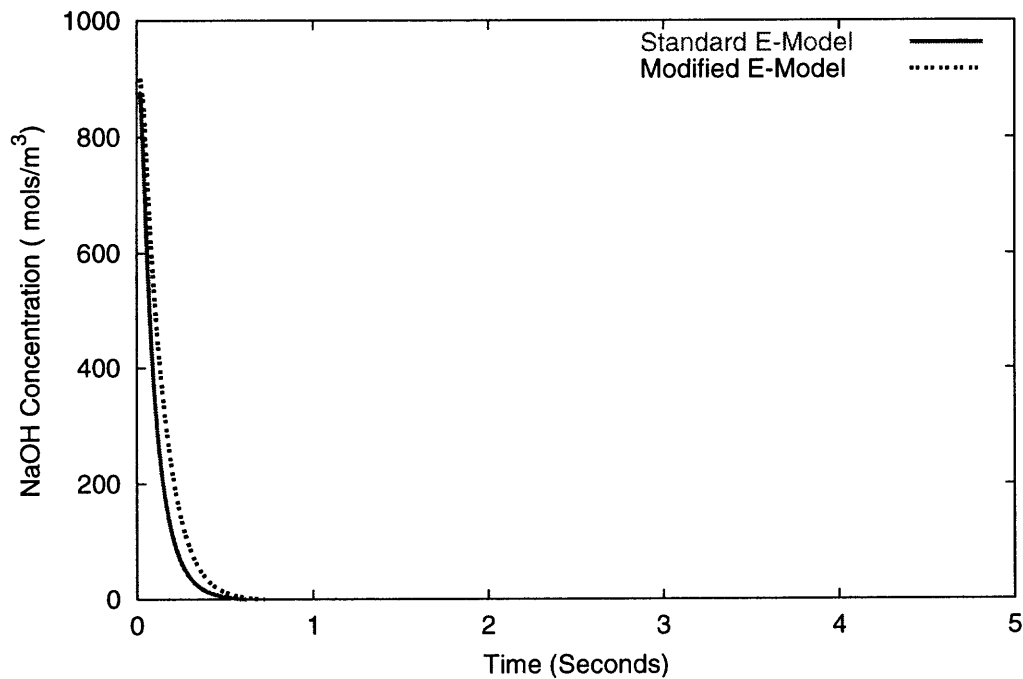
Figure 5.85: Reaction profile for System D at 100rpm. Feed location Fi.
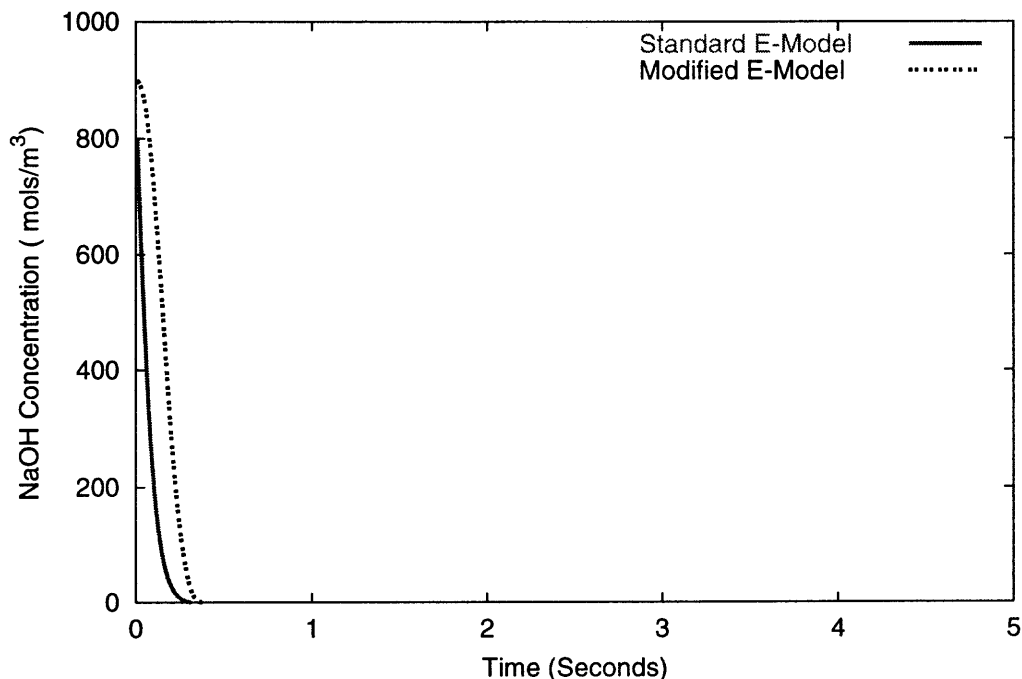
**Figure 5.86:** Reaction profile for System D at 300rpm. Feed location Fs.

5.6.6 Effect of Impeller Off-bottom Clearance

As mentioned earlier, raising the the impeller off-bottom clearance for the Rushton-based systems had the effect of lowering the amount of undesired by-product that was formed. Results for System A3 are presented with results for System D, for feed location Fs, in Figure 5.91 for ease of comparison.

The difference between the predicted data is greater than the difference between the experimental data. Nonetheless, it is evident that increasing the impeller off-bottom clearance impacts the yield of the undesired by-product.
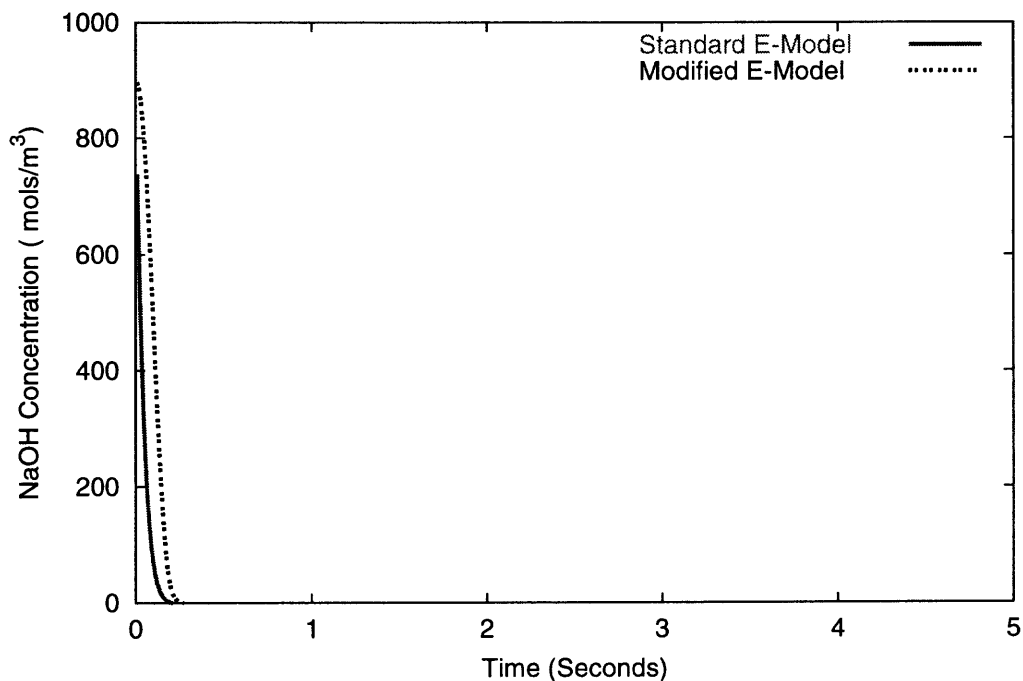
Figure 5.87: Variation of product yield with feed time for System D at 300rpm. Feed location Fi.
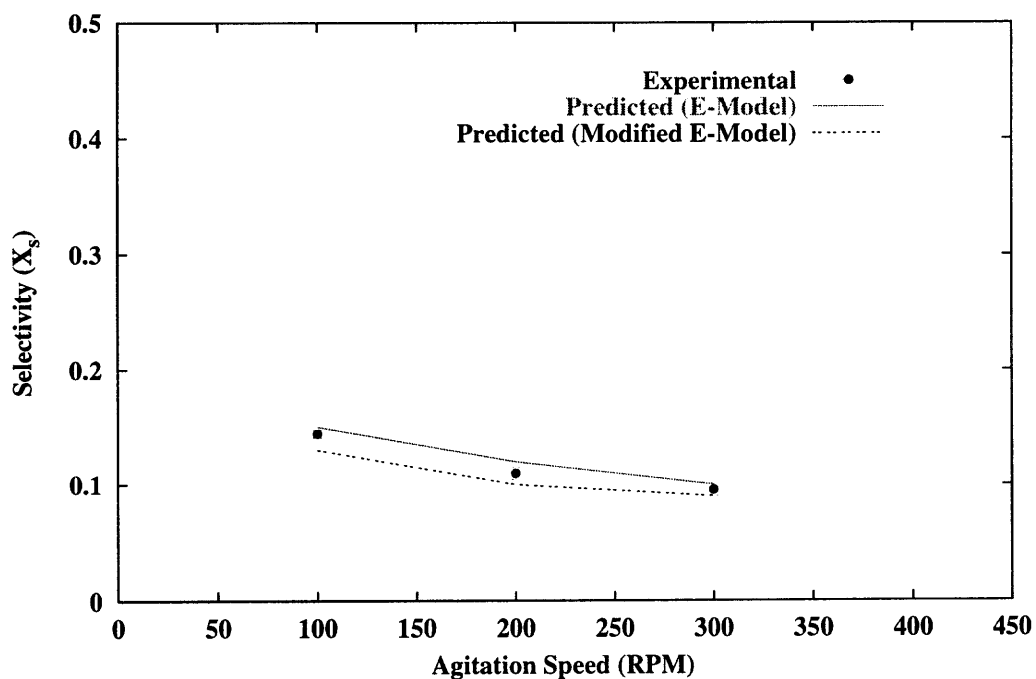
Figure 5.88: Variation of product yield with agitation speed for System D. Feed Location Fs.
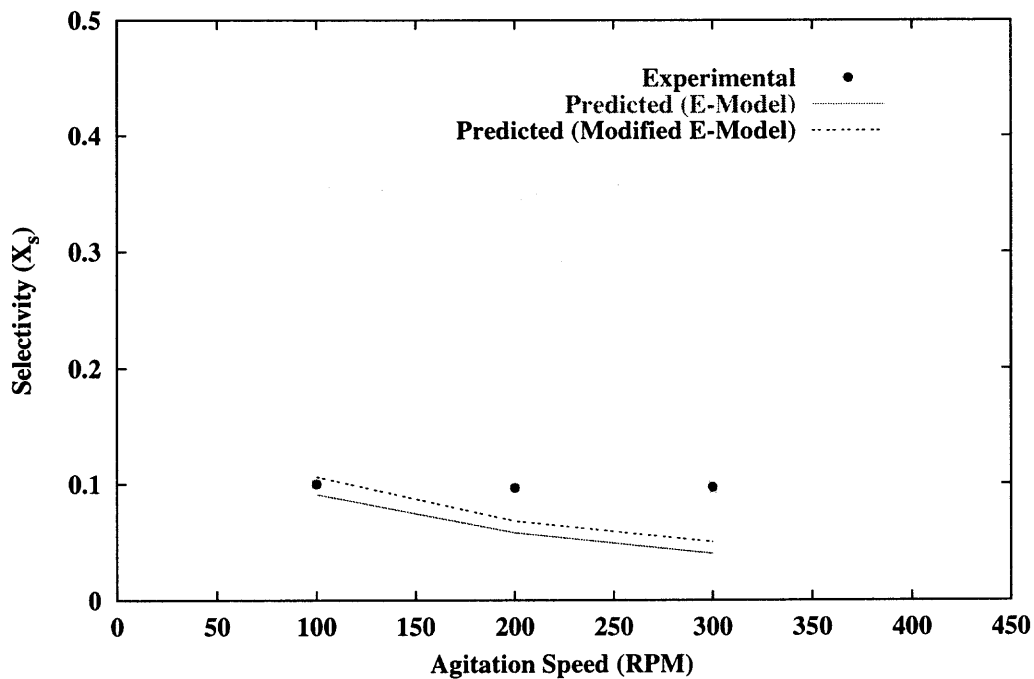
Figure 5.89: Variation of product yield with agitation speed for System D. Feed location Fi.
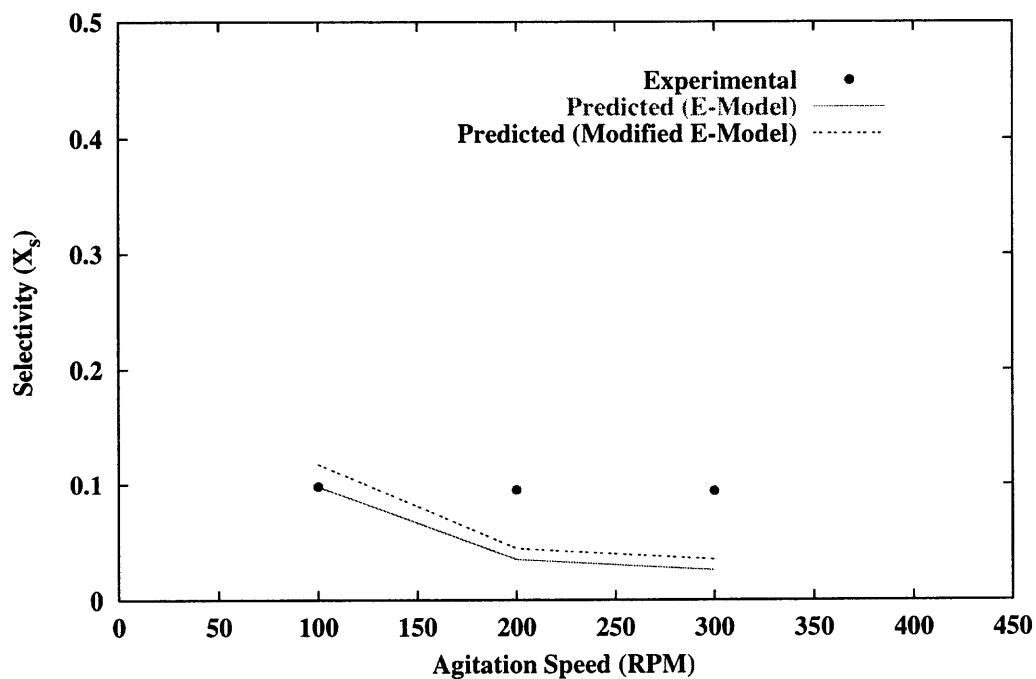
Figure 5.90: Variation of product yield with agitation speed for System D. Feed location Fd.
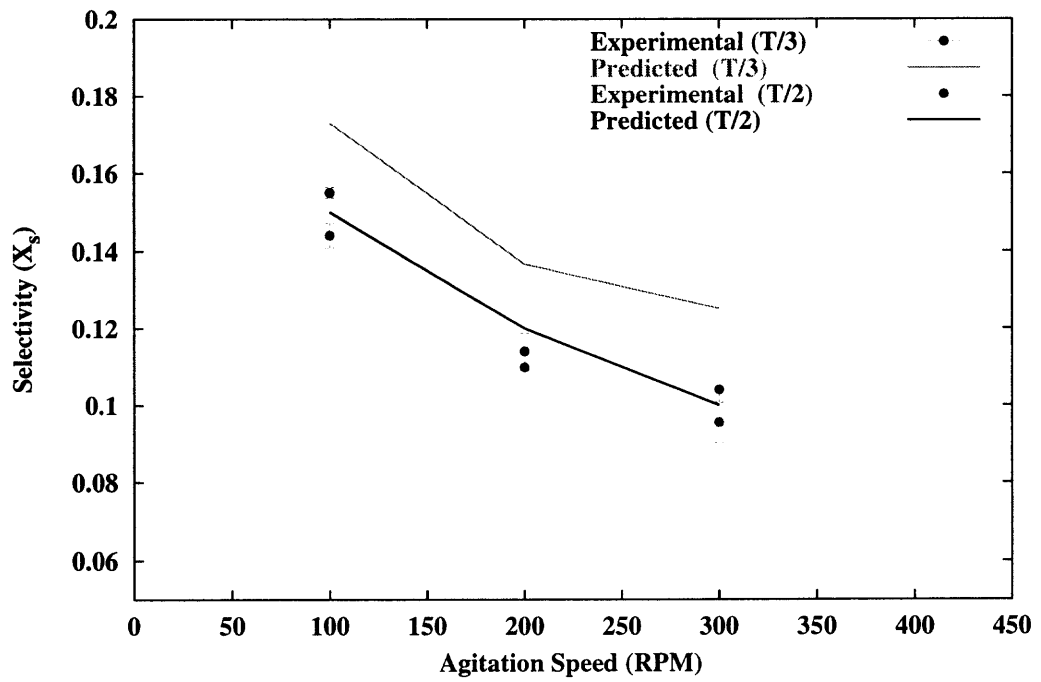
Figure 5.91: Effect of increasing the impeller off-bottom clearance: Comparing System A3 and System D

CHAPTER 6

CONCLUSION

In this work two state of the art technologies, Laser Doppler Velocimetry (LDV) and Computational Fluid Dynamics (CFD), were used to investigate the effect of turbulent mixing fast parallel competing reactions in baffled stirred tanks. A commercially available CFD package (FLUENT) was used to predict the three dimensional velocity profile and profiles of turbulent kinetic energy and local energy dissipation rates, as well as power consumption within the mechanically agitated vessels. The Reynolds Stress Model (RSM) was used to account for turbulence effects in the flow field and the Multiple Reference Frames (MRF) model was used to simulate the motion of the agitator. A novel model that combined CFD, and micromixing models was developed and used to investigate the effect of mixing on chemical reactions for a variety of systems.

There were two components to the experimental phase of this work. The first component involved carrying out the reaction scheme in the mixing laboratory in the department of Chemical Engineering, Chemistry and Environmental Science at the New Jersey Institute of Technology, under a variety of conditions. This involved varying the following parameters:

- **The agitator**: Three different impellers were used used in this study. These were namely the Rushton turbine, the 6 Bladed Pitched Blade turbine (6 PBT) and the Chemineer High Efficiency impeller (HE-3). The three impellers cover the range of mixers used in industrial practice for low viscosity blending applications.

- **The agitation speed**: For each impeller studied, the agitation rate was varied in order to determine its effect on the yield of the reactions.

- **The feed point location**: The location in the vessel where the feed was introduced was varied to study what effects this would have on the yield.

- **The fluid viscosity**: The viscosity of the fluid was varied for two of the systems,

namely the Rushton equipped system and the 6 PBT equipped system.

- **The impeller off bottom clearance**: The impeller off bottom clearance was varied for the Rushton equipped systems.

The experimental data served not only to validate the novel approach developed in this work, but also to study how turbulent mixing for complex reactions systems is influenced by the reactor setup. In so doing the general applicability and flexibility of the new model were also established.

The second component of the experimental work involved the use of the LDV apparatus to experimentally measure the three dimensional velocity profile of the flow field within the agitated vessels along with the fluctuating components of these velocities. The fluctuating components of the velocity were used to determine the turbulent kinetic energy of the flow within the vessels. This experimental work served primarily to validate the predictions furnished by the CFD model.

The micromixing effects were accounted for using *Engulfment* based models. The standard E-Model and a variant which accounted for mesomixing as well as micromixing by engulfment were used. The reactant fed to the system was simulated using the Volume of Fluid (VOF) multiphase model. The micromixing model, VOF model, and the information furnished by CFD were then coupled in a novel way to yield a novel model that can be used to predict the yield of reaction systems exhibiting complex chemistry in baffled stirred tanks.

The main results for the baffled cylindrical vessel fitted with a Rushton turbine can be summarized as follows:

- While the three dimensional velocity profile was well predicted, turbulence and power were under predicted. This had the effect of over predicting the product yields.

- The model was able to successfully capture the effect of varying the agitation speed, fluid viscosity and impeller off bottom clearance on the reaction system.

- Increasing the agitation speed of the impeller resulted in a decrease of the level of by-product formation.

- Increasing the viscosity of the fluid had the effect of increasing amount of by-product formation. The observed phenomena highlight the importance of micromixing in determining the outcome of parallel competitive reactions in turbulent environments.

- When the impeller off bottom clearance was increased, a drop in by-product formation was observed for feed material introduced near the liquid surface indicating an increase in the turbulence level for that region.

The main results for the baffled cylindrical vessel fitted with a 6 bladed pitched blade turbine can be summarized as follows:

- The three dimensional velocity profile was well predicted, as well as the turbulence and power.

- Again, the model was able to successfully capture the effect of varying the agitation speed, fluid viscosity on the levels of by-product formation.

- Increasing the agitation speed of the impeller resulted in a decrease of the level of by-product formation as for the Rushton based systems.

- Increasing the viscosity of the fluid had the effect of increasing amount of by-product formation.

The main results for the baffled cylindrical vessel fitted with a Chemineer High Efficiency impeller can be summarized as follows:

- The three dimensional velocity profiles were well predicted, as well as the turbulent kinetic energy and power delivered to the system by the impeller.

- Again, the model was able to successfully capture the effect of varying the agitation speed on the levels of by-product formation.

- Increasing the agitation speed of the impeller resulted in a decrease of the level of by-product formation as for the Rushton and 6 PBT based systems.

- The overall levels of by-product formation for this system were similar for this system as the 6 PBT based system and higher than those for the Rushton based system, a consequence of the prevailing lower levels of turbulence for this system.

In summary, the overall results obtained were most encouraging. CFD in conjunction with the MRF model adequately predicted the turbulent velocity profile and turbulence levels with the systems studied. The model predicted by-product yields in good agreement with the experimentally determined values. It was shown that for some systems (6 PBT and HE-3), the inclusion of mesomixing into the model yielded better results than when engulfment only was considered. The power level in the Rushton based systems was higher than in the 6 PBT based system or the HE-3 based system. This is a consequence of more power being delivered to the system by the Rushton impeller than by either the 6 PBT or the HE-3. The Rushton based system also produced the lowest by-product yields while the HE-3 and PBT based system produced similar by-product yields. It was also observed for all the systems studied that material fed into the impeller stream yielded lower by-product yields than material introduced near the feed surface, a consequence of the higher level of turbulence prevailing in the impeller region. Increasing the fluid viscosity had the effect of increasing the yield of by-product formation. This occurred because the increase in viscosity slows the mesomixing and engulfment processes thereby allowing the second and slower side reaction to proceed to a greater extent. Increasing the impeller clearance as was done for the Rushton turbine based systems resulted in higher overall levels of turbulence delivered to the system thereby producing lower by-product yields than in the standard configuration.

All the experimentally observed phenomena and trends were predicted consistently by the novel model. This works thus demonstrates that turbulent mixing and its influence on fast parallel reactions may be simulated using the developed novel computational approach.

The approach is completely general requiring no adjustable parameters and is therefore applicable to a wide variety of systems.

APPENDIX A

FORTRAN CODE USED IN THE EVALUATION OF THE MICROMIXING

MODEL EQUATIONS

A.1   Runge-Kutta Solver

The Runge-Kutta code used in solving the model equations was obtained from an online numerical library, *Netlib*. Pertinent information are as follows:

RKSUITE Release 1.0 November 1991
written by
R.W. Brankin (*), I. Gladwell(**), and L.F. Shampine (**)

(*) Numerical Algorithms Group Ltd.

Wilkinson House
Jordan Hill Road
Oxford OX2 8DR
U.K.
email: richard@nag.co.uk
       na.brankin@na-net.ornl.gov
International phone: + 44 865 511245
International fax: + 44 865 310139

(**) Department of Mathematics
Southern Methodist University
Dallas, Texas 75275
U.S.A.
email: h5nr1001@vm.cis.smu.edu
U.S. phone: (214) 692-2542
U.S. fax: (214) 692-4138

RKSUITE is a suite of codes based on Runge-Kutta methods for the numerical
solution of the initial value problem for a first order system of ordinary
differential equations. It is the result of decades of research and
development of such methods and software by the authors. It supersedes
some very widely used codes written by the authors and their coauthors,
namely, the RKF45 code that is available in several books and its descendant
DDERKF in the SLATEC library, and D02PAF and the associated codes in the NAG
Fortran library.

RKSUITE is being made available free of charge to the scientific community as a public service. It is expected that anyone making a substantial use of the software will acknowledge this use and in particular, give a proper citation in any publication resulting from its use. A suitable reference is:

R.W. Brankin, I. Gladwell, and L.F. Shampine, RKSUITE: a suite of Runge-Kutta codes for the initial value problem for ODEs, Softreport 92-S1, Department of Mathematics, Southern Methodist University, Dallas, Texas, U.S.A, 1992.

A.2 Driver Module

The driver module was written to read in the initial conditions and system parameters, these include initial concentrations and the amount of feed discretization. The driver module was also responsible for performing the necessary mass balances and updating the boundary conditions.

```
      program emodel`driver

      implicit real (a-h,o-z)

c.....................................................c
c    Simulation of micromixing in stirred tank            c
c    Choice of Model used is as follows:                  c
c                                           c
c  1. Original E-Model (R14)                    c
c  2. Modified E-Model (R10)                    c
c                                           c
c                                           c
c The W-Z Transformation was used so that it was possible to solve the c
c problem with a Runge-Kutta Scheme and NOT collocation          c
c this file emodel`driver`vof.f goes with emodel`solve`vof.f      c
c and rksuite.f                              c
c                                           c
c    -Otute 25 Jan 1999                        c
c.....................................................c


c-------------------------------------------------------------------c
```

```
c   my variable declarations                          c
c-------------------------------------------------------------------c

c---nsize denotes the max number of I slices
c---ncomp denotes the max number of species
      integer ncomp,nrow,ncol,ntimes
      parameter(ncomp=7,nrow=500,ncol=3)
c...........................................................
      real conc(1:ncomp),avgconc(1:ncomp)
      real edata(1:nrow,1:ncol)
      real avgdiss,avgkin
c........status is used to determine whther the soln process is
c       running smoothly or not. if not, then the process is terminated
c       and answers up to that point are printed out.
      status = 0
      step = 1
c   read in the file conating the epsilon and ke values from FLUENT
      open(10,file='vof˙fs.data')
      kount = 0
      write(*,*) 'Reading Data'
      do 93 krow = 1,nrow
        read(10,1020,end=94) (edata(krow,kcol), kcol=1,ncol)
        write(*,1020) (edata(krow,kcol), kcol=1,ncol)
 93     continue
 94     continue
c   back one step from the EOF marker
      kount = kount - 1
c   first time will be used as time zero
      time0 = edata(1,1)
c............................................................
c
c   USER INPUTS
c............................................................

c Model to be used:
c 1 -¿ Standard E Model
c 2 -¿ Modified E Model
      nmodel = 1
c   parameters to send
c   va,vb,average dissipation rate,concentrations
c Tank Bulk Volume
      vb    = 0.019e0
      vb1   = vb
c Volume Added to the Tank
      vatot  = vb/50.0e0
```

```
c number of parts feed is discretized into -¿ sigma
      sigma  = 50.0e0
      ntimes = NINT(sigma)
c volume of first part
      va1    = vatot/sigma
c.......initial concentrations
      CAo = 900.0e0
      CBo = 0.00e0
      CCo = 0.00e0
c.....initial average concentrations - zone 1
      CAavg = 0.0d0
      CBavg = 18.0e0
      CCavg = 18.0e0
c......put the above concentrations into arrays
      conc(1) = CAo
      conc(2) = CBo
      conc(3) = CCo
      avgconc(1) = CAavg
      avgconc(2) = CBavg
      avgconc(3) = CCavg
c loop sigma times until all the feed has been added
      open(12,file='ca´profile´start.data')
      open(13,file='ca´profile´end.data')
      do 401 nfeed = 1,ntimes
        nstep   = 2
        nstep1  = nstep - 1
        va      = va1
c...parameters wanted
c...new concentrations, new va,new vb
c    loop until  all the feed has been consumed
 503      continue
          tstart  = edata(nstep1,1)
          tend    = edata(nstep,1)
          tstart  = tstart - time0
          tend    = tend   - time0
          avgdiss = edata(nstep,2)
          avgkin  = edata(nstep,3)
          print*,'nstep',nstep
          print*,'tstart',tstart
          print*,'tend',tend
            call rkmixer(va,vb,avgdiss,avgkin,
     &              conc,avgconc,tstart,tend,nmodel)
          print 1505
          print 3005,conc(1),conc(2),conc(3)
c update concentrations in entire tank
```

```
      nstep = nstep + 1
      nstep1= nstep - 1
      if (nfeed .eq. 1) then
         write (12,1030) tend,conc(1),conc(2),conc(3)
      elseif (nfeed .eq. ntimes) then
         write (13,1030) tend,conc(1),conc(2),conc(3)
      endif
      if (conc(1) .gt. 0.0e0) goto 503
   do 402 nspec = 1,3
      avgconc(nspec) = (avgconc(nspec)*vb+conc(nspec)*va)/(va+vb)
402   continue
c Echo Results to Screen
      print*,'vafinal ',va
      vb = vb + va
      va = 0.0e0
      conc(1) = CAo
      conc(2) = CBo
      conc(3) = CCo
401   continue
      print*,'The final Concentrations in the Bulk Are: '
      print 1500
      print 3000,avgconc(1),avgconc(2),avgconc(3)
      print*,'The Final Volumes Are'
      print*,'VA',va
      print*,'VB',vb
      print*,'Computing the selectivity'
      xs = (CCavg*vb1-avgconc(3)*(vb))/(CAo*vatot)
      print*,'Xs',xs
      close(10)
      close(12)
      close(13)
1500 Format(6x,6x,'CAavg',12x,'CBavg',12x,'CCavg')
3000 Format(9x,1x,3(E14.6,3x))
1505 Format(6x,6x,'CA',12x,'CB',12x,'CC')
3005 Format(9x,1x,3(E14.6,3x))
1020 format(1x,e15.6,2x,e15.6,2x,e15.6)
1030 format(1x,4(E14.6,2x))
      end
```

A.3   Solver Module

The solver module interfaced directly with the Runge-Kutta solver. It takes the necessary parameters from the driver module passes them on to the Runge-Kutta code. The solutions are then returned to the driver module for updating. It also contains the equations that need to be solved.

```
      subroutine rkmixer(avol,bvol,avgdiss,avgkin,conc,
     &   avgconc,t1,t2,nmodel)

c.................................................................c
c    This subroutine solves two verions of the emodel            c
c                                             c
c    nmodel = 1 -¿ Conventional E-Model R14             c
c    nmodel = 2 -¿ Modified Emodel    R10            c
c    c
c    The W-Z Transformation was used so that it was possible to solve the c
c    problem with a Runge-Kutta Scheme and NOT collocation          c
c    this file emodel`solve`vof.f goes with emodel`driver`vof.f      c
c    and rksuite.f                          c
c                                 c
c    -Otute 25 Jan 1999                      c
c.................................................................c

C    NOTES:   Typically problems are solved for a number of tolerances, initial
C    conditions, intervals, parameter values, ... . A prudent person
C    would make at least one run with global error assessment as a
C    spot check on the reliability of the results.  Variant 1b shows
C    how to do this.
C
C    For TOL in this range, METHOD = 2 is generally the most efficient
C    choice.  Indeed, for this specific problem and tolerance (and a
C    specific computer, precision, compiler, ... ), the results found
C    in tmpl1.out show that the cost with METHOD = 2 is 109 calls to
C    the subroutine F, with METHOD = 1 it is 292 calls, and with
C    METHOD = 3 it is 105 calls. At relaxed tolerances, METHOD = 1 is
C    generally the most efficient choice, and at stringent tolerances,
C    METHOD = 3 is generally the most efficient.
C
C    In typical use of UT, the cost is scarcely affected by the
C    number of answers, but when a "large" number of answers is
C    required, this is not true of METHOD = 3.  In such a situation
```

```
C    its cost is proportional to the number of answers.
C
C    Working storage must be provided in the array WORK(*) of length
C    LENWRK.  Because storage is no problem with only NEQ = 2
C    equations, LENWRK is taken here to be 32*NEQ, enough to handle
C    all three methods with and without global error assessment.
C
C    .. Parameters ..
c----------------------Make changes NEQ,METHOD----------------------------

      implicit double precision (a-h,o-z)

      INTEGER        NEQ, LENWRK, METHOD,ncomp
      PARAMETER      (NEQ=3,LENWRK=64*NEQ,METHOD=3,ncomp=7)
c-------------------------------------------------------------------------
C    .. Local Scalars ..

      DOUBLE PRECISION  HNEXT, HSTART, T, TEND,
     &    TLAST, TOL, TSTART, TWANT, WASTE
      INTEGER        L, NOUT, STPCST, STPSOK, TOTF, UFLAG
      LOGICAL        ERRASS, MESAGE
C    .. Local Arrays ..
      DOUBLE PRECISION  THRES(NEQ), WORK(LENWRK), Y(NEQ), YMAX(NEQ),
     &    YP(NEQ), YSTART(NEQ)

c..................MY VARIABLES ARE DECLARED FROM HERE ON...................

c.....imported real variables
      real conc(1:ncomp),avgconc(1:ncomp),
     .    time,avgdiss,avgkin

      real avol,bvol,t1,t2

c.....parameters needed to solve the eqns. these will be declared in
c.....a common block

      double precision dengulf,corrsin,dkval1,dkval2
      double precision kvisc
      double precision x,xb,ke
      double precision CAo,CBo,CCo
      double precision CAbar,CBbar,CCbar
c...................................................................
      common /oparams/dengulf,corrsin,dkval1,dkval2,vao
      common /oavgs/ uavg,CCbar
```

```
C    .. External Subroutines ..
     EXTERNAL      F1,F2, SETUP, STAT, UT


C    .. Executable Statements ..


c-------------Make changes: TSTART,YSTART(NEQ),TLAST,TEND. ---------------


C................................................................
C    Set the initial conditions.  Note that TEND is taken well past      .
C    the last output point, TLAST.  When this is possible, and it        .
C    usually is, it is good practice.                                    .
C................................................................

     print*,'entering rkmixer1 subroutine to solve eqns'


c.....volume
     ova   = DBLE(avol)
     ovb   = DBLE(bvol)
     vao   = ova
     ovtot = ova + ovb

     print*,'VA',avol
     print*,'VB',bvol


c.....initial concentrations - micro mixed phase
     CAo = DBLE(conc(1))
     CBo = DBLE(conc(2))
     CCo = DBLE(conc(3))

     print*,'concentrations updated'


c.....initial average concentrations - bulk zone
     CAbar = DBLE(avgconc(1))
     CBbar = DBLE(avgconc(2))
     CCbar = DBLE(avgconc(3))

     print*,'average concentrations updated'
c................................................................
     print*,'Initial Concentrations Before Solving'
     print 1000
     print 2000,CAo,CBo,CCo
     print*,'Average Concentrations Before Solving'
     print 1500
     print 3000,CAbar,CBbar,CCbar
```

```
c    stop
c.........................................................
     viscosity = 9.0d-4
     density = 1.0d3
     pi = 3.14159265359
     diss   = DBLE(avgdiss)
     ke     = DBLE(avgkin)
     kvisc  = viscosity/density
c.....diffusivity
     diff = 1d-9
c.....lifetime of a vortex
     alpha  = 12.0d0*(kvisc/diss)**0.5
c    alpha = 1d-5
     x      = alpha
c.....ENGULFMENT RATE
c    dengulf = 0.058d0*(diss/kvisc)**0.5
     dengulf = DLOG(2.0d0)/alpha
     dengulf2=dengulf
c.....CORSSIN TIME CONSTANT
     schmidt = viscosity/(density*diff)
c    tms    = 5.74*(ke/diss) +
c    .        (1.0/2.0)*(kvisc/diss)**(1.0/2.0)*DLOG(schmidt)
     tms = 0.5d0*(ke/diss)
c    A = 2.0d0
c    D = 0.1d0
c    rlambda = D/10.0d0
c    tms = A*(rlambda**2/diss)**(1.0d0/3.0d0)
     corssin = 1/tms
c.........................................................
     xb=0
     dkval1  = 1.0d5
     dkval2  = 0.020d0
     dtemp   = 273.15d0 + 23.0d0
     dR      = 8.314
     dkval2  = 2.0d5*dexp(-3.891d4/(dR*dtemp))
     print*,'Parameters are as follows:'
     print*,'viscosity: ',viscosity
     print*,'density: ',density
     print*,'dissipation: ',diss
     print*,'ke',ke
     print*,'schmidt',schmidt
     print*,'k1: ',dkval1
     print*,'k2: ',dkval2
     print*,'kinematic viscosity',kvisc
     print*,'Vortex Lifetime: ',alpha
```

```
      print*,'E: ',dengulf2
      print*,'corssin',corssin
c     transform the variables - micro mixed phase
      uavg  = CAbar  - CBbar
      uo    = CAo    - CBo
      CCbar = CCbar * 1.0d0
c     boundary conditions
c     TSTART   = 0
      YSTART(1) = uo
      YSTART(2) = CCo
c.....and then the volumes
      YSTART(3) = ova
      YSTART(4) = ovb
      TSTART  = DBLE(t1)
      TEND    = 2*DBLE(t2)
      TWANT   = DBLE(t2)
C.................................................................
C     Initialize output.
C
c     print out the initial conditions
      print 9010
      print 9030,TSTART
      print 9040,TWANT
      print 9070
      print 9020
C---------------------------------------------------------------
C.............................
C     Set error control parameters.
C.............................
      TOL = 5.0D-5
      DO 20 L = 1, NEQ
        THRES(L) = 1.0D-10
  20  CONTINUE
C
C     Call the setup routine. Because messages are requested, MESAGE = .TRUE.,
C     there is no need later to test values of flags and print out explanations.
C     In this variant no error assessment is done, so ERRASS is set .FALSE..
C     By setting HSTART to zero, the code is told to find a starting (initial)
C     step size automatically .
C
      MESAGE = .TRUE.
      ERRASS = .FALSE.
      HSTART = ZERO
C
c.................................................................
```

```
c    results are obtained here. where twant is the point at which a soln .
c    is wanted
c...............................................................
     if (nmodel .eq. 1) then
       print*,'calling setup routine for R14'
       CALL SETUP(NEQ,TSTART,YSTART,TEND,TOL,THRES,METHOD,'Usual Task'
     &      ,ERRASS,HSTART,WORK,LENWRK,MESAGE)
       print*,'calling ut routine for R14'
       CALL UT(F1,TWANT,T,Y,YP,YMAX,WORK,UFLAG)
     else if (nmodel .eq. 2) then
       print*,'calling setup routine for R10'
       CALL SETUP(NEQ,TSTART,YSTART,TEND,TOL,THRES,METHOD,'Usual Task'
     &      ,ERRASS,HSTART,WORK,LENWRK,MESAGE)
       print*,'calling ut routine for R10'
       CALL UT(F2,TWANT,T,Y,YP,YMAX,WORK,UFLAG)
     endif
C
     IF (UFLAG.GT.2) GO TO 60
C    Success. T = TWANT. Output computed and true solution components.
c    print solutions after first transforming the variables back to
c    concentrations
     u        = Y(1)
     CC       = Y(2)
     ova      = Y(3)
c    ovb      = Y(4)
     ovb = ovtot - ova
     CA = (DABS(u)+u)/2
     CB = (DABS(u)-u)/2
c...............................................................
     print 1000
     print 2000,CA,CB,CC

     avol     = REAL(ova)
     bvol     = REAL(ovb)

c.....update the concentrations...............................

     conc(1)  = REAL(CA)
     conc(2)  = REAL(CB)
     conc(3)  = REAL(CC)


c...............................................................


c    stop
```

```
C    The integration is complete or has failed in a way reported in a
C    message to the standard output channel.
 60  CONTINUE
C
C    YMAX(L) is the largest magnitude computed for the solution component
C    Y(L) in the course of the integration from TSTART to the last T.  It
C    is used to decide whether THRES(L) is reasonable and to select a new
C    THRES(L) if it is not.
C
     print 9070
     print *

c    WRITE (*,'(A/)') '        YMAX(L) '
c    DO 80 L = 1, NEQ
c    WRITE (*,'(13X,1PE8.2)')   YMAX(L)
c 80  CONTINUE
C
C    The subroutine STAT is used to obtain some information about the progress
C    of the integration. TOTF is the total number of calls to F made so far
C    in the integration; it is a machine-independent measure of work.  At present
C    the integration is finished, so the value printed out refers to the overall
C    cost of the integration.
C
     print 9070

c    stop

     CALL STAT(TOTF,STPCST,WASTE,STPSOK,HNEXT)
     WRITE (*,'(/A,1PE10.2,0P/A,I10/A,I10/A,F10.2/A,I10)')
    &    ' The integration reached            ', TNOW,
    &    ' The cost of the integration in calls to F was', TOTF,
    &    ' The number of calls to F per step is     ', STPCST,
    &    ' The fraction of failed steps was        ', WASTE,
    &    ' The number of accepted steps was        ', STPSOK

c    print line to signal end of results
     print 9070
c--------------format statements for displaying results------------------
9010 format(1x,32('-'),'Results',31('-'))
9020 format(1x,'Initial Conditions')
9030 format(1x,'Start Time = ',f10.4)
9040 format(1x,'End Time = ',f10.4)
```

```
9050 format(1x,'Results')
9060 format(1x,5x,'Y',I2,' = ',f10.4)
9070 format(1x,70('-'))

1000 Format(1x,6x,'CA',15x,'CB',15x,'CC')
1500 Format(6x,6x,'CAavg',12x,'CBavg',12x,'CCavg')
1505 Format(6x,6x,'CAb',14x,'CBb',14x,'CCb')
2000 Format(1x,1x,3(D14.6,3x))
3000 Format(9x,1x,3(D14.6,3x))

      RETURN
      END


C--------------------------------------------------------------------------
      SUBROUTINE F1(T,Y,YP)
      implicit double precision(a-h,o-z)
C    .. Scalar Arguments ..
      DOUBLE PRECISION  T
      DOUBLE PRECISION  dengulf,corrsin,dkval1,dkval2,vao
      DOUBLE PRECISION  uavg,CCavg
C    .. Array Arguments ..
      DOUBLE PRECISION  Y(*), YP(*)
C    .. Executable Statements ..
      common /oparams/dengulf,corrsin,dkval1,dkval2,vao
      common /oavgs/  uavg,CCbar
c     print*, 'corrsin',corrsin
c     print*,'dengulf',dengulf
c     print*,'dkval2',dkval2
      corrsin = corrsin*1.0d0
      dengulf = dengulf*1.0d0
      dkval2  = dkval2 *1.0d0
      uavg    = uavg*1.0d0
      CCbar   = CCbar*1.0d0
      ca    = ( DABS(Y(1))+Y(1) )/2.0
      cc    =  Y(2)
      YP(1) = (dengulf)*(uavg - Y(1)) - dkval2*ca*cc
      YP(2) = (dengulf)*(CCbar - Y(2)) - dkval2*ca*cc
      YP(3) = (dengulf)*Y(3)
      RETURN
      END


C--------------------------------------------------------------------------
      SUBROUTINE F2(T,Y,YP)
      implicit double precision(a-h,o-z)
C    .. Scalar Arguments ..
```

```
      DOUBLE PRECISION  T
      DOUBLE PRECISION  dengulf,corrsin,dkval1,dkval2,vao
      DOUBLE PRECISION  uavg,CCavg
C    .. Array Arguments ..
      DOUBLE PRECISION  Y(*), YP(*)
C    .. Executable Statements ..
      common /oparams/dengulf,corssin,dkval1,dkval2,vao
      common /oavgs/ uavg,CCavg
      factor = (1 - (Y(3)*DEXP(- T*corssin)/vao))
      ca    = ( DABS(Y(1))+Y(1) )/2
      cc    =   Y(2)
      YP(1) =   dengulf*factor*(uavg - Y(1))  - dkval2*ca*cc
      YP(2) =   dengulf*factor*(CCavg - Y(2)) - dkval2*ca*cc
      YP(3) =   dengulf*factor*Y(3)
      RETURN
      END
C-------------------------------------------------------------------------
```

REFERENCES

Armenante, P. M. and C. Chou. "Experimental LDV Measurements and Numerical CFD Determination of the Fluid Velocity Distribution in an Unbaffled Vessel." *AICHE Symposium Series* 90 (1994): 33–40.

Armenante, P. M., C. Chou, and R. R. Hemrajani. "Comparison of Experimental and Numerical Fluid Velocity Distribution Profiles in an Unbaffled Mixing Vessel Provided with a Pitched-Blade Turbine." *Institution of Chemical Engineers Symposium Series 136*. Cambridge, England: Institution of Chemical Engineers, September 1994, 349–356.

Armenante, P. M., C. Luo, C. Chou, I. Fort, and Jaroslav Medek. "Velocity Profiles in a Closed, Unbaffled Vessel: Comparison Between Experimental LDV Data and Numerical CFD Predictions." *Chemical Engineering Science* 52 (1997): 3483–3492.

Aubry, C. and J. Villermaux. "Représentation du Mélange Imparfait de Deux Courants de Reactifs dans un Réacteur Agité Continu." *Chemical Engineering Science* 30 (1975): 1309–1313.

Bakker, R. A. and H. E. A. van den Akker. "A Computational Study of Chemical Reactors on the Basis of Micromixing Models." *Transactions of the Institution of Chemical Engineers* 72 (November 1994): 733.

Bakker, R. A. and H. E. A. van den Akker. "A Lagrangian Description of Micromixing in a Stirred Tank Reactor Using 1D-micromixing Models in a CFD Flow Field." *Chemical Engineering Science* 51 (1996): 2643–2648.

Baldyga, J. "Turbulent Mixer Model with Application to Homogeneous, Instantaneous Chemical Reactions." *Chemical Engineering Science* 44 (1989): 1175–1182.

Baldyga, J. "A Closure Model for Homogeneous Chemical Reactions." *Chemical Engineering Science* 49 (1994): 1985–2003.

Baldyga, J. and J. R. Bourne. "A Fluid Mechanical Approach to Turbulent Mixing and Chemical Reaction - Part II: Micromixing in the Light of Turbulent Theory." *Chemical Engineering Communications* 28 (1984): 243–258.

Baldyga, J. and J. R. Bourne. "A Fluid Mechanical Approach to Turbulent Mixing and Chemical Reaction: Part I Inadequacies of Available Methods." *Chemical Engineering Communications* 28 (1984): 231–241.

Baldyga, J. and J. R. Bourne. "A Fluid Mechanical Approach to Turbulent Mixing and Chemical Reaction: Part III Computational and Experimental Results for the New Micromixing Model." *Chemical Engineering Communications* 28 (1984): 259–281.

Baldyga, J. and J. R. Bourne. "Mixing and Fast Chemical Reaction — VIII: Initial Deformation of Material Elements in Isotropic, Homogeneous Turbulence." *Chemical Engineering Science* 39 (1984): 329–334.

Baldyga, J. and J. R. Bourne. "Calculation of Micromixing in Inhomogeneous Stirred Tank Reactors." *Chemical Engineering Research Design* 66 (January 1988): 33–38.

Baldyga, J. and J. R. Bourne. "Simplification of Micromixing Calculations I, Derivation and Application of New Model." *The Chemical Engineering Journal* 42 (1989): 83–92.

Baldyga, J. and J. R. Bourne. "Simplification of Micromixing Calculations II. New Applications." *The Chemical Engineering Journal* 42 (1989): 93–101.

Baldyga, J. and J. R. Bourne. "Interaction Between Mixing on Various Scales Scales in Stirred Tank Reactors." *Chemical Engineering Science* 47 (1992): 1839–1848.

Baldyga, J., J. R. Bourne, and S. J. Hearn. "Interaction between chemical reactions and mixing on various scales." *Chemical Engineering Science* 52 (1997): 457–466.

Baldyga, J. and M. Henczka. "Turbulence Mixing and Parallel Chemical Reactions in a Pipe: Application of a Closure Model." *MIXING IX: Recent Advances in Mixing.* Paris, France: Technique et Documentation-Lavoisier, 1997, 341–348.

Baldyga, J. and R. Pohorecki. "Turbulent micromixing in chemical reactors." *The Chemical Engineering Journal* 58 (1998): 183–195.

Bird, R. B., W. E. Stewart, and E. N. Lightfoot. *Transport Phenomena.* USA: John Wiley and Sons, 1960.

Bourne, J. R. and J. Baldyga. *Turbulent Mixing and Chemical Reactions.* England: John Wiley and Sons, 1999.

Bourne, J. R. and S. Yu. "An Experimental Study of Micromixing Using Two Parallel Reactions." *7th European Congress on Mixing.* Brugge-Belgium: Royal Flemish Society of Engineers, September 1991, 67–75.

Bourne, J. R. and S. Yu. "Investigation of Micromixing in Stirred Tank Reactors Using Parallel Reactions." *Industrial and Engineering Chemistry Research* 33 (1994): 41–55.

Bourne, J.R. "What Does the Modeling of Reactive Flows ask of CFD." *Revue de L'institut Français du Pétrole* 48 (Novembre–D'ecembre 1993).

Bourne, J.R., R.V. Gholap, and V.B. Rewatkar. "The influence of viscosity on the product distribution of fast parallel reactions." *The Chemical Engineering Journal* 58 (1995): 15–20.

Brucato, A., M. Ciofalo, F. Grisafi, and G. Micale. "Numerical prediction of flow fields in baffled stirred vessels: A comparison of alternative modeling approaches." *Chemical Engineering Science* 53 (1998): 3653–3684.

Chakrabarti, M. and J. C. Hill. "First-Order Closure for Series Parallel Reaction in Simulated Homogeneous Turbulence." *AIChE Journal* 43 (1997): 902–912.

Coy, D. "Computer Simulation Helps Design Laboratory Equipment that Accurately Models Production Plant." *Simulation* 67 (1996): 206–208.

David, R., H. Muhr, and J. Villermaux. "The Yield of consecutive-competitive reaction in a double semi-batch reactor: comparison between experiments and a multi zone mixing model." *Chemical Engineering Science* 47 (1992): 2841–2846.

David, R. and J. Villermaux. "Micromixing Effect on Complex Reactions in a CSTR." *Chemical Engineering Science* 30 (1975): 1309–1313.

Denn, M. M. *Process Fluid Mechanics*. Englewood Cliffs, NJ. USA: Prentice-Hall, 1980.

Dickey, D. S. and J. G. Fenic. "Dimensional Analysis for Fluid Agitation Systems." *Chemical Engineering* (January 1976): 7–13.

Dutta, A. and J. M. Tarbell. "Closure Models for Turbulent Reacting Flows." *AIChE Journal* 35 (December 1989): 2013–2027.

Fasano, J. B., A. Bakker, and W. R. Penney. "Advanced impeller geometry boosts liquid agitation." *Chemical Engineering* (August 1994).

Fasano, J. B. and W. R. Penney. "Avoid Blending Mix-Ups." *Chemical Engineering Progress* 87 (October 1991): 56–63.

Finlayson, B. A. *Nonlinear Analysis in Chemical Engineering*. New York, USA: McGraw-Hill Inc., 1980.

Fox, R. O. "Computation of Turbulent Reactive Flows: First-Principles Macro/Micromixing Models Using Probability Density Function Methods." *Chemical Engineering Science* 47 (1992): 2853–2858.

Fox, R. O. "The Spectral Relaxation Model of the Scalar Dissipation Rate in Homogeneous Turbulence." *Physics of Fluids* 7 (May 1995): 1082–1094.

Fox, R. O. "Computational Methods for Turbulent Reacting Flows in the Chemical Process industry." *Revue de L'institut Français du Pétrole* 51 (Mars–Avril 1996): 215–243.

Gray, D. J., R.E. Treybal, and S. M. Barnett. "Mixing of Single and Two Phase Systems: Power Consumption of Impellers." *AIChE Journal* 28 (March 1982): 195–198.

Griebel, M., T. Dornseifer, and T. Neunhoeffer. *Numerical Simulation in Fluid Dynamics*. Philadelphia, USA: SIAM, 1998.

Harnby, H., M. F. Edwards, and A. W. Nienow. *Mixing in the Process Industries*. U.K.: Butterworths, 1985.

Hinze, J. O. *Turbulence*. Second edition. USA: Mc Graw Hill, 1975.

Hirt, C. W. and B. D. Nichols. "Volume of Fluid (VOF) Method for the Dynamics of Free Boundaries." *Journal of Computational Physics* 39 (1981): 201–225.

Jaworski, J., A. W. Nienow, and K. N. Dyster. "An LDA Study of the Turbulent Flow Field in a Baffled Vessel Agitated by an Axial, Down-pumping Hydrofoil Impeller." *The Canadian Journal of Chemical Engineering* 74 (February 1996): 3–15.

Kresta, S. M. and P. E. Wood. "Prediction of the Three-Dimensional Turbulent Flow in Stirred Tanks." *AIChE Journal* 37 (1991).

Kruis, F.E. and L. Falk. "Mixing and Reaction in a Tubular Jet Reactor: A comparison of Experiments with a Model based on a prescribed PDF." *Chemical Engineering Science* 51 (1996): 2439–2448.

Leng, D. L. "Succeed at Scale Up." *Chemical Engineering Progress* 6 (June 1991): 23–31.

Luo, J. Y., R. I. Issa, and A. D. Gosman. "Prediction of Impeller Induced Flows in Mixing Vessels Using Multiple Frames of Reference." *Institution of Chemical Engineers Symposium Series No.136.* Cambridge, England: Institution of Chemical Engineers, 1994, 549–556.

Fluent Inc. *Fluent v4.3 Manual.* Fluent Inc., Lebanon, New Hampshire, 4.3 edition, 1992.

Harvey III, A. D. and S.E. Rogers. "Steady and Unsteady Computation of Impeller-Stirred Reactors." *AIChE Journal* 42 (October 1996): 2701–2712.

Myers, K., J. B. Fasano, and R. R. Corpstein. "The influence of solid properties on the just suspended agitation requirements of pitched-blade and high-efficiency impellers." *The Canadian Journal of Chemical Engineering* 72 (August 1994): 745–748.

Pipino, M. and R. O. Fox. "Reactive Mixing in a Tubular Jet Reactor: A Comparison of PDF Simulations with Experimental Data." *Chemical Engineering Science* 49 (1994): 5229–5241.

Ranade, V.V., J.R. Bourne, and J.B. Joshi. "Prediction of the Three-Dimensional Turbulent Flow in Stirred Tanks." *AIChE Journal* 37 (March 1991): 448.

Ranade, V.V. and J.B. Joshi. "Flow Generated by Pitched Blade Turbines I: Measurements Using Laser Doppler Anemometer." *Chemical Engineering Communications* 81 (1989): 197–224.

Ranade, V.V. and J.B. Joshi. "Flow Generated by Pitched Blade Turbines II: Simulation Using the k-e Model." *Chemical Engineering Communications* 81 (1989): 225–248.

Ranade, V.V. and J.B. Joshi. "Flow Generated By a Disk Turbine: Part I Experimental." *Transactions of IChemE* 68 (1990): 19.

Ranade, V.V. and J.B. Joshi. "Flow Generated By a Disk Turbine: Part II Mathematical Modeling and Comparison with Experimental Data." *Transactions of IChemE* 68 (January 1990): 34.

Rewaltker, V. B., R. Rao, and J. B. Joshi. "Power dissipation in mechnical agitated contactors using a pitched blade turbine impeller." *Chemical Engineering Communications* 88 (1990): 69–90.

Rodi, W. *Turbulence Models and Their Applications in Hydraulics - A State of the Art Review.* Second edition. Delft, The Netherlands: International Association for Hydraulic Research, February 1984.

Smith, J. M. "Industrial Needs for Mixing Research." *Transaction of the Institution of Chemical Engineers* 68 (January 1990): 3–6.

Tatterson, G. B., R. S. Brodkey, and R.V. Calabrese. "Move mixing technology into the 21st Century." *Chemical Engineering Progress* 6 (June 1991): 45–48.

TSI. Technical Bulletin 25a: Laser Doppler Velocimeter Techniques. Technical report, TSI Incorporated, 1979.

Villermaux, J. and L. Falk. "A Generalized Mixing Model for Initial Contacting of Reactive Fluids." *Chemical Engineering Science* 49 (1994): 5127–5140.

Villermaux, J. and L. Falk. "Recent Advances in Modeling Micromixing and Chemical Reactions." *Revue de l'Institut Français du Pétrole* 51 (Mars–Avril 1996).

Wang, D. M. and J. M. Tarbell. "Closure Models for Turbulent Reacting Flows with a Non-Homogeneous Concentration Field." *Chemical Engineering Science* 48 (1993): 3907–3920.

Wang, Y. D. and R. Mann. "Partial Segregation in Stirred Batch Reactors: Effect of Scale-up on the Yield of a Pair of Competing Reactions." *Transactions of IChemE* 70 (May 1992): 282–290.

Zhou, G. and S.M. Kresta. "Distribution of Energy Between Convective and Turbulent Flow for Three Frequently Used Impellers." *Transactions of IChemE* 74 (1996).